

Scale-Up of Continuous Monoclonal Antibody Precipitation

by

Michael Martinez

A thesis submitted for the degree of

Doctor of Engineering

in

The Department of Biochemical Engineering

UCL

October 2020



I, Michael Martinez, hereby declare that the work presented in this thesis is my own. Where information has been derived from other sources, I can confirm that this has been indicated in the thesis.

Signature _____ Date _____

Acknowledgements

I am forever grateful for the guidance and support provided by my supervisor Daniel Bracewell throughout this work. I would also like to kindly thank my industrial sponsors Mari Spitali at UCB and Edith Norrant at IPSOMEDIC for their continuous input, without which none of this work would have been possible. A special mention must be made to Gareth Mannall for his assistance in pilot-scale downstream processing training and contribution to the pilot-scale work presented in the thesis.

I want to thank my family and friends for their encouragement and support throughout the whole EngD process, aiding me in times of difficulty and always helping to keep things in perspective. I want to specifically thank my mother Nasly for her undeniable support throughout this endeavour and continuously feeding me with deliciously cooked meals. I also would like to specifically acknowledge the following individuals: Maximillian Lularevic, Sheun Oshinbolu, Charnett Chau, Chika Nweke, Darryl Kong, Rosalia Cardos, Greta Jasualitye, Jose Martins Bufajer and Nehal Patel for all the great moments we've shared together within and outside the department. Last, but not least, I want to specially thank the UCL Dance Society for providing me an outlet for when times were tough and allowing me to embrace my passion for dance, as well as for granting me with the special connections I made at UCL.

Abstract

The scale-up of protein precipitation processes proves to be a challenging task due to the complexity of the reactions and transport processes involved. A good understanding of the molecular processes underpinning precipitate formation and the reaction kinetics are therefore required in order to devise a scale-up strategy. The doctoral project was first set out to establish micro-mixing as an engineering tool for the scale-up of antibody precipitation from cell culture, and secondly to design a downstream process with the goal of purifying a therapeutic mAb to clinical grade levels.

Studies were first conducted in batch and transferred to a continuous process, with the scale-up approach focusing on the latter. Interactions between precipitation conditions and centrifugal recovery were then examined by employing an ultra scale-down (USD) methodology to mimic large-scale centrifugation. The downstream process design was on the basis of integrating precipitation with non-affinity chromatography steps to avoid the cost of affinity chromatography.

Precipitate formation in batch and continuous settings was governed by the mixing at the molecular scale, which determined the final particle properties. Based on this, the mean energy dissipation rate for a continuous precipitation process proved an effective scale-up criterion, enabling high process throughputs relative to batch operation. The strength of protein precipitates, as evaluated by exposing particles to turbulent shear in a rotating disc device, was shown to correlate with particle fractal dimensions. Despite excellent precipitate solids removal from the USD methodology, these could not be predicted by disc-stack centrifugation. Differences in hindered settling between the systems were proposed to explain this observation which suggests routes to resolve this scale-up challenge.

To provide an integrated DSP solution for therapeutic mAbs processes anion exchange and mixed-mode chromatography steps subsequent to precipitation were designed. Parameter ranges were studied to identify the optimal conditions in maximising antibody yield and HCP removal. Using optimal conditions, precipitation and anion exchange demonstrated an 18-fold removal in HCPs, whilst precipitation and mixed-mode provided a 40-fold removal. For a three step process comprising the sequence precipitation, anion exchange and mixed mode, an overall HCP removal of 260-fold was seen; however such levels remain at least 38-fold higher than the typical specification of a clinical grade product. This therefore necessitates further optimisation in one or more steps.

Impact Statement

The costs associated with conventional manufacturing of biologics, in particular monoclonal antibodies, make these classes of drugs one of the most expensive in the therapeutic market (Farid, 2007; Kaufman and Kalaitzandonakes, 2011). This is due to the complexity of the manufacturing process requiring specific equipment (e.g. bioreactors), the need for high doses, marketing costs and the price point set by early innovative treatments (Shaughnessy, 2012). Developing and delivering a new drug to the market reaches an average cost of \$1 billion (Danzon, 2007), taking approximately 10 years with only 11% chance of commercial success (DiMasi, Hansen and Grabowski, 2003). Nevertheless, continued investment towards the development of these agents is required in order to combat some of the complex and severe illnesses not treatable by other means. In order to reduce manufacturing costs which enable wider patient access, a concept known as process intensification has been implemented (Reay, Ramshaw and Harvey, 2013; Xu *et al.*, 2020). This involves the adoption of innovative methods to protein purification. Process intensification aims to provide major improvements to the purification process by improving overall productivity that not only lowers process costs but also reduces facility footprint.

The adoption of continuous precipitation to bio-manufacturing can be considered as a strategy to process intensification and has shown to provide a solution to the economic and technological constraints imposed by conventional chromatography (Reay, Ramshaw and Harvey, 2013; Martinez *et al.*, 2019). The relatively low costs of precipitating agents in comparison to chromatography resins and the required column hardware enables a significant reduction in cost of goods (CoGs) for downstream processing. An added benefit is the ability to cope with high titres often seen in current mammalian cell culture practices, where chromatography would normally struggle in providing the same level of productivity. As a result, efforts from both academia and the biopharmaceutical industry have focused on downstream process intensification through implementing precipitation, amongst other techniques.

The use of ultra scale-down models has become a key component to rapidly explore bioprocess sequences so that full-scale processes can be developed at speed and at low cost while assuring product safety and efficacy (Rayat *et al.*, 2016). These become particularly valuable when attempting to translate the discovery of new and complex therapies to market as well as minimise the risks encountered during scale-up. One such risk with regards to the work outlined herein is stress exposure during large-scale semi-continuous centrifugation and how it may negatively impact the biologic. As such an event is not often captured in a laboratory setting, a shear mimic characterising this would have

considerable utility. Therefore, an existing methodology was applied in this work to evaluate centrifugal recovery of protein precipitates in terms of efficiency and risk, and further, to develop an integrated precipitation process. Implementation of USD tools can drive further research in this area and has applicability in a range of purification schemes, whether in alternative precipitation methods or other methods.

As a final remark, the impact of the research has been disseminated through publications and presented at regional and international conferences. The foundation of the work lays out an approach in which future biologics could be manufactured at reduced costs by industrial companies such as UCB, providing them a competitive advantage.

Table of Contents

Acknowledgements.....	3
Abstract.....	4
Impact Statement.....	5
List of Figures.....	11
List of Tables.....	15
List of Equations.....	16
Nomenclature.....	17
Chapter 1: Introduction and Literature Review.....	22
1.1 Introduction.....	22
1.2 Thesis overview.....	22
1.3 Project objectives.....	24
1.4 Role of precipitation to bioprocessing.....	24
1.5 Monoclonal antibody manufacturing.....	26
1.6 Precipitation methods.....	28
1.6.1 Conventional precipitants.....	28
1.6.2 Concluding remarks.....	36
1.7 Theory of solubility.....	36
1.7.1 Protein and solvent structural considerations.....	37
1.7.2 Colloidal approach of protein solubility.....	38
1.7.3 Solubility with the Cavity Model.....	40
1.8 Principle of precipitation.....	41
1.9 Precipitate formation.....	42
1.9.1 Nucleation and growth by diffusion.....	43
1.9.2 Growth by fluid motion.....	45
1.9.3 Aging.....	46
1.9.4 Precipitate conditioning.....	47
1.10 Considerations in mixing for precipitation.....	47
1.11 Prospects for scale-up.....	49
1.12 Future prospects and concluding remarks.....	52
Chapter 2: Materials and Methods.....	53

2.1	Materials	53
2.1.1	Clarified cell culture fluid	53
2.1.2	Purified IgG ₄	53
2.1.3	Purification reagents	54
2.1.4	Chromatography media	54
2.2	Precipitation methods	54
2.2.1	Batch precipitations	54
2.2.2	Continuous precipitations	55
2.3	Analytical methods	56
2.3.1	Antibody quantification	56
2.3.2	Antibody purity	57
2.3.3	Circular dichroism (CD) spectroscopy	60
2.3.4	Particle size measurements	61
2.3.5	Ultra scale-down (USD) centrifugation	62
2.4	Disc-stack centrifugation	62
2.5	Chromatographic methods	63
2.5.1	Predictor plates	63
2.5.2	Column chromatography	63
Chapter 3: Characterisation of monoclonal antibody precipitation with salting-out		64
3.1	Introduction	64
3.2	Salting-out screen	65
3.3	Effect of salt type, salt concentration and pH on purified IgG ₄ precipitation performance	68
3.4	Effect of protein concentration on precipitation performance	74
3.5	Solubilisation efficiency of purified IgG ₄ precipitates	79
3.5.1	Solubilised IgG ₄ yields	79
3.5.2	Impact of precipitation on antibody structure and aggregate levels	81
3.6	IgG ₄ precipitation from cell culture fluid	84
3.6.1	Effect of salts on IgG ₄ precipitation and recovery	84
3.7	IgG ₄ precipitation kinetics	89
3.8	Re-solubilisation efficiency of CCCF precipitates	92
3.9	Design of Experiments study on cell culture fluid precipitation with ammonium sulphate	95
3.10	Antibody purity with ammonium sulphate precipitation	98
3.10.1	Relative antibody purity upon ammonium sulphate precipitation	98

3.10.2	Effect of precipitate washing on impurity removal.....	101
3.10.3	HCP and DNA levels on precipitated antibody	102
3.11	Fractional precipitation	104
3.12	Summary	108
Chapter 4:	Design of precipitation reactor systems based on analysis of mixing.....	110
4.1	Introduction.....	110
4.2	Villiermaux's Iodide-iodate reaction test	116
4.3	Estimation of micro-mixing times	119
4.4	Macro-mixing test results	122
4.4.1	Batch stirred reactor.....	122
4.4.2	Continuous tubular reactor.....	124
4.5	Characterization of residence time distribution in tubular reactors.....	124
4.6	Micro-mixing tests results.....	128
4.6.1	Micro-mixing in stirred batch reactor	128
4.6.2	Micro-mixing characterisation in the lab-scale and pilot-scale continuous reactors	132
4.7	Summary	135
Chapter 5:	Micro-mixing on protein precipitation as a tool for scale-up	136
5.1	Introduction.....	136
5.2	Theoretical considerations	138
5.2.1	Particle fractal dimension	138
5.2.2	Sigma theory	140
5.3	Batch precipitation trials	142
5.3.1	Effect of mixing during micro-mixing-controlled precipitation	142
5.3.2	Effect of increased agitation on precipitates	146
5.3.3	UltraUltra scale-down centrifugation of batch precipitates.....	147
5.4	Continuous precipitation trials	154
5.4.1	Lab-scale continuous precipitation	154
5.4.2	Effect of flow rate and residence time on particle size, PSD and yield.....	154
5.4.3	Effect of antibody concentration on particle size	158
5.4.4	Effect of tube diameter in the lab-scale reactor	160
5.4.5	Pilot-scale precipitation results.....	162
5.5	Impact of turbulent processing on continuous protein precipitates	165
5.6	Effect of Camp Number on strength of continuous precipitates	167

5.7	Ultra scale-down centrifugation study	172
5.9	Summary	179
Chapter 6: Integrating salt precipitation with chromatography.....		181
6.1	Introduction.....	181
6.2	IgG ₄ purification with Capto Q in FT-mode.....	183
6.2.1	Determination of IgG ₄ binding conditions with microscale chromatography screening	183
6.2.2	Evaluation of loading conditions on IgG ₄ yield and impurity removal.....	187
6.3	IgG ₄ purification with Capto MMC in bind-and-elute mode.....	195
6.3.1	Determination of non-precipitating loading conditions.....	195
6.3.2	Microscale purification study	196
6.3.3	Verification of IgG ₄ purification using selected lead conditions with lab scale chromatography.....	204
6.4	Integration of precipitation and two-step chromatography process.....	209
6.4.1	Purification with Capto Q on an XK 16 column.....	210
6.4.2	Capto MMC Loading Range selection	210
6.4.3	Predictor plate purification results.....	210
6.4.4	Verification of IgG ₄ purification using selected lead conditions with lab scale chromatography.....	213
6.5	Comparison of integrated processes with PrA chromatography.....	215
Chapter 7: Conclusions and Future Work.....		217
7.1	Conclusions.....	217
7.2	Scope for future work.....	219
7.2.1	Short-term.....	219
7.2.2	Mid-term.....	221
7.2.3	Long term.....	223
Chapter 8: Process Validation.....		226
8.1	Regulatory considerations for bioprocess manufacturing	226
8.2	Regulatory considerations for implementation of precipitation processes	227
References		231
Appendix A: IgG ₄ amino acid sequence		245
Appendix B: IgG physicochemical properties		246

List of Figures

Figure 1-1. Graph showing the evolution of new patent submissions regarding therapeutic purification with precipitation of various protein classes between 2010 and 2017.	26
Figure 1-2. A typical mAb platform process showing key upstream and downstream unit operations.....	27
Figure 1-3. A schematic of DLVO interaction energy as a function of separation distance (Adair et al., 2001).....	39
Figure 1-4. Qualitative illustration of a phase diagram showing zones of precipitation and crystallisation of macromolecules, based on protein concentration and precipitant concentration (or any other relevant parameter).	41
Figure 1-5. A generic schematic showing the effect of the degree of supersaturation on particle nucleation and growth rates, and ultimate crystal/precipitate size.	43
Figure 1-6. Schematic illustration of different continuous reactors.	50
Figure 3-1. Step-by-step procedure implemented for the precipitation screening experiments in the 96-well plate format.....	66
Figure 3-2. IgG ₄ solubility profile with increasing ammonium sulphate concentration at pH 6, 7 and 8.	70
Figure 3-3. IgG ₄ solubility profile with increasing sodium sulphate concentration at pH 6, 7 and 8.	71
Figure 3-4. IgG ₄ solubility profile with increasing sodium citrate concentration at pH 6, 7 and 8.	72
Figure 3-5. Precipitation midpoints for IgG ₄ precipitation with ammonium sulphate, sodium sulphate and sodium citrate as a function of pH.	73
Figure 3-6. Ammonium sulphate precipitation profiles at various final IgG ₄ concentrations. .	75
Figure 3-7. Sodium sulphate precipitation profiles at various final IgG ₄ concentrations.....	76
Figure 3-8. Sodium citrate precipitation profiles at various final IgG ₄ concentrations.	77
Figure 3-9. Precipitation midpoints for ammonium sulphate, sodium sulphate and sodium citrate precipitation as a function of IgG ₄ concentration.....	78
Figure 3-10. Contour plot displaying IgG ₄ recoveries at various ammonium sulphate concentrations and resuspension buffer volumes.....	80
Figure 3-11. SEC-HPLC profiles of IgG ₄ before and after ammonium sulphate precipitation at 1.5 mL scale.....	82
Figure 3-12. CD spectra overlay of Protein-A purified IgG ₄ before (<i>black</i>) and after precipitation (<i>red</i>) in the wavelength range from 200 to 250 nm using an antibody concentration of 0.8 mg/mL.	83
Figure 3-13. Comparison of IgG ₄ precipitation profiles with ammonium sulphate between purified and cell culture supernatant feedstock.	85
Figure 3-14. Visualisation of CCCF precipitates with ammonium sulphate (AS), sodium citrate (SC) and sodium sulphate (SS) precipitation after centrifugal recovery.....	87
Figure 3-15. Particle size distribution profiles of CCCF precipitates with ammonium sulphate, sodium sulphate and sodium citrate precipitation at 40 mL scale.	88
Figure 3-16. Kinetics of antibody precipitation with ammonium sulphate.	91

Figure 3-17. Antibody yields upon re-solubilisation with various buffers and buffer volumes with respect to the initial starting volume.	93
Figure 3-18. Overlay of particle size distribution between clarified cell culture supernatant and re-solubilised precipitate.....	94
Figure 3-20. Contour plots showing IgG ₄ recovery as a function of ammonium sulphate (AS) concentration and pH at (A) 0.5 g/L, (B) 2.75 g/L and (C) 5 g/L IgG ₄	97
Figure 3-21. Protein G HPLC profile of clarified cell culture fluid (CCCF) and IgG ₄ precipitate samples.	99
Figure 3-22. Bar plot of the impact of pH and ammonium sulphate (AS) concentration on the purification factors achieved with ammonium sulphate precipitation with a target antibody concentration of 0.5 g/L.....	100
Figure 3-23. Non-reduced SDS-PAGE of composition of precipitated IgG ₄ from cell culture fluid with increasing ammonium sulphate concentration in the range 1 to 1.7 M.....	101
Figure 3-24. Protein G HPLC profiles of resolubilised IgG ₄ precipitate (Ppt) with and without washing.....	102
Figure 3-25. DNA levels in nanograms per milligram of antibody as a function of ammonium sulphate concentration for precipitation.....	103
Figure 3-26. Non-reduced SDS-PAGE of composition of IgG ₄ purified samples from single ammonium sulphate (AS) precipitations with increasing salt concentration.....	106
Figure 3-27. Non-reduced SDS-PAGE of composition of IgG ₄ samples from fractional two-step ammonium sulphate precipitations.	107
Figure 4-1. Schematic representation (A) and photographic illustration (B) of the 150 mL stirred batch vessel with feed additions made through a 0.5 mm diameter bore positioned adjacent to the impeller.	113
Figure 4-2 Schematic representation (A) and photographic illustration (B) of the continuous tubular reactor fitted with an in-line T-mixer for initial mixing of two solutions.....	114
Figure 4-3. Configuration of the coiled-flow inversion reactor (CFIR) employed for pilot scale mixing and precipitation studies.....	115
Figure 4-4. Relationship between segregation index, X_s , and micro-mixing time, t_m , based on experimental conditions in the continuous tubular reactors (lab and pilot-scale) using the incorporation model.	121
Figure 4-5. Evolution of macro-mixing times as a function of impeller mixing speed and two acid injection viscosities in a 150 mL stirred batch vessel.....	123
Figure 4-6. Residence time distribution experiments in the lab-scale continuous reactor. ..	126
Figure 4-7. Residence time distribution experiments in the pilot-scale reactor.....	127
Figure 4-8. Effect of the sulphuric acid injection time (t_{add}) at 100 rpm impeller speed on the segregation index at two different acid viscosity injections: 1 and 2.5 mPa.s.	130
Figure 4-9. Effect of Reynolds number on the micromixedness ratio, α , at the critical injection time, t_{crit} ($t_{add} = 480$ s), and at two different viscosities: 1 and 2.5 mPa.s.....	131
Figure 4-10. Re vs estimated t_m from lab-scale continuous reactor micro-mixing experiments.	133
Figure 4-11. Re vs estimated t_m from pilot-scale continuous reactor (CFIR) micro-mixing experiments.....	134
Figure 5-1. Log-log plot for the estimation of the fractal dimension, f_D , of a protein precipitates with laser light diffraction.	140

Figure 5-2. Effect of impeller speed on the average mean particle size, d_{50} , of CCCF precipitates with ammonium sulphate in a 150 mL baffled-stirred vessel under micro-mixing-controlled conditions.	144
Figure 5-3. Effect of batch mixing speed on the PSD profiles of CCCF precipitates under micro-mixing-controlled conditions.	145
Figure 5-4. Representative micrographs of protein precipitate particles prepared during batch precipitation experiments.	146
Figure 5-5. Effect of turbulent shear stress on batch precipitates.	149
Figure 5-6. Representative micrographs of batch-formed precipitates after exposure to turbulent stress at 6000 rpm in the rotary disc device.	150
Figure 5-7. Ultra scale-down centrifugation analysis of non-sheared (black circles) and sheared (crossed open circles) precipitate samples from the batch precipitation experiments conducted at (A) 150 rpm, (B) 200 rpm, (C) 300 rpm, (D) 400 rpm and (E) 500 rpm mixing.	153
Figure 5-8. Change in the mean particle size, d_{50} , of clarified cell culture fluid protein precipitates as a function of flow rate over various reactor lengths in 1 mm diameter tubing.	156
Figure 5-9. Representative particle size distributions (PSD) of protein precipitates formed at (A) 1 mL/min, (B) 2 mL/min, (C) 4 mL/min, (D) 7 mL/min, (E) 10 mL/min, (F) 14 mL/min and (G) 20 mL/min.	157
Figure 5-10. Representative micrograph images of protein precipitates obtained at (A) 1 mL/min, (B) 2 mL/min, (C) 4 mL/min, (D) 7 mL/min, (E) 10 mL/min, (F) 14 mL/min.	158
Figure 5-11. Effect of CCCF antibody concentration on the mean particle size, d_{50} , of continuous protein precipitates as a function of total flow rate.	159
Figure 5-12. Mean particle sizes in various tubing diameters for continuous precipitation at lab-scale.	161
Figure 5-13. Pilot-scale precipitation results and comparison with small-scale data.	163
Figure 5-14. Effect of flow rate on the PSD, on a volume basis, of protein precipitates formed at pilot-scale in a CFIR.	164
Figure 5-15. Effect of turbulent processing in a rotating disc device on lab-scale protein precipitates formed from various flow rate conditions.	165
Figure 5-16. Effect of turbulent processing in a rotating disc device on pilot-scale protein precipitates formed from various flow rate conditions.	166
Figure 5-17. Effect of precipitate Camp Number, N_{Ca} , by varying reactor length, on the change of mean particle size, d_{50} , with exposure to turbulent shear stress in the rotating disc device.	169
Figure 5-18. Effect of batch aging on the mean particle size, d_{50} , and strength of continuous tubular precipitates.	170
Figure 5-19. Effect of tube constrictions on the mean particle size, d_{50} , and strength of continuous tubular precipitates.	171
Figure 5-20. Ultra scale-down centrifugation analysis of non-sheared (black squares) and sheared (red circles) lab-scale precipitate samples.	174
Figure 5-21. Ultra scale-down centrifugation analysis of non-sheared (black squares) and sheared (red circles) pilot-scale precipitate samples.	175
Figure 5-22. Validation of the USD method for the prediction of CCCF precipitate recovery by disc-stack centrifuge with Pathfinder PSC-1.	177

Figure 5-23. Effect of disc-stack centrifugation on CCCF precipitate recovery.....	178
Figure 6-1. High-throughput workflow using 50 μ L Capto Q 96-well Predictor plates for the development of an anion exchange (AEX) chromatography step.	184
Figure 6-2. Capto Q screening to determine IgG ₄ loading conditions.	186
Figure 6-3. Effect of salt concentration on antibody yield and remaining HCP levels in CaptoQ processing of (A) post-precipitated and (B) non-precipitated CCCF samples at microscale.	189
Figure 6-4. Capto Q chromatogram profiles representing IgG ₄ purification from (A) post-precipitated and (B) non-precipitated CCCF samples in a 1 mL HiTrap column.	191
Figure 6-5. Effect of salt concentration on antibody yield and HCP levels in Capto Q processing of (A) post-precipitated and (B) non-precipitated CCCF samples in FT-mode using lab-scale chromatography.	193
Figure 6-6. Effect of salt concentration on residual DNA levels in Capto Q processing of (A) post-precipitated and (B) non-precipitated CCCF samples in FT-mode using lab-scale chromatography.....	194
Figure 6-7. Capto MMC Predictor Plate workflow schematic for antibody purification screening.	197
Figure 6-8. Contour plots showing the effect of pH, salt type and salt concentration of IgG ₄ binding to Capto Q resin and HCP removal during loading in 50 μ L Predictor plates as a function of pH and salt concentration.....	199
Figure 6-9 Desirability plots highlighting leading loading conditions from sodium chloride, SC, (A) and ammonium sulphate, AS, (B) screening using Design Expert 12.....	200
Figure 6-10. IgG elution profiles with sodium chloride at pH 8.	201
Figure 6-11. Contour maps showing antibody yield and HCP eluate pools from the various loading conditions in the presence of ammonium sulphate.....	203
Figure 6-12. UV chromatograms of post-precipitated antibody samples loaded onto 1 mL HiTrap Capto MMC and eluted with sodium chloride at pH 8 with a linear gradient over 20 CVs.....	205
Figure 6-13. Antibody and HCP level compositions in Capto MMC eluate fractions corresponding to the main peak in the chromatograms presented in Figure 6-12.	207
Figure 6-14. Contour maps showing from Capto MMC Predictor screening on post- Capto Q samples using ammonium sulphate (AS).....	212
Figure 6-15. UV chromatograms representing Capto MMC purification of Capto Q FT samples.(....	214
Figure 8-1. Quality by design (QbD) approach for quality assurance.....	228

List of Tables

Table 1-1. List of main centrifuge types and advantages/disadvantages to precipitate solids recovery (Bell et al., 1983; Bell and Dunnill, 1982a).....	51
Table 3-1. List of salts, stock solutions and pH and concentration ranges tested for the precipitation screening experiments.....	65
Table 3-2 Selection of factors and factor levels tested for full factorial DoE study.....	95
Table 3-3. List of factor terms included in the reduced DoE model for precipitated IgG ₄ yield.	96
Table 3-4. Yield and purity comparison of single and double cut precipitations for IgG ₄ purification from CCCF using ammonium sulphate (AS).	105
Table 4-1. Summary of micro-mixing results from batch mixing experiments.	129
Table 5-1. Determined f_D values of non-sheared and sheared batch precipitate samples as a function of mixing.	151
Table 5-2. Experimental conditions employed for the pilot-scale precipitation runs in a CFIR.	162
Table 6-1. Details of Capto Q and Capto MMC resin media.	182
Table 6-2. Examination of non-precipitating and precipitating conditions across a salt range from 0 to 1.25 M sodium chloride (SC) and ammonium sulphate (AS) for Capto MMC chromatography loading.....	196
Table 6-3. Purification results of selected leading conditions for Capto MMC on a 1 mL HiTrap column.	209
Table 6-4. Comparison of integrated precipitation and chromatography purification processes for IgG ₄ from CCCF with each other and with standard and UCB platform PrA capture chromatography processes.....	215

List of Equations

Equation 1-1. Cohn salting-out equation.	28
Equation 1-2. Thermodynamic model for protein solubility in non-ionic polymer solutions. ...	31
Equation 1-3. Foster's simplified expression on protein solubility with non-ionic polymers. ..	32
Equation 1-4. Expression for protein solubility as a function of the solution dielectric constant with the addition of organic solvents.	33
Equation 1-5. Sinanoğlu's cavity model.....	40
Equation 1-6. Smoluchowski's perikentic growth model.	44
Equation 1-7. Stokes-Einstein relationship for translational diffusion.	44
Equation 1-8. Fuchs' perikinetic growth model.....	44
Equation 1-9. Determination of stability ratio, W	44
Equation 1-10. Smoluchowski's orthokinetic growth model.	45
Equation 1-11. Integral of Smoluchowski's orthokinetic growth model.....	45
Equation 1-12. Calculation of Camp number, N_{Ca}	46
Equation 1-13. Determination of segregation number, N_{seg} , with the droplet diffusion model.	48
Equation 2-1. Transformation of polarised angle ellipticity to molar circular dichroism, $\Delta\epsilon$	60
Equation 2-2. Percentage of solids remaining as a function of OD600 values for feed, supernatant and well-clarified supernatant samples.	62
Equation 3-1. Calculation of minimum centrifugation time, t_c , required for effective particle separation.....	67
Equation 3-2. Sigmoidal precipitation curve fitting.	68
Equation 4-1. Dushman reaction rate law.	116
Equation 4-2. Calculation of equilibrium rate constant, K , for tri-iodide formation based on iodide, iodide and tri-iodide concentrations.....	117
Equation 4-3. Calculation of equilibrium rate constant, K , as a function of solution temperature, T	117
Equation 4-4. Calculation of micro-mixedness ratio, α	118
Equation 4-5. The incorporation model for the estimation of micro-mixing times in reactors.	119
Equation 4-6. Series of micro-mixing time, t_m , calculations for stirred batch reactors using defined reagent concentrations.....	120
Equation 4-7. Estimation of macro-mixing time in continuous tubular reactors.....	124
Equation 4-8. Calculation to estimate micro-mixing time, t_m , in a baffled vessel with fully developed turbulence (i.e. $Re > 10^4$).....	128
Equation 5-1. Calculation of scattering wave vector, Q	139
Equation 5-2. Log-log correlation of deflected laser light intensity, I , at each scattering angle, Θ , to estimate particle fractal dimension, f_D	139
Equation 5-3. Sigma theory correlation between two types of industrial centrifuges which provide similar clarification.....	141
Equation 5-4. Calculation of equivalent settling area for disc-stack centrifuges.	141
Equation 5-5. Calculation of equivalent settling area for laboratory centrifuges.	141
Equation 5-6. Sigma theory correlation to mimic clarification of an industrial centrifuge with a laboratory centrifuge.	141

Nomenclature

α – Micro-mixedness ratio

μ – Absolute dynamic viscosity

ε – Mean energy dissipation rate

Σ – Equivalent settling area

B – Salting-out constant

ω – Angular velocity

ν – Kinematic viscosity

f_D – Fractal dimension

X_s – Segregation Index

2D-DiGE – Two Dimensional Difference Gel Electrophoresis

AEX – Anion Exchange Chromatography

AS – Ammonium Sulphate

CCCF – Clarified Cell Culture Fluid

CD – Circular Dichroism

CEX – Cation Exchange Chromatography

CFD – Computation Fluid Dynamics

CFIR – Coiled Flow Inversion Reactor

CHO – Chinese Hamster Ovary

CMC – Chemical, Manufacturing and Controls

CoGs – Cost of Goods

CPP(s) – Critical Process Parameters

CV(s) – Column Volume(s)

CQA(s) – Critical Quality Attribute(s)

D - Diffusivity

d_{10} – Portion of particles with diameters smaller than this value is 10%

d_{50} – Portion of particles with diameters smaller than this value is 50%. Also known as median diameter.

d_{90} - Portion of particles with diameters smaller than this value is 90%

Da_M – Dahmkohler Number

DLS – Dynamic Light Scattering

DoE – Design of Experiments

DLVO – Derjaguin-Landau-Verwey-Overbeek

D_s – Dielectric constant

DNA – Deoxyribonucleic Acid

ELISA – Enzyme-linked Immunosorbent Assay

EMA –European Medicines Agency

Fab – Fragment antibody binding

FDA – Food and Drug Administration

FBRM – Focused Beam Reflectance Measurement

F_c – Fragment constant

FMEA – Failure Mode of Effect Analysis

FTIR – Fourier-transform Infrared

G – Shear Rate

GMP – Good Manufacturing Practice

HCP(s) – Host Cell Protein(s)

HPLC – High Performance Liquid Chromatography

HMWS – High Molecular Weight Species

HRP – Horseradish Peroxidase

I – Ionic strength

ICH – International Council for Harmonisation

IgG – Immunoglobulin G

k – Boltzmann Constant

K– Equilibrium Constant

LDS – Lithium Dodecyl Sulphate

mAb – Monoclonal Antibody

MCB – Master Cell Bank

MES – (N-morpholino)ethanesulfonic acid

MMC – Mixed Mode Chromatography

MWCO – Molecular Weight Cut-Off

N – Particle number concentration

N_{Ca} – Camp Number

NDA – New Drug Application

NEM – N-Ethylmaleimide

OD – Optical Density

PAT – Process Analytical Technology

PBS – Phosphate Buffered Saline

PDADMAC - Poly(diallyldimethyl ammonium chloride)

PEG – Polyethylene glycol

PEI – Polyethyleneimine

PES - Polyethersulfone

pI – Isoelectric point

PrA – Protein A

PrG – Protein G

PSD – Particle Size Distribution

PVC – Polyvinyl Chloride

r – rate of reaction

QbD – Quality by Design

QTPP – Quality Target Product Profile

R&D – Research & Development

Re – Reynold's Number

RNA – Ribonucleic Acid

RTD – Residence Time Distribution

RT-PCR – Real-time Polymerase Chain Reaction

S – Solubility

S_o – Extrapolated initial solubility

SC – Sodium Citrate

SDS-PAGE – Sodium Dodecyl Sulphate-Polyacrylamide Gel Electrophoresis

SEC – Size Exclusion Chromatography

SS – Sodium Sulphate

T - Temperature

t_m – Micro-mixing time

TFF – Tangential Flow Filtration

TIJ – Two-impinging jets

TMB – Tetramethylbenzidine

USD – Ultra Scale-Down

W – Stability Ratio

Y - the ratio of acid mole number consumed by Dushman reaction

YST - value of Y in the case of total segregation

Chapter 1: Introduction and Literature Review

1.1 Introduction

For over a century, the technique of precipitation has seen wide use in multiple applications including the purification of low-value products. In some instances, precipitation has played a key role in the manufacture of some high-value therapeutics, most notably in the plasma fractionation process (Cohn *et al.*, 1946). This is otherwise known as Cohn's process. In recent years, precipitation has been considered as a potential cost-effective technique for the purification of monoclonal antibodies (mAbs) (Sommer *et al.*, 2014; Hammerschmidt *et al.*, 2015; Krepper *et al.*, 2019).

Developments in upstream processing have greatly benefited from stable cell lines with improved mAb expression, which has resulted in lower CoGs (Low, O'Leary and Pujar, 2007). However, the financial bottleneck has shifted towards downstream processing with conventional chromatography struggling to keep up the pace. Consequently, the search for alternative downstream methods is necessary. Despite the potential of precipitation steps in reducing downstream CoGs relative to for instance Protein A (PrA) chromatography during mAb capture, the complexity of such processes and the mechanisms responsible are not well understood. Moreover, precipitation is strongly influenced by many factors including temperature, pH, ionic strength, protein concentration, protein chemical nature (i.e. distribution of polar and nonpolar residues) and the precipitating agents. Whilst various precipitation studies on mAb purification show promise at small scale, a scale-up approach has not yet been established. Despite the knowledge gained from earlier studies which have attempted to provide scalable precipitation process for protein systems, developing a precipitation method for a specific macromolecule remains an empirical procedure and requires extensive characterisation.

1.2 Thesis overview

The aim of the thesis is to produce a scalable downstream process for mAb purification directly from clarified mammalian cell culture supernatant using precipitation. The project focused on an engineering study which looked to test small scale systems to establish key parameters influencing the formation of viable precipitates at scale. This required an

integrative approach involving the examination of the interactions between precipitation conditions on precipitate recovery. Such an approach would be useful in constructing process models linking precipitation and recovery stages.

It was also envisioned that a non-affinity based downstream process, commencing with precipitation as the capture step, could be designed to grant a purified mAb to clinical grade standards. Among the available technologies, focus was made on integrating precipitation with typical chromatography polishing steps.

The thesis is divided into eight chapters:

Chapter 1 – This chapter provides a literature review introducing protein precipitation concepts and methods, with particular emphasis on the role of precipitation within bioprocessing.

Chapter 2 – This chapter details the materials and methods describing the experimental procedures employed in the studies outlined in subsequent chapters.

Chapter 3 – This chapter reports small-scale screening studies in evaluating mAb precipitation with neutral salts.

Chapter 4 – This chapter details mixing concepts relevant to precipitation and demonstrates a characterisation study on the mixing phenomena in batch and continuous reactors, based on established mixing models.

Chapter 5 – This chapter provides an assessment on the effect of mixing regimes and mixing times on the control of precipitation performance based on particle properties which are critical to centrifugal performance. A study linking final precipitate properties to the settling behaviour in an industrial centrifuge through the application of an ultra scale-down methodology is also performed.

Chapter 6 – In this chapter, a non-affinity based purification process is designed which integrates salt precipitation with conventional chromatography steps to provide a clinically grade purified mAb.

Chapter 7 – This chapter provides a summary of the preceding results and conclusions of the main findings. Scope for future work is also presented.

Chapter 8 – This chapter describes how a precipitation step would undergo process validation as set out by the recommended regulatory guidelines.

1.3 Project objectives

In order to achieve our specified aims, the following objectives were devised:

- 1) To reproduce a precipitation methodology for the purification of a therapeutic mAb using neutral salts to determine suitable precipitation conditions for recovery. As well as gain an initial insight into relative product purity.
- 2) To experimentally characterise mixing times in batch and continuous reactor designs, focusing on micro-mixing and its relevance to precipitate properties during particle formation which infers reactor design. Concurrently, to establish micro-mixing as a tool for the scale-up of a continuous precipitation step.
- 3) To determine the effect of final precipitate properties, as influenced by mixing and other key engineering parameters, on the ease of centrifugal recovery using an ultra scale-down method for the prediction of disc-stack centrifugation performance by:
 - i. Investigating the impact of turbulent shear processing of protein precipitates in a shear device as an indication for particle strength
 - ii. Determining the ease of clarification of processed precipitates over a range of throughputs in a lab-scale centrifuge
 - iii. Verifying USD clarification results on a pilot scale disc-stack centrifuge.
- 4) To design a non-affinity based purification process using precipitation and conventional chromatography steps, with the goal of purifying a therapeutic mAb to clinical standard with respect to process-related impurities including host cell proteins (HCPs) and genomic DNA.

1.4 Role of precipitation to bioprocessing

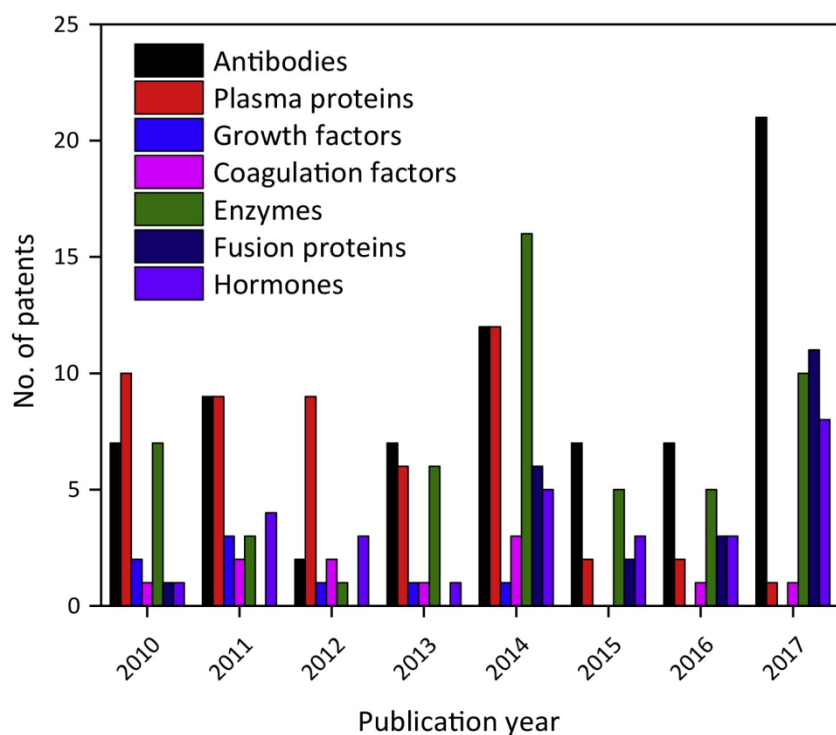
Precipitation is a process involving the conversion of macromolecules from an aqueous state to an insoluble state upon a change in the solution environment causing destabilisation. A solid precipitate is formed as a result and is subsequently separated from the mother liquor using centrifugation or filtration steps. The precipitate is then re-dissolved into an appropriate buffer solution. Precipitation has two approaches: precipitating the target protein of interest

and separating it from the soluble impurities (product precipitation) or precipitating the target impurities whilst keeping the protein of interest in solution (impurity precipitation). The latter approach can be taken one step further by precipitating the target protein. In doing so, less co-precipitation of impurities is observed in comparison to the first approach. The product precipitation approach in some cases can be irreversible which prevents dissolution of the precipitate and often leads to loss of native structure and activity (Salt *et al.*, 1982). By contrast, impurity precipitation leaves the target molecule in solution, mitigating the risk of protein denaturation.

Precipitation can be induced by a wide variety of reagents including neutral salts, organic solvents, non-ionic polymers, polyelectrolytes, acids, affinity ligands and metal ions. Precipitation enables the preparation of high-protein concentration formulations in significantly lower volumes that are easier to handle. Before the advent of chromatography, purification of protein isolates using precipitation was rather common and primarily employed for low value products. Given the high resolution attainable in chromatography steps and thus their widespread use in bioprocesses, precipitation is often considered as a supplementary step for the pre-treatment of process solutions ahead of chromatography or during the final formulation stages. The capital and operating costs associated with chromatography steps however demonstrate an economic incentive to re-evaluate process designs. Thus, investigating and designing alternative methods with the potential to alleviate the economic burden would be valuable; one such example is precipitation.

Bioprocesses implementing precipitation have already been established for the purification of some important bio-therapeutics, including human serum albumin (Cohn *et al.*, 1940) and erythropoietin (Miyake, Kung and Goldwasser, 1977). Precipitation has additionally been reported for the production of high-value intracellular enzymes such as β -galactosidase (Higgins *et al.*, 1978; Zhang, Chisti and Moo-Young, 1995) and prolyl-tRNA synthetase (Dunnill *et al.*, 1967; Dunnill, Currie and Lilly, 1970). Some recent developments have revolved around mAb, antibody fragment (Fab) and Fc-fusion protein purification directly from cell culture harvest as an alternative to PrA chromatography (Balasundaram, Sachdeva and Bracewell, 2011; Oelmeier, Ladd-Effio and Hubbuch, 2013; Greene *et al.*, 2018; Swartz *et al.*, 2018). Such developments have led to the growth in the number of publications reporting novel precipitation strategies, as well as an influx in patent submissions by some biopharmaceutical companies including Novartis and Amgen (Martinez *et al.*, 2019). A notable increase in patents concerning mAb and Fc-fusion protein precipitation processes have been observed between 2014 and 2017, of which report both product and impurity precipitation methods, as well as combined precipitation strategies (Figure 1-1). The number of plasma protein fractionation patents, by contrast, has however declined. This is most likely

due to the already well-established commercial process of Cohn's method and adaptations thereof, thereby indicating a shift in R&D focus towards mAb process development.



Trends in Biotechnology

Figure 1-1. Graph showing the evolution of new patent submissions regarding therapeutic purification with precipitation of various protein classes between 2010 and 2017. Figure obtained from *Martinez et al 2018*.

1.5 Monoclonal antibody manufacturing

The current approach to therapeutic mAb manufacture involves a platform process in which fully humanised IgG molecules are produced in Chinese hamster ovary (CHO) cells and subsequently purified to pharmaceutical grade standard. A typical mAb production process is illustrated in Figure 1-2. In upstream processing, CHO cells from a Master Cell Bank (MCB) are expanded through a sequence of inoculum steps and seed bioreactors, before transferring to the production bioreactor where mAb is expressed extracellularly. The culture is then harvested by centrifugation followed by depth filtration to isolate the extracellular fluid from the cells and cell debris. Purification of mAb from the impurities is then accomplished by downstream processing, which involves a series of chromatography, viral inactivation and filtration unit operations. Filtration steps consist of depth filtration for the clarification of cell

culture harvest, ultrafiltration/diafiltration (UF/DF) for buffer exchange in preparation for sample loading onto column chromatography, nano-filtration for virus removal and germ filtration.

As a gold standard in therapeutic mAb processes, PrA chromatography is employed as the capture step owing to the specific affinity of PrA ligand towards Fc regions of mAbs. The high resolution of a PrA step enables the vast majority of process related impurities including host cell proteins (HCPs), DNA and lipids to be removed at the early stage. Despite its capabilities, standard PrA resins achieve low binding capacities which is a notable bottleneck when considering the processing of high-titre feeds (Ramos-de-la-Peña, González-Valdez and Aguilar, 2019). Moreover, resin costs can reach up to £14,000 per litre, contributing to almost 50% of total manufacturing costs (dos Santos, Carvalho and Roque, 2017). In Figure 1-2, cation exchange (CEX) and anion exchange (AEX) chromatography are mAb polishing steps which remove product-related impurities such as aggregates, acidic/basic mAb variants as well as further reduce HCPs and DNA to acceptable levels. Depending on the nature of the product, the platform process can be designed using other modes of chromatography for polishing steps.

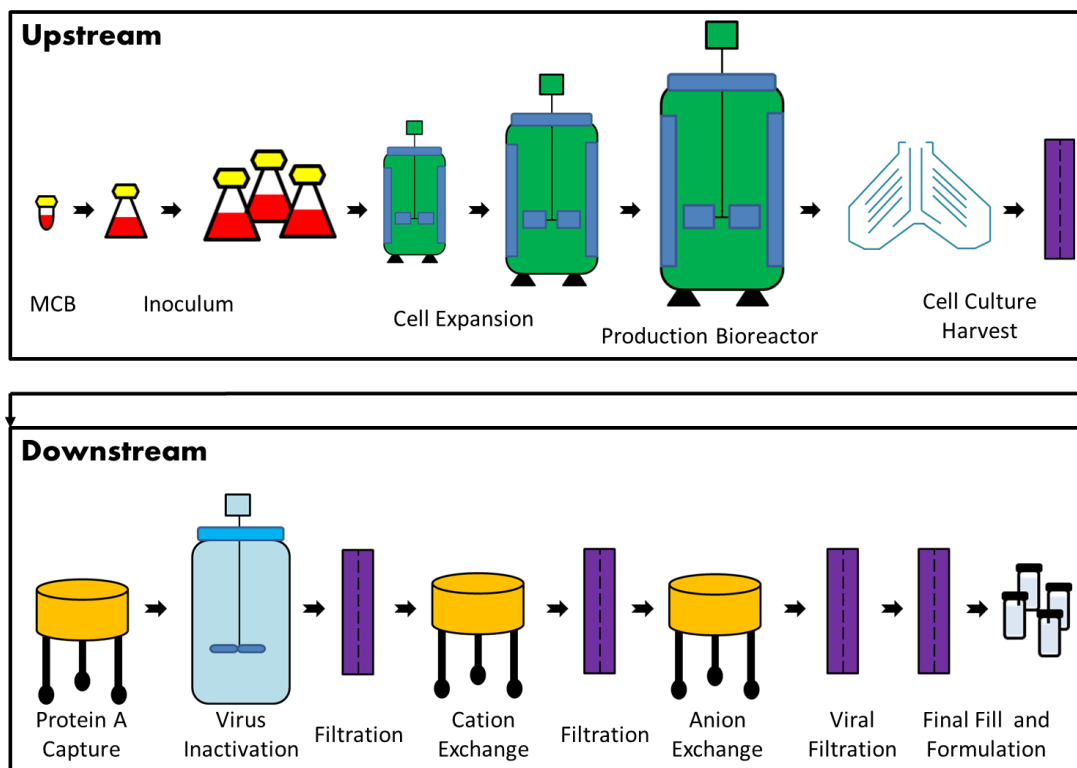


Figure 1-2. A typical mAb platform process showing key upstream and downstream unit operations.

1.6 Precipitation methods

The range of precipitation techniques in the purification of protein solutions is considerable, each influencing macromolecular solubility by a different mode of action. One general mechanism to initiate precipitation is through the means of preferential dehydration caused by the addition of high precipitant concentrations. The other general mode of action involves direct changes to the target solute at low precipitant concentrations. It is therefore instructive to provide a comprehensive overview of precipitation methods and current understanding of the mechanisms governing precipitation behaviour. Those methods relevant to therapeutic bioprocessing, as reported in the literature, are explored herein.

1.6.1 Conventional precipitants

1.6.1.1 Neutral salts

Neutral salts have the dual ability in either increasing protein solubility at low concentrations through salting-in or reducing protein solubility at high concentrations via the salting-out effect. Only a small subset of proteins are in fact soluble in pure water and small amounts of salt promote their solubility, as is the case for the euglobulins (Sandor, 1966). This can be explained by the effect of non-specific electrostatic interactions between the salt ions and charged groups on the protein surface, which leads to a decrease in the electrostatic free energy of the solute and overall promotes solubility (Arakawa and Timasheff, 1984). Salting-in was first observed by Mellanby in globulin-salt solutions and a relationship between ionic strength and solubility was established (Mellanby, 1904).

Above reaching a certain salt concentration, the salting-out effect takes place, and protein solubility decreases proportionally with salt concentration. An empirical correlation was deduced by Cohn to represent the solubility of a single protein component under conditions of salting-out (Cohn, 1925)

$$\text{Log}S = \beta - K_s I$$

Equation 1-1. Cohn salting-out equation.

where S is the protein solubility at ionic strength I , and β and K_s are constants. β is the solubility constant which represents the hypothetical solubility of a protein at zero ionic

strength, and is a function of the net charge and strongly dependent on pH, having a minimum at the protein isoelectric point (pI). K_s is the salting-out constant describing the slope of the solubility curve and varies with protein and salt type but is independent of pH and temperature. Based on one study, the surface hydrophobicity of a given protein was suggested to correlate with the value of K_s (Salahuddin *et al.*, 1983). In a real system, that is one which comprises of multiple macromolecular components, such correlation is much less applicable. Precipitation with salting-out does not often provide high selectivity in targeting specific proteins, however a common trend in larger proteins precipitating at lower salt concentrations is observed.

The mechanism underlying salting-out remains not fully understood. It has been suggested that precipitation on the basis of salting-out is due to protein dehydration due to the competition between introduced salt ions and proteins with water (Shih, Prausnitz and Blanch, 1992). Due to the increased interactions between the salt ions and water, fewer water molecules are available to interact with charged groups on the protein surface, which leads to stronger protein-protein interactions through hydrophobic patches eventually excluding the solute from the solvent. Suffice to say that proteins with a larger distribution of hydrophobic regions will precipitate more readily and under lower salt concentrations, which would provide a useful tool for fractionation procedures (Madhusudhan, Raghavarao and Nene, 2008).

At equivalent ionic strengths, the ability to induce salting-out between different salts varies dramatically. Hofmeister first reported this effect to be strongly dependent on the specific cation and anion constituents of the salts employed. From this, a series known as the Hofmeister or lyotropic series was established ranking the constituents in terms of their salting-out effectiveness (Baldwin, 1996; Zhang and Cremer, 2006). Anions provide the more dominant force in precipitation initiation and are ranked as follows:

citrate > phosphate > sulphate > acetate > chloride > nitrate > thiocyanate

The leftmost species are described as anti-chaotropic since they create a high surface tension, lower the solubility of hydrocarbons, minimise protein denaturation and promote protein stability. Progressing down the series, a decrease in surface tension, increase in hydrocarbon solubility, and increase in protein denaturation and reduction in protein stability are all observed. The positioning of the salts in the lyotropic series is indicative of the tendency to cause structural protein damage. For instance, the chaotropic ions such as thiocyanate and nitrate destabilise native structure by disrupting the organised water structure around the protein molecules. In contrast, the kosmotropic ions such as sulphate enable protein stabilisation through strong interactions with water, causing large hydration

numbers and result in structure-making phenomena. It is important to note that there are a number of exceptions in which Hofmeister series does not follow. In the salting-out of insulin, Fredericq and Neurath report optimal precipitation using thiocyanate (Fredericq and Neurath, 1950). In another study, the precipitation/crystallisation efficiency of insulin followed the reverse order of Hofmeister series (Ries-Kautt and Ducruix, 1989; Watanabe *et al.*, 2009). Based on these studies, it was therefore postulated that the Hofmeister series generally holds when the solution pH exceeds the target protein's pI and the reverse is true.

Amongst the various neutral salts, ammonium sulphate is the most commonly used in protein precipitation applications due to its high solubility, inexpensiveness and protein stabilisation over longer periods. Its extensive use has been reported in the purification of soya protein isolates (Chan, Hoare and Dunnill, 1986), yeast enzymes (Foster, Dunnill and Lilly, 1976; Madhusudhan, Raghavarao and Nene, 2008), plasma proteins (Harms, 1946; Schilling *et al.*, 1953) and more recently for the purification of antibodies (McKinney and Parkinson, 1987; Ahmad and Dalby, 2011; Oelmeier, Ladd-Effio and Hubbuch, 2013). One caution in employing ammonium sulphate is ensuring that process solutions do not exceed pH values beyond 8 to mitigate the production of ammonia gas, which is rather toxic and difficult to handle industrially. Alternatives such as sodium sulphate have also been studied; however due to the low solubility of the salt below 40°C, its application is often restricted to some thermostable enzymes (Shih, Prausnitz and Blanch, 1992). A patent broadly claiming protein precipitation with citrate salts, with specific mention of sodium citrate, was filed in 2011 (Arunakumari and Ferreira, 2011) which showed a potential alternative to overcome some of the bottlenecks associated with other salt reagents.

An interesting avenue that has not been explored extensively is the use of salt combinations or dual salt precipitation by exploiting the different properties of salt types to improve precipitation performance. An example of the use of dual salt precipitation is the purification of a Fab molecule produced in *Escherichia coli* using a combination of ammonium sulphate and sodium citrate (Balasundaram, Sachdeva and Bracewell, 2011). In altering the product solubility profiles through synergistic or antagonistic effects, a route to improved product recovery and removal of process contaminations was achieved. It can be assumed that a similar approach would be both feasible and beneficial in mAb purification from mammalian cell culture and thus would be interesting to investigate.

1.6.1.2 Non-ionic polymers

Precipitation of protein solutions with non-ionic polymers, namely polyethylene glycols (PEG), has seen more recent application, in particular with mAbs and other industrially relevant therapeutics (Foster, Dunnill and Lilly, 1973; Ramshaw, Bateman and Cole, 1984; Kuczewski *et al.*, 2010). In contrast to salting-out, by tuning of the precipitant conditions and selection of the PEG type, improved product selectivity could be obtained in single and two-step precipitation methods (Kuczewski *et al.*, 2010; Giese *et al.*, 2013; Muendges *et al.*, 2015). In addition, where desalting applications is often necessary after a salt precipitation step to aid further processing, non-ionic polymers can be removed with appropriately designed chromatography techniques.

The mechanism underlying precipitation with non-ionic polymers has not been fully explained but the current theory is protein molecules are sterically excluded from the volume of solution occupied by the larger polymer (Asakura and Oosawa, 1958; Iverius and Laurent, 1967; Edmond and Ogston, 1970; Polson, 1977). The theory states that two masses cannot occupy the same space simultaneously and in turn incurs a displacement reaction (Bhat and Timasheff, 1992). The introduction of a polymer with a large Stokes radius such as PEG reduces the effective amount of water available to solvate protein molecules. As a result, protein solubility is exceeded and in turn initiates precipitation. The thermodynamic behaviour of protein solubility in the presence of non-ionic polymers is closely related to that of two phase systems comprising of two partially immiscible aqueous phases as studied by Albertsson and others (Albertsson and Frick, 1960). Such close relation allows for the following expression to apply:

$$\mu_i = \mu_i^0 + RT(\ln m_i + f_{ii}m_i + f_{ij}m_j)$$

Equation 1-2. Thermodynamic model for protein solubility in non-ionic polymer solutions.

where μ_i^0 is the standard chemical potential of component i , μ_i is the chemical potential of component i , R the gas constant, T the absolute temperature, m_i and m_j the molality of component i and j respectively, f_{ii} and f_{ij} are the appropriate protein-protein and protein-precipitation interaction coefficients respectively.

Studies conducted by Foster and colleagues (Foster, Dunnill and Lilly, 1973) on the precipitation of intracellular yeast enzymes using PEG led to the derivation of a simplified expression to describe protein solubility in the presence of non-ionic polymers in the form:

$$\ln S + fS = X - aC$$

Equation 1-3. Foster's simplified expression on protein solubility with non-ionic polymers.

where S is the protein solubility, f the protein self-interaction coefficient, $X = (\mu - \mu_i^0)/RT$, a is the PEG interaction coefficient and C the PEG concentration.

A general observation is that the effectiveness for proteins to precipitate increases as the molecular weight of the polymer increases up to a limiting value of 6000 Daltons (Polson *et al.*, 1964). The precipitation of low molecular weight proteins often requires higher polymer concentrations and vice versa. Both observations are consistent with the precipitation mechanism of volume exclusion resulting in the unavailability of water molecules to maintain protein solubility. Polymers of molecular weight exceeding 6000 Da do not show any particular differences in their excluded volumes which explains why no further increase in precipitation effectiveness above the limiting size is observed (Juckles, 1971; Foster, Dunnill and Lilly, 1973).

PEG6000 is the most widely used PEG species because of its lower viscosity relative to other precipitants within the same class and, like other PEG species, has the advantage in stabilising a wide range of proteins (S.-L. Sim *et al.*, 2012). It can also be used at ambient temperatures without concern for protein denaturation. The required PEG concentration to fully precipitate proteins is typically below 20 % (w/v) but can vary substantially depending on the application. Based on recent works to develop mAb precipitation processes, working PEG concentrations have been specifically reported to be in the range 3 – 15 % w/w (Carol *et al.*, 2009; Sommer *et al.*, 2015; Hammerschmidt, Hobiger and Jungbauer, 2016). One example is the development of a bioprocess which consists of a two-step PEG-based precipitation strategy using PEG6000: the addition of 3% PEG6000 to cell culture harvest at pH 4 to precipitate impurities, followed by mAb precipitation with 14% PEG6000 at a specified pH giving an overall product yield above 90% and above 96% purity (Hammerschmidt, Hobiger and Jungbauer, 2016).

A general concern for adding PEG is potential binding to proteins that may not be easily removed in the process and may illicit side effects during treatment. Furthermore, the viability for commercial application at scale is questionable considering the result of PEG in creating viscous process fluids which impair mass transfer during mixing, pumping, centrifugation and filtration (S. L. Sim *et al.*, 2012). Difficulties in cleaning must also be addressed.

1.6.1.3 Organic solvents

The addition of alcohols and other water-miscible solvents to protein solutions has been frequently employed, most notably the use of ethanol in Cohn's method for human plasma fractionation (Cohn *et al.*, 1946). Prior to this, the use of miscible organic solvents up to 40% in concentration has been reported for concentrating a number of proteins from animal plasma (Mellanby, 1907; Percival, 1925; Merrill and Fleisher, 1932). Ethanol-based precipitation processes have recently been in development for mAb purification strategies (Tscheliessnig *et al.*, 2014; Hammerschmidt *et al.*, 2015). In combination with impurity precipitation via inorganic acids as a pre-treatment method, such processes have achieved purification levels exceeding 90% in both yield and purity using a maximum ethanol concentration of 20%. Although less common, methanol, acetone, acetonitrile and isopropanol have also been reported as viable precipitating reagents (Polson *et al.*, 2003; Crowell, Wall and Doucette, 2013; Crowe, 2014; Tscheliessnig *et al.*, 2014; Faizal Wong, Ariff and Stuckey, 2017).

The mechanism underlying alcohol-based precipitation is thought to be based on the reduction of the dielectric constant of an aqueous solution upon the addition of weakly polar solvents (Oss, 1989). In the case of ethanol whose dielectric constant is about one third of that of water, the addition of the reagent promotes the increase in intramolecular and intermolecular electrostatic interactions, resulting in a considerable reduction in protein solubility (Bell, Hoare and Dunnill, 1983; Harrison, 1994). The change in solubility of a protein at its pI as a function of the solution dielectric constant is expressed as:

$$\log\left(\frac{S}{S_0}\right) = \frac{K}{D_s^2}$$

Equation 1-4. Expression for protein solubility as a function of the solution dielectric constant with the addition of organic solvents.

where D_s is the solution dielectric constant, K is a constant representing the dielectric constant of the original aqueous solution and S_0 is the extrapolated initial protein solubility.

The presence of neutral salts in ethanol-water mixtures has been shown to induce salting-in effects on proteins where salting-out effects would be prominent in the absence of organic solvents. Therefore, refined fractionation procedures can be designed by controlling protein solubilisation at low salt concentrations against the precipitation action of an organic solvent. This demonstrates a key benefit for employing organic solvent precipitation in which protein solubility can be finely modulated through careful alterations in pH, temperature and ionic

strength in order to effectively provide relatively pure protein isolates based on solubility behaviour alone.

Due to the large enthalpy change accompanied with organic solvents at high concentrations, it was identified that such operations demand the precipitation be carried out and controlled at low temperatures (typically as low as -10°C) to minimise protein denaturation (Mellanby, 1907; Schubert and Finn, 1981). In order to control this in a batch precipitation process, good mixing with slow additions of precipitant would be required to minimise heat generation with each addition. Despite organic solvents allowing effective protein extraction, the huge risk concerning potential explosive activity raises the question on the scalability. In a plant facility, control measures must be put in place in order to mitigate this risk (e.g. proper ventilation and flame-proofing).

1.6.1.4 Ionic Polyelectrolytes

Precipitation with polyelectrolytes works in a similar fashion to the process of flocculation, some of which are in fact common flocculating agents including polyethyleneimine (PEI) and poly(diallyldimethyl ammonium chloride) (PDADMAC) (Burgess, 2009; Espuny Garcia del Real, Davies and Bracewell, 2014). In contrast to the mechanism of preferential dehydration, the ionisable groups of polyelectrolytes form insoluble complexes with the target protein of interest under suitable conditions. The control of protein-polyelectrolyte complex formation requires the optimisation of process parameters including pH, ionic strength, and polyelectrolyte type – the two former parameters having a strong influence in polyelectrolyte precipitation. This was evident in the examination of whey protein precipitation using a range of anionic and cationic polymers (Hill and Zadow, 1978). The precipitation profiles followed a parabolic relationship with small changes in pH showing a sharper transition from the soluble state of a protein or protein mixture to the insoluble state as compared to the effect of ionic strength. Therefore, it becomes imperative to explore a wide range of conditions and reagents within the family group.

Most polyelectrolyte applications concern the purification of enzymes (Sternberg and Hershberger, 1974; Clark and Glatz, 1992; Zhang *et al.*, 2005); however some recent studies have reported their potential for mAb systems (McDonald *et al.*, 2009; Fahrner *et al.*, 2011). In one study, a range of polyamines were screened to evaluate HCP removal from CHO cell culture harvest (Ma *et al.*, 2010). The purification was designed on the basis of forming bridging complexes with bulk HCPs whilst keeping the antibody in solution and

separating the two phases by filtration. Such a process provided significant clearance of HCPs making it feasible to eliminate affinity-based chromatography steps. One advantage to this approach is that the resulting soluble fraction containing the product is absent or in minimal amounts of polyelectrolyte. If the protein of interest is the target, downstream operations would need to be designed to ensure its dissociation and subsequent removal.

Whilst polyelectrolytes confer better protein specificity at low concentrations over salts and organic solvents, these agents are generally costly and therefore reduce the economic incentive for their application at scale (Clark and Glatz, 1987). The recovery and re-use of these agents could however be considered.

1.6.1.5 Tag and affinity-based precipitants

Similarly to the approach of precipitation with polyelectrolytes, a range of novel protein tags and affinity ligands have been developed to form specific complexes, via targeting or direct attachment to certain moieties, which precipitate under finely tuned conditions. Adopting this method provides a more selective mode of precipitation than the aforementioned methods. Furthermore, it has the potential to simulate an affinity chromatography step whilst bypassing some of the disadvantages associated with it such as column fouling, scale-up and flow rate limitations. One such example of an approach is the fusion of *Corynebacterium glutamicum* cell surface protein B tag to proinsulins, Teriparatide and Bivalirudin, the former responding to changes in solution pH and enabling a reversible process for unstable therapeutics at non-physiological conditions with near to 100 % recovery (Nonaka *et al.*, 2018). The also pH-responsive Eudragit S-100 tag fused to *Staphylococcus aureus* PrA provided an effective affinity ligand to precipitate mAbs at pH 5.2 with around 90% yield and above 95% purity (Janoschek, Freiherr von Roman and Berensmeier, 2014). Z-domain-elastic-like polypeptide nanocages containing an IgG-binding domain have been demonstrated to provide comparable purification performance by precipitation for a range of mAbs and Fc-fusion proteins (Swartz *et al.*, 2018). In another study, a rapid purification for trastuzumab and rituximab involving a two-step precipitation process using salting-out via ammonium sulphate (to precipitate high molecular weight proteins) followed by affinity precipitation based on synthetic trivalent haptens has been in development (Handlogten *et al.*, 2013).

A promising avenue for the use of affinity tags is the potential for precipitant recycling that can be accomplished by dissociation of the complex by dissolution, chromatography or

filtration where recycling of classical precipitants proves to be rather challenging. However, because of the relatively higher costs in the generation of such ligands, implementing these for a platform process must be highly justified. In some cases, it may be difficult to reverse the binding interaction or enable complete removal of the tag throughout the process.

1.6.2 Concluding remarks

Whilst isoelectric and metal ion precipitations are reported in the literature, these were not covered since they have very little application in mAb purification. Moreover, these techniques often lead to major irreversible, undesired changes in proteins limiting their suitability in bioprocesses. Therefore, focus was made on the more conventional and novel precipitation approaches to protein purification. Details of these approaches can be found elsewhere (Bell, Hoare and Dunnill, 1983).

From a bioprocess perspective, it is important to consider the key aspects of available precipitation methods such as reagent cost, required concentrations to maximise protein recovery, potential impact on denaturation, recoverability, reversibility of the reaction, scale-up implications and environmental impact. Much of these can be quickly assessed with laboratory-scale studies using high-throughput process development strategies and via automated systems, enabling many precipitating agents and conditions to be screened in a short time. However, these studies are not able to capture some of the key issues that will be encountered at the industrial scale, particularly those directly related to particle recovery efficiency. For this reason, the choice of precipitation method should be a compromise between purification performance and precipitate recovery efficiency.

1.7 Theory of solubility

Early models of solubility theory described biomolecules as aqueous particles, existing as colloidal dispersions with a surface charge allowing favourable interactions with the solvent (van Oss, Good and Chaudhury, 1986; Oss and Good, 1989). More complex models based on solution thermodynamics were also developed (Middaugh *et al.*, 1980; Schellman, 1990; Livingstone, Spolar and Thomas Record, 1991). The development of solubility theory is described herein, and is critical in understanding the physical processes involved in precipitation. An important aspect of protein solubility is to address not only how it ties in with

the protein structure, but also the structural changes of solvent molecules in the presence of a protein.

1.7.1 Protein and solvent structural considerations

In the folding of a globular protein, the tertiary structure is such that the majority of the hydrophobic amino acids are buried into the interior constituting the hydrophobic core, whilst most of the hydrophilic amino acids are exposed to the surface (Scopes and Scopes, 1982). In reality, due to steric constraints, a proportion of the hydrophobic side chains pertain in the exterior, whilst a proportion of the hydrophilic ones are buried into the core. Thus, a degree of surface hydrophobicity is established and varies between proteins. This characteristic determines the level of hydration as result of the interactions between the protein surface groups and the solvent. Moreover, such solvation interactions will introduce a structural order of solvent molecules towards the solute whose depth and rigidity is dependent on the strength of solute-solvent and solvent-solvent interactions. This forms the basis of the hydrophobic effect.

Upon the dispersion of a macromolecule containing hydrophobic groups, such as that of a protein, repulsive forces between the solvent and solute induce the formation of ice-like structures of water around these groups, which is accompanied with an increase in the order in the system. This process is thermodynamically favourable since the large decrease in entropy associated with the ordering of water molecules over-compensates the enthalpy change due to hydrogen bond formation. As the surface area of a non-polar moiety increases, so does the free energy due to a larger decrease in entropy of the system and its lower solubility in water. The relation concerning the solubilising action of non-polar groups was initially used to describe the limited solubility of hydrocarbons in water (Frank and Evans, 1945).

Kauzmann extended the concept of the hydrophobic effect to describe protein solubility in aqueous environments (Kauzmann, 1959). The internalisation of hydrophobic residues which establishes the protein core is an entropically driven process, whereby non-polar groups will tend to cluster together to reduce the extent of hydrophobic surface that is accessible to water. In doing so, intramolecular interactions (e.g. hydrogen bonds, van der Waals interactions) and electrostatic interactions between charged and polar groups with the solvent are maximised.

Studies on protein-solvent interaction were described using the electrical double layer model (Smoluchowski, 1917). Stern first characterised the presence of positive counter-ions from an electrolyte which were attracted to the negative charge of the protein to form the first layer. This is otherwise known as the Stern layer (Stern, 1924). Further, Guoy-Chapman identified a second, more diffusible layer from more existing counter-ions adjacent to the first layer giving rise to what has been referred to as the electrical double layer (Gouy, 1910; David Leonard Chapman, 1913). The strength of the layer depicts the extent of repulsive attractions between two proteins in solution when these come into close contact with each other. Changes in the solvent composition may perturb the stability and rigidity of the electrical double layer, which can reduce protein solubility and in turn drive aggregation/precipitation.

1.7.2 Colloidal approach of protein solubility

Aqueous protein systems were originally treated as colloidal particles in the range of 1 to 1000 nm in size, whose properties were primarily determined by surface characteristics (Saunders, 1951). Colloidal stability is inferred by the magnitude of the colloidal particle interactions, which results in either a meta-stable dispersed phase (lyophobic solution) or a thermodynamically stable phase (lyophilic solution). The latter is the case for many water-based protein solutions. Protein precipitation was postulated to be a result of the solution becoming thermodynamically unstable.

Two similar theories were developed to describe the destabilisation of hydrophobic colloid dispersions, and were later combined into Derjaguin-Landau-Verwey-Overbeek (DLVO) theory (Derjaguin *et al.*, 1987). The DLVO model identifies the energy sum of the repulsive electrostatic forces due to the electrical double layer and attractive van der Waals interactions between two particles as a function of separation distance, as depicted in Figure 1-3. In a dilute electrolyte solution, a stable dispersion is characterised by long range net positive charges that result in overall particle repulsion. At closer distances up to 2 nm, an energy barrier is established to prevent contact between particle surfaces.

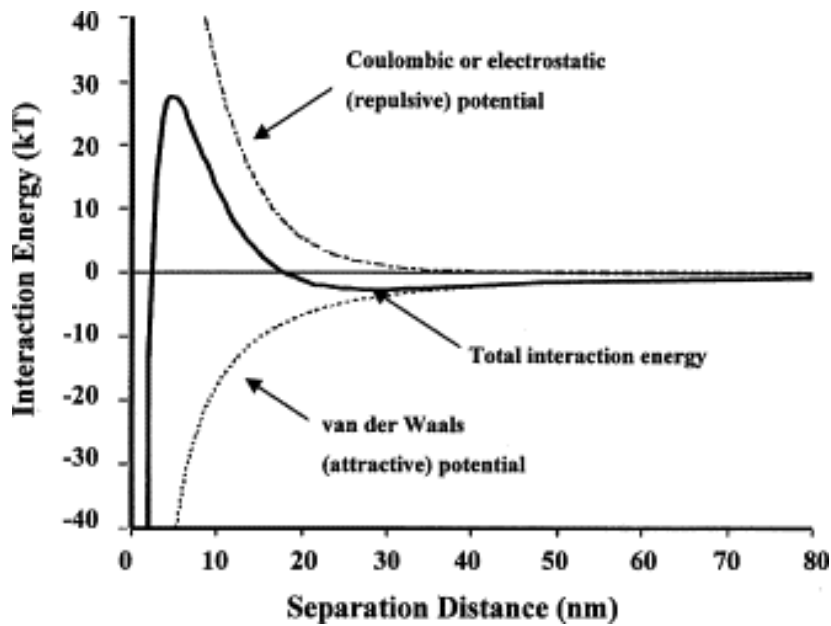


Figure 1-3. A schematic of DLVO interaction energy as a function of separation distance (Adair, Suvaci and Sindel, 2001). Reprinted from Encyclopedia of Materials: Science and Technology, Surface and Colloid Chemistry, Adair, J.H., Pages 1-10, 2001, with permission from Elsevier. Total interaction energy (solid line) corresponds to the summation of double layer repulsion and attractive van der Waals energy potentials (dashed lines).

According to DLVO theory, destabilisation of hydrophobic solutions is indicated by the reduction in the maximum free energy of colloidal interactions. This increases the probability of particle collisions by Brownian motion, which ultimately leads to aggregation. The DLVO theory applies well to the prediction of the stability of colloidal dispersions in dilute electrolyte solutions, comprising of negatively charged proteins accompanied with small cation concentrations. This however places a severe limitation on describing protein solubility with the DLVO theory during salting-out procedures where high salt concentrations are often employed. At such conditions, the contribution of the electrical double layer potential to colloidal stability becomes negligible. Moreover, DLVO does not take into account hydration forces, hydrophobic interactions and steric exclusion forces, all of which are postulated to play key roles in protein solubility and precipitation mechanisms. Nonetheless, the DLVO approach remains useful in understanding and modelling protein aggregation kinetics.

1.7.3 Solubility with the Cavity Model

Sinanoğlu proposed the cavity model to describe the influence of solvent on solute solubility in terms of the difference in free energy of the solute in the gas phase, as compared to in the aqueous phase (Sinanoğlu, 1980). The accommodation of a solute was postulated to occur in two steps: the creation of a cavity large enough to accept the solute and the placement of the solute in the cavity to interact with its surroundings. The net change is determined by the free energy of cavity formation, the free energy of solute-solvent interactions in the wall of the cavity and the loss of solute free volume going from the gas to the aqueous phase. The work expended in the formation of cavities is considerable for solvents with high surface tensions, such as that of water and dilute salt solutions, by which solvent-solvent interactions are particularly strong and confer great structural stability. The free energy of cavity formation is also influenced by the molecular size and shape of the solute. More work has to be done to form the cavity to accommodate solutes with larger excluded volumes. In terms of the free energy of solute-solvent interactions, this will greatly depend on the chemical environment and the prominence of London dispersion and electrostatic components (attractive or repulsive).

An extension of the cavity theory was performed by Melander and Horváth to describe protein stability with neutral salts (Melander and Horváth, 1977). The surface tension of water is known to increase upon the addition of inorganic salts which in turn affects the hydrophobic interactions between aqueous protein molecules. The unitary free energy required to convert a protein molecule from a gaseous phase to an aqueous salt solution, ΔG° , is given by:

$$\Delta G^{\circ} = \Delta G_{cav} + \Delta G_{es} + \Delta G_{vdw} + f$$

Equation 1-5. Sinanoğlu's cavity model.

where ΔG_{cav} is the free energy associated with cavity formation, ΔG_{es} and ΔG_{vdw} are the free energy changes due to electrostatic and van der Waals interactions, respectively, and f being the solute free volume change.

1.8 Principle of precipitation

Precipitation refers to the conversion of a molecule or subset of molecules in solution from the soluble state to the insoluble state, often induced by a change in one or more solution parameters. In some cases, the terms precipitation and crystallisation are used interchangeably; however these are in fact distinct processes and yield different solid structures despite sharing the same fundamental steps towards solid formation: supersaturation, nucleation and growth.

Macromolecular crystallisation involves the slow formation of crystalline solids that become arranged in an ordered lattice. The main pathways to crystallisation involve vapour diffusion, micro-batch, dialysis and free interface diffusion (dos Santos, Carvalho and Roque, 2017). By contrast, precipitation typically sees the formation of amorphous solids under initial conditions of high supersaturation, where rapid nucleation and growth of solid particles occur. Figure 1-4 displays a phase diagram representing crystallisation and precipitation as a function of protein concentration and a second parameter such as precipitant concentration. The phase diagram defines regions of under-saturation, metastable conditions which see nuclei crystal growth, and supersaturation where nucleation or precipitation occurs spontaneously.

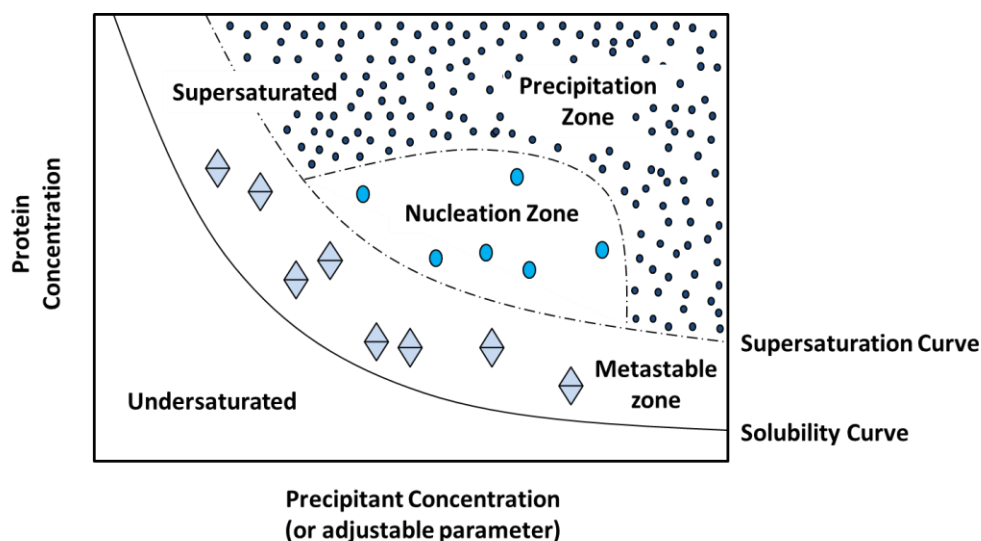


Figure 1-4. Qualitative illustration of a phase diagram showing zones of precipitation and crystallisation of macromolecules, based on protein concentration and precipitant concentration (or any other relevant parameter).

Figure was adapted from (Chayen, 2005).

1.9 Precipitate formation

Precipitate formation is generally comprised of two distinct phases occurring in sequence: nucleation and growth (Nelson and Glatz, 1985). The nucleation phase sees the formation of sub-micron particles which then act as nucleic centres for solute molecules to condense onto. Nucleation is initiated when a solution proceeds to a metastable supersaturated state, which establishes the energy requirement for the process to occur (Rothstein, 1994).

As illustrated in Figure 1-5, the rate of nuclei formation is greatly influenced by the degree of supersaturation in the system, as is the rate of particle growth; however both processes occur at different rates (Çelikbilek, 2012). Depending on the rates of these processes, a crystal or precipitate of a certain size is obtained. Therefore, desired particle size ranges can be attained via control of supersaturation levels. Nucleation rates increase exponentially with increasing supersaturation levels, whilst growth rates increase in a linear fashion (Klein, 1965; Harrison, 1994). At very high supersaturation levels where nucleation rates dominate, significantly smaller particles are formed in comparison to those formed at low supersaturation. To yield maximum sizes, supersaturation levels should be kept at a minimum where growth greatly exceeds nucleation, which can be facilitated with efficient mixing processes (Chi *et al.*, 2003). The impact and role of mixing to precipitation processes is discussed in section 1.10. Aging is an additional process to describe the continued growth in size, strength and density of aggregates under conditions of shear. These processes are discussed in further detail in the subsequent sections.

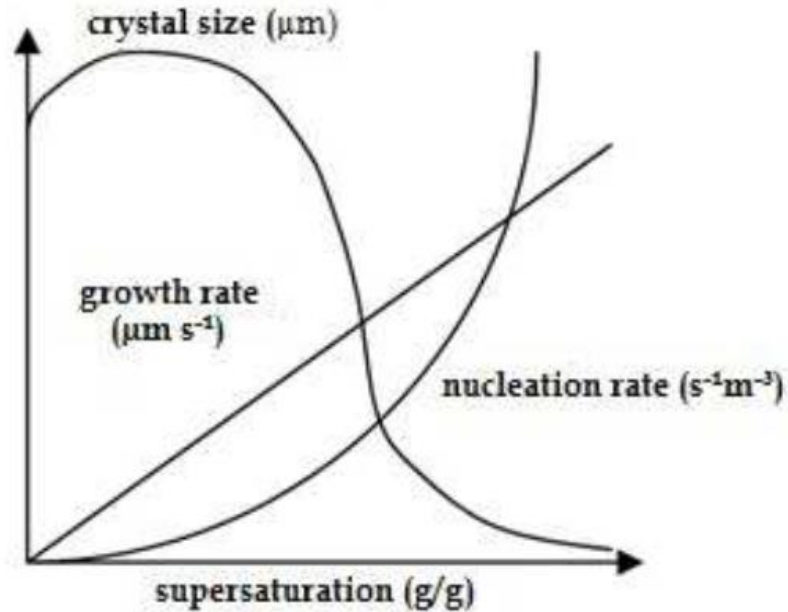


Figure 1-5. A generic schematic showing the effect of the degree of supersaturation on particle nucleation and growth rates, and ultimate crystal/precipitate size. Figure obtained with permission from (Çelikkilek, 2012)

1.9.1 Nucleation and growth by diffusion

Nucleation comprises the first stage of the precipitate formation process and often occurs spontaneously (Parker and Dalgleish, 1977). Thereafter, stable clusters increase in size through inter-particle collisions, driven by Brownian motion, up to a limiting size. This growth mechanism is referred to as perikinetic growth (Ives, 1978; Berre, Chauveteau and Pefferkorn, 1998). The perikinetic growth rate can be considered to be affected by: the time taken to induce a thermodynamic in-stabilisation of the macromolecules, the time taken for the association of two insoluble entities driven by the influence of each other's attractive forces (as determined by the relative rate of diffusion) and finally the frequency of particle-particle collisions.

A kinetic model to describe the rate of perikinetic growth for a monodisperse system was determined by Smoluchowski (Smoluchowski, 1917) in which the initial decrease in dispersed particle concentration as a result of aggregate growth, in the assumption that all collisions are 100% effective, is a second order process given by:

$$\frac{-dN}{dt} = K_A N^2$$

Equation 1-6. Smoluchowski's perikentic growth model.

where N is the particle number concentration and K_A is the aggregate growth rate constant equal to $8\pi Dd$. D is the particle diffusivity and d is the dispersed particle diameter. The particle diffusivity, D , can be estimated using the Stokes-Einstein relationship for translational diffusion and is given by:

$$D = \frac{kT}{3\pi\mu d}$$

Equation 1-7. Stokes-Einstein relationship for translational diffusion.

where k is the Boltzmann constant, T the absolute temperature and μ the solution viscosity. The aggregate growth model has been experimentally verified for latex particle suspensions (Higuchi *et al.*, 1963) and colloidal metal dispersions (Turkevich, Stevenson and Hillier, 1951).

An extension of Smoluchowski's theory was then posited by Fuchs (Fuchs, 1964) to consider the diffusion of particles in a force field and take into account electrical barriers which reduce aggregation rates upon particle collisions using a stability ratio, W :

$$\frac{-dN}{dt} = \frac{K_A N^2}{W}$$

Equation 1-8. Fuchs' perikinetic growth model.

$$W = d \int_0^{\infty} \frac{e^{\left(\frac{\phi(h)}{kT}\right)}}{(h+d)^2} dh$$

Equation 1-9. Determination of stability ratio, W .

where $\phi(h)$ is the potential energy of interaction, as determined by DLVO theory, and h is the separation distance between the particles.

Both Smoluchowski and Fuchs' theories however only consider the removal of the stabilising layer around protein molecules, and do not account for the presence of hydration barriers of associated water, where their removal may be limiting on the aggregation kinetics.

1.9.2 Growth by fluid motion

Upon exceeding the primary particle limiting size, of which approaches the scale of turbulence of the fluid, growth continues via orthokinetic aggregation. This continued growth becomes largely governed by the fluid motion and shear field which promote the collisions of primary particles. Whilst a proportion of these collisions will lead to growing aggregates, many can also result in aggregate break-up, the extent of which becomes dependent on the level of shear imposed onto the fluid system. The final particle sizes and spread of the particle size distribution tends to show an inverse relation with shear rate (Virkar *et al.*, 1982; Petenate and Glatz, 1983; Glatz, Hoare and Landa-Vertiz, 1986; Brown and Glatz, 1987; Byrne *et al.*, 2002a). At low levels of shear, the extent of hydrodynamic-controlled breakup is minimal which enables the orthokinetic growth of larger aggregates. At high levels of shear, the reverse is true. Therefore, the growth of particles to an equilibrium size results in the balance between orthokinetic aggregation, shear-controlled erosion and particle-particle collisions. Particle collisions with vessel walls may also be considered to describe aggregate dissociation.

Smoluchowski studied orthokinetic aggregation and approximated the rate of aggregation of uniformly sized spherical particles in a uniform shear field using the relationship (Smoluchowski, 1917):

$$\frac{-dN}{dt} = \frac{2}{3} \alpha G d^3 N^2 = \frac{4}{\pi} \alpha \phi_v G N$$

Equation 1-10. Smoluchowski's orthokinetic growth model.

where α is the collision effectiveness factor or number of collisions which contribute to a growing aggregate, G is the shear rate and ϕ_v is the volume fraction of particles (assumed to be constant and is equal to $\pi d^3 N/6$). The relationship implies that the rate of aggregate growth during orthokinetic aggregation is proportional to the shear rate and particle concentration. Integrating the above expresses the ratio of the final to initial particle number concentration (N_t/N_0) after exposure to shear over time t in the form:

$$\frac{N_t}{N_0} = e^{(-4\alpha\phi_v Gt/\pi)}$$

Equation 1-11. Integral of Smoluchowski's orthokinetic growth model.

In this case, the growth of aggregates should increase at an exponential rate over time, as the dispersed particle concentration decreases at the same rate.

1.9.3 Aging

During the aging process, particles continue to collide with each other and grow, as well as undergo restructuring events contributing to precipitate physicochemical properties including size, strength and density over time (Hoare, 1982a). The nature of such characteristics is of utmost importance for the recovery stages (Raphael and Rohani, 1999). In addition to particle size and density that both determine the ease of separation based on settling velocity, the strength of a particle defines its susceptibility to breakage under the turbulent shear forces common in industrial centrifuges and filtration systems. The resistance to shear break up has been shown to correlate with the dimensionless Camp number, N_{Ca} , which describes the shear history of precipitate particles and is given by (Camp, 1955):

$$N_{Ca} = Gt$$

Equation 1-12. Calculation of Camp number, N_{Ca} .

G is the average shear rate and t , the time of exposure to shear. It has been suggested that precipitates with Camp numbers above 10^5 have optimal strength in withstanding turbulent shear forces. Such correlation has been identified in the aging of soya precipitate via isoelectric precipitation (Bell and Dunnill, 1982a). The authors postulate that an increase in the precipitate strength at higher Camp numbers is attributed to a mechanism of structural rearrangement which results in more highly compact, stable particles. The study infers that Camp number can be adopted as a basis for the scale-up of a precipitation process. However, the perikinetic and orthokinetic processes must also be accounted for.

The aging process also allows reversing the effects of over-precipitation caused through poor mixing by readjustment of precipitation concentration gradients. Over time, any local precipitant excesses become evenly dispersed through the liquid to reach the final equilibrium state. In some cases, proteins that initially precipitate will redissolve during aging. Such an effect was demonstrated in aging studies concerning Cohn's plasma fractionation method (Watt, 1970). In other instances, over-precipitation cannot be reversed; an example being an overshoot in pH during isoelectric precipitation which often leads to irreversible protein denaturation, as well as difficulties in re-dissolving the precipitate even if the protein maintains its native state.. Therefore, mixing quality becomes an important consideration for

the control of parameters that are critical to precipitation performance. Considerations on the mixing for precipitation reactions are discussed in section 1.10.

1.9.4 Precipitate conditioning

The required residence time for precipitate aging processes can vary greatly and in some cases can be extensively long, which becomes impractical from a manufacturing point of view. For these processes, methods of acoustic conditioning have been employed to accelerate precipitate aging by exposing suspensions to low-frequency acoustic waves which result in improved particle characteristics as to facilitate solid-liquid separation. The idea is that the acoustic conditioning acts as a catalyst in promoting particle-particle collisions between the smaller particles through improved micro-mixing (Bell and Dunnill, 1984; Titchener-Hooker and McIntosh, 1992; Titchener-Hooker *et al.*, 1992). The technique has also been proposed to improve dewatering characteristics (Muralidhara, Ensminger and Putnam, 1985). The application of acoustic conditioning for protein systems was first reported by Jewett in improving the sedimentation properties of antihemophilic factor by PEG precipitation (Jewett, 1974). Later, an industrial application was reported for the conditioning of continuous flow plasma protein precipitates (Sandberg, 1978). However, the technology has not seen widespread use due to the lack of understanding of the mechanisms involved.

1.10 Considerations in mixing for precipitation

For the purposes of protein recovery and yield, mixing is often not deemed critical provided proteins are not exposed to extreme conditions which may incur negative effects such as loss of activity. Mixing has however been demonstrated to influence precipitation kinetics through nucleation and growth rates via the control of supersaturation, and hydrodynamic-controlled break-up. The former case is particularly important for fast reactions such as in the case of isoelectric and calcium precipitation of casein (Parker and Dalgleish, 1977). This necessitates the rapid distribution of reagents to the final supersaturated state, such that mixing is completed before the initial events of precipitation take place. Incorporating zones of turbulence such as that of the impeller zone in a stirred tank by jet mixing or a static mixer in continuous tubular reactor usually achieves good mixing. This process involves large packets of incoming fluid being broken up to some limiting size through the mechanism of

macro-mixing. Thereafter, isotropic turbulent shear can no longer affect the size of eddies and molecular diffusion becomes the controlling mechanism. This process is known as micro-mixing. The lifetime of these packets is then determined by the protein diffusivity and the recirculation rates of the fluid. The size of the primary precipitate particles becomes a function of the relative rate of protein precipitation and dissipation of proteins from the packets.

A slow mixing process on the other hand risks the onset of nucleation within a heterogeneous environment which can greatly influence the outcome. In the alcohol precipitation of catalase (Schubert and Finn, 1981) and the precipitation of fumarase with ammonium sulphate (Foster, Dunnill and Lilly, 1976), due to nucleation times being in the order of minutes, rapid mixing was less significant for particle formation but rather had marked effects on their solubility profiles. Amongst these studies and various others, attempts to define the relationship between mixing conditions and final protein precipitate characteristics have led to the general consensus that the rate of mixing influences the primary particle size and subsequent particle growth kinetics.

In order to determine the significance of mixing in precipitation processes and to build a suitable model that can infer process scale-up, it is important to consider the time constants for mixing and compare with the characteristic time constants. Given that nucleation and particle growth are essentially molecular-level processes, mixing on the molecular scale i.e. micro-mixing, can directly affect the course of precipitation. The larger-scale mixing mechanisms such as meso- and macro-mixing should also be considered when generating a complete mixing model as, in reality, they take place in parallel. Where micro-mixing is important for precipitation processes, the use of a segregation number can be a tool to determine the state of micro-mixing in a fluid. To describe the micro-mixing process by a droplet diffusion model, the segregation number of Naumann, N_{seg} , has been suggested:

$$N_{seg} = R^2 / \pi^2 Dt$$

Equation 1-13. Determination of segregation number, N_{seg} , with the droplet diffusion model. where R is the limiting droplet size, D the species diffusivity and t the mean residence time. For a fully segregated fluid, $N_{seg} > 1$ whilst for a fluid in a state of maximum mixedness $N_{seg} < 1$.

In addition to understanding the mixing mechanisms in the importance of precipitation kinetics, the effect of mixing on particle break-up must also be considered. Within regions of turbulence where stress levels are significant, a higher rate of particle break up is observed and generally leads to small particle sizes. This can become problematic for shear-sensitive

precipitates and greatly affects formation, especially during the orthokinetic growth stage. This effect has been highlighted in the ageing of casein precipitates produced with salting-out in a helical ribbon stirred reactor (Hoare, 1982a). The study showed that final precipitate sizes were an inverse function of the mean velocity gradient (or shear rate) in the reactor which supports the idea of particle formation being a balanced process between growth and break-up. Therefore, to aid solid-liquid separation, the mixing should be designed to reduce the effects of localized high concentrations of reagents but not be so intense to induce significant particle breakage. One may adopt an approach of initial rapid mixing in bringing reagents to the point of homogeneity and induction of nucleation, followed by a reduction in the mixing intensity.

1.11 Prospects for scale-up

Scaling up precipitation processes remains a considerable challenge considering the complexity of the nucleation and aggregation phenomena involved, and how these can be greatly affected by operating conditions (e.g. mixing, choice and concentration of precipitant, protein concentration and contacting procedure). This makes developing a robust precipitation step rather difficult. Moreover, precipitation performance is likely to differ between scales. It is worth mentioning that the developments of scale-down models which are capable of mimicking large scale precipitation processes would be valuable and can reduce development times.

In the design of a precipitation process, both batch and continuous reactor configurations should be considered. Whilst most industrial precipitation procedures have been conducted in batch mode, multiple designs based on continuous reactors have seen much development (Zydney, 2015; Kateja *et al.*, 2016; Li *et al.*, 2019; Liu *et al.*, 2019). In some applications, the volume requirement of precipitant relative to protein solution can often be substantial, which necessitates very large batch reactors and introduces a mixing challenge to control critical process parameters. The relatively small sizes of continuous reactor systems offer the benefit of enhancing the mixing rate by reducing the mixing volume. In addition, reaction parameters that are critical to product quality (e.g. residence time, temperature, pressure) are better controlled. Continuous reactors also carry the benefit of reducing overall carbon footprint. A continuous fractionation process to separate human plasma was developed by Watt and co-workers, enabling better control of ethanol and plasma mixing as well as cooling over the batch approach (Watt, 1970). Various studies on mAb precipitation primarily report

the use of continuous reactors over batch reactors since higher productivities can be achieved with the former and are amenable to scale-up. Some reactor designs are illustrated in Figure 1-6. Although these systems have not been scaled-up per se, a scale-out approach involving multiple parallel units could be adopted. Otherwise, an option to scale up could include increasing the pipe diameter and flow rate to have equivalent residence times.

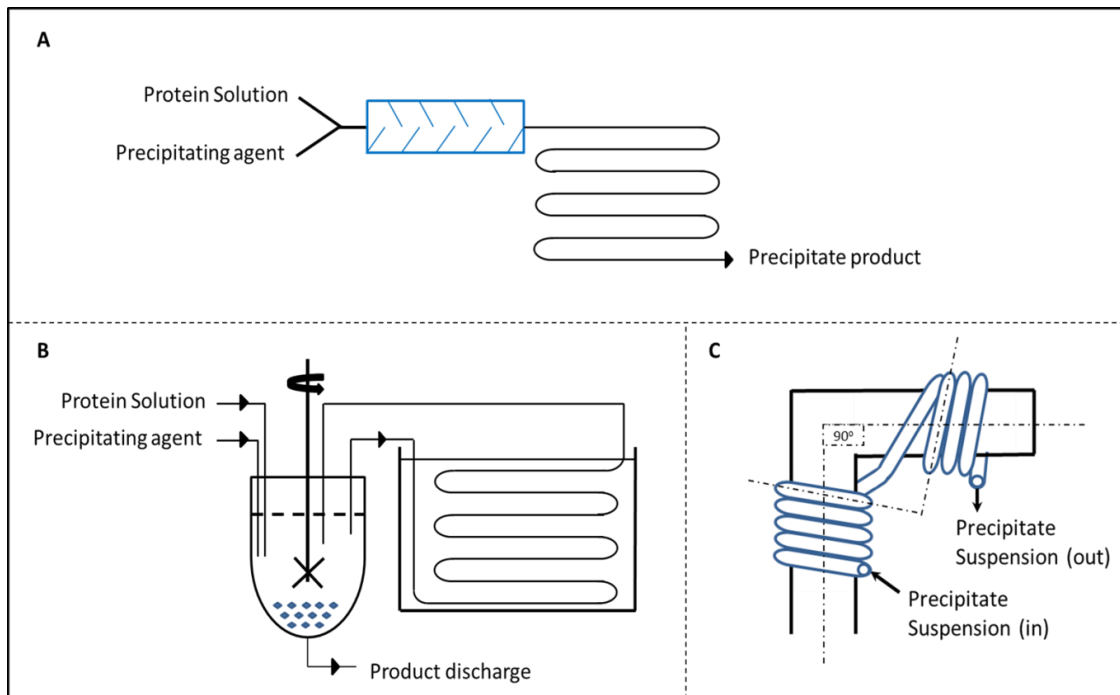


Figure 1-6. Schematic illustration of different continuous reactors. (A) Continuous tubular reactors; (B) stirred reactors with a tubular reactor in bypass and (C) coiled flow inversion reactors for precipitation applications. The reactor set up in (B) has been developed for protein crystallisation but is equally applicable for precipitation (Hekmat *et al.*, 2017).

Even though continuous processing appears to be the more desirable option, the example of soya protein precipitation described by Chan and co-workers demonstrates differences in the particle properties between batch and continuous processing (Chan, Hoare and Dunnill, 1986). Continuous-formed precipitate particles were shown to be less compact and more susceptible to breakage than those formed in a batch reactor, thereby indicating batch-formed precipitates would be more suitable for recovery in industrial centrifuges. In order to maximise strength, the design of a continuous reactor should enable the aging of an aggregated precipitate for sufficient time as can be guided by the Camp number. Depending on the required residence time, this could lead to rather long tube lengths and an impractical design. Therefore, it is imperative that designing a precipitation step should have the solid-liquid separation technique in mind. A number of centrifugal recovery options including disc-

stack centrifuges, tubular bowls, multi-chamber bowls and scroll discharge systems have been considered

Table 1-1 lists some of the advantages and disadvantages for these centrifuge types which can guide the engineering design of a precipitate recovery step.

Table 1-1. List of main centrifuge types and advantages/disadvantages to precipitate solids recovery (Bell and Dunnill, 1982b; Bell, Hoare and Dunnill, 1983)

Centrifuge Type	<i>Advantages</i>	<i>Disadvantages</i>
<i>Disc-stack centrifuge</i>	<ul style="list-style-type: none"> • Bowl cooling possible • Semi-continuous operation with solids discharge possible • Backpressure on supernatant eliminates foaming 	<ul style="list-style-type: none"> • Poor dewatering • Difficult to clean or long CIP cycles • Imposes very high shear on particles during solids discharge
<i>Tubular Bowl</i>	<ul style="list-style-type: none"> • High centrifugal force • Good dewatering • Easy to clean 	<ul style="list-style-type: none"> • Requires dismantling to recover solids • Limited solids capacity • Can only be operated in batch mode
<i>Carr Powerfuge</i>	<ul style="list-style-type: none"> • Good dewatering • High centrifugal force • Automated solids removal 	<ul style="list-style-type: none"> • Limited solids capacity • Scraping cycle may damage materials
<i>Multi-chamber Bowl</i>	<ul style="list-style-type: none"> • Large solids capacity • Good dewatering • Bowl cooling possible 	<ul style="list-style-type: none"> • No solids discharge • Difficult to clean • Difficult to recover solids
<i>Scroll Discharge</i>	<ul style="list-style-type: none"> • Solids are discharged continuously • Can accommodate high feed solids concentration 	<ul style="list-style-type: none"> • Low centrifugal force • Scroll creates turbulence which may induce solids break-up.

Recently, a shift from traditional centrifugal recovery of protein precipitates has been observed via the implementation of filtration systems including depth filters and hollow fiber membranes which are thought to impose reduced levels of shear on particles (Kang *et al.*,

2013; Hammerschmidt, Hobiger and Jungbauer, 2016; Liu *et al.*, 2019). Moreover, integrating these systems with a continuous precipitation process demonstrates the potential for a fully continuous process. It's worth noting that the compressibility of protein precipitates can often lead to membrane fouling issues which reduces protein transmission. Moreover, issues with protein binding to membrane materials can significantly impact the overall recovery. Therefore, depending on the nature of the precipitate, centrifugation may in fact be simpler and more suitable for separation.

1.12 Future prospects and concluding remarks

The application of precipitation to bioprocessing is a promising one considering the increased demand for therapeutic production at reduced costs. The biopharmaceutical industry is expected to face a higher production demand in the future and current techniques may not be able to cope. Therefore, it may be imperative to explore alternative methods. Precipitation offers the flexibility in using a number of low-cost reagents to purify therapeutic proteins at any stage across the purification process. Furthermore, precipitation has the advantage of scaling-up with process volume, instead of product titre as in chromatography processes. An additional consideration is the ability to recycle precipitating agents to further reduce costs. This is unlikely for many precipitating agents such as those belonging to the neutral salts, mineral acids and non-ionic polymers. On the other hand, organic solvents can be recycled via distillation processes, whilst tag and affinity ligands may be re-used after dissociation of the protein complex and subsequent purification.

The literature review highlights the progress that has gradually been made in the design of protein precipitation methods. Major developments have seen the adoption of continuous processes which show potential in aid of supporting product supply (Jungbauer, 2013). Although successful, understanding of the mechanisms and transport processes involved are still somewhat lacking, making the scale-up a cumbersome task. This necessitates the identification of optimal process parameters governing an efficient protein precipitation process based on optimal particle growth characteristics, which in turn enables effective separation performance. High-throughput screening methods and scale-down models in combination with statistical tools such as Design of Experiments (DoE) can yield a more comprehensive process understanding and accelerate process implementation at the same time. This will then be followed by scaling-up of the optimised conditions (provided that those tested successfully mimic the conditions at large scale) based on key engineering principles, forms the primary basis of the studies presented in the thesis.

Chapter 2: Materials and Methods

This chapter describes all the materials and analytical methods employed for the scope of the study presented in the thesis. Specific experiments and any deviations from the methods described herein are detailed in their appropriate chapters. All chemicals used in the study were of analytical grade and sourced from Sigma-Aldrich, Fisher Scientific or Acros-Organics, unless otherwise stated.

2.1 Materials

2.1.1 Clarified cell culture fluid

Clarified cell culture fluid (CCCF) containing humanized IgG₄ with molecular weight of 145 kDa, pI of 7.89, and 1.5 g/L titre was harvested at UCB Pharma (Slough, UK). The CCCF material provided is a research candidate and therefore not dedicated for a therapeutic process. Fed-batch fermentations were performed for CHO cell growth and antibody production. Harvesting was performed by centrifugation of the cell culture followed by depth filtration and finally 0.22 µm filtration. Aliquots were either stored at 4°C for short term storage (<1 week) or at -20°C for long term storage (<12 months) to mitigate issues associated with freeze-thawing. Prior to experimentation, thawed aliquots underwent 0.22 µm filtration in order to remove potential particulates formed during storage. Residual material was stored at 2-8°C for as long as 4 days, if required. Adjustments to feed pH were performed via the addition of 1 M NaOH/1 M HCl, if required.

2.1.2 Purified IgG₄

A proportion of CCCF was purified with PrA affinity chromatography using an XK50 column (Amersham Biosciences, UK), packed with 400 mL of Mab Select Sure resin (GE Healthcare, Uppsala, Sweden), to a bed height of 20 cm. The linear flow rate during the equilibration, sample loading, washing and elution steps was fixed at 150 cm/h. The column was first equilibrated with 5 column volumes (CVs) of Dulbecco's PBS pH 7.4. CCCF was then loaded to 30 mg mAb per mL of resin. The column was then washed with Dulbecco's

phosphate buffered saline (PBS) pH 7.4 for 5 CVs. Product elution was performed with 100 mM citrate pH 3.6. The eluate pH was adjusted to pH 6 via the addition of 2 M Tris-HCl pH 8.5. The sample was subsequently concentrated to approximately 50 mg/mL and dialysed into 50 mM sodium phosphate pH 7 by ultrafiltration/diafiltration using an AKTA Crossflow system. A T-series 0.2m² 30kDa molecular weight cut-off (MWCO) membrane (Pall Life Sciences, UK) was fitted and equilibrated with the dialysis buffer prior to processing. As with the CCCF, the purified and concentrated feed was 0.22 µm filtered and stored at 4°C for short-term storage (<1 week) or at -20°C for long term storage (<12 months).

2.1.3 Purification reagents

Monosodium phosphate monobasic, disodium phosphate dibasic, PBS, ammonium sulphate, lithium sulphate, sodium chloride, sodium sulphate and sodium acetate were purchased from Sigma Aldrich. Tri-sodium citrate was obtained from Alfa Aesar; HEPES, glycine, glacial acetic acid, hydrochloric acid and sodium hydroxide were purchased from Fisher Scientific. Buffer and stock solutions were filtered by vacuum filtration using 0.22 µm membranes to remove any undissolved solids.

2.1.4 Chromatography media

Capto Q and Capto MMC 96-well Predictor plates, 1 mL HiTrap Capto Q, 1 mL HiTrap Capto MMC, 1 mL HiTrap Protein G, Capto Q and Mab Select Sure resins were all purchased from GE Healthcare.

2.2 Precipitation methods

2.2.1 Batch precipitations

At 1.5 mL scale, antibody precipitation was performed in 2 mL 96-well V or U-bottomed polypropylene plates (Corning, UK) by combining various volumes of protein solution, buffer and precipitant at the desired pH values. Plates were incubated on an orbital shaker (Thermomixer C, Eppendorf, UK) at 500 rpm for at least one hour at 20°C. At 40 mL scale,

precipitation was performed by adding a fixed amount of precipitant to protein solution in a 50 mL test tube via a pipette with constant agitation using a stirrer bar on a magnetic plate. At 100 mL scale, precipitation was performed by adding a fixed amount of precipitant to a 150 mL Pyrex glass beaker pre-charged with protein solution at a defined flow rate. Details of the reactor design are described in Chapter 3. Precipitates were separated from the mother liquor either by centrifugation or filtration. Separation by centrifugation was performed using either an Eppendorf 5420R centrifuge (Eppendorf, UK) equipped with a 45° fixed angled rotor for 0.5 to 2 mL test tubes or an Eppendorf 5910R centrifuge equipped with a swing-bucket rotor for 10 and 50 mL test tubes. In the 96-well plate format, precipitates were separated by centrifuging at 4500 rpm for 45 minutes in a swing-bucket rotor. At 40 and 100 mL scales, precipitates isolated with centrifugation were attained at various conditions which have been detailed in Chapters 3 – 6. Filtration was performed using either 33 mm diameter, 0.22 µm pore size PES syringe filters (Millipore, UK) or Nalgene Rapid-Flow sterile disposable filter units with 50 mm diameter, 0.22 µm pore size membranes (Thermo Fisher Scientific, UK).

2.2.2 Continuous precipitations

Continuous precipitation was performed in self-designed continuous tubular reactors by feeding protein solution and precipitant through a T-mixer at equivalent flow rates and passing the mixture through coiled tubing of defined length and diameter. At small scale, a 0.5 mm internal diameter T-mixer (Upchurch Scientific, UK) was used, whilst the reactor length and diameter ranged between 1 to 10 m and 0.5 to 2 mm, respectively. Pumping of solutions was accomplished with a Harvard Apparatus PHD ULTRA double-barrelled syringe pump (Harvard Apparatus, UK) fitted with either 20 or 50 mL Plastipak syringes. At pilot scale, a 4.8 mm internal diameter T-mixer (Swagelok, UK) was used whilst the tubing had an internal diameter of 6.4 mm and a length of 5 m. Solutions were pumped using the main and gradient pumps on an AKTA Ready system (GE Healthcare, UK). A minimum of 5 reactor volumes of processing was performed before the collection of samples for analysis. Precipitates were separated from the soluble fractions by either centrifugation or filtration.

2.3 Analytical methods

2.3.1 Antibody quantification

2.3.1.1 Determination of antibody concentration using absorbance at 280 nm

Concentrations of purified IgG₄ samples (post-PrA chromatography) were determined based on absorbance values at 280 nm using a Nanodrop 1000 spectrophotometer (Thermo Fisher Scientific, UK). The IgG₄ has an extinction coefficient of 1.38Lg⁻¹cm⁻¹ (personal communication, UCB Pharma). Therefore, the unknown concentration of antibody in samples was deduced using the Beer-Lambert law relationship: $A_{280} = \epsilon_{280}cl$, where A_{280} is the absorbance value at 280 nm, ϵ_{280} is the IgG₄ molar extinction coefficient at 280 nm, c is the antibody concentration and l is the path length. It is important to note that the Beer-Lambert law only applies over the range 0.1 to 1.0 absorbance units. Above this range, the relation between protein concentration and absorbance is no longer linear. When required, dilutions were performed in order to ensure absorbance values were within this range.

2.3.1.2 Determination of antibody concentration with Protein G-HPLC

Non-PrA chromatography purified samples were determined using analytical Protein G (PrG) affinity chromatography on an Agilent Technologies Biosystem 1200 (Agilent, UK). A 1 mL HiTrap PrG column was used. The column was equilibrated with 5 CVs of 20 mM sodium phosphate pH 7 at 1 mL/min. 100 μ L of an IgG₄ reference standard, blank (containing only buffer) and samples were injected into the column. The antibody standard was an in-house reference with a molar extinction coefficient of 1.43 Lg⁻¹cm⁻¹. This was prepared using a purification sequence comprising PrA, cation exchange and anion exchange chromatography steps in that order. The final concentration of the antibody was 3.68 mg/mL. The standard was diluted with equilibration buffer in the range 0.18 to 2.2 mg/mL to generate a 5 to 7 point standard curve by which the unknown antibody concentration in samples could be deduced with linear regression. Elution was performed with 20 mM glycine pH 2.8 at 1 mL/min. Post-run analysis was performed with Chemstation software. Column cleaning and storage was performed by washing with 5 CVs of MilliQ water, followed by 5 CVs of 20% ethanol, each at 1 mL/min. In between runs, the column was stored at 4°C according to the manufacturer's recommendation.

2.3.2 Antibody purity

2.3.2.1 PrG-HPLC

Chemstation software was capable of automatically integrating the peaks present in each of the samples and expresses them as a percentage of the sum of the peak areas. Unbound species (the impurities) were detected in the flow-through fraction whilst the main antibody peak was detected at a retention time of 5.8 ± 0.2 minutes during elution with 20 mM glycine pH 2.8. Whilst not a specific assay, the method provided an initial metric of the relative purity level when compared against the CCCF feed. For precipitated samples, this was a rather a quick metric on precipitation performance between various conditions.

2.3.2.2 Total protein Determination with Bradford Assay

Pierce Coomassie (Bradford) assay kit (Thermo Fisher Scientific, UK) was initially used to determine total protein concentrations in samples. This method relies on the binding of proteins to a Coomassie dye forming a complex which shifts the maximum absorbance of the dye from 465 nm to 595 nm. Absorption is proportional to the concentration of total protein in the sample within the range 0.1 – 1.4 mg/mL of an albumin standard (Thermo Fisher Scientific, UK).

Samples were diluted with 50 mM sodium phosphate pH 7.0 to bring the protein concentration within the linear range of the assay. Upon addition of samples and assay mix, the mixtures were incubated at room temperature for at least 10 minutes prior to reading the absorbance at 595 nm with a spectrophotometer (GENYSYS™ 10S UV-Vis spectrophotometer, Thermo Fisher Scientific, UK) in 10 mm cuvettes.

The assay was discontinued during the early stages of the work since it was found that PrG-HPLC produced more reliable findings and required fewer resources. It however remains a good application for other protein systems.

2.3.2.3 SDS-PAGE

As a qualitative analysis of antibody purity, non-reduced SDS-PAGE were run on samples using 1.5 mm 12 or 15-well NuPAGE 4-12% Bis-Tris 8 x 8 cm pre-cast gels (Thermo Fisher Scientific, UK). 5 μ L of sample was combined with 8 μ L of MilliQ water, 2 μ L of NEM and 5 μ L of NuPAGE 4x LDS Sample Buffer (Thermo Fisher Scientific, UK). In the initial analysis, samples were incubated on a heating block at 80°C for 5-10 minutes. However, this was found to induce the formation of antibody degradation products which misled purity analysis. Therefore, heating was not performed in subsequent analyses. A short, full-speed centrifugation (i.e 16,000 x g for 1 minute) was performed to draw liquid to the base of the tubes. An XCell SureLock Mini-Cell gel tank (Thermo Fisher Scientific, UK) was filled with 1x MES running buffer, prepared from NuPage 20x MES running buffer (Thermo Fisher Scientific, UK), before fitting gel cassettes and loading samples. 15-20 μ L of samples were loaded into each individual well, along with 7 μ L of Mk12 unstained standard protein ladder (Thermo Fisher Scientific, UK) in a separate lane. A sample of the PrA-purified IgG₄, diluted to ~1 mg/mL, was also included as a reference. Gels were run at a constant voltage of 200 V for 35 mins. After electrophoresis, the gels were removed from their cassettes and placed in polypropylene trays. Gel staining was either performed with the Coomassie-based Instant Blue stain (Expedeon, UK) or SYPRO Ruby (BioRad, UK).

For Instant Blue staining, the gels were briefly washed with MilliQ water and incubated in stain overnight for best sensitivity. For SYPRO Ruby staining, gels were washed with 10% ethanol, 7% acetic acid solution for 30 minutes and subsequently stained overnight with the pre-mixed SYPRO Ruby stain solution. The stain was then removed and gels were washed with 10% ethanol, 7% acetic acid for 30-60 minutes. Gels were finally washed with MilliQ water after both staining procedures prior to imaging. Imaging was performed using the Amersham Imager 600 (GE Healthcare). For Coomassie-stained gels, the trans-illumination colorimetric capturing method was used, whereas for SYPRO ruby-stained gels, epi-illumination fluorescence was used.

2.3.2.4 HCP-ELISA

The quantification of host-cell proteins (HCPs) in samples was performed using CHO-HCP ELISA 3rd generation kits (Cygnus Technologies, North Carolina, USA). The kits comprised of 96-well anti-CHO coated microtiter strips, CHO HCP standards (0, 1, 3, 12, 40 and 100

ng/mL), anti-CHO:HRP, TMB substrate, wash concentrate (20x) and 0.5 M H₂SO₄ stop solution. The assay involves a direct ELISA in which CHO HCPs first react with the anti-CHO:HRP antibody to form a solid-phase complex in each of the wells. Addition of TMB substrate induces a hydrolysis reaction by which the amount of hydrolysed TMB is directly correlated to the concentration of CHO HCPs present in the sample. Samples were serially diluted with a proprietary sample diluent buffer provided by Cygnus Technologies in order to be within the range of the HCP standard curve. To each well, 100 µL of anti-CHO:HRP was dispensed, followed by 50 µL of CHO HCP standard, buffer (as a negative control) and samples. The strips were then covered and incubated on an orbital shaker (Eppendorf Thermomixer C, Thermo Fisher Scientific, UK) at 500 rpm for 2 hours at 24°C. The wells were washed with 1x wash concentrate for a total of four washes, with the contents dumped between each wash in order to remove unbound reactants. 100 µL of TMB substrate was added to each of the wells and allowed to incubate at room temperature for 30 minutes with no shaking. 100 µL of 0.5 M H₂SO₄ stop solution was then added, at which point absorbance was read at 450 nm with a reference wavelength of 650 nm using a Tecan Safire 2 Multi-mode plate reader (Tecan, UK). HCP concentration levels were expressed in terms of parts per million (ppm) or nanograms of HCP per milligram of antibody (ng HCP/mg mAb). Samples were analysed in triplicate for assay reproducibility.

2.3.2.5 dsDNA quantification

The concentration of double-stranded DNA (dsDNA) in samples was quantified using the Quant-iT Picogreen dsDNA assay kit (Thermo Fisher Scientific, UK) in fluorescent black bottom 96-well plates. The assay procedure according to the manufacturer's instructions was followed. In short, samples and λ DNA standard (2 µg/mL DNA stock concentration) were serially diluted in 1 x TE buffer (200 mM Tris-HCl, 20 mM EDTA pH 7.5), and 100 µL of each were transferred onto the 96-well plates. 100 µL of the Quant-iT Picogreen dsDNA colour reagent, pre-diluted in 1 x TE, was then added to each well. Immediately after, the fluorescence signals were measured in a Tecan Safire 2 Multi-mode plate reader using an excitation wavelength of 480 nm and emission wavelength of 520 nm, each with a bandwidth of ± 20 nm. Unknown dsDNA levels were then determined from the λ DNA standard curve. Samples were measured in triplicate for assay reproducibility.

2.3.2.6 High molecular weight species (HMWS) determination using size-exclusion chromatography HPLC (SEC-HPLC)

Antibody monomer and residual aggregate levels were determined by size-exclusion HPLC using a TSK gel UP-SW3000, 2 μm particle size, 4.6 mm ID x 30 cm SEC column (Tosoh Biosciences, UK) and Agilent Biosystems 1200 instrument (Agilent Biotechnologies, UK). The column was first equilibrated with 0.1 M sodium phosphate pH 6.7 running buffer by flowing liquid at 0.1 mL/min and gradually increasing the flow rate to 0.3 mL/min. Equilibration continued at 0.3 mL/min for at least 10 CVs. 5 μL of samples at ~ 1 mg/mL IgG₄ were injected onto the column and running buffer was run at 0.3 mL/min. Post-data analysis to determine the ratio of HMWS to monomer antibody was performed with Chemstation software. At the end of each run, the column was stored in 20% ethanol and at room temperature.

2.3.3 Circular dichroism (CD) spectroscopy

CD spectra of samples were generated using an Aviv 400 Circular Dichroism spectrophotometer (Biomedical Inc, Lakewood, USA) equipped with thermoelectric temperature control. Samples were buffer exchanged into 50 mM sodium phosphate by dilution and adjusted to 0.8 mg/mL before transferring into a quartz cuvette with 1 mm path length. CD data was analysed in the far-UV range from 200 to 250 nm in 1 nm steps, using a 1 nm bandwidth and a 1 second averaging time. Temperature was controlled at 25°C. Triplicate scans were performed to ensure data reproducibility. The buffer baseline was subtracted from the samples spectra. The CD signal given in millidegrees, Θ , was converted to molar circular dichroism, $\Delta\epsilon$, using the relationship:

$$\Delta\epsilon = \Theta \cdot \frac{(0.1 \times MRW)}{(c \times l \times 3298)}$$

Equation 2-1. Transformation of polarised angle ellipticity to molar circular dichroism, $\Delta\epsilon$.

where c is the antibody concentration, l is the path length and MRW is the mean residual weight (= antibody molecular weight/number of amino acids in sequence).

2.3.4 Particle size measurements

2.3.4.1 *Dynamic light scattering*

Particle size distributions of samples comprising particle populations in the range 0.3 nm to 2 μm were measured using the Malvern Zetasizer NS (Malvern Instruments Ltd., UK), based on dynamic light scattering. Samples were dispensed in 1 mL cuvettes and inserted into the cell holder of the instrument. Since the refractive and absorption indices of the protein molecule were not known, the optical properties of a standard acrylic latex particle was used for the measurements (RI = 1.59, AI = 0). Changes in these values showed no adverse changes in the particle size distributions and hence were used throughout the analyses. Five individual measurements were taken, of which a technical average was computed by the Zetasizer software.

2.3.4.2 *Laser light diffraction*

Particle size distributions of samples comprising of particles in the size range 0.1 – 1000 μm were measured using the Malvern Mastersizer 3000 (Malvern Instruments Ltd., UK), on the basis of laser light diffraction. The Hydro SV dispersion unit was used to disperse samples and make measurements. Background measurements containing only dispersant was made, after which samples were dispersed with the dispersant and thoroughly mixed by means of a stirrer bar at 1500 rpm. Sample was continuously added until the red laser obscuration level in the flow cell reached between 10 and 20%. The same refractive and absorption indices stated in section 2.3.4.1 were used during the analysis. Five measurements were taken per sample with 5 seconds delay between each measurement and an average was computed by the Masteriszer 3000 software.

2.3.4.3 *Light microscopy*

Precipitated samples were loaded onto pre-cleaned glass microscopic slides (VWR, UK) with cover slips (VWR, UK) carefully placed over. Phase contrast images were taken with a Nikon TE2000-PFS inverted microscope (Nikon, UK) and processed with Image J.

2.3.5 Ultra scale-down (USD) centrifugation

CCCF precipitate samples were exposed to shear stress in a rotary disc device developed by the Department of Biochemical Engineering at UCL. Details of the USD method are described by Chatel *et al* (Chatel, Kumpalume and Hoare, 2014). The construction and device components are detailed elsewhere (Hutchinson *et al.*, 2006). In short, 20 mL of sample was exposed to 6000 rpm shear, corresponding to a maximum energy dissipation rate of $0.045 \times 10^6 \text{ Wkg}^{-1}$, for 20 s. This condition was selected to be representative of a hydro-hermetic feed zone of a well-operated disc-stack centrifuge. 1, 1.5 and 2 mL of sheared samples were centrifuged in a fixed angle rotor for 10 mins at 4000 or 8000 rpm. Non-sheared samples were also spun using the equivalent conditions for comparison purposes. Approximately half of the supernatant from each condition was recovered with minimal disturbance of the solids sediment and measured for solids content using OD_{600} readings. The clarification performance was recorded in terms of the percentage of solids remaining, S, according to the relation:

$$S (\%) = 100 \times \frac{OD_S - OD_O}{OD_F - OD_O}$$

Equation 2-2. Percentage of solids remaining as a function of OD_{600} values for feed, supernatant and well-clarified supernatant samples.

where OD_S is the optical density of the supernatant, OD_F is the optical density of the feed prior to centrifugation and OD_O is the optical density of a well-spun sample which is used as a baseline value for clarification. The well-spun sample was prepared by centrifuging a sample at $16000 \times g$ for 30 minutes. All centrifugation conditions were performed at $22 \text{ }^\circ\text{C}$ in duplicate.

2.4 Disc-stack centrifugation

A pilot-scale clarification run was performed using the GEA Westfalia Pathfinder PSC 1-06-177 (GEA Westfalia, Germany) at 13,500 rpm ($20,000 \times g$) with a flow rate of 35 L/H. PSC-1 has 8 discs, a bowl volume of 1 L and a solids capacity of approximately 850 g. Pre-operation set-up was performed according to the manufacturer's instructions. The centrifuge bowl and equipment piping were filled with reverse osmosis water to test the efficiency of bowl opening and closing. The centrifuge feed was constantly agitated in a 20 L Nalgene

heavy duty cylindrical tank (tank diameter: 28 cm) using a 6-blade Rushton impeller (impeller diameter: 12 cm) and overhead stirrer at ~300 rpm to prevent solids sedimentation during operation. The feed was pumped through the centrifuge via a centripetal pump for a total of 7 minutes. The bulk supernatant was collected after 1 min of processing. The solids were recovered from the bowl via three complete discharges. Samples of the feed, supernatant and discharged solids were taken and analysed for particle size, antibody recovery and clarification.

2.5 Chromatographic methods

2.5.1 Predictor plates

Details of the chromatography screening experiments using 96-well Predictor plates are described in Chapter 6. Samples were buffer exchanged into the respective mobile phases using Vivaspin 20 centrifugal concentrators comprising of either 3 or 30 kDa MWCO PES membranes (Sartorius, UK) prior to loading. Preparation of the resin wells were performed according to the manufacturer's recommendations.

2.5.2 Column chromatography

Lab scale column chromatography was performed on an AKTA Pure system (GE Healthcare). A standard pre-operation procedure was followed: lines were first primed with MilliQ water to remove 20% ethanol storage solution and then primed with the relevant buffers as per the mode of operation. Depending on the application, either pre-packed 1 mL HiTrap columns or an XK16 packed with resin slurry to a specified bed height was used. Details of the chromatography procedures can be found in Chapter 6. As in section 2.5.1, samples were prepared with buffer exchange in the same way.

Chapter 3: Characterisation of monoclonal antibody precipitation with salting-out

3.1 Introduction

In this chapter, a salting-out study on an IgG₄, provided by UCB Pharma, was reproduced from previous work conducted on an IgG₁ (Morris, 2019). Despite belonging to the same class of antibodies, it could not be assumed that the precipitants and process conditions previously identified for IgG₁ would perform in the same way for a different antibody. Differences in the structural and physicochemical properties of these antibodies could greatly influence precipitation behaviour (Hekmat, 2015; dos Santos, Carvalho and Roque, 2017). Thus, it was necessary to perform small-scale studies involving an initial screening methodology to identify suitable precipitation conditions as a benchmark for the later studies presented in subsequent chapters. Rather than designing a whole set of screening experiments to investigate a wide range of precipitants and process conditions, since this was not the main focus of the thesis, it was decided to characterise and evaluate the potential of the salts identified from the previous work on IgG₄ precipitation.

Prior to identifying the suitability of the salt agents for the precipitation and recovery of IgG₄ from CCCF, studies began with using a purified feedstock. This feed was prepared from the purification of CCCF using PrA chromatography in which IgG₄ would be captured on the column resin, whilst removing the bulk of impurities that do not bind and reside in the flow-through fraction. Provided that antibody purities above 95% are typical with PrA chromatography (Hammerschmidt *et al.*, 2015), quantification of precipitation could be rapidly elucidated with techniques that are often limited to single-component systems such as simple A₂₈₀ measurements. More complex systems in which impurities such as HCPs and DNA are present would require more extensive and time-consuming methods. Indeed, the precipitation behaviour of a single component system may not necessarily translate to a multicomponent system but can provide useful information.

As described in the literature review in Chapter 1, protein precipitation can be affected by many factors including pH, precipitating agent, precipitant concentration, temperature, ionic strength and protein concentration. In this study, the effect of salt type, salt concentration, pH and antibody concentrations were evaluated on the precipitation behaviour of IgG₄ using a multi-well plate methodology. One of the advantages for using a multi-well plate approach

is the ability to test a wide range of conditions simultaneously and generate many data with minimal sample usage.

From the previous work, ammonium sulphate, sodium sulphate, lithium sulphate and sodium citrate were considered as potential candidates. All precipitants were prepared as highly concentrated stock solutions near to saturation. Whilst lithium sulphate could theoretically be made up to 2.5 M in solution, the salt often crashed out of solution with short-term storage. Additionally, the incorporation of a buffer system also caused lithium sulphate to crystallise, making pH control difficult. Consequently, lithium sulphate was discontinued as a precipitant candidate. Thus, ammonium sulphate, sodium citrate and sodium sulphate were carried forward. The conditions identified for precipitation of IgG₄ in the purified system were linked to cell culture fluid in order to test the potential of salt precipitation as an antibody capture step in terms of recovery and relative purity.

3.2 Salting-out screen

The salt stock solutions (with buffering systems) and the range of conditions employed for the precipitation screening are shown in Table 3-1.

Table 3-1. List of salts, stock solutions and pH and concentration ranges tested for the precipitation screening experiments.

Salt Precipitant	Stock Concentration (M)	Buffer System Used	Concentration Range Tested (M)	System pH
Ammonium Sulphate (AS)	3.6	Sodium Phosphate (50 mM)	0 – 2.75	6, 7, 8
Sodium Sulphate (SS)	2	Sodium Phosphate (50 mM)	0 - 1.65	6, 7, 8
Sodium Citrate (SC)	1.8	Sodium Phosphate (50 mM)	0 – 1.5	6, 7, 8

Precipitations of purified IgG₄ were performed in 2 mL V-bottomed deep 96-well polypropylene plates at the desired antibody concentration. The steps taken for precipitation in the 96-well plate format and subsequent analysis are described in Figure 3-1. In summary, various volumes of precipitant and diluent (i.e. buffer) were initially mixed, at which point antibody solution was introduced, mixed and incubated at room temperature with constant mixing for up to 2 hours.

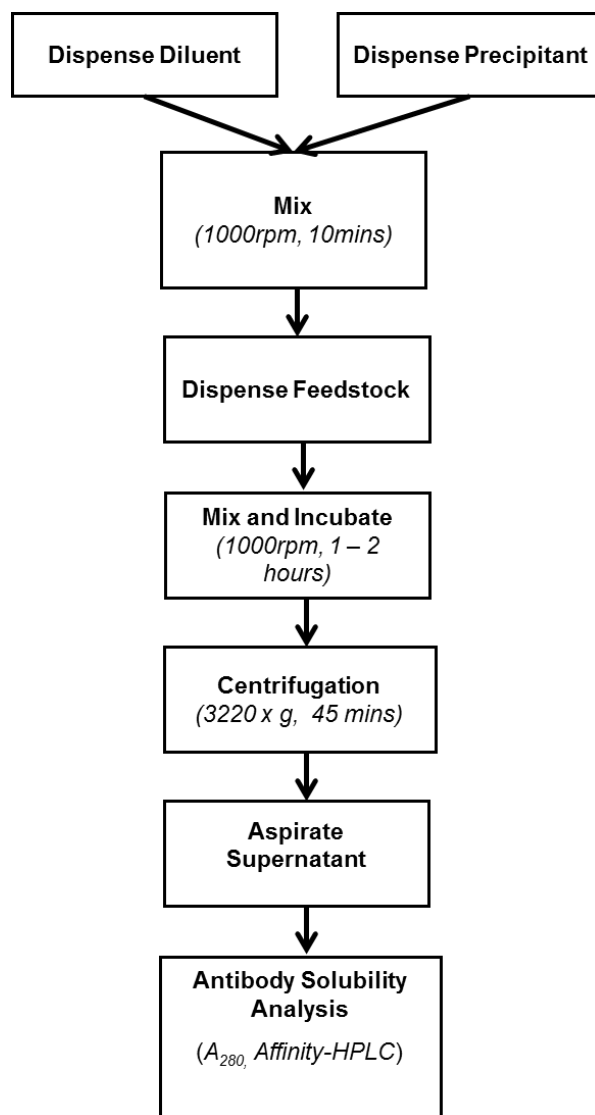


Figure 3-1. Step-by-step procedure implemented for the precipitation screening experiments in the 96-well plate format.

Preliminary studies showed that no change in the final solubility was observed between 1 and 2 hours, therefore suggesting the attainment of precipitation equilibrium within 1 hour. Additionally, depending on the conditions, precipitation was observed to occur immediately upon the addition of feed. A more thorough study on the precipitation kinetics is described in section 3.7. Selected centrifugation conditions showed that all precipitate particles were able to pass from the top of the mother liquor to the base of the wells, whilst the liquid layers appeared particle-free by observation. This enabled withdrawal of the supernatant to determine antibody content without disturbing the pellet. Whilst 45 minutes was selected for the centrifugation time benchmark in the 96-well plate format, similar centrifugal performance may have been achieved with reduced centrifugation times. According to Stoke's Law, the minimum centrifugation time, t_c , required for a precipitate particle to pass through the liquid phase at a defined speed can be determined based on the relationship:

$$t_c = \frac{\text{Ln} \left(\frac{R}{R_0} \right) 18\mu}{(\rho_p - \rho_f) D_p^2 \omega^2}$$

Equation 3-1. Calculation of minimum centrifugation time, t_c , required for effective particle separation.

where R and R_0 are the distances from the centre of rotation to the top and bottom of the liquid of a centrifuge tube, respectively, μ is the liquid viscosity, ρ_p is the density of the particles, ρ_f is the density of the liquid D_p is the average diameter of the precipitate particles and ω is the angular velocity.

The critical parameters driving the separation of a precipitate particle from the liquid suspension according to the derived equation are the density difference between the precipitate and liquid phase ($\rho_p - \rho_f$), the average diameter of the precipitate particle D_p and the angular velocity of the centrifuge ω . In principle, a faster and more effective phase separation can be achieved for large particle sizes, large density differences between the solid and suspension phases, high centrifuge speed and low viscosity. From laser diffraction analyses, the mean sizes of precipitate particles based on volume distribution were above 5 μm . Protein precipitates were assumed to have an average density of 1300 kgm^{-3} based on previous protein precipitation studies (Hoare, Dunnill and Bell, 1983; Fischer, Polikarpov and Craievich, 2009). The densities of the salt stock solutions used in the study were determined gravimetrically and were in the range $1100\text{-}1150 \text{ kgm}^{-3}$. Therefore, the density differences were expected to be sufficient in separating the particles from the suspension with centrifugation.

Precipitation efficiency data were represented in terms of the fraction of soluble antibody plotted against precipitant concentration. These data could be fitted with a sigmoidal curve function using OriginPro 2018, giving the following expression in terms of antibody solubility and salt concentration:

$$\frac{S}{S_0} = S_{min} + \frac{S_0 - S_{min}}{1 + e^{\frac{[Salt] - [Salt]_{1/2}}{Slope}}}$$

Equation 3-2. Sigmoidal precipitation curve fitting.

where S is the final soluble antibody concentration after the addition of salt, S_0 is the initial soluble antibody concentration in the absence of added salt, S_{min} is the minimum soluble antibody concentration where maximum precipitation is observed and $[Salt]_{1/2}$ is the salt concentration at the precipitation midpoint where 50% of protein has precipitated. This expression can provide useful predictions of precipitation performance between different conditions. Moreover, the function can be rearranged to determine the precipitation midpoints, providing a useful metric and identification for the factors that exhibit the largest effects on precipitation.

3.3 Effect of salt type, salt concentration and pH on purified IgG₄ precipitation performance

Antibody precipitation profiles with ammonium sulphate, sodium sulphate and sodium citrate at pH 6, 7 and 8 are shown in Figure 3-2 to Figure 3-4. A phosphate buffer was used to control the pH in this range. The final antibody concentration in the samples was set to 1 mg/mL. It can be seen that all three salts induced IgG₄ precipitation with increasing saturation. The S-shaped curves between salt concentration and antibody solubility demonstrate steep transitions from fully soluble to fully precipitated antibody within a small salt concentration range. Depending on the pH of the system, in order to precipitate above 95% IgG₄ from the purified feedstock solution, a minimum salt concentration of 1.45, 1 and 0.9 M for ammonium sulphate, sodium sulphate and sodium citrate, respectively, was required.

There was a notable shift in the precipitation curves at pH 6 compared to the curves at pH 7 and pH 8, particularly at low salt concentrations. It can be seen that a higher minimum salt concentration was required to initiate precipitation when the solution was at pH 6. Also, at

the same salt concentration, depending on the salt, the amount of antibody in the precipitate was markedly reduced compared to precipitations at pH 7 and pH 8. This is likely a result of enhanced electrostatic interactions at below pH 7 which promote protein solubility at the lower end of the salt concentration range. As the concentration increases to very high saturation levels, these electrostatic interactions become superseded by the hydrophobic interactions driving the association of protein molecules and eventually induce precipitation.

The significance of the reaction pH to the precipitation behaviour was further evaluated by determining the precipitation midpoints at each pH value. As depicted in Figure 3-5, a slight decrease in the precipitation midpoint was observed with increasing pH which is consistent with the theory that protein solubility is reduced at pH conditions close to the protein's isoelectric point (Leavis and Rothstein, 1974). Electrostatic interactions are minimised as the protein net charge reaches zero and become superseded by the hydrophobic interactions. This therefore drives the precipitation process as a result of increased ionic strength. The precipitation midpoints for ammonium sulphate precipitation were the least affected by changes in pH with only a 5.45% decrease observed over two pH units. For sodium sulphate and sodium citrate precipitations, a 15.6% and 20.5% decrease in the precipitation midpoints, respectively, were observed over the same pH change. This result indicated that ammonium sulphate provides a more robust salting-out system for IgG₄ precipitation with pH and also infers better reliability for pH variabilities in process feed. It would have been interesting to investigate the effect of pH outside of the studied range. However, lower pH values would be expected to precipitate process-related impurities more readily given the relatively low pI of HCP pools. Higher pH systems with ammonium sulphate precipitation are not favourable since it becomes prone to the release of ammonia gas.

For the amounts of salt required to maximise precipitation, it was noted that the volume fraction of salt solution to feed solution is approximately 1-to-1 for sodium sulphate and sodium citrate-based precipitations. For ammonium sulphate precipitation, the ratio is less than 1-to-1 (0.7-to-1) which corresponds to an ammonium sulphate saturation of 41.7% with a 3.6 M starting stock solution. From a fully saturated ammonium sulphate solution (4M), the saturation level required drops to 37.5%. This means that lower process volumes would be expected during a large scale batch process which confers an advantage for employing ammonium sulphate precipitation over sodium sulphate and/or sodium citrate precipitation.

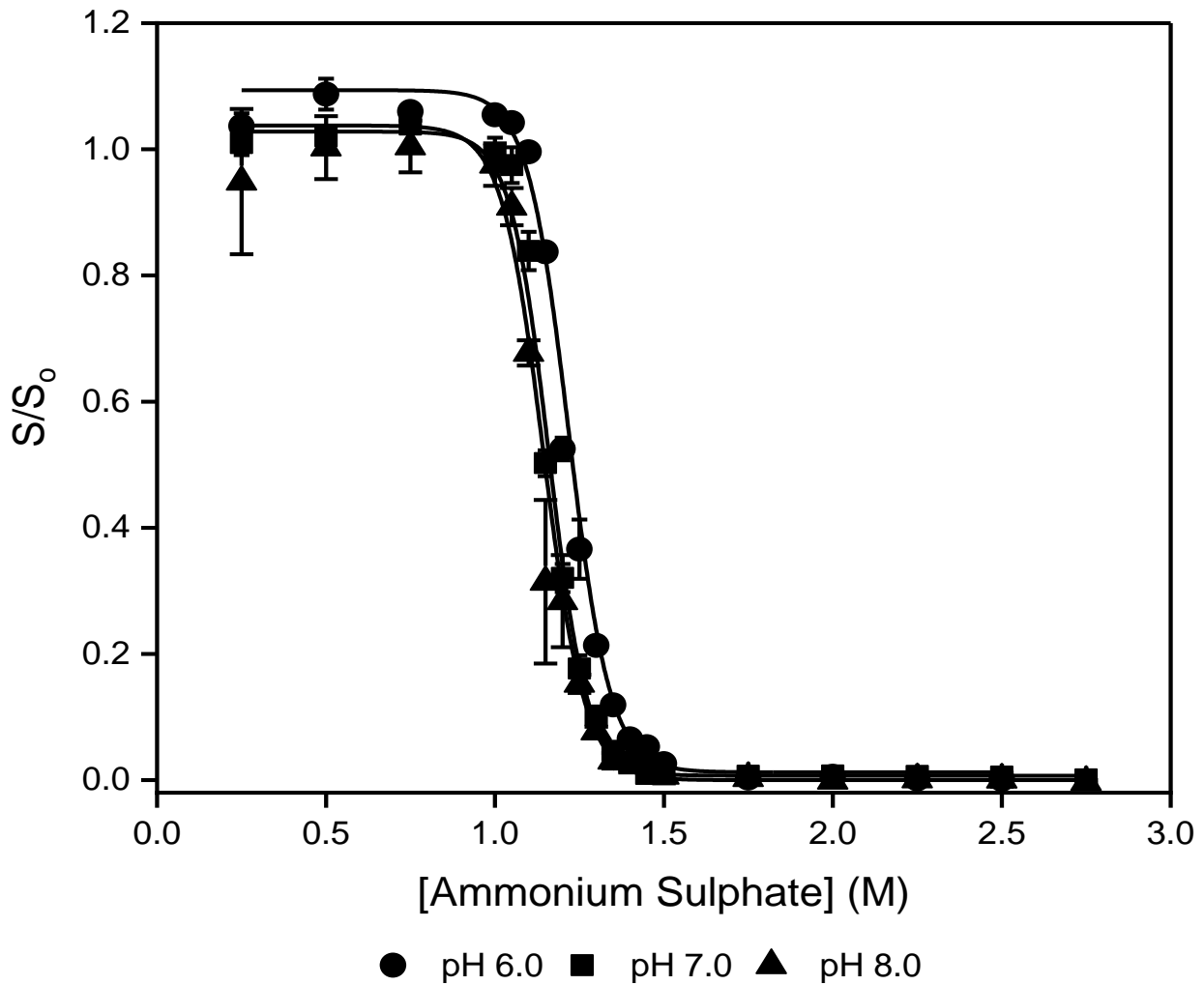


Figure 3-2. IgG₄ solubility profile with increasing ammonium sulphate concentration at pH 6, 7 and 8. Precipitations were carried out in 2 mL V-bottomed 96-deepwell plates at 1.5 mL working volume with initial mixing performed with manual pipetting of antibody feed into various ammonium sulphate concentrations to a target final antibody concentration of 1 mg/mL. This was followed by orbital mixing at 1000 rpm for 1 hour and subsequent centrifugation at 4000 rpm for 45 mins at room temperature. The upper layer was withdrawn and measured for non-precipitated antibody. Average solubility values are displayed from n=3 experiments with one standard deviation around the mean.

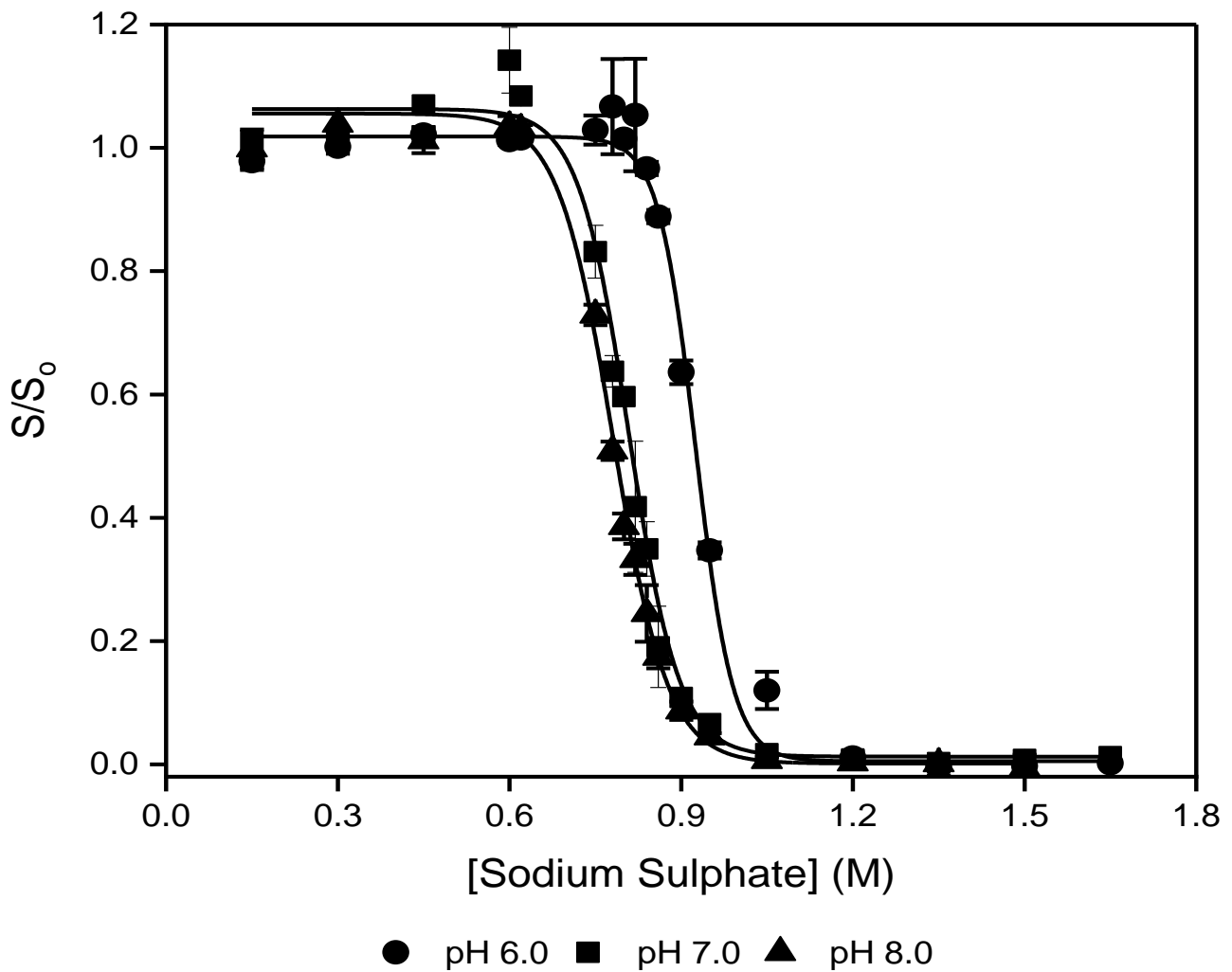


Figure 3-3. IgG₄ solubility profile with increasing sodium sulphate concentration at pH 6, 7 and 8. Precipitations were carried out in 2 mL V-bottomed 96-deepwell plates at 1.5 mL working volume with initial mixing performed with manual pipetting of antibody feed into various sodium sulphate concentrations to a target final antibody concentration of 1 mg/mL. This was followed by orbital mixing at 1000 rpm for 1 hour and subsequent centrifugation at 4000 rpm for 45 mins at room temperature. The upper layer was withdrawn and measured for non-precipitated antibody. Average solubility values are displayed from n=3 experiments with one standard deviation around the mean.

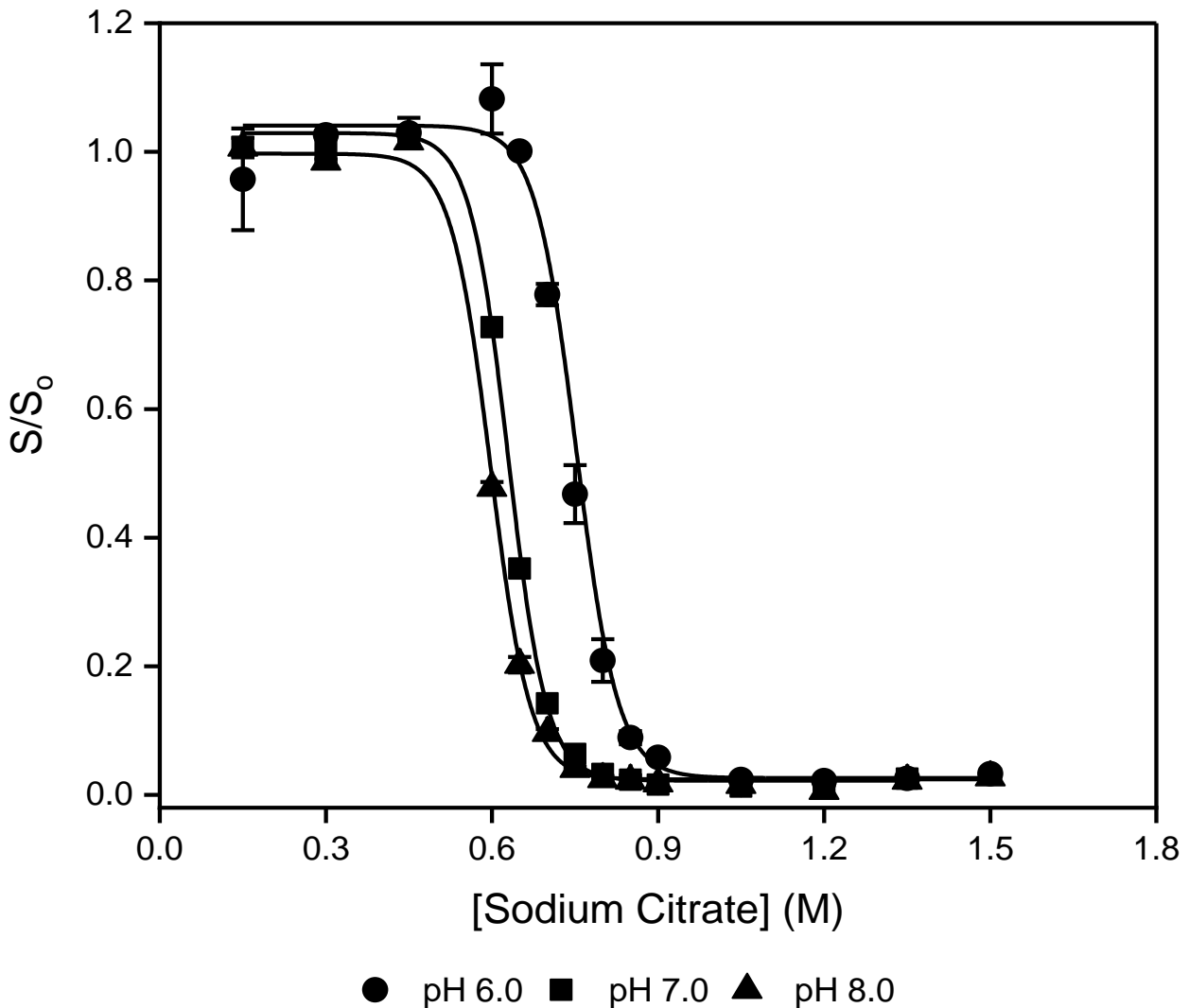


Figure 3-4. IgG₄ solubility profile with increasing sodium citrate concentration at pH 6, 7 and 8. Precipitations were carried out in 2 mL V-bottomed 96-deepwell plates at 1.5 mL working volume with initial mixing performed with manual pipetting of antibody feed into various sodium citrate concentrations to a target final antibody concentration of 1 mg/mL. This was followed by orbital mixing at 1000 rpm for 1 hour and subsequent centrifugation at 4000 rpm for 45 mins at room temperature. The upper layer was withdrawn and measured for non-precipitated antibody. Average solubility values are displayed from n=3 experiments with one standard deviation around the mean.

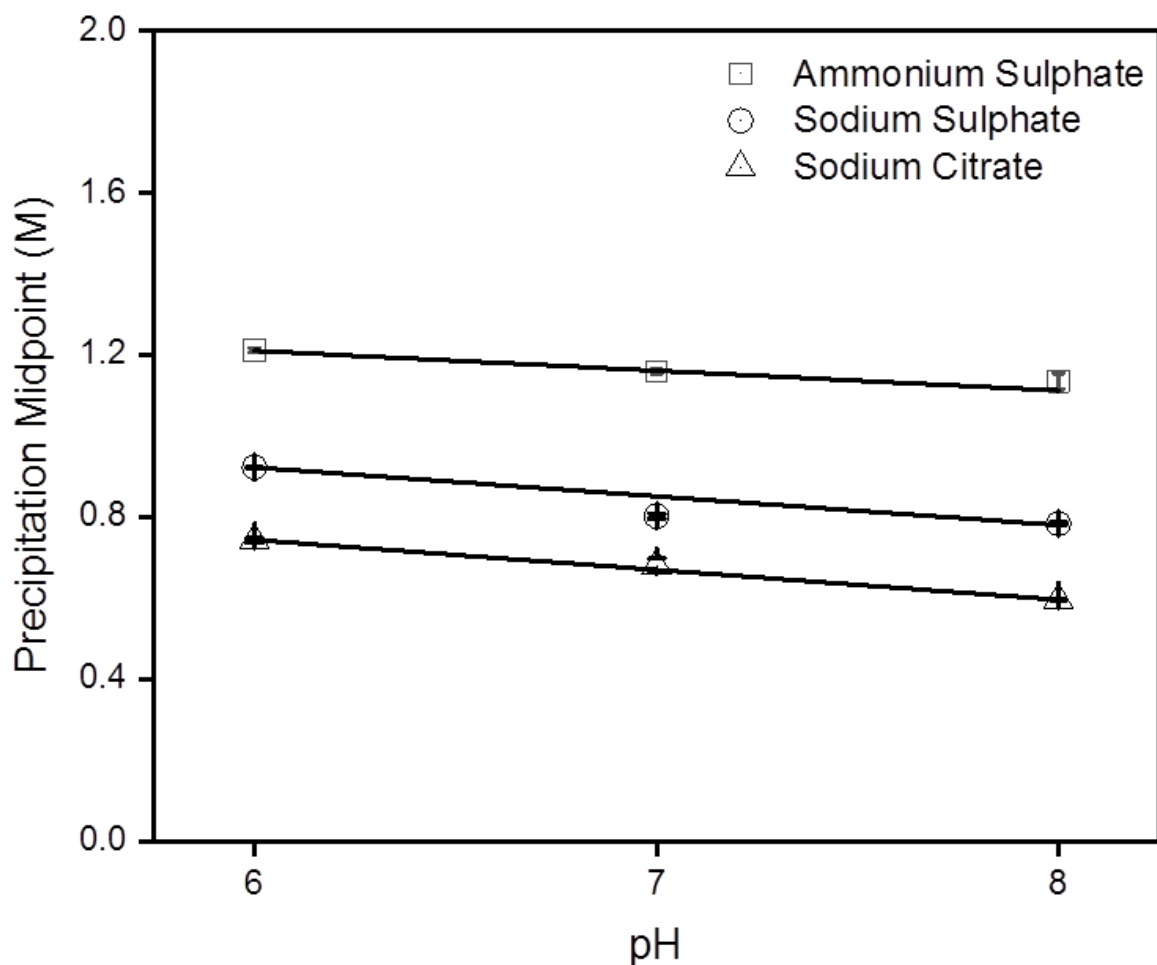


Figure 3-5. Precipitation midpoints for IgG₄ precipitation with ammonium sulphate, sodium sulphate and sodium citrate as a function of pH. Values for the precipitation midpoints were sourced from the sigmoidal fitting of the precipitation curves presented in Figures 3-2 to 3-4. Symbols represent an average of each precipitation midpoint against pH with error bars showing one standard deviation around the mean. Error bars are sufficiently small such that are difficult to observe with data symbols. A linear fit was applied for appropriate treatment of the data (ammonium sulphate precipitation midpoint $R^2 = 0.956$; sodium sulphate precipitation midpoint $R^2 = 0.958$; sodium citrate precipitation midpoint $R^2 = 0.999$).

3.4 Effect of protein concentration on precipitation performance

Another parameter known to influence the precipitation performance is the protein concentration in suspension. Combining this parameter with salt concentration would be expected to enhance the precipitation propensity of antibodies. Screening on antibody concentration was performed using a reduced range of salt concentration based on the observations made in section 3.3. The precipitation reactions were fixed at pH 7 and performed at ambient temperature. The antibody concentration in the precipitation mixtures was varied between 0.5 and 15 g/L. The upper concentration limit was selected as to be representative of the antibody titres currently achievable in industrial processes (Kim, Kim and Lee, 2012).

Figure 3-6 to Figure 3-8 show the effect of the final antibody concentration in suspension on the precipitation profile as a function of ammonium sulphate, sodium sulphate and sodium citrate concentration, respectively. It can be seen that an increase in the final antibody concentration has a major effect on the precipitation profiles. By increasing the amount of antibody, the precipitant requirement is reduced to provide the same performance. Similarly to section 3.3, the precipitation midpoints were plotted as a log function of the IgG₄ concentration as shown in Figure 3-9. The data show that increasing the antibody concentration 30-fold (0.5 to 15 g/L) decreases the precipitation midpoint by 0.2, 0.27 and 0.325 M for sodium citrate, sodium sulphate and ammonium sulphate, respectively. As the antibody concentration continues to increase up to 15 g/L, the differences in salt concentrations to provide similar precipitation become less significant. This finding is useful as it highlights the benefit of employing salt precipitation for highly concentrated protein solutions. As precipitation scales with volume, starting with a high protein concentration reduces the amount of precipitant required and overall reduces the process volume. This becomes more manageable for large scale applications.

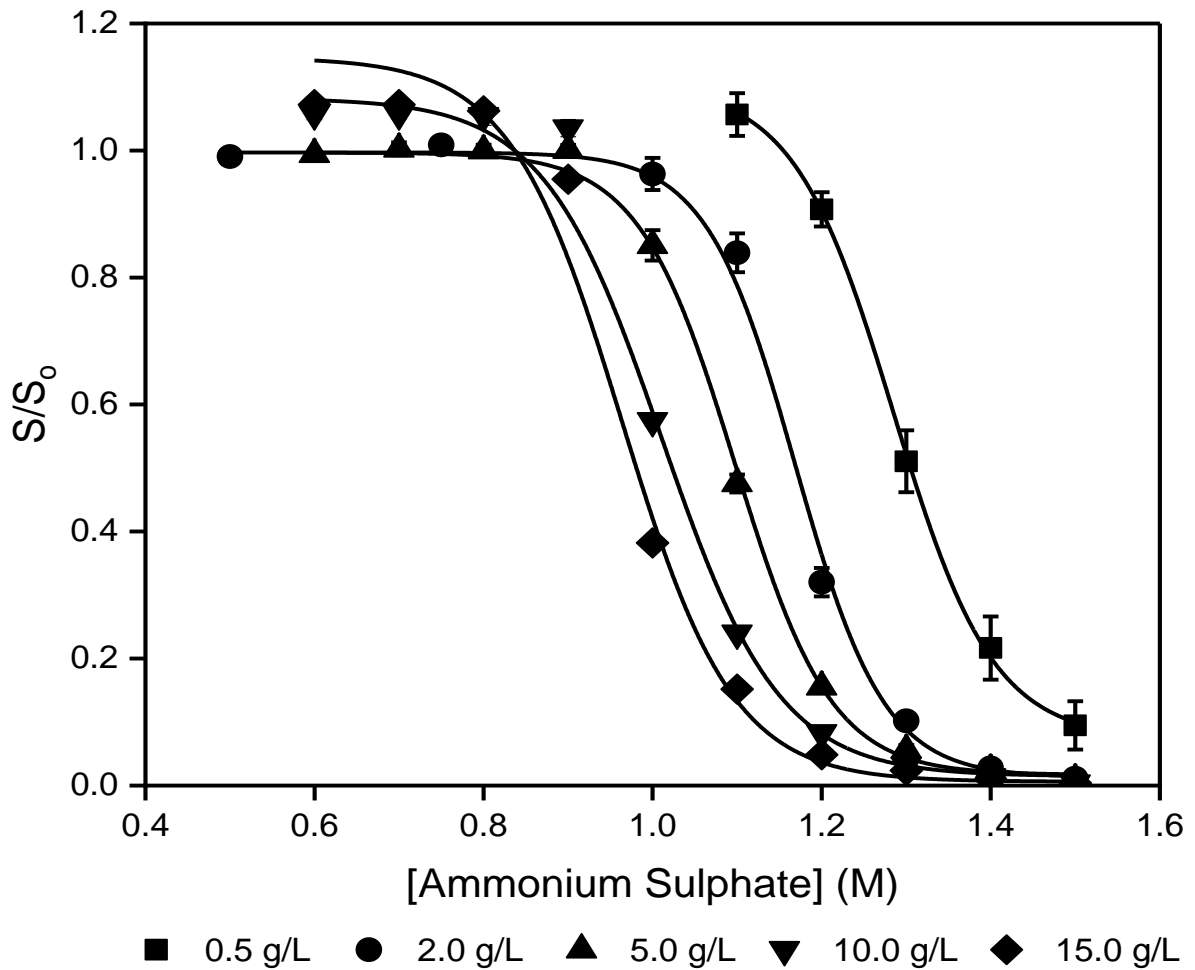


Figure 3-6. Ammonium sulphate precipitation profiles at various final IgG₄ concentrations. Precipitations were carried out in 2 mL V-bottomed 96-deepwell plates at 1.5 mL working volume with initial mixing performed with manual pipetting of antibody feed into various ammonium sulphate concentrations to the desired target final antibody concentration in the range 0.5 to 15 g/L. This was followed by orbital mixing at 1000 rpm for 1 hour and subsequent centrifugation at 4000 rpm for 45 mins at room temperature. The upper layer was withdrawn and measured for non-precipitated antibody. Average solubility values are displayed from n = 3 experiments with one standard deviation around the mean.

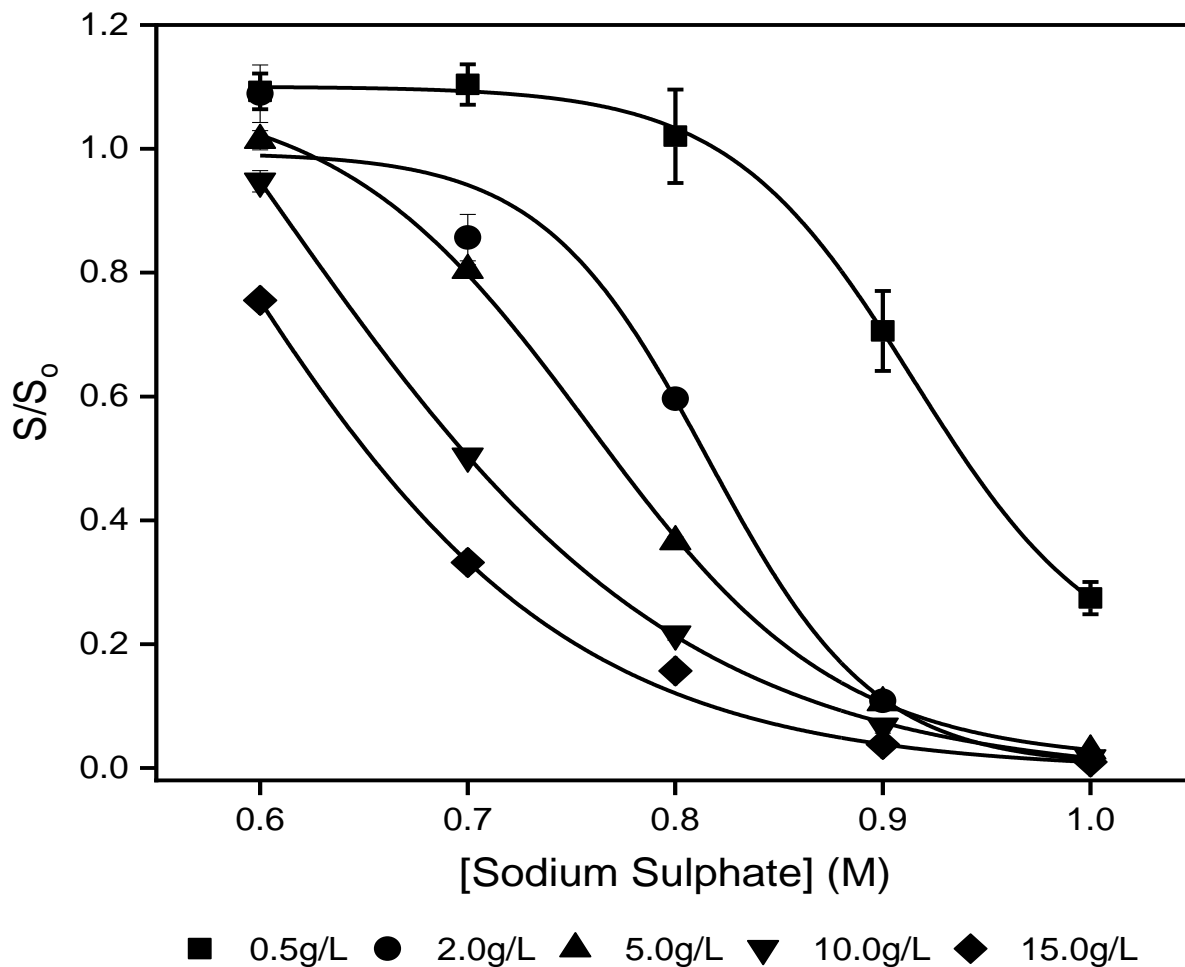


Figure 3-7. Sodium sulphate precipitation profiles at various final IgG₄ concentrations. Precipitations were carried out in 2 mL V-bottomed 96-deepwell plates at 1.5 mL working volume with initial mixing performed with manual pipetting of antibody feed into various sodium sulphate concentrations to the desired target final antibody concentration in the range 0.5 to 15 g/L. This was followed by orbital mixing at 1000 rpm for 1 hour and subsequent centrifugation at 4000 rpm for 45 mins at room temperature. The upper layer was withdrawn and measured for non-precipitated antibody. Average solubility values are displayed from n = 3 experiments with one standard deviation around the mean.

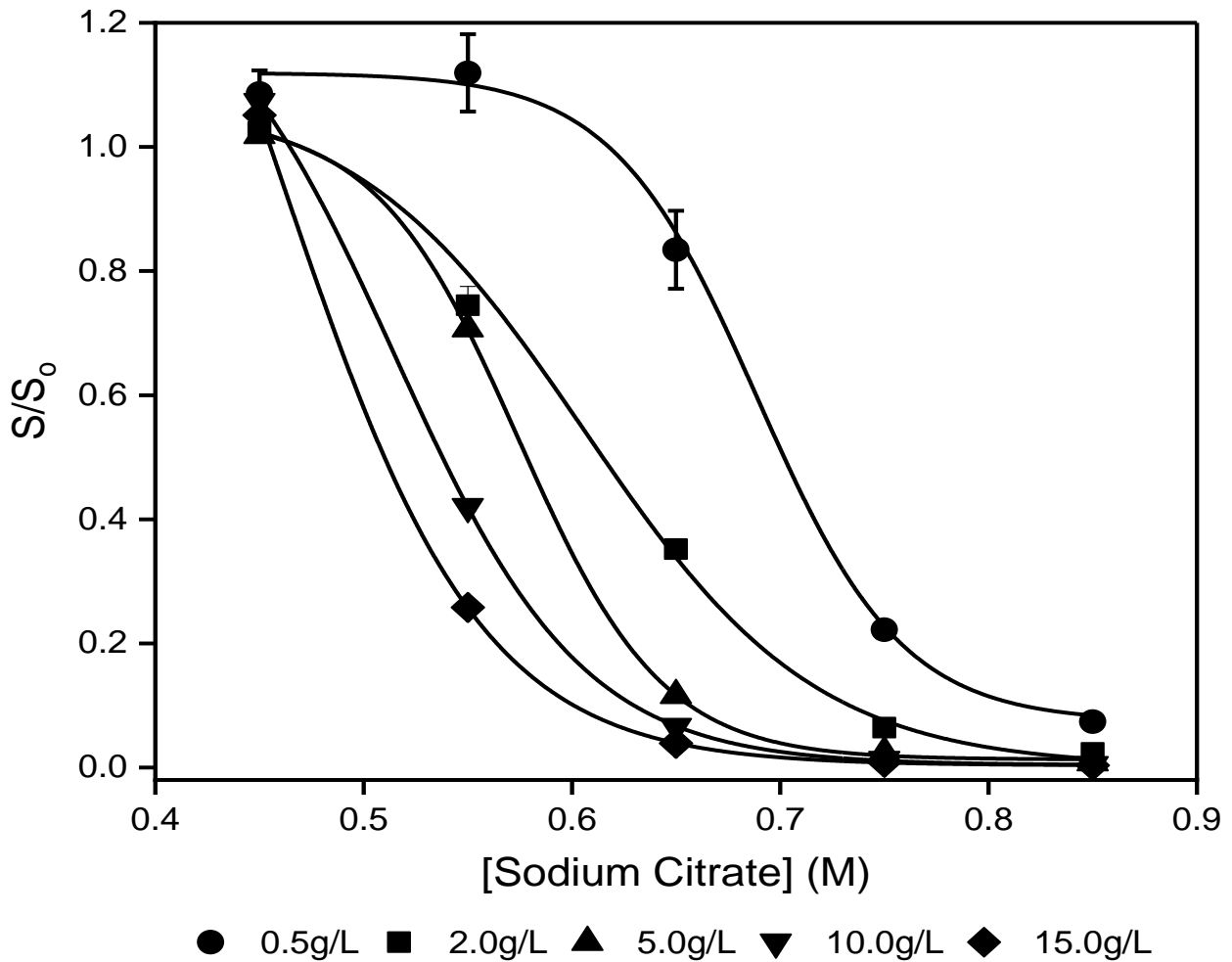


Figure 3-8. Sodium citrate precipitation profiles at various final IgG₄ concentrations. Precipitations were carried out in 2 mL V-bottomed 96-deepwell plates at 1.5 mL working volume with initial mixing performed with manual pipetting of antibody feed into various sodium citrate concentrations to the desired target final antibody concentration in the range 0.5 to 15 g/L. This was followed by orbital mixing at 1000 rpm for 1 hour and subsequent centrifugation at 4000 rpm for 45 mins at room temperature. The upper layer was withdrawn and measured for non-precipitated antibody. Average solubility values are displayed from n = 3 experiments with one standard deviation around the mean.

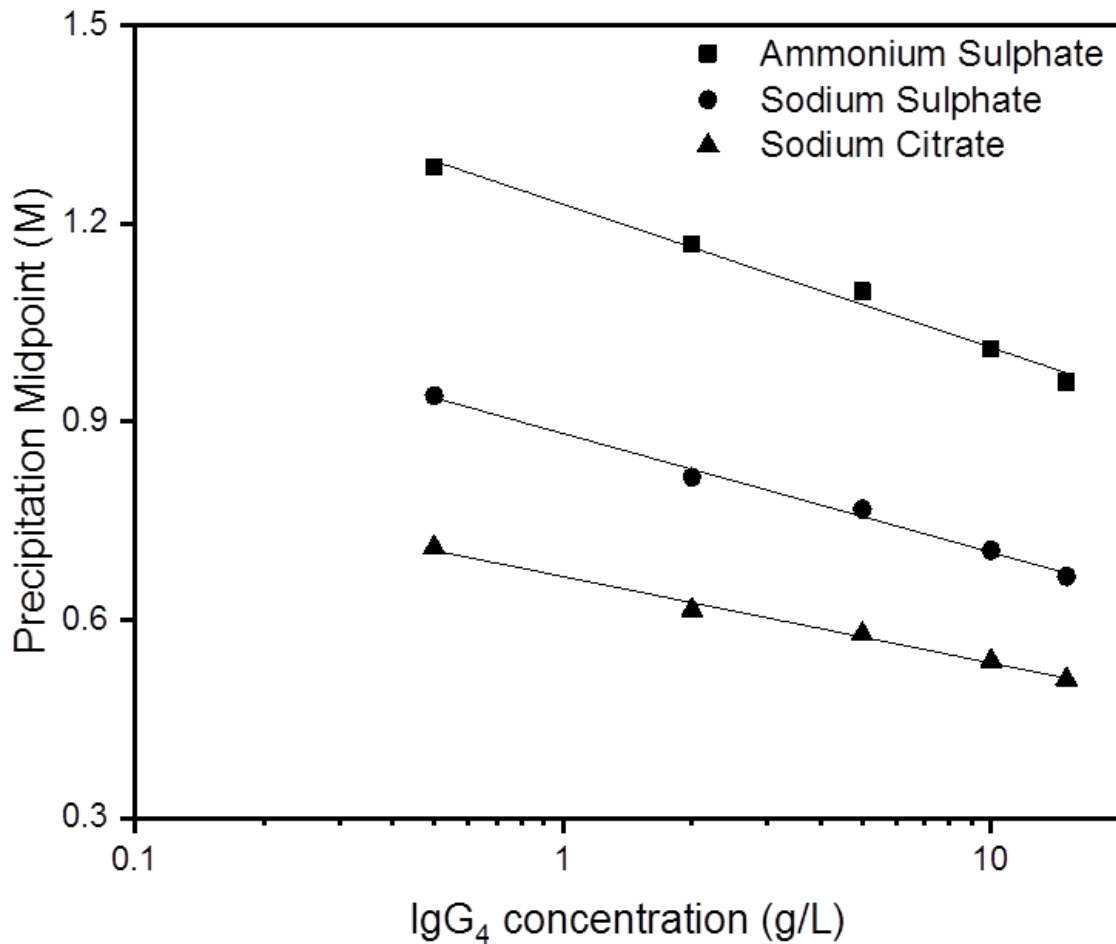


Figure 3-9. Precipitation midpoints for ammonium sulphate, sodium sulphate and sodium citrate precipitation as a function of IgG₄ concentration. Values for the precipitation midpoints were determined using analysis of the sigmoidal-fitted data of the precipitation curves presented in Figures 3-6 to 3-8 Symbols represent an average of each precipitation midpoint against antibody concentration condition tested with error bars showing one standard deviation around the mean. Error bars are sufficiently small such that are difficult to observe with data symbols. A linear fit was applied for appropriate treatment of the data: ammonium sulphate precipitation midpoint = $1.229 - \log [\text{IgG}_4]^{0.217}$, $R^2 = 0.986$; sodium sulphate precipitation midpoint = $0.882 - \log [\text{IgG}_4]^{0.18}$, $R^2 = 0.991$; sodium citrate precipitation midpoint = $0.665 - \log [\text{IgG}_4]^{0.131}$, $R^2 = 0.990$.

3.5 Solubilisation efficiency of purified IgG₄ precipitates

Results in the previous section have demonstrated the efficiency of IgG₄ salting-out with the precipitant candidates tested, with efficiencies near to 100%. Since the precipitate contains the product of interest, it is imperative to address product recoverability with solubilisation. This is particularly important for bioprocess applications in which further downstream processing would be required or during drug formulation (Kurinomaru *et al.*, 2014; Hekmat, 2015). Salt-based precipitations are often reversible which confers an advantage over other methods of precipitation. For instance, poor control of acid-based precipitations often yields precipitates that are difficult to dissolve back into solution (Virkar *et al.*, 1982). Also, it is important to characterise product changes that may occur as a result of the precipitation reaction which may include protein activity, protein structure and increased aggregate levels, all of which are relevant to the development of therapeutics. Dissolving the precipitates in small volumes carries the advantage of reduced process volumes downstream, whilst dissolving the precipitates in high volumes minimises the concentration of residual salts which would need to be removed downstream in the process. To overcome this, buffer exchange systems can be employed; however at the cost of an extra purification step.

3.5.1 Solubilised IgG₄ yields

Precipitations were carried out by combining ammonium sulphate, buffer and purified IgG₄ feedstock to a target IgG₄ concentration of 1 mg/mL and target ammonium sulphate concentration in the range 1.2 – 2 M with pH fixed at 7.0. After mixing and incubation for 1 hour, the precipitates were isolated from 1.5 mL aliquots with centrifugation and re-solubilised in various volumes of sodium phosphate buffer.

The IgG₄ yields upon resolubilisation with various volumes of buffer relative to the initial spun down volume (i.e. 1.5 mL) against ammonium sulphate concentration are displayed as a contour plot in Figure 3-10.

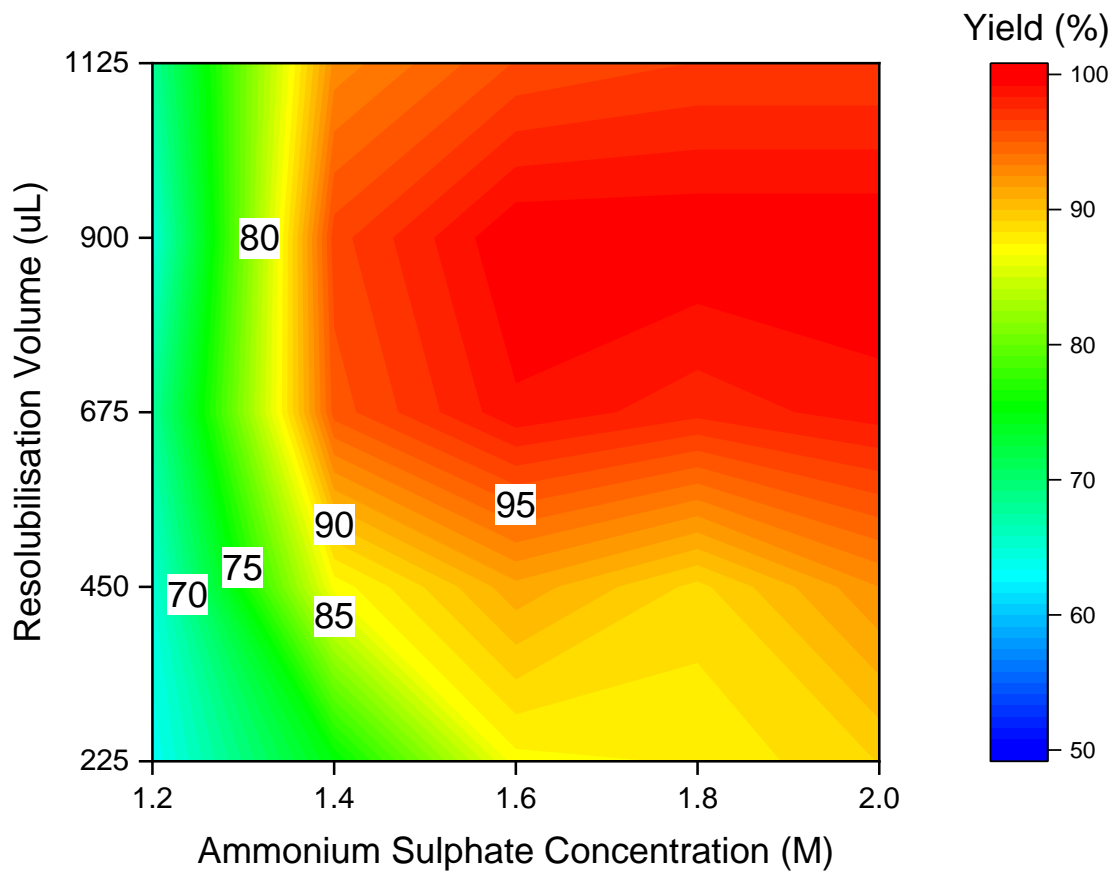


Figure 3-10. Contour plot displaying IgG₄ recoveries at various ammonium sulphate concentrations and resuspension buffer volumes. Precipitations were carried out in 2 mL Eppendorf tubes with 1.5 mL working volume with mixing induced via manual pipetting followed by orbital mixing at 1000 rpm for 1 hour. This was followed by centrifugation at 13000 xg for 20 mins using a fixed angle rotor. Pellets were re-solubilised in various volumes of 50 mM sodium phosphate pH 7.0 Data above has been fitted using least mean squares.

The data was fitted using the method of least mean squares in Origin Pro 2018. IgG₄ precipitations at an ammonium sulphate concentration less than 1.4 M were limited to a maximum yield of 80% upon resuspension with various volumes. Above 1.4 M ammonium sulphate, at least 500 µL (i.e. three tenths of the initial sample volume) was required to achieve IgG₄ yields in the range 90 – 100%. Considering the relative high solubility of the IgG₄ (up to 50 g/L and possibly higher), it was surprising that calculated yields were lower with resuspension volumes less than 500 µL. One explanation for this could be due to inaccuracies in volume determination with smaller resuspension volumes. Also, re-suspending precipitates in small volumes may have required a more extensive mixing regime to ensure no particles were left behind. One method to ensure that all the precipitate particles have been dissolved back into solution is by means of turbidity measurements. However, this requires a few millilitres of sample to provide reliable measurements. Another useful method is by means of comparing particle size measurements between pre and post-precipitated and re-solubilised precipitate measurements. These methods were not employed for this part of the study but are discussed in a later section which addresses IgG₄ precipitation from process relevant cell culture fluid.

3.5.2 Impact of precipitation on antibody structure and aggregate levels

In another set of experiments, the same precipitation methodology was performed with the precipitate re-dissolved in buffer back up to 1 mg/mL. This concentration was chosen to facilitate structural analysis using size-exclusion HPLC and circular dichroism (CD), given the concentration limits posed by each method. Figure 3-11 overlays the monomer and aggregate profiles of IgG₄ before and after ammonium sulphate precipitation, whilst Figure 3-12 overlays the secondary structure profile of the equivalent samples. A small change in the SEC profile can be observed between precipitated and non-precipitated samples with the precipitated samples showing at most an increase of 0.7% in high molecular weight species and a decrease in 0.4% in IgG₄ monomer. Provided that HMWS should be maintained below 5%, according to target specifications set by the regulatory authorities, the ammonium sulphate precipitation did not appear to compromise product quality. Figure 3-12 shows expected antibody CD signals which are characteristic of primarily B-sheet-based proteins. A negative control was performed using 50 mM sodium phosphate pH 7 buffer (the buffer matrix of the protein samples) to form a baseline measurement. This ensured that the observed signals from the sample measurements were not due to noise. The almost perfectly aligned CD signal between both samples indicates that ammonium sulphate

precipitation did not impact the antibody secondary structure. This finding was not surprising as ammonium sulphate is known to be an effective stabilizer for proteins.

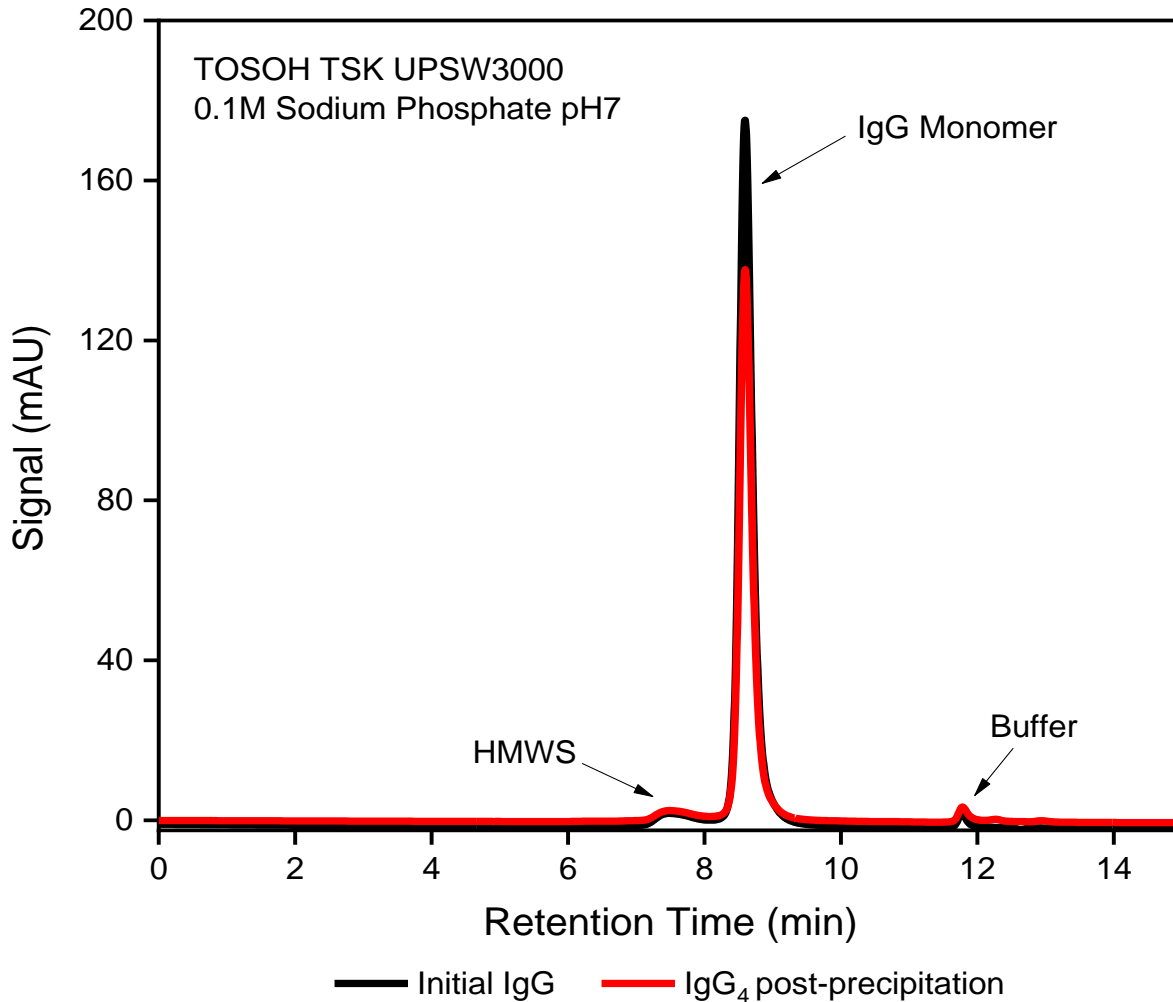


Figure 3-11. SEC-HPLC profiles of IgG₄ before and after ammonium sulphate precipitation at 1.5 mL scale. The precipitate was re-solubilised with 100 mM sodium phosphate buffer to a target antibody concentration of 1 mg/mL for analysis. Samples were run on a TSKgel UP-SW3000, 2 µm particle size, 4.6 mm ID x 30 cm SEC column (Tosoh Biosciences) with guard column, at 0.3 mL/min flow rate with 0.1 M sodium phosphate pH 6.7 as the running buffer.

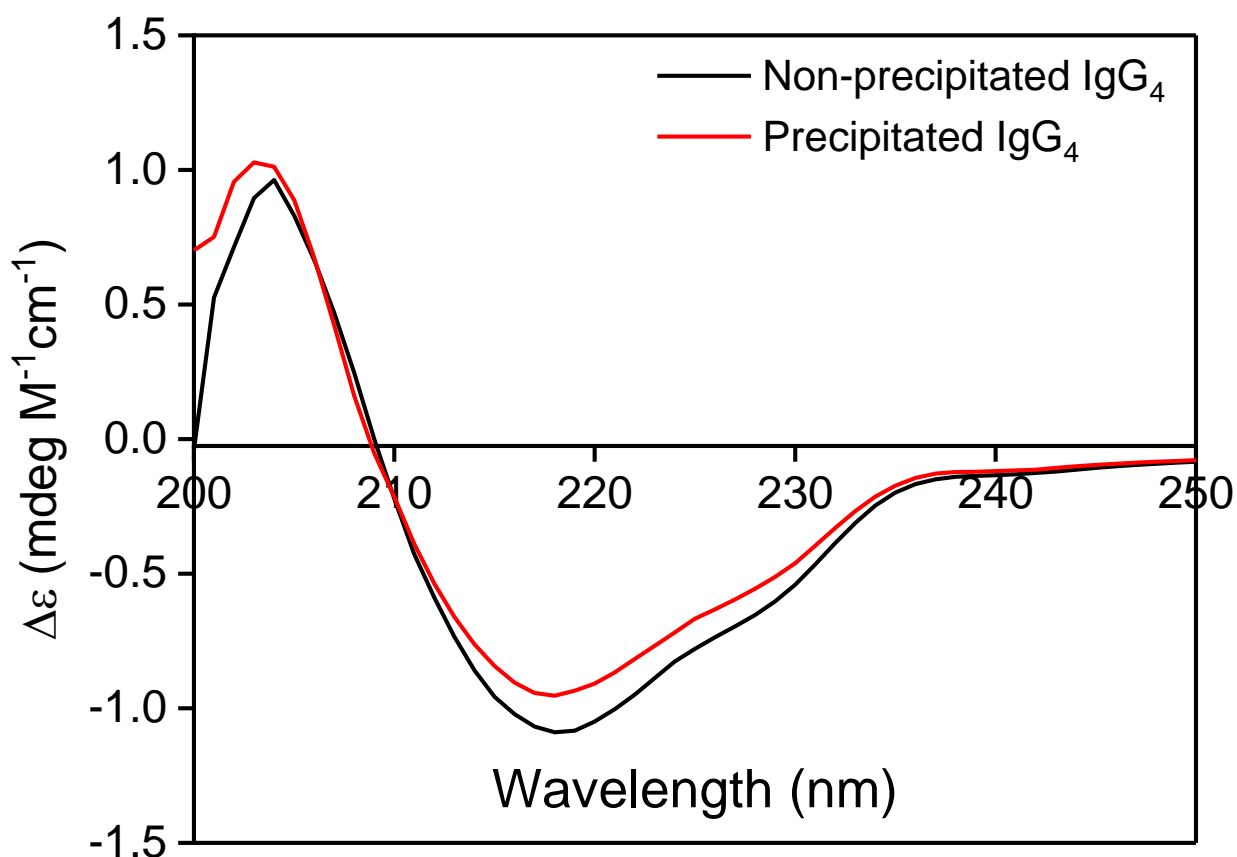


Figure 3-12. CD spectra overlay of Protein-A purified IgG₄ before (*black*) and after precipitation (*red*) in the wavelength range from 200 to 250 nm using an antibody concentration of 0.8 mg/mL. Antibody molar ellipticity is expressed in terms of delta epsilon units as an average of three separate CD scans for each sample. Negative bands at 208 and 222 nm correspond to α -helix; a negative band at 218 nm corresponds to β -sheet and positive bands at 212 nm correspond to random coils.

3.6 IgG₄ precipitation from cell culture fluid

Whilst salt precipitation has been well-characterised with the purified IgG₄ model, the question lies whether the results demonstrated previously translate to IgG₄ precipitation from cell culture supernatant. Indeed, precipitation may behave differently owing to the complexity of the feed mixture which contains many additional components (e.g. HCPs, DNA, lipids and other cellular-based components).

As all three salts tested during the purified IgG₄ precipitation studies showed promising results, the same salts were tested on cell culture fluid with an IgG₄ titre of 1.4 g/L, as determined by PrG-HPLC. Cell culture fluid precipitations were carried out with the same methodology as previously employed, with a final antibody concentration of 0.5 g/L. Due to the presence of interfering species, antibody content in the soluble fractions would be overestimated using UV-Vis spectroscopy measurements. For accurate quantification of antibody concentrations, PrG-HPLC was applied instead. Using a standard curve of purified antibody with various known concentrations, unknown antibody content in samples could be determined by means of linear regression.

3.6.1 Effect of salts on IgG₄ precipitation and recovery

A set of precipitation experiments were performed on cell culture supernatant IgG₄ with ammonium sulphate, sodium sulphate and sodium citrate at 0.5 g/L final antibody concentration and at ambient temperature. The precipitation profiles were compared with those from the purified feedstock models. Figure 3-13 provides an overlay of the precipitation profiles with ammonium sulphate at pH 7 in which these were observed to be comparable. At most the precipitation midpoints differed by 100 mM ammonium sulphate. The slightly higher demand for ammonium sulphate in the crude system to precipitate the same amount of antibody may be attributed to an increase in the stabilisation of the feed components that influence antibody solubility.

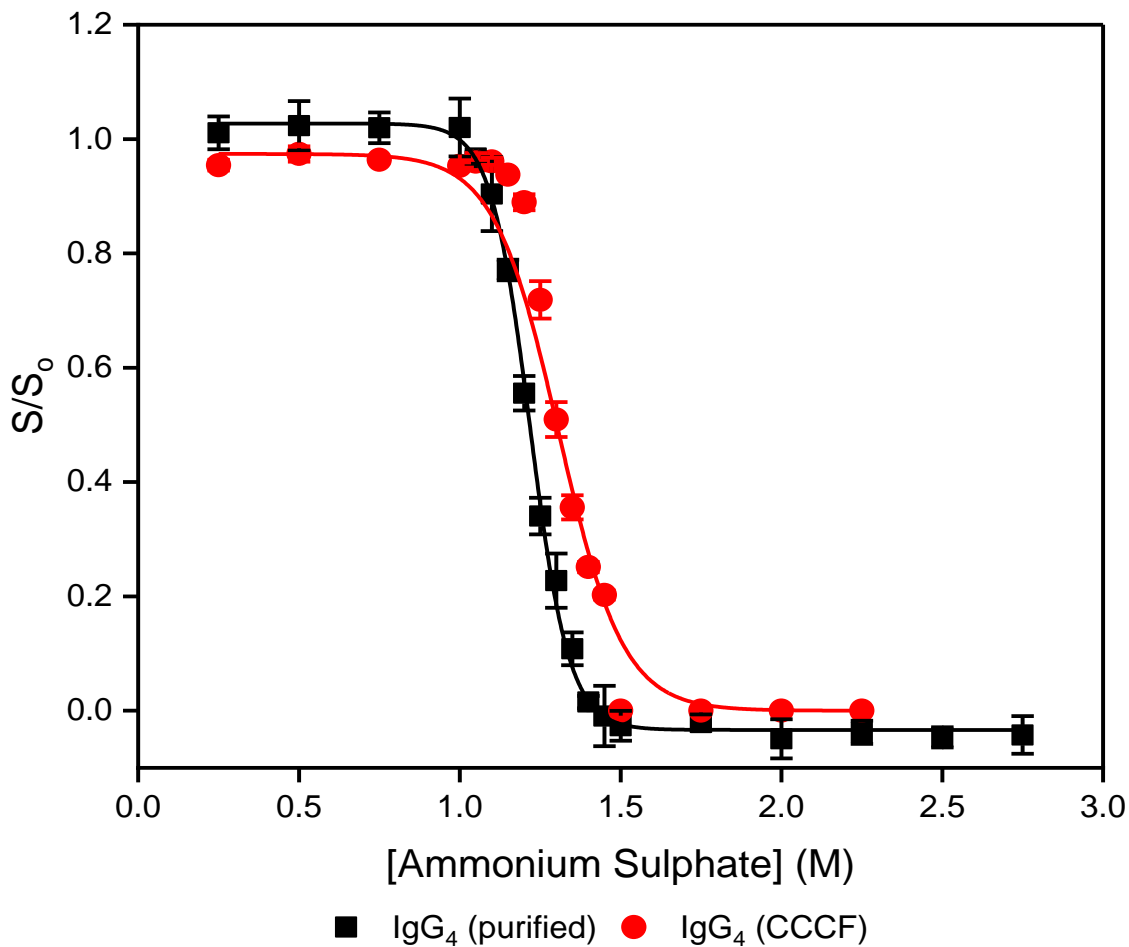


Figure 3-13. Comparison of IgG₄ precipitation profiles with ammonium sulphate between purified and cell culture supernatant feedstock. Precipitations were carried out in 2 mL V-bottomed 96-deepwell plates at 1.5 mL working volume with initial mixing performed with manual pipetting of antibody feed into various sodium sulphate concentrations to a target final antibody concentration of 0.5 mg/mL. This was followed by orbital mixing at 1000 rpm for up to an hour and subsequent centrifugation at 4000 rpm for 45 mins at room temperature. The upper layer was withdrawn and measured for non-precipitated antibody. Soluble fractions of precipitated purified antibody were analysed with absorbance at 280 nm, whilst the soluble fractions of precipitated antibody in cell culture fluid were analysed with affinity HPLC. Average solubility values are displayed from n = 3 experiments with one standard deviation around the mean.

The solubility plots for sodium sulphate and sodium citrate precipitation are not shown because of the separation challenge that was encountered during centrifugal recovery. Where precipitates formed in the presence of ammonium sulphate settled to the bottom of the wells, those formed during sodium sulphate and sodium citrate precipitation did not. Instead, the precipitates either rose to the surface of the mother liquor in the form of an upper layer or formed clumps in suspension. This therefore made it difficult to isolate the soluble fraction without disturbing the precipitate. To confirm this behaviour, a series of precipitation reactions were carried out in 50 mL falcon tubes with a working volume of 40 mL. Mixing of the solutions was achieved with an overhead impeller at 300 rpm. Figure 3-14 demonstrates the visual recoverability of the precipitates upon centrifugation. As in the micro-well plate format, the protein precipitate from 1.5 M ammonium sulphate precipitation settled effectively to the base of the suspension. In the case of 0.9 M sodium citrate, the precipitate localised to the surface and to one side of the tube wall. For sodium sulphate precipitation at 1.1 M, the precipitate was randomly distributed across the suspension and the supernatant was distinctly more turbid.

AS Precipitation

SC Precipitation

SS Precipitation

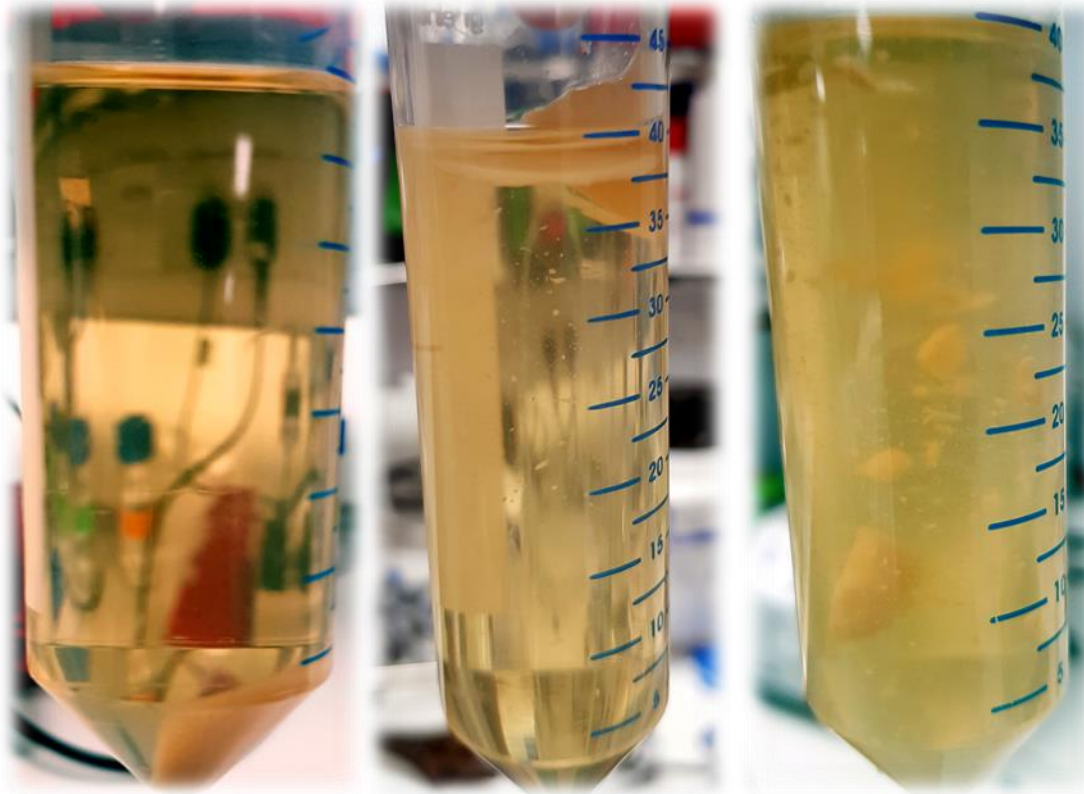


Figure 3-14. Visualisation of CCCF precipitates with ammonium sulphate (AS), sodium citrate (SC) and sodium sulphate (SS) precipitation after centrifugal recovery. Precipitations were carried out in 50 mL falcon tubes with a 40 mL working volume. Precipitants were introduced to cell culture fluid with stirring at 300 rpm with a Rushton turbine for 1 hour at room temperature. Precipitate separation was conducted by centrifuging falcons at 13000 x g for 30 mins.

Figure 3-15 compares the particle size distribution (PSD) profiles for each of the precipitation systems. Despite the differences observed in the PSD, 90% of the particles would have been expected to settle successfully given that d_{10} was above 2 μm . This therefore suggests that the inefficiency to separate the precipitate from the mother liquor could be attributed to density. Some components in cell culture fluid, including lipids, are known to exhibit relatively low densities and, when precipitated, may cause an adverse effect on the settling behaviour of particles. Precipitates may also float due to the salting-out of dissolved gas. Since this was not observed for the salting-out of Protein A purified IgG₄ with the same salts, the behaviour was more likely due to the presence of lipids. Despite the disappointing centrifugal recovery, if indeed lipids were removed by the effect on precipitation, this could have proven advantageous for minimising lipid effects on column fouling.

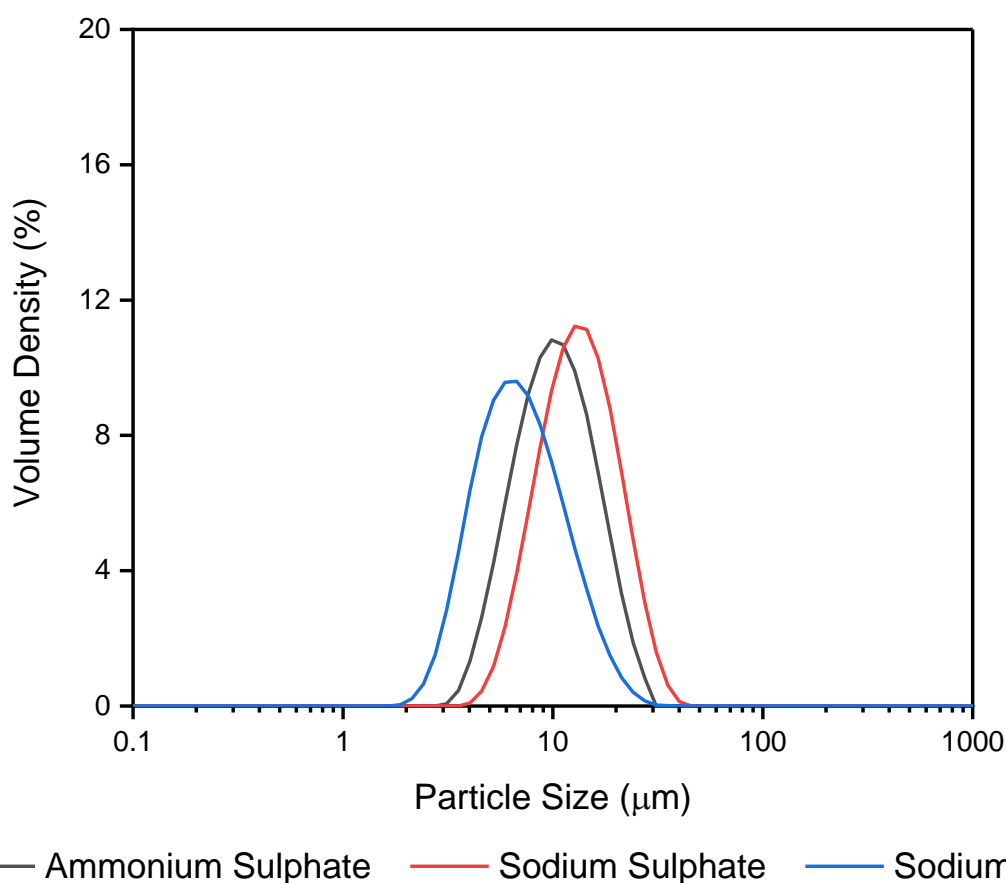


Figure 3-15. Particle size distribution profiles of CCCF precipitates with ammonium sulphate, sodium sulphate and sodium citrate precipitation at 40 mL scale. Distributions are presented as technical averages of five individual particle size measurements. Sample refractive and absorption indices: 1.59, 0; dispersant refractive indices: 1.37 – 1.38; stirrer speed: 1500 rpm; laser obscuration: minimum 10%, maximum 20%; weighted residual : <1%; COV: < 5%.

Alternatively, precipitates could be recovered from suspension via filtration; however this would have required an enormous quantity of filters given the number of experiments carried out, which in turn significantly reduces the experimental throughput. Furthermore, recovery of the captured precipitate would involve feeding a set amount of buffer through the filter and allowing time for re-solubilisation. Otherwise various flushes could be performed at the expense of a diluted filtrate. Whilst both options are feasible, these would not be appropriate for a high-throughput screening strategy.

It would have been interesting to further investigate and characterise the differences between precipitates to show how this could influence recoverability. Methods such as Fourier-transform infrared (FTIR) spectroscopy could provide information on precipitate composition and identify interfering materials. Alternatively, sucrose gradient ultracentrifugation could be applied to separate particle populations with different densities. This works by applying the sample through a sucrose gradient and particles of different densities will settle across different layers that align with the same density of sugar. Once the particles are separated, sugar fractions are withdrawn and analysed with a refractometer.

Ammonium sulphate was selected as the model precipitant for future studies outlined in the scope of the thesis as a reduced level of precipitant was required to maximise IgG₄ precipitation, is a good protein stabiliser, and more importantly, enabled efficient centrifugal clarification.

3.7 IgG₄ precipitation kinetics

In the previous experiments, precipitation reactions were allowed to incubate for a minimum of one hour in order to ensure equilibrium despite observing instantaneous precipitation. In order to determine the 'true' equilibrium for IgG₄ precipitation, a precipitation was performed by combining CCCF, diluent and ammonium sulphate solution to a target ammonium sulphate concentration of 1.5 M and 1 mg/mL IgG₄ with the solution maintained at pH 7. Ammonium sulphate was introduced in bolus whilst mixing was performed at 300 rpm with an overhead stirrer. Samples of the suspension were withdrawn at various time points up to 1 hour and subsequently filtered through 0.22 µm PES syringe filters to determine IgG₄ solubility as a function of residence time.

In addition to antibody solubility, particle size measurements using either dynamic light scattering (DLS) or laser diffraction were also performed. As a control, the particle size distribution of the non-precipitated cell culture supernatant, determined by DLS, is shown in Figure 3-18 which displays a particle size distribution in the range 7.9 and 350 nm. Analysis of precipitate particle sizes with DLS was not possible owing to the presence of particles with sizes exceeding the upper range detected by the method. This was also confirmed by performing a precipitation titration experiment in which ammonium sulphate was added to the feed in 0.125 M increments up to 1.5 M, with measurements taken at each of the intervals. A gradual shift in the size distribution was observed towards the upper range as the salt concentration increased. Upon reaching the upper range of the salt concentration, the quality of the data from DLS was poor. For this reason, laser diffraction with the Malvern Mastersizer 3000 was employed, enabling the identification of particle sizes above 1 μm .

The precipitation was repeated with precipitate analysis performed with laser diffraction. The effect of incubation or residence time on the solubility of IgG₄ and precipitate particle size using ammonium-sulphate driven precipitation of cell culture supernatant is shown in Figure 3-16. The data shows that precipitation was complete within the first minute of precipitant addition. Also, the average particle size is maintained at $5.2 \pm 0.3 \mu\text{m}$ over the course of 1 hour. This implies that the precipitation is a very rapid process. This contrasts with some of the earlier work performed with other protein precipitation systems in which complete precipitation occurs over much longer periods (Madhusudhan, Raghavarao and Nene, 2008). However, recent studies concerning the development of antibody precipitation processes have also shown similarly rapid kinetics using PEG and ethanol as precipitating agents (Kuczewski *et al.*, 2010; Hammerschmidt *et al.*, 2015; Hammerschmidt, Hobiger and Jungbauer, 2016).

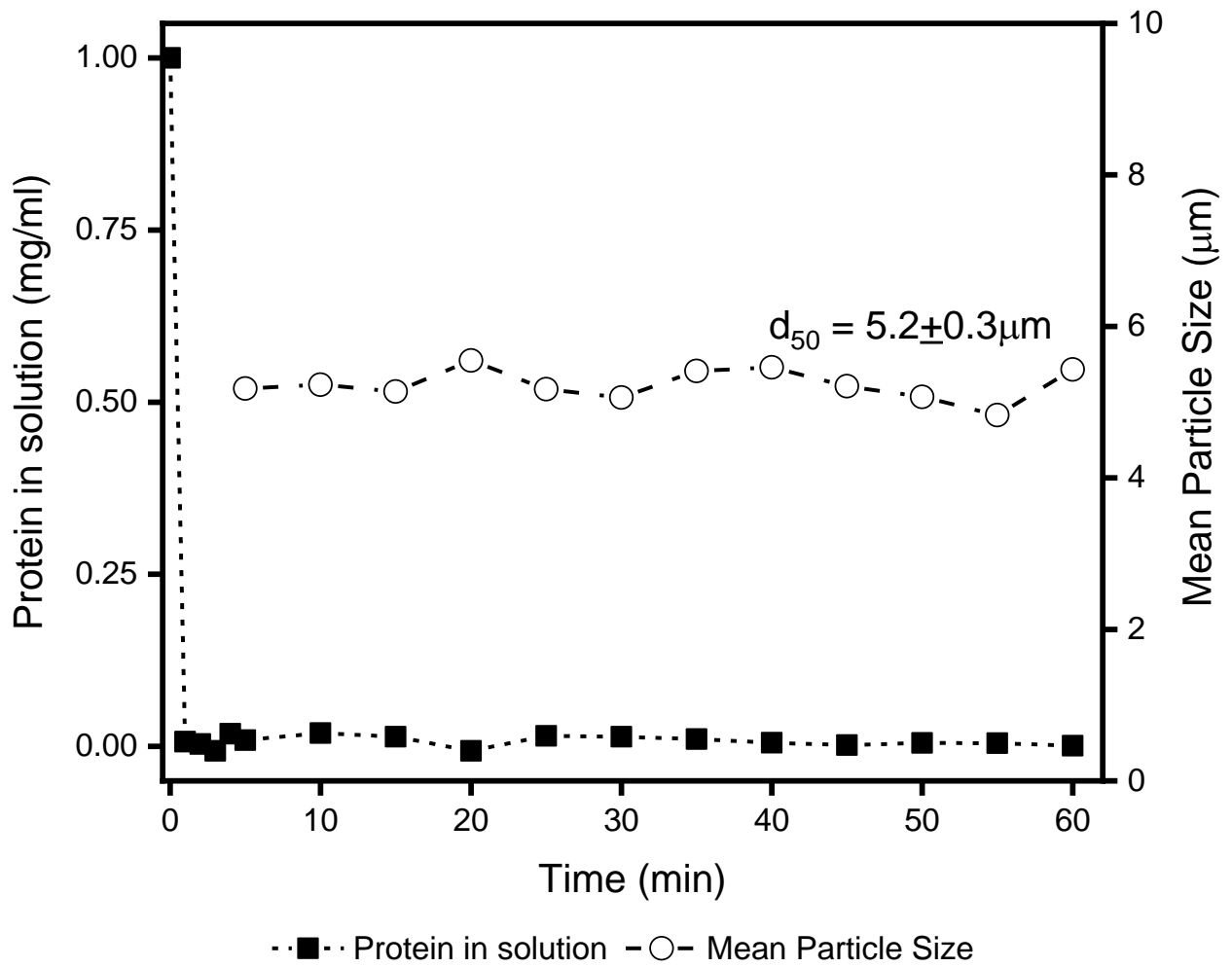


Figure 3-16. Kinetics of antibody precipitation with ammonium sulphate. Solubility of protein and average particle size, as determined by laser diffraction, is represented as a function of time up to 60 mins. Precipitation was performed in a 40 mL fully-baffled beaker with stirring at 300 rpm. The technical average d_{50} values from five individual particle size measurements are plotted.

3.8 Re-solubilisation efficiency of CCCF precipitates

The solubilisation of precipitates formed from precipitating cell culture fluid was investigated in a similar way to that of purified IgG₄ precipitations as described in section 3.5. A more detailed analysis of the re-solubilised precipitates was performed. The efficiency of re-solubilisation with various buffers commonly used for chromatography loading conditions was also tested.

A 50 mL precipitation as described in section 3.6 was performed. After approximately 10 mins of mixing, 1 mL aliquots were spun down and the precipitates were re-solubilised with various buffers using 1 in 2, 1 in 3, 1 in 4 and 1 in 8 volume ratios with respect to the initial precipitate suspension volume. This corresponded to a solubilisation volume range of 125 to 500 μ L. The antibody yields upon re-solubilisation are summarised in Figure 3-17. In all cases, antibody yields were comparable (>90%) which demonstrates the wide range of buffers that can be used during recovery. Provided the solubility limit is not exceeded, higher protein concentrations could be achieved. This could have been tested; however samples of very low volume would have been generated and would be insufficient for analyses.

As shown in Figure 3-18, DLS on the clarified cell culture fluid and the resolubilised precipitate revealed wide and polydisperse particle size distributions with particles ranging in size ~10 to 300 nm. Koehler and colleagues observed a similar PSD for clarified CHO cell culture harvested for the purification of a tocilizumab biosimilar (Koehler *et al.*, 2019). The polydispersity of the clarified cell culture sample is characteristic of the diverse mixture of components such as HCPs, host cell DNA, and the target protein. A similarly diverse mixture appears to be present in the resolubilised precipitate which indicated that the same components become precipitated and re-solubilised. The peak centred around 12-15 nm is consistent with the sizes of protein-based species, including mAbs, whilst the peak centred around 80 nm might be characteristic of chromatin-based species (Koehler *et al.*, 2019) . This was also corroborated by OD₆₀₀ measurements between both samples, as well as against a particle-free buffer solution

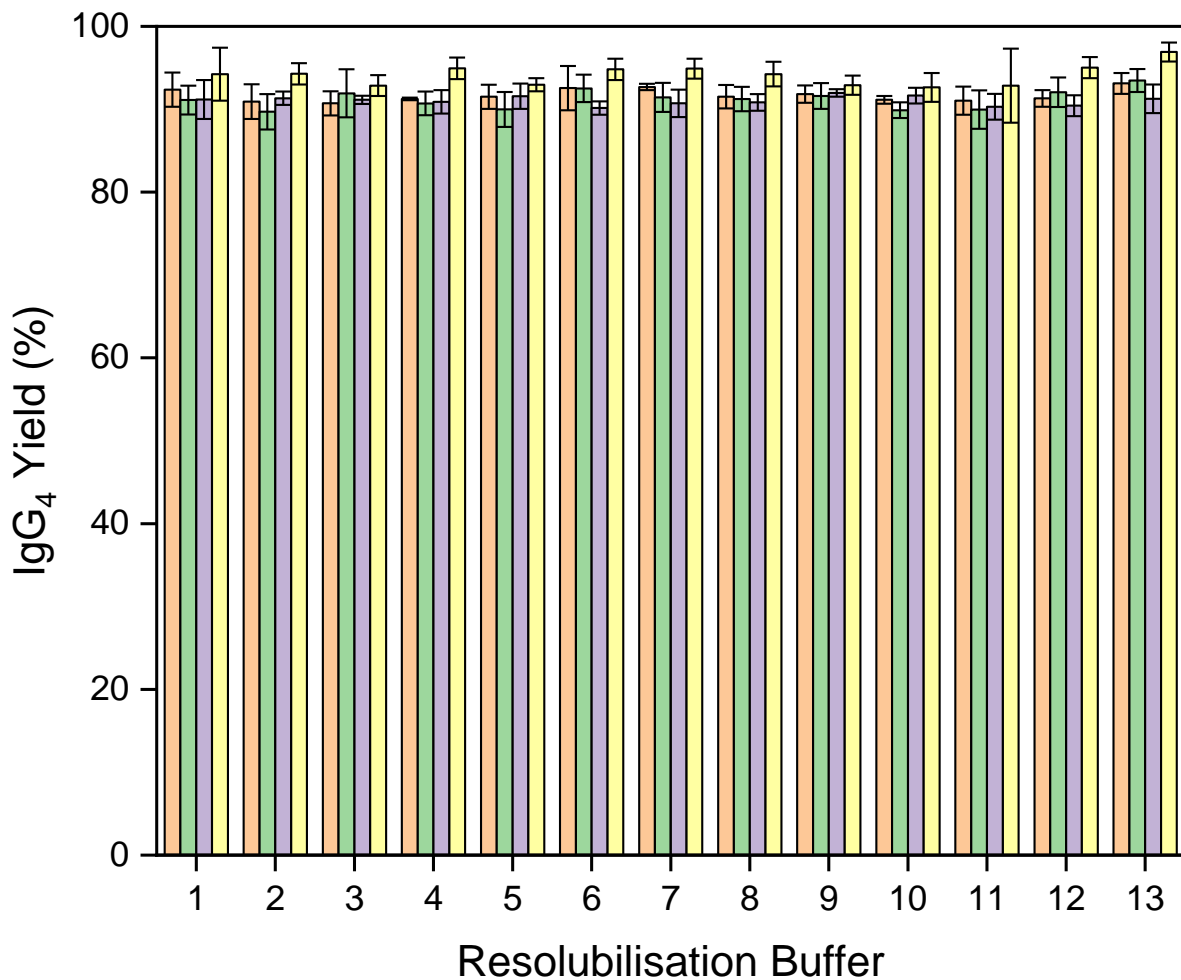


Figure 3-17. Antibody yields upon re-solubilisation with various buffers and buffer volumes with respect to the initial starting volume. Orange - 1 in 2, green - 1 in 3, purple - 1 in 4, yellow - 1 in 8. Precipitation was carried out with a working volume of 40 mL. Key: 1- 50 mM sodium phosphate pH 6; 2 – 50 mM sodium phosphate pH 7; 3 – 50 mM sodium phosphate; 4 – phosphate buffer saline pH 7.4, 5 – 50 mM sodium acetate pH 4, 6 – 50 mM sodium acetate pH5, 7 – 50 mM sodium acetate pH 5.8, 8 – 50 mM Tris-HCl pH 6.9, 9 – 50 mM Tris-HCl pH 8, 10 – 50 mM Tris-HCl pH 9, 11 – 50mM sodium citrate pH 3.5, 12 – 50mM sodium citrate pH 4.5, 13 – 50 mM sodium citrate pH 6.

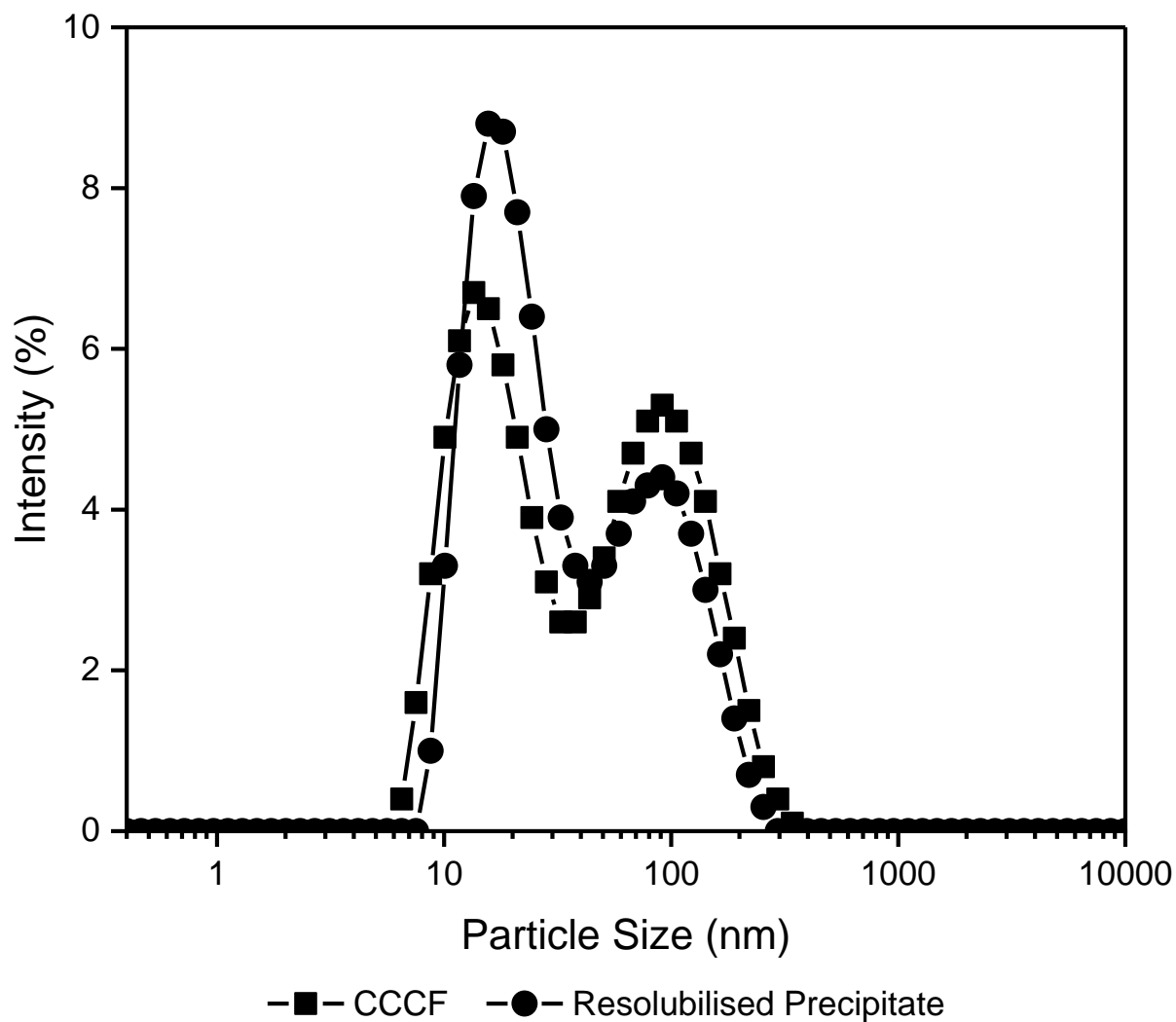


Figure 3-18. Overlay of particle size distribution between clarified cell culture supernatant and re-solubilised precipitate. Curves are displayed as technical averages of triplicate measurements of size intensities by dynamic light scattering.

3.9 Design of Experiments study on cell culture fluid precipitation with ammonium sulphate

In order to identify an operating window based upon key process parameters influencing precipitation performance, a Design of Experiments (DoE) study was conducted using Design Expert 12 software. A full factorial 3 level quadratic DoE was run with 3 replicates of the centre point to detect any curvature in the model. This resulted in 32 total experimental runs. The precipitations were carried out on cell culture fluid in 1 mL Eppendorf tubes. Three factors were selected for the study: ammonium sulphate concentration, pH of the precipitation system and antibody concentration, as depicted in Table 3-2. To adjust the antibody concentration, the cell culture fluid was spiked with purified IgG₄ feed which mitigated the requirement for a concentration step by ultrafiltration.

Table 3-2 Selection of factors and factor levels tested for full factorial DoE study.

Factor	Unit	Low	Mid	High
[Ammonium Sulphate]	M	1.1	1.425	1.75
pH	n/a	6	7	8
[IgG ₄]	g/L	0.5	2.75	5

The response of the study was set to the percentage of IgG₄ recovered from the precipitate which was measured through the PrG-HPLC method. Precipitates were re-dissolved with 500 µL of sodium phosphate buffer. The DoE model was built using a Standard Least Squares approach and included factors that were statistically significant at the 5% significance level ($\alpha = 0.05$). Factors which were not statistically significant were removed from the model in a stepwise approach, with a threshold p-value of 0.05.

Table 3-3 lists the model terms that were identified as statistically significant along with the corresponding coefficient estimates and p-values.

Table 3-3. List of factor terms included in the reduced DoE model for precipitated IgG₄ yield. Coefficient estimate represents the expected change in yield per unit change in the factor value when all other factors are held constant. SE: standard error.

Model Term	Coefficient Estimate (\pm SE)	p-value
[AS]	39.9 (\pm 3.06)	<0.0001
pH	9.5 (\pm 3.06)	0.0045
[IgG ₄]	8.4 (\pm 3.06)	0.0103
[AS] (quadratic)	-26.7(\pm 4.62)	<0.0001

It can be seen that the ammonium sulphate concentration was the most significant factor and contributes the most to the change in precipitated IgG₄ yield as denoted by the high coefficient value. Curvature was detected for this factor as evident from the statistical significance of its quadratic term. pH was the next significant factor, followed by IgG₄ concentration. The coefficient estimates for both factors were similar which indicated that their effects on IgG₄ yield were comparable when either factor is varied whilst the other two factors are held constant. The quadratic model provided a good fit of the data with adjusted and predicted R² values of 0.875 and 0.840, respectively.

The contour plots in Figure 3-19 show that optimum yields for precipitation (i.e. above 90%) are obtained with increasing pH, increasing salt concentration and increasing antibody concentration in suspension. The influence of ammonium sulphate concentration on precipitation yield is notable which is consistent with previous data. The effect of pH shows better precipitation performance at conditions closer to the pI of the antibody. The antibody concentration has a marked effect on the amount of ammonium sulphate required to provide similar performance at low antibody concentrations.

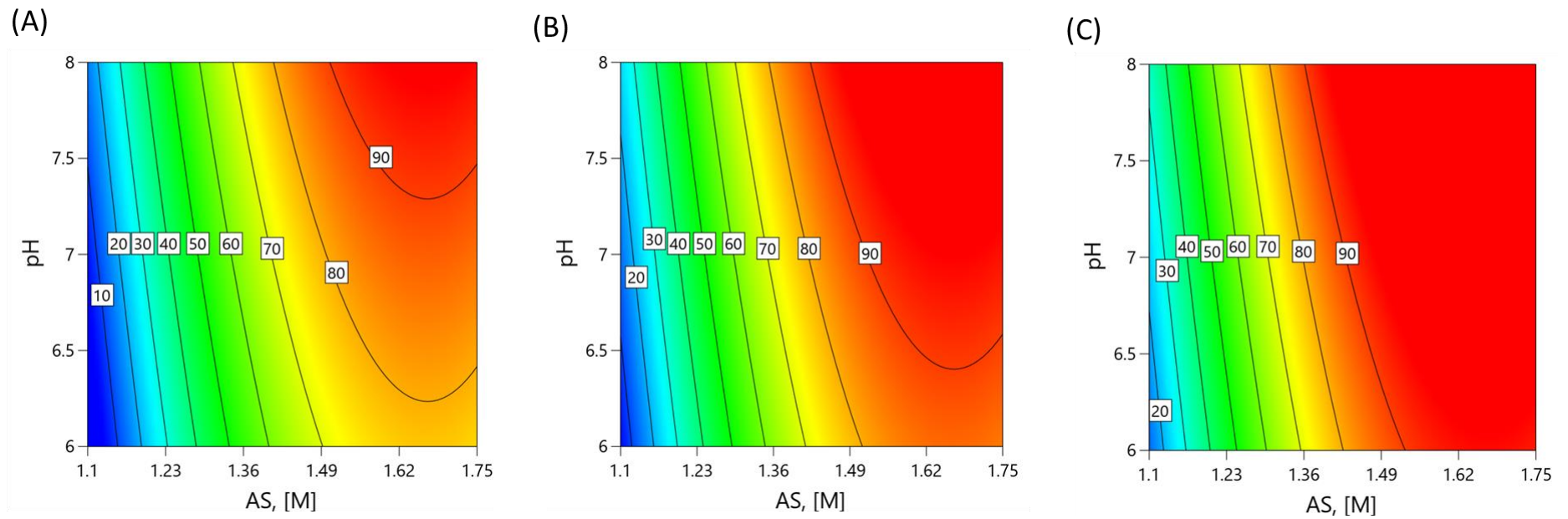


Figure 3-19. Contour plots showing IgG₄ recovery as a function of ammonium sulphate (AS) concentration and pH at (A) 0.5 g/L, (B) 2.75 g/L and (C) 5 g/L IgG₄. Precipitated IgG₄ yield data were fitted using a quadratic model and standard least squares approach. Model Adjusted R²: 0.887, Predicted R²: 0.791.

3.10 Antibody purity with ammonium sulphate precipitation

An important question to address, from a purification standpoint, is whether ammonium sulphate can provide a selective method of precipitation for IgG₄ whilst maintaining the solubility of process-related impurities in the mother liquor which become ultimately discarded. Initially, antibody purity was characterised with affinity-HPLC using a HiTrap PrG column which separates the target antibody molecule from all other components in the sample. This method provided a relative estimate of the level of purification acquired under various precipitation conditions. A more detailed analysis was then performed to quantify more specific impurity populations including DNA and HCPs. The purification factor i.e. the change in antibody purity from cell culture supernatant to that in a precipitated sample, is a good metric in comparing performance between various conditions.

3.10.1 Relative antibody purity upon ammonium sulphate precipitation

One way of estimating the relative purification factor achieved by ammonium sulphate precipitation was performed through the analysis of the PrG-HPLC profiles prior to and after precipitation, as depicted in Figure 3-20. Since PrG has a specific affinity for the Fc region of IgG molecules, most of the impurities which are not antibody related are gathered in the flowthrough fraction, corresponding to the first peak with a characteristic retention time of 0.5 ± 0.2 min. The eluate peak comprising of IgG₄ is detected at 5.8 ± 0.2 min.

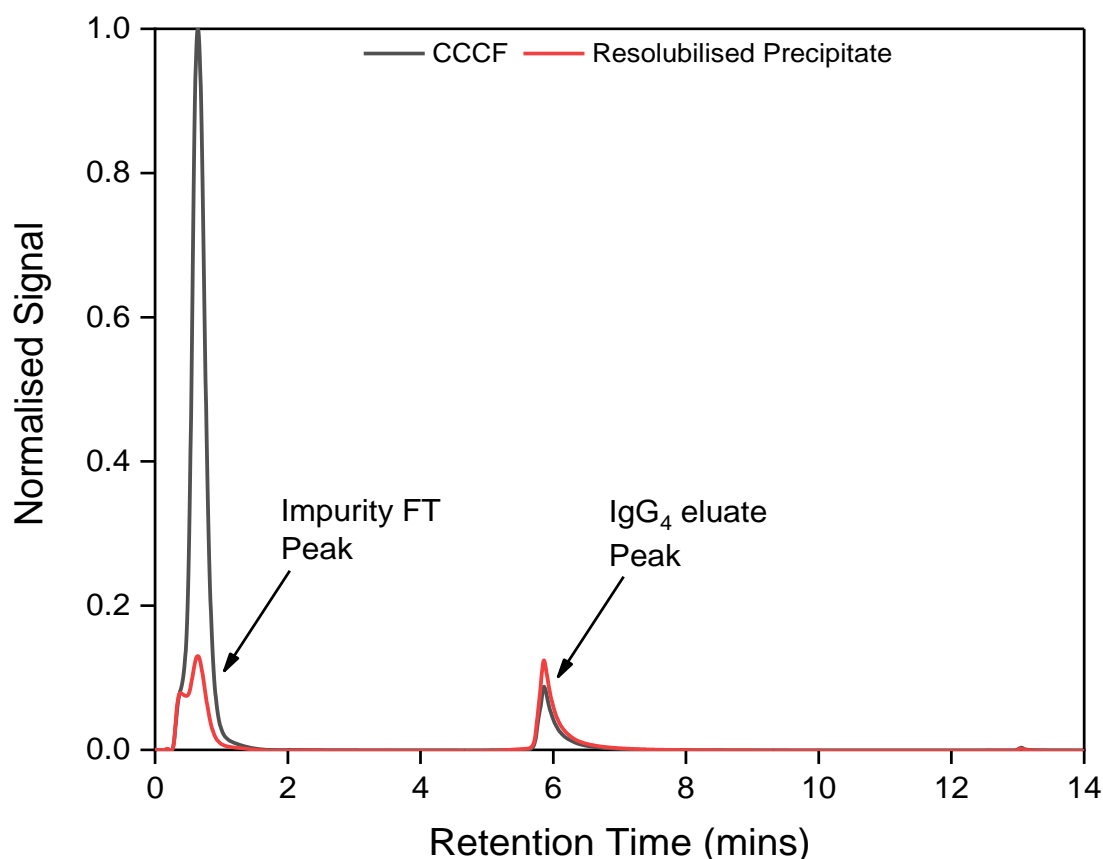


Figure 3-20. Protein G HPLC profile of clarified cell culture fluid (CCCF) and IgG₄ precipitate samples. First peak corresponds to the flow-through fraction of impurities that are unbound to the PrG stationary phase. The second peak corresponds to the presence of antibody in the sample with a characteristic retention time of 5.8 ± 0.2 min.

Post-run analysis with Chemstation software evaluates the area of each peak in terms of an absolute value which can be used to determine protein concentrations against a standard curve as well as a percentage of the sum of the areas of the detected peaks. Assuming the eluate peak primarily comprises IgG₄, the calculated peak area percentage provides an approximation of the relative purity. For the starting cell culture fluid, the IgG₄ purity is approximately 6-7%. Using an antibody concentration precipitation target of 0.5 g/L, the effect of pH and ammonium sulphate concentration on the purification of IgG₄ was investigated. Figure 3-21 shows the purification factors achieved using each of these conditions of which were determined by the ratio of the final purity to the initial purity.

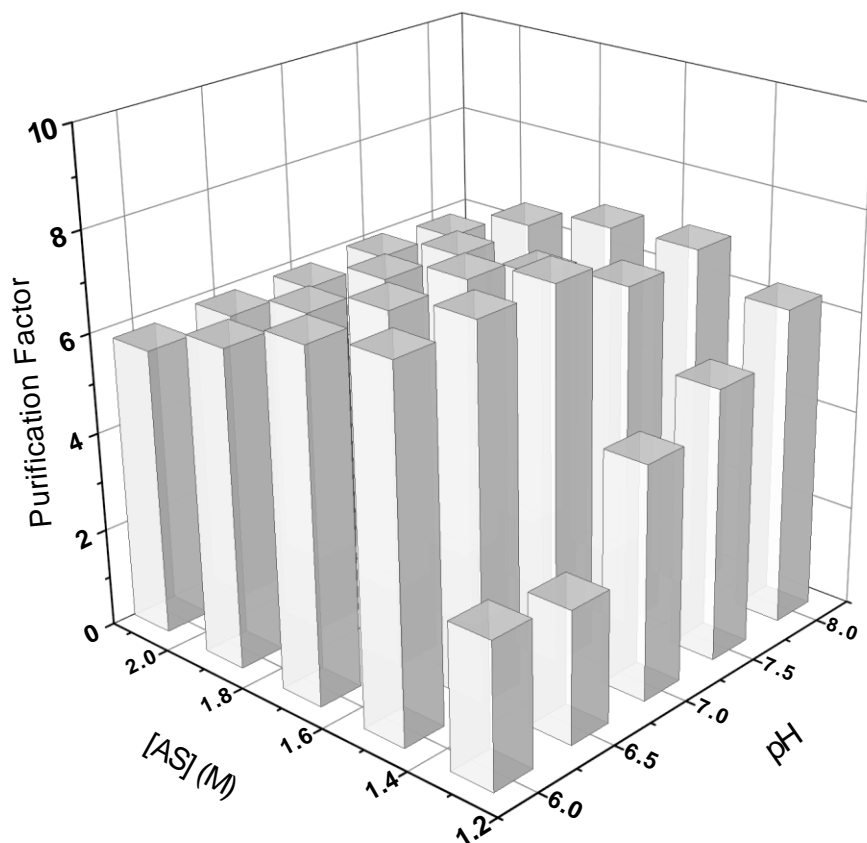


Figure 3-21. Bar plot of the impact of pH and ammonium sulphate (AS) concentration on the purification factors achieved with ammonium sulphate precipitation with a target antibody concentration of 0.5 g/L.

It can be seen that gradual reductions in purity occur as the salt concentration increases beyond 1.5 M which can be justified by increased co-precipitation of impurities. An increase in the pH at salt concentrations equal to or higher than 1.5 M also appeared to reduce the overall purity. Based on these data, the best purity level was obtained at approximately 1.5 M salt at pH 7 with an overall purity level of 47-48%, corresponding to an average purification factor of 7.3. Furthermore, yields obtained under these conditions were always above 90%. Based on these estimations, ammonium sulphate precipitation lacks the ability to purify IgG₄ to the level achievable with PrA chromatography. The protein profile shown in Figure 3-22 from SDS-PAGE supports this when comparing precipitated samples against the PrA-purified reference standard. Indeed, it was expected that impurities would co-precipitate based on the non-selectivity of ammonium sulphate precipitation. If the salt concentration were to increase, the effect of co-precipitation becomes more pronounced. Reduced salt concentrations could be used if the carry-over of impurities was more concerning than antibody yield.

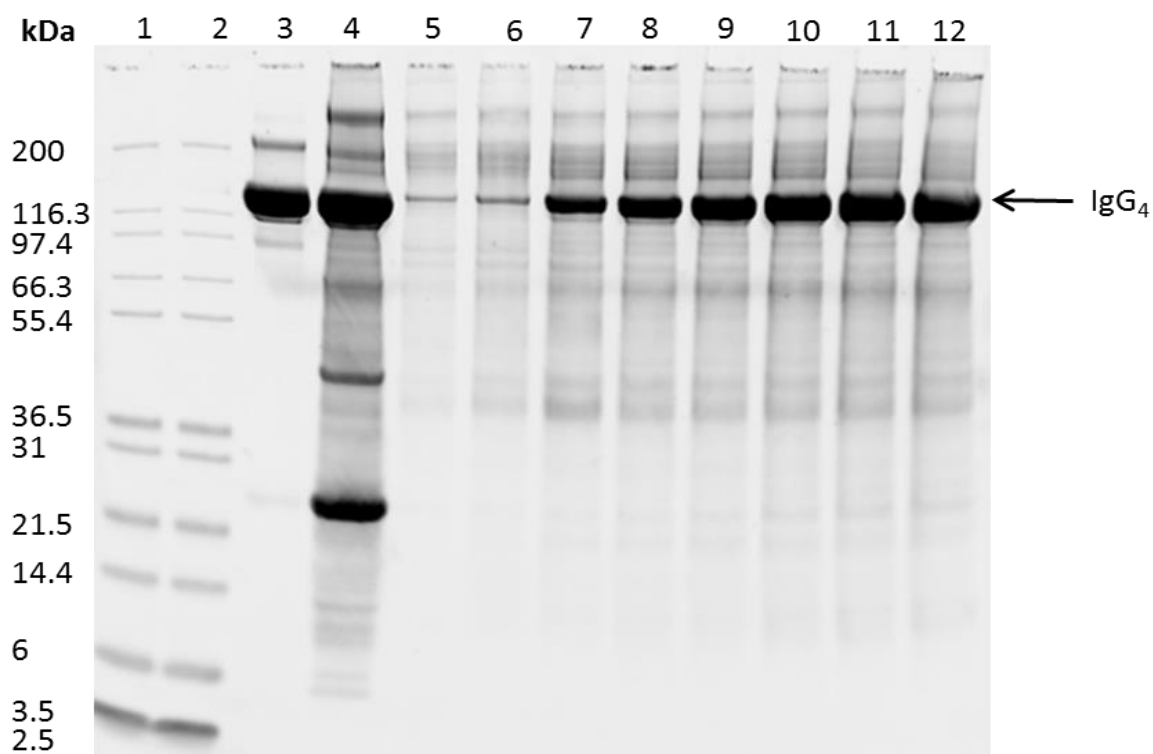


Figure 3-22. Non-reduced SDS-PAGE of composition of precipitated IgG₄ from cell culture fluid with increasing ammonium sulphate concentration in the range 1 to 1.7 M. Lanes 1) and 2) Protein ladder (Invitrogen Mk12), 3) purified IgG₄ standard, 4) cell culture fluid, 5) 1 M AS precipitation, 6) 1.1 M AS precipitation, 7) 1.2 M AS precipitation, 8) 1.3 M AS precipitation, 9) 1.4 M AS precipitation, 10) 1.5 M AS precipitation, 11) 1.6 M AS precipitation, 12) 1.7 M AS precipitation.

3.10.2 Effect of precipitate washing on impurity removal

Sequential washing of the precipitate with the same conditions used for precipitation prior to resolubilisation is one method in aiding the removal of the non-precipitated components in the immediate vicinity of the precipitate. The impact of washing the precipitate with ammonium sulphate on the impurity profile is demonstrated in Figure 3-23. Performing a single wash increased the relative purity to 55% as demonstrated by a reduction in the flow-through peak, whilst an additional wash slightly increased the purity further to 58%. Purity would not be expected to improve with further washes.

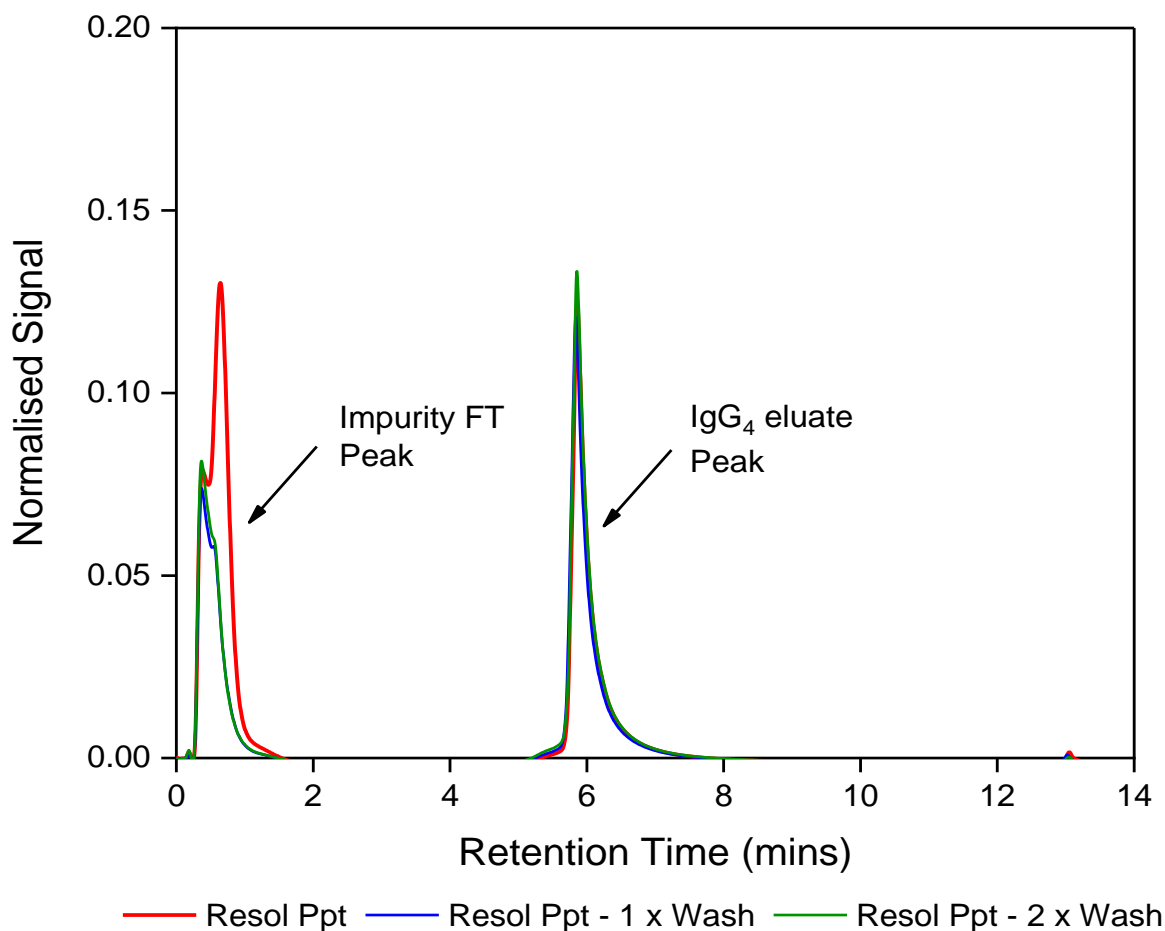


Figure 3-23. Protein G HPLC profiles of resolubilised IgG₄ precipitate (Ppt) with and without washing. The signals are normalised to the signal of the CCCF profile presented in Figure 3-20.

3.10.3 HCP and DNA levels on precipitated antibody

Information on the identity and population of the impurities present could not be gathered from the chromatograms and therefore a more detailed analysis would be required. For host cell proteins, ELISA kits have been developed to detect those specific to CHO cell lines. However, the presence of a large population of HCPs can often give misleading values owing to the excessive dilutions required to bring levels down to the detectable range of the assay. Using the assay developed by Cygnus Technologies, HCP levels ranged between 550,000 and 1,180,000ppm for starting cell culture fluid, whilst resolubilised precipitate HCP levels were in the range 250,000 to 500,000 ppm with replicate measurements. This method would be more reliable at the later stages of a purification process. In the quantification of DNA levels, the results from the Picogreen assay demonstrated approximately a 4-fold reduction in DNA levels under maximal precipitation conditions. Figure 3-24 shows

increasing DNA levels per milligram of antibody up to 1.1 M ammonium sulphate, most likely due to the propensity of DNA to precipitate at lower ammonium sulphate concentrations. After which antibody begins to precipitate and the level of DNA per quantity of antibody is reduced.

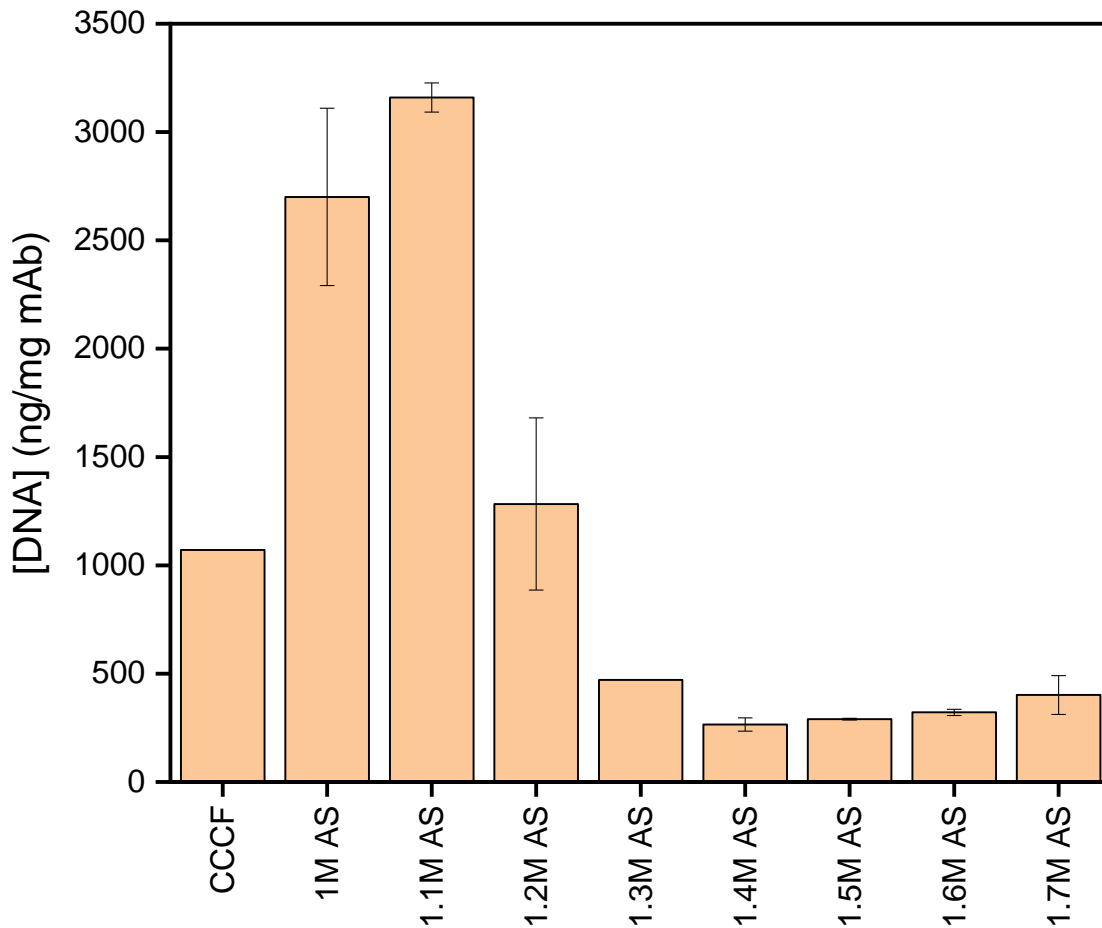


Figure 3-24. DNA levels in nanograms per milligram of antibody as a function of ammonium sulphate concentration for precipitation. DNA amounts were quantified using the Quant-iT Picogreen dsDNA Assay, in triplicate.

3.11 Fractional precipitation

A further improvement of impurity removal may be facilitated by performing precipitation cuts based on the identification of the precipitation region with a particular precipitant. This involves inducing precipitation at a lower concentration of precipitant, followed by increasing the concentration to the final target value. This approach is synonymous to Cohn's fractionation method of plasma proteins (Cohn *et al.*, 1940). In doing so, compromised yields would be expected; however if the effect on purity is more significantly affected then the loss of yield would be less of a concern.

To demonstrate the potential of a fractional precipitation procedure as a proof of concept for antibody purification with ammonium sulphate precipitation, a series of precipitation reactions were performed at 20 mL scale in batch mode with final ammonium sulphate concentrations of 1.05, 1.1, 1.15, 1.2, 1.25, and 1.5 M. The final antibody concentration in the precipitated cell culture harvest was 0.5 mg/mL. At the end of the precipitation reactions and following centrifugation, the supernatants were adjusted to a 1.5 M final ammonium sulphate concentration via the gradual addition of ammonium sulphate solid. Adding ammonium sulphate in the form of a solid carried the advantage of decreasing the amount of volume increase when adding a saturated stock solution, meaning the change in protein concentration is minimised. All precipitates were solubilised in buffer and analysed.

Table 3-4 compares the antibody yields and purity levels of antibody precipitates obtained from a single precipitation at 1.5 M AS versus the fractional or double-cut precipitation procedures.

Table 3-4. Yield and purity comparison of single and double cut precipitations for IgG₄ purification from CCCF using ammonium sulphate (AS). A single cut precipitation refers to the addition of precipitant to the target concentration to precipitate and recover antibody. A double-cut precipitation refers to adding a pre-set amount of precipitant to feed to at a lower concentration to remove impurities, keeping as much IgG₄ in the soluble fraction, to which further precipitant is added to the final desired concentration.

	Precipitation Condition	Yield (%)	Purity (%)
<i>Single- Cut Precipitation</i>	1.5 M AS	91	40
<i>Double-cut precipitation</i>	1.05 M AS (first step) + 1.5 M AS (second step)	81.65	55.2
	1.1 M AS (first step) + 1.5 M AS (second step)	78.4	57.2
	1.15 M AS (first step) + 1.5 M AS (second step)	73.6	61.6
	1.2 M AS (first step) + 1.5 M AS (second step)	52.1	58
	1.25 M AS (first step) + 1.5 M AS (second step)	37.2	56.2

A qualitative indication of the relative purification is also given from the SDS-PAGE gel profiles in Figure 3-25 and Figure 3-26. From the fractional precipitation data, it can be seen that an increase in the ammonium sulphate concentration during the first precipitation improves impurity removal upon the final precipitation but decreases the yield. Precipitating antibody at 1.15 M ammonium sulphate, followed by increasing the ammonium sulphate to 1.5 M in the supernatant provides a significantly ‘cleaner’ feed compared to precipitating at 1.5 M ammonium sulphate alone; although at a cost of approximately 20% in yield. Further impurity removal could be additionally achieved through precipitate washing after the second precipitation, as observed from the results presented in section 3.10.2. Alternatively, a low pH with 1.15 M ammonium sulphate, followed by precipitation with 1.5 M ammonium sulphate at higher pH could be employed.

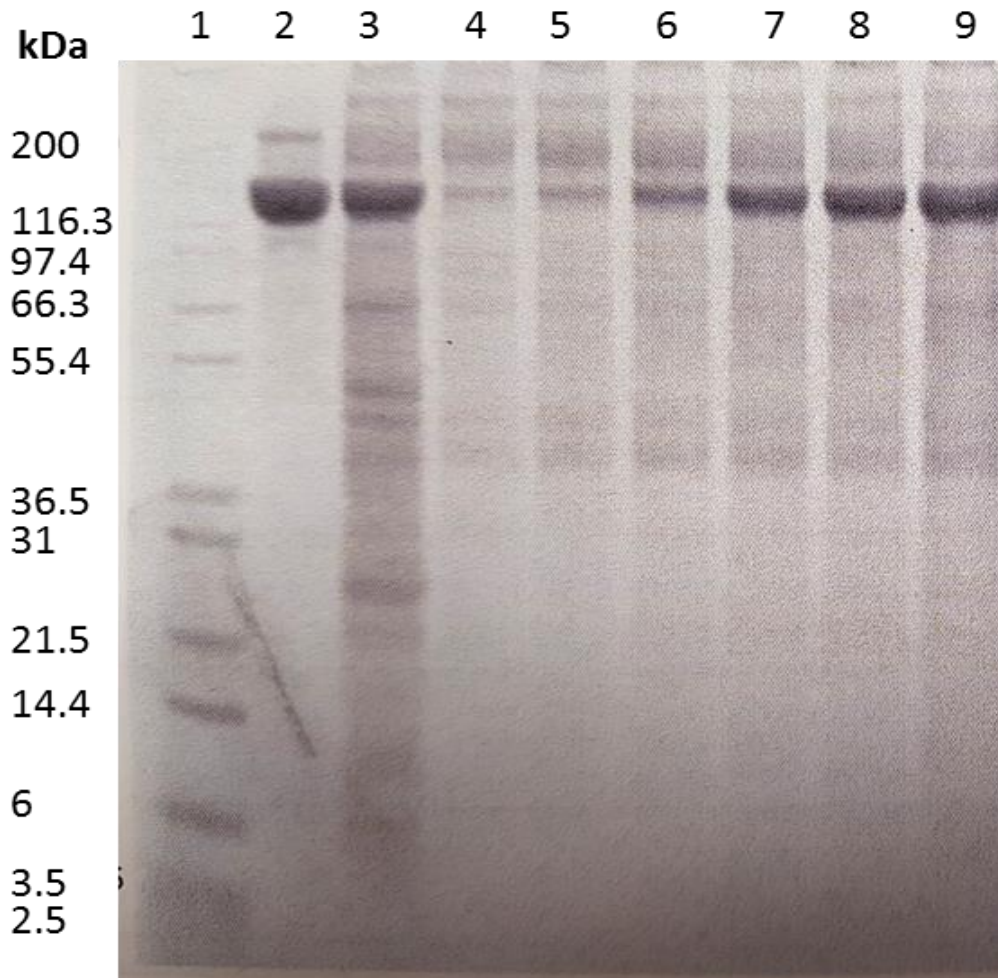


Figure 3-25. Non-reduced SDS-PAGE of composition of IgG₄ purified samples from single ammonium sulphate (AS) precipitations with increasing salt concentration. Lanes 1) Protein ladder (Invitrogen Mk12), 2) IgG₄ reference standard, 3) cell culture fluid, 4) 1.05 M AS precipitation, 5) 1.1 M AS precipitation, 6) 1.15 M AS precipitation, 7) 1.2 M AS precipitation, 8) 1.25 M AS precipitation, 9) 1.5 M AS precipitation.

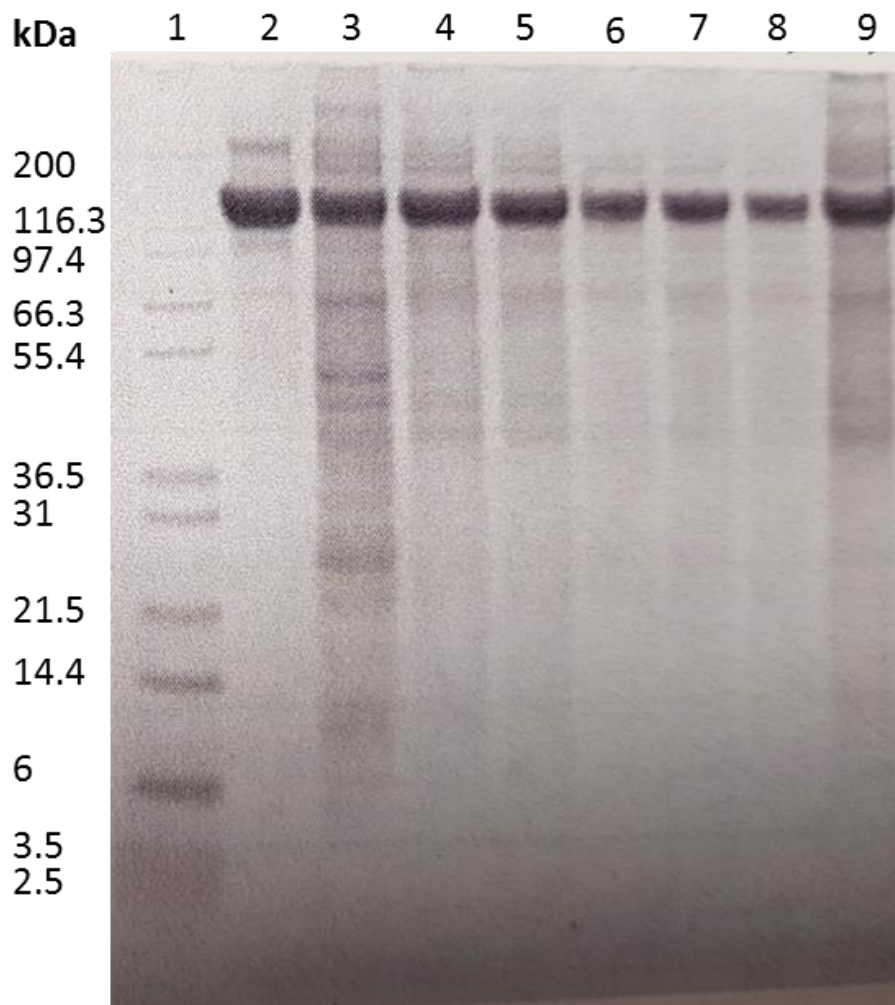


Figure 3-26. Non-reduced SDS-PAGE of composition of IgG₄ samples from fractional two-step ammonium sulphate precipitations. Lanes 1) Protein ladder (Invitrogen Mk12), 2) purified IgG₄ standard, 3) cell culture fluid, 4) 1.05 – 1.5 M AS precipitation, 5) 1.1 -1.5 M AS precipitation, 6) 1.15 -1.5 M AS precipitation, 7) 1.2 – 1.5 M AS precipitation, 8) 1.25 – 1.5 M AS precipitation, 9) 1.5M AS precipitation (control).

The fractional precipitation approach was not further developed as this was out of the scope of the work. The studies presented in the following chapters focused on the development of reactor systems to control the performance of a single precipitation step to target the molecule of interest. A second reactor system might be required in addition to the reactor performing the product precipitation which adds further complexity to the process design. Nonetheless, it remains a useful strategy for early process development studies if the conditions for precipitation are well characterised and the composition of the precipitates is well understood.

3.12 Summary

Previous research conducted at UCL involving salt-driven precipitation on a monoclonal antibody was reproduced on another antibody molecule of the subclass IgG₄ (Morris, 2019). In comparison to this work, similar precipitation performance using salts was observed, at least for the purified antibody model. For cell culture supernatant precipitation, although precipitation was successful, the centrifugal recovery was severely impacted when employing sodium sulphate or sodium citrate precipitation. It was suspected that the nature of the feed tested was 'less' clean than what had been previously used and therefore the presence of particular components may have impacted recovery. Ammonium sulphate precipitation, on the other hand, enabled good precipitate recovery and showed comparable precipitation behaviour between purified and crude antibody feeds. Furthermore, the increase in volume required was less than the other two agents to achieve the same level of precipitation, of which can be further reduced through adjustment of process parameters including pH and final antibody concentration. Since proteins are generally stable at high saturation levels of ammonium sulphate, the precipitate could potentially be stored for long periods under appropriate conditions, if required. For instance, if issues are encountered further downstream of the process and manufacturing comes to a halt. Future experiments exploring the impact of storage conditions on antibody stability as a precipitate would have been an interesting avenue to investigate, analogous to the study on the storage of PEG-induced antibody precipitates conducted by Krepper et al (Krepper *et al.*, 2019).

A drawback of ammonium sulphate precipitation for antibody purification is the occurrence of precipitating impurities along with the target protein. This method tends to be more useful at the later stages of processing for protein concentration and formulation. In order to maximise target protein recovery whilst removing as many impurities as possible, fractional or dual

precipitation strategies could be applied to reach purification levels which potentially compete with affinity chromatography. These approaches are feasible for precipitation in a batch vessel where adjustments can be made for process control; however adaptation to a continuous process requires greater complexity. Also, additional purification techniques following salt precipitation including ion-exchange, HIC and mixed-mode chromatography may be required.

The next step is to investigate the potential of ammonium sulphate precipitation from a scale-up perspective. Despite successful antibody recovery with ammonium sulphate precipitation at small scale, a large scale application is far more complex considering factors such as mixing and shear effects begin to play a pivotal role. A good understanding of the impact of these effects on the nucleation and growth processes governing protein precipitation reactions is necessary when devising a scale-up strategy and selecting the appropriate design for a precipitation reactor.

Chapter 4: Design of precipitation reactor systems based on analysis of mixing

4.1 Introduction

Mixing plays a significant role for many industrial processes as the extent of contact between two or more species often depicts the output of the process or reaction (Gao *et al.*, 2015). For instance, a poorly mixed system can have a detrimental effect on the yield and purity of a desired product whilst increasing the yield of an undesired by-product. This therefore necessitates the identification of the mixing mechanisms controlling the process. Mixing occurs at three distinct scales, that is macro-mixing, meso-mixing and micro-mixing (Guichardon, Falk and Andrieu, 2001). Macro-mixing describes mixing on the largest scale i.e. the residence time distribution (RTD) of a fluid entering the vessel which can be determined from the analysis of input and output tracer concentrations (Bałdyga, Bourne and Hearn, 1997; Gobert *et al.*, 2017). Macro-mixing evaluation is useful since it can provide information on the flow behaviour in a reactor (e.g. plug flow, mixed flow, laminar flow etc.). Meso-mixing is considered as the intermediate scale of mixing which occurs via turbulent dispersion and large eddy disintegration (Bałdyga, Bourne and Hearn, 1997). This scale of mixing is particularly relevant for semi-batch operated vessels in which reagents fed through a pipe are dispersed shortly after entering the reactor (Zauner and Jones, 2000). Micro-mixing is defined as the smallest scale of mixing which occurs in the smallest eddies, below the Kolmogorov scale (Guichardon, Falk and Villiermaux, 2000; Commenge and Falk, 2011). Micro-mixing is the final stage of the complex mixing process and is governed by deformation, engulfment and molecular diffusion of the reacting species at the molecular scale (Bałdyga and Pohorecki, 1995; Guichardon and Falk, 2000). For many chemical reactions, and in particular crystallisation and precipitation reactions, meso-mixing and micro-mixing tend to be more influential in their performance owing to the reactions occurring at the molecular scale.

Physical and chemical models to evaluate micro-mixing quality in various reactor designs have been under much development. Physical techniques involve optical methods including fluorescent tracers and laser-induced fluorescence to detect changes in reagent concentrations as a function of time and space (Kling and Mewes, 2004; Lehwald, Thévenin and Zähringer, 2010); however these methods are limited to the detection of relatively large mixing eddies. Chemical methods are generally more suitable for micro-mixing evaluation

and rely on the selectivity of competitive reactions which directly correlate to the micro-mixing efficiency. The iodide-iodate and diazo coupling between naphthol and diazotized sulphanic acid methods are frequently used for micro-mixing tests in stirred and in-line mixing reactors (Guichardon, Falk and Andrieu, 2001; Gholap, Sergio and Bourne, 2018). The former test system is cheaper to use, easier to handle and adaptable to investigate viscosity effects (Pinot *et al.*, 2014), as might be expected in precipitation applications.

When the characteristic reaction time of the process is longer than the mixing time, the selectivity of the reaction becomes dependent on the mixing efficiency. Conversely, when the mixing time is shorter or on the same magnitude as the characteristic reaction time, the reaction depends on the reaction rate or a combination of both reaction and mixing rates. The ratio between these rates is defined as the Damköhler number, Da_M , whose value describes kinetically-controlled ($Da_M < 0.001$) or mixing-limited reactions ($Da_M > 1000$) or both ($0.001 < Da_M < 1000$) (Gobert *et al.*, 2017). Therefore, reactions with reaction times of 1 s require maximum mixing times of 1 ms to minimise mixing limitations on the reaction kinetics. For fast reactions such as that observed for organic synthesis, precipitation, crystallisation and polymerization reactions, the scale of micro-mixing would be particularly important. Therefore, a reactor design capable of delivering the required level micro-mixing is sought for optimal performance.

Factors which can impact the quality of mixing and thus should be considered for an appropriate mixer design include: the solution rheology which is directly related to its viscoelastic properties, the mode of feeding, the hydrodynamic forces exerted by the mixing equipment and the mixing volume. A number of reactor designs incorporating various mixers have been developed including Rushton impellers (Bourne and Dell'ava, 1987), helical ribbon and screw impellers (Ameur, Kamla and Sahel, 2018), propellers and turbines in stirred batch vessels as well as T-mixers (Forney and Gray, 1990; Cozewith *et al.*, 1991), V-mixers (Kolbl and M, 2003; Falk and Commenge, 2010), Y-mixers (Gobert *et al.*, 2017), static mixers (Lehwald, Thévenin and Zähringer, 2010; Ghanem *et al.*, 2014), impinging jets (Mahajan and Kirwan, 1996; Tummers, Jacobse and Voorbrood, 2011) and rotating packed-beds (Yang *et al.*, 2005; Chen *et al.*, 2006) for continuous flow systems. Employing continuous flow systems has been of increased interest since they have been shown to improve heat transfer, mixing, are safer to operate and potentially offer higher-throughput over stirred batch vessels (Gobert *et al.*, 2017). Given the vast range of systems available, choosing the optimal reactor requires a clear understanding of the mixing characteristics and on the reaction taking place. Owing to the complexity of the mixing process with the added complexity of a precipitation process, establishing a general approach to scale-up based upon mixing has proven difficult.

The study presented in this chapter aims to establish the mixing characteristics of stirred batch vessel and continuous tubular reactor systems using macro-mixing and micro-mixing models. First, macro-mixing was evaluated using phenolphthalein, a dye which responds to pH and induces a colour change. Second, micro-mixing evaluation was performed by applying the iodide-iodate method developed by Villermaux, the details of which are presented in section 4.2.

The reactor designs studied are displayed in Figure 4-1 to Figure 4-3. Figure 4-1 displays and details the configuration and dimensions of a 150 mL stirred-batch vessel. A short piece of tubing with an internal diameter of 0.5 mm internal diameter was inserted into the reactor and placed at a distance of 5 mm from the impeller blade. This served as an injection point for the addition of reagents during micro-mixing evaluation. For the macro-mixing experiments, reagents were added directly to the surface of the bulk liquid. Figure 4-2 and Figure 4-3 display self-constructed lab and pilot-scale continuous flow reactor systems, respectively. These systems utilise a T mixer to bring solutions into contact and promote the initial mixing. For the lab-scale continuous flow system, the T-mixer had an internal diameter of 0.5 mm whilst the outlet tubing had an internal diameter of 0.5, 1 or 2 mm. Tubing diameters were altered to investigate how these affected the mixing. The total length of the reactor was 5 or 10 m. To be able to fit a tubing size of 2 mm a small piece of 1 mm size tubing was incorporated upstream to allow direct connection. The tubing was arranged in a coil with a diameter of 16.5 cm which minimised spacing. In Figure 4-3, a coiled-flow inversion reactor (CFIR) proposed by various authors (Rathore *et al.*, 2015; Kateja *et al.*, 2016), was constructed for pilot-scale experiments. Here, the T-mixer had an internal diameter of 4.8 mm, whilst the tubing had an internal diameter of 6.4 mm, arranged into a coil of eight helical turns around a polyvinyl chloride (PVC) pipe with a diameter of 75 mm, followed by a 90° bend, and finally eight additional helical turns.

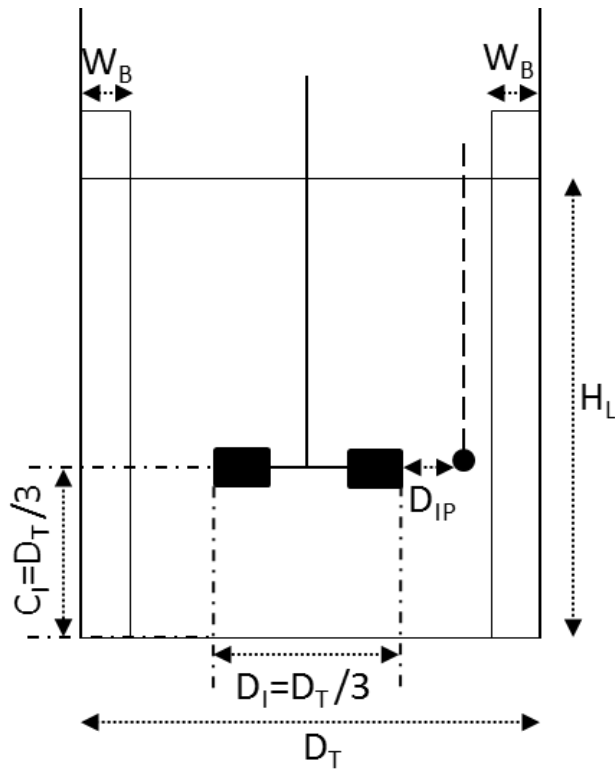
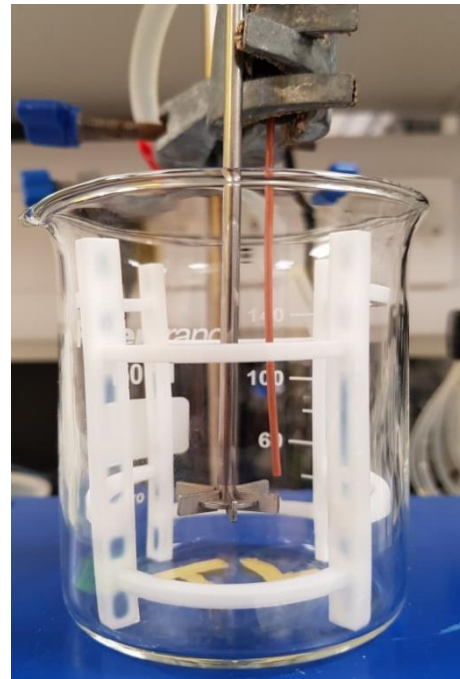
A**B**

Figure 4-1. Schematic representation (A) and photographic illustration (B) of the 150 mL stirred batch vessel with feed additions made through a 0.5 mm diameter bore positioned adjacent to the impeller. The dimensional specifications are as follows: D_T (tank diameter) = 58 mm; D_I (impeller diameter) = 20 mm; H_L (liquid height) = 58 mm (~100 mL with baffles); C_I (impeller clearance) = 20 mm; W_B (baffled width) = 4 mm; D_{IP} (distance of injection point from edge of impeller blade) = 5 mm.

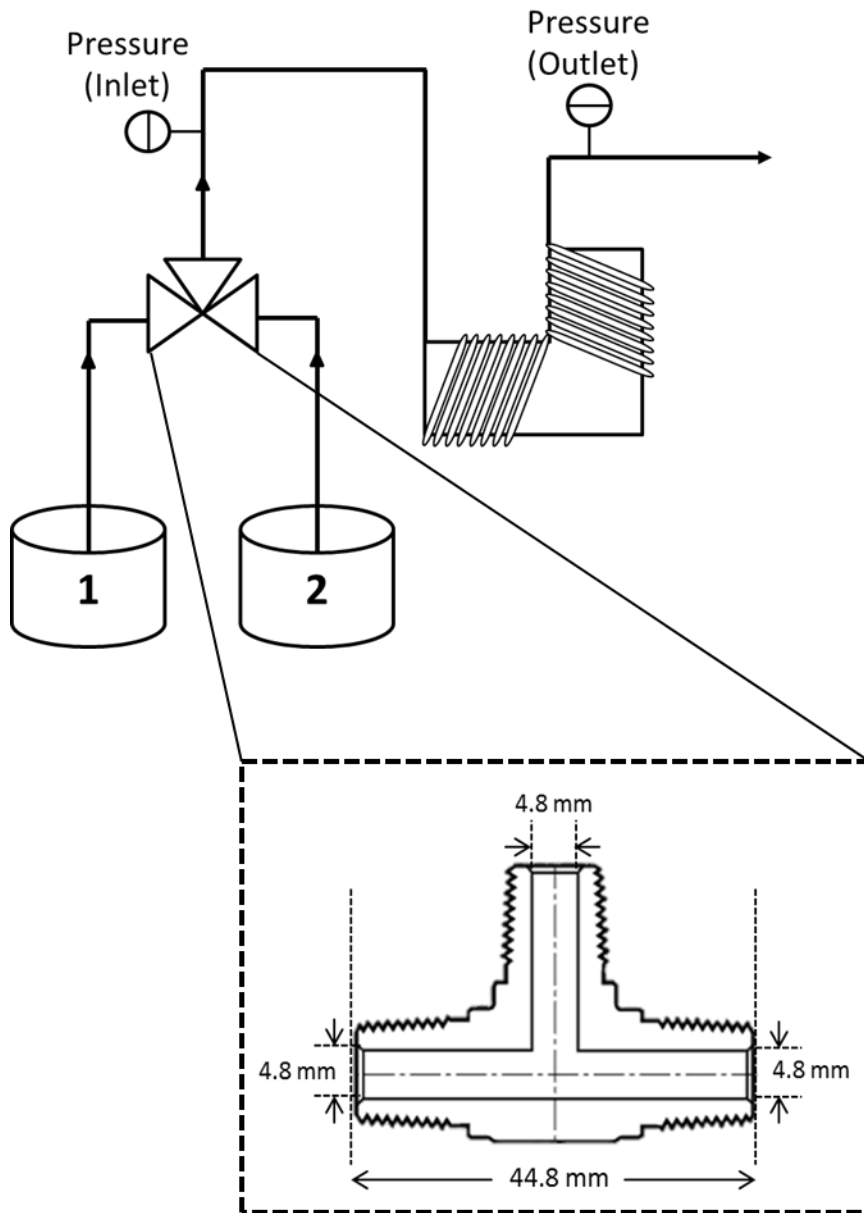
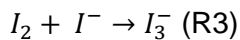
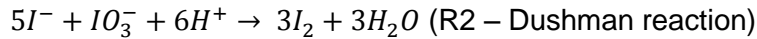


Figure 4-3. Configuration of the coiled-flow inversion reactor (CFIR) employed for pilot scale mixing and precipitation studies.

4.2 Villermaux's Iodide-iodate reaction test

The iodide-iodate reaction test developed by Villermaux (Guichardon, Falk and Villermaux, 2000) to assess micro-mixing in various reactors involves a series of parallel competing reactions as follows:



The neutralisation and Dushman reactions both consume acid at different rates. R1 is instantaneous, whilst the rate of the R2 is fast but much slower than R1 and comparable to the micro-mixing process. The kinetics of R2 was studied by many authors and they have demonstrated that the rate of the reaction is a function of the mixture composition and mixing conditions. An empirical model to describe the rate law for R2 is given by:

$$r = k[H^+]^2[I^-]^2[IO_3^-]$$

Equation 4-1. Dushman reaction rate law.

where k is the kinetic constant which is a function of the ionic strength, I , of the mixture:

$$\text{If } I < 0.16M \text{ then: } \log(k) = 9.28 - 3.66\sqrt{I}$$

$$\text{If } I > 0.16M \text{ then: } \log(k) = 8.38 - 1.5115\sqrt{I} + 0.23I$$

In the presence of acid, as long as the pH is kept above 9 upon good mixing, R2 does not occur to a significant extent in relation to R1. However, when local excesses of acid occur as a result of inefficient mixing, R2 proceeds and iodine formation occurs which then becomes instantly trapped by I^- to form I_3^- in reaction 3 (R3). The equilibrium constant for R3 can be calculated using the correlation:

$$K = \frac{[I_3^-]}{[I^-][I_2]}$$

Equation 4-2. Calculation of equilibrium rate constant, K , for tri-iodide formation based on iodide, iodine and tri-iodide concentrations.

where K is the equilibrium constant and has a value of 736 L/mol at 298 K. The following correlation can also be used to determine the equilibrium constant as a function of absolute temperature:

$$\log(K) = \frac{550}{T} + 7.355 - 2.575 \log T$$

Equation 4-3. Calculation of equilibrium rate constant, K , as a function of solution temperature, T .

In our experiments, the value of T consistently remained in the range 295.5 K to 296.5 K., giving an average K value of 715 L/mol which was used for all micro-mixing calculations. The concentration of I_3^- was determined using Beer Lambert law ($A = \epsilon cl$) with an absorbance wavelength at 353 nm and molar extinction coefficient of 26047 L/cm as reported in the literature, although some authors have determined slight variations of this value (Guichardon, Falk and Villermaux, 1997; Rousseaux *et al.*, 1999; Yang *et al.*, 2009). The amount of I_3^- produced allows the characterisation of the micro-mixing efficiency through the segregation index X_s . The segregation index X_s is defined as Y/Y_{ST} where Y is the ratio of acid mole number consumed by Reaction (2) to the total acid mole number injected ($Y = 2(n_{I_2} + n_{I^-})/n_{H^+}$) and Y_{ST} is the value of Y in the case of total segregation when the micro-mixing process is infinitely slow ($Y_{ST} = 6[IO_3^-]_0 / (6[IO_3^-]_0 + [H_2BO_3^-]_0)$). The value of X_s is within the range $0 < X_s < 1$ for partial segregation. For $X_s = 0$, perfect micro-mixing is indicated, whereas total segregation is indicated for $X_s = 1$. The amount of I_2 can be determined based on a mass balance of iodine atoms and the value of K . It is important to note that absorbance measurements are only valid in the range 0.1 to 2.5 and thus the path length of the optical cell must be considered. Since the values obtained are also dependent on the starting reagent concentrations according to the rate law of R2 and the tested mixing conditions, some trial-and-error experiments may be required during initial investigation to define the appropriate ranges.

The procedure in assessing micro-mixing in a stirred batch vessel consists in adding in stoichiometric defect a small amount of sulphuric acid to the mixture of iodide, iodate and borate ions. This ensures that any iodine formation is governed by the mixing process alone.

Further treatment of X_s gives a second dimensionless constant known as the micro-mixedness ratio, α . This constant is defined as the ratio of perfectly micro-mixed fluid versus the volume fraction which remains completely segregated and is given by:

$$\alpha = \frac{1 - X_s}{X_s}$$

Equation 4-4. Calculation of micro-mixedness ratio, α .

The micro-mixedness ratio may also describe the ratio between the characteristic reaction and mixing times.

X_s is sensitive to the concentrations of the reagents used in Villermaux's micro-mixing test; hence comparing mixing performance between different reactors on the sole basis of X_s or α is only valid when the reagent concentrations are matched. Otherwise, the use of a different concentration set requires further treatment of the data to obtain a micro-mixing time which is independent of the reagent concentrations. Depending on the systems that are being compared, it may be necessary to adjust the concentration set for one or more systems when the initial set does not reliably offer valid measurements.

Various reports on micro-mixing in batch-stirred vessels use borate-iodate solutions comprising the following concentrations of reagents (Baldyga and Pohorecki, 1995; Baldyga, Bourne and Hearn, 1997; Guichardon and Falk, 2000; Yang *et al.*, 2005): 0.1818 M H_3BO_3 , 0.0909 M NaOH, 0.0023 M KIO_3 and 0.01167 M KI, whilst the acid concentration is typically in the range 0.5 to 2 M.

Micro-mixing in continuous tubular flow reactors is typically evaluated for systems operating with equal inlet flow rates through T, V or Y-mixers as this enables direct treatment of the data using the methods described in previous reports (Falk and Commenge, 2010; Commenge and Falk, 2011; Pinot *et al.*, 2014). The acid concentrations employed for batch mixing cannot be used for these continuous flow systems since the acid would be in much greater excess relative to the iodate-borate solution and form large amounts of iodine. For these systems, the acid concentration should be in the range 0.01 to 0.1 M. Also, the pH value of the buffer solution must be higher (close to 11) to avoid natural formation of iodine with borate ions being in large excess to the amount of acid. This pH adjustment has also been demonstrated to avoid such formation in the presence of glycerol if viscosity effects are to be accounted for with respect to the micro-mixing quality (Guichardon, Falk and Villermaux, 1997). Commenge and Falk have defined a number of reagent concentration

sets which are appropriate for the characterisation of micromixers operating with continuous flow.

4.3 Estimation of micro-mixing times

In order to determine micro-mixing times, many phenomenological models have been proposed to describe mixing phenomena (Villermaux, 1986; Villermaux and Falk, 1994; Bałdyga and Pohorecki, 1995; Fournier, Falk and Villermaux, 1996). One simple model, the incorporation model (Fournier, Falk and Villermaux, 1996) can be used for estimating micro-mixing times in batch and continuous mixers. Despite originally applied in turbulent flow systems, it has been shown to equally apply for laminar flow. The model assumes that the incoming acid is divided into aggregates and is progressively invaded by the fluid containing the borate-iodate-iodide buffer mixture. The acid aggregates grow progressively incorporating the surrounding liquid where the reactions take place. The characteristic time of incorporation, t_m , is assumed to be equivalent to the micro-mixing time. The aggregate volume grows according to the equation $V_2 = V_{20}g(t)$, where $g(t)$ is the incorporation function and is given by $g(t) = \exp(t/t_m)$. The concentrations of j species, according to the model, are given by:

$$\frac{dC_j}{dt} = \frac{C_{j10} - C_j}{t_m} + R_j$$

Equation 4-5. The incorporation model for the estimation of micro-mixing times in reactors.

where C_j denotes the concentration of reactants in the system, C_{j10} represents the initial concentration of reactants in the surrounding liquid and R_j is the net production rate of each reactant. By assuming a series of t_m values, the concentration of species can be calculated by solving the differential equations for each of the species. The integration continues until all the acid has been consumed. Details of the method are presented elsewhere (Yang *et al.*, 2005). The value of the corresponding X_s and corresponding α can then be derived. In the batch micro-mixing experiments, the reagent concentrations used by Rousseaux and colleagues (Rousseaux *et al.*, 1999) were suitable in generating valid absorbance measurements from which X_s and α could be determined. In addition, t_m could be calculated based on the following equations given that $2 < \alpha < 20$:

$$\begin{aligned} 2 < \alpha < 5 & \quad t_m = 0.73\alpha^{-2.26} \\ 5 < \alpha < 7 & \quad t_m = 0.82\alpha^{-2.30} \\ 7 < \alpha < 20 & \quad t_m = 0.158\alpha^{-1.45} \end{aligned}$$

Equation 4-6. Series of micro-mixing time, t_m , calculations for stirred batch reactors using defined reagent concentrations.

In the case for the continuous mixing experiments, we use the theoretical relationship between t_m and X_s as calculated from the incorporation model based on the reagent concentrations selected, as displayed in Figure 4-4. The marked region corresponds to the range of X_s values determined experimentally.

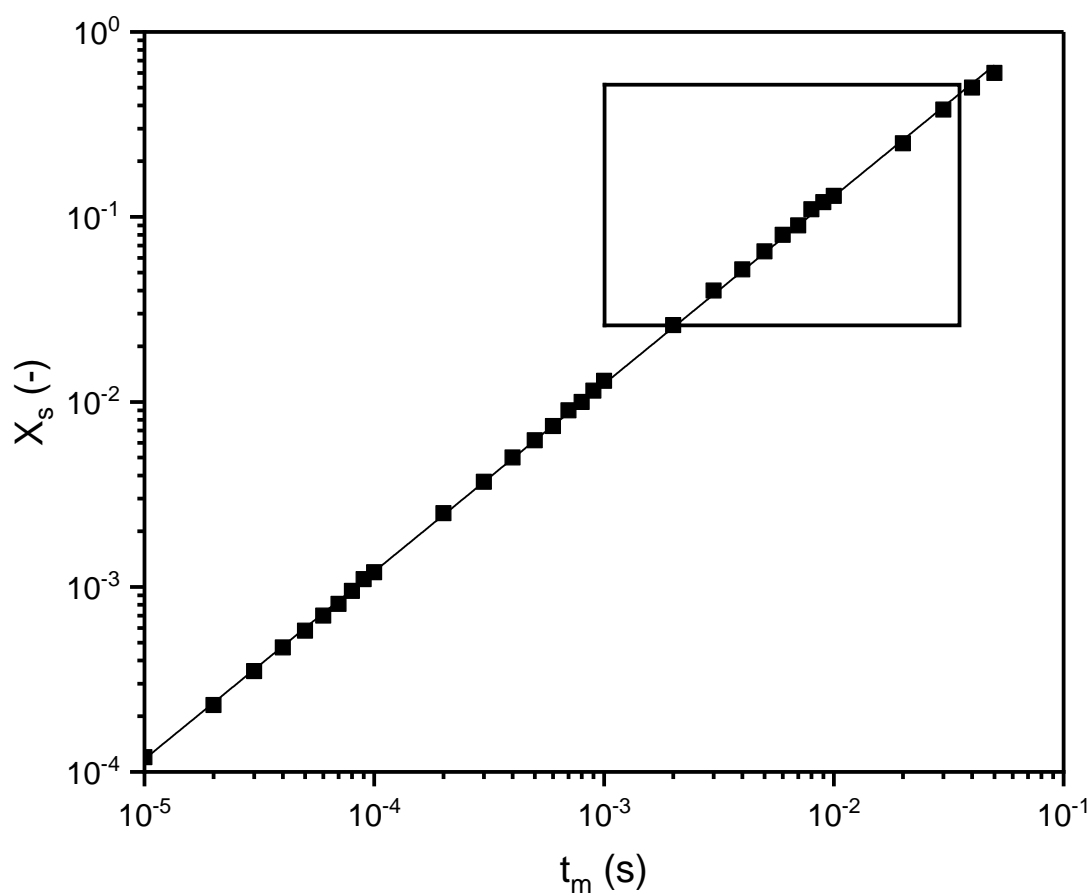


Figure 4-4. Relationship between segregation index, X_s , and micro-mixing time, t_m , based on experimental conditions in the continuous tubular reactors (lab and pilot-scale) using the incorporation model. Reagent concentrations: $[H_2SO_4] = 0.02$ M, $[H_3BO_3] = 0.045$ M, $[KIO_3] = 0.003$ M, $[KI] = 0.016$ M. Highlighted region corresponds to the experimentally determined values of X_s .

4.4 Macro-mixing test results

4.4.1 Batch stirred reactor

Additions of hydrochloric acid were made in an instantaneous fashion to the surface of the bulk liquid consisting of phenolphthalein in sodium hydroxide. The time taken to observe a fully developed colour change (dark pink to colourless) as a function of agitation speed was measured. In order to understand the influence of viscous agents, such as that of a highly concentrated ammonium sulphate solution, on the mixing quality, hydrochloric acid was combined with glycerol to increase the viscosity of the addition. A 3.6 M ammonium sulphate solution has a dynamic viscosity, μ , of 2.55 mPa.s at 22.5°C over the shear rate range 100 to 1000 s⁻¹. To provide a similarly viscous solution, glycerol was added to the hydrochloric acid solution to a final concentration of 26 % v/v ($\mu = 2.50$ mPa.s at 22.5°C) over the same shear rate range.

The effect of impeller agitation in the range 100 to 500 rpm (1.67 – 8.3 s⁻¹) on the macro-mixing times at the two viscosities are shown in Figure 4-5. For the range of impeller speeds studied, the flow regime is transitional with Reynolds number ranging between 670 and 3300. Since the tested range does not describe a fully developed turbulent system ($Re < 10^4$), a constant power number of 5.7 could not be assumed for energy dissipation calculations. Based on a global fitting of power number versus Reynolds number, $P_o = 4$ was approximated.

As expected from Figure 4-5, for a given viscosity, higher agitation rates leads to more efficient mixing and hence reduced macro-mixing times. At low agitation rates, the effect of increasing the injection viscosity on the mixing time is more pronounced whereas the effect is reduced when operating at higher agitation rates. Across the board, we observed a difference of approximately 30% change in mixing efficiency between the two viscosities. For an agitation speed of 500 rpm and above, macro-mixing times were below 3 s, suggestive of rapid mixing. Whilst operating at high agitation provides better mixing, caution should be taken to prevent air-liquid interfaces which likely incur protein damage. Despite including baffles into the mixing vessel to reduce the occurrence of these interfaces, the extent of mixing must be a compromise between the energy dissipation and protein stability. Typically, medium level agitation rates in batch vessels are employed or high mixing speeds are used to provide rapid mixing followed by a low mixing regime during precipitate aging. For the batch precipitation trials described in Chapter 5, it was decided to limit the maximum amount of agitation to 500 rpm since the mixing was rapid.

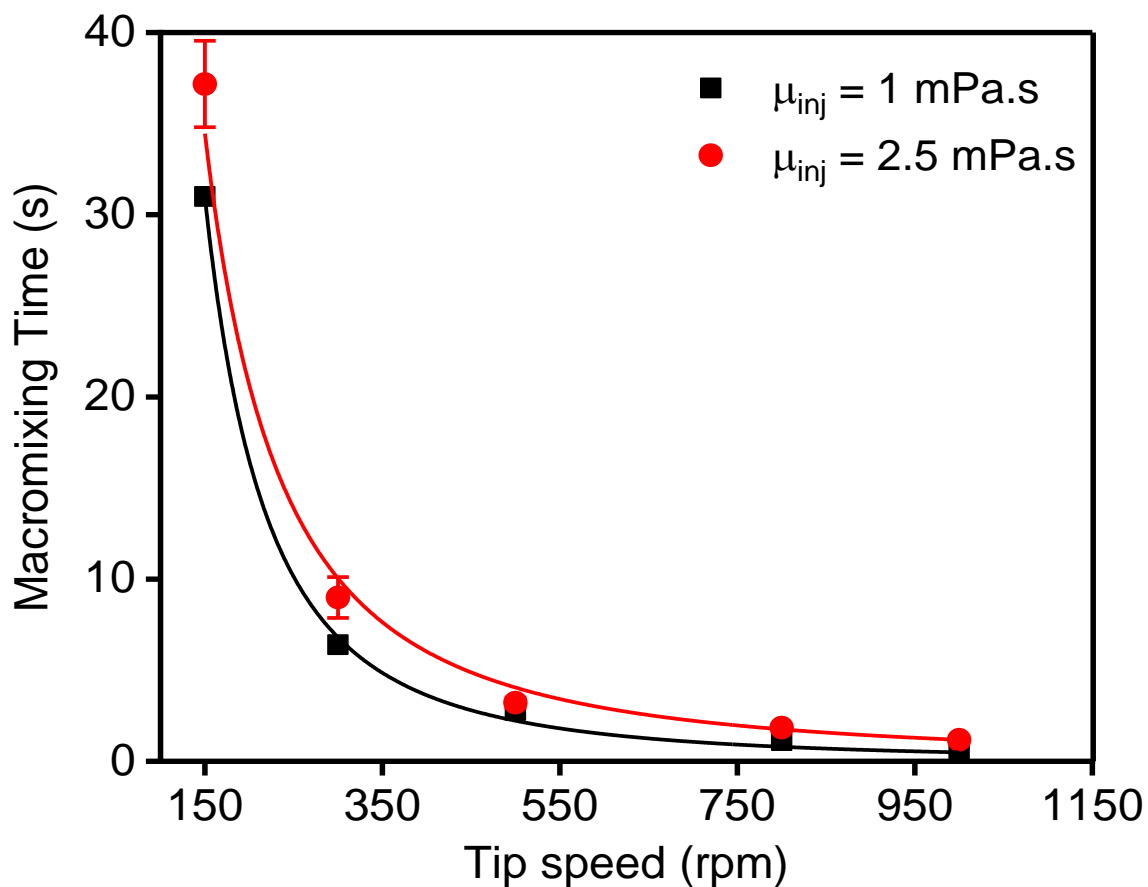


Figure 4-5. Evolution of macro-mixing times as a function of impeller mixing speed and two acid injection viscosities in a 150 mL stirred batch vessel. Injections were made instantaneously to the surface of the liquid and the time taken to induce a colour change of phenolphthalein from dark pink to colourless was deduced. Experiments were carried out in triplicate with data displaying the average mixing times with one standard deviation around the mean.

4.4.2 Continuous tubular reactor

For the continuous tubular reactors, the time to complete macro-mixing was estimated by measuring the distance from the outlet of either T-mixer (0.5 mm T or 4.8 mm T) to the point of the tubing downstream where the complete colour change had fully developed. Macro-mixing times can be approximated using the following relation:

$$\text{Macromixing time (s)} = \frac{L_p}{u}$$

Equation 4-7. Estimation of macro-mixing time in continuous tubular reactors

where L_p is the distance of the tubing or pipe from the Tee outlet that remains incompletely mixed and u is the linear flow velocity. Depending on the flow rate, the colour change was either observed some distance along the tubing (< 5 cm) or immediately at the T outlet. In the former case, at low flow rates, the above equation could be applied to give a reliable approximation of the macro-mixing time. However, for high flow rates, the entire length of tubing appeared colourless suggesting macro-mixing was completed within the mixing chamber of the Tees. Therefore, the exact point where the solutions were fully mixed could not be determined. From this we assumed macro-mixing was complete in less than 1 s. The same behaviour was observed in the case of adding glycerol to 21% v/v to one of the inlet streams. This glycerol concentration was selected based on the viscosity of a 3 M ammonium sulphate solution that was used during the continuous precipitation trials described in Chapter 5. Both solutions had a matching viscosity of 2 mPa.s.

4.5 Characterization of residence time distribution in tubular reactors

The self-designed continuous tubular reactors were characterised in terms of residence time distribution to determine the likely flow regime during operation. A step input of saturated ammonium sulphate was measured by conductivity readings at the outlet on an AKTA Pure system for the lab-scale reactor, whilst an AKTA Ready system was used for the CFIR. Residence time distribution of the lab-scale reactor was characterised with 1 mm diameter tubing. This was not performed for the 0.5 or 2 mm diameter tubing.

Figure 4-6 displays the conductivity profiles and corresponding residence time distribution curves for the lab-scale reactor whilst Figure 4-7 displays the equivalent information for the CFIR. It can be seen that for the lab-scale reactor with a 1 mm pipe connection, the flow profiles are constant over the range of flow rates examined. For the CFIR, we observed a

greater delay in the evolution of conductivity for 100 and 145 L/hr compared to the other flow rates. This may be explained by the slower response time of the conductivity sensor relative to the flow rate. Nonetheless, the transition to the final conductivity value is much steeper compared to low flow rates. The residence time distribution analyses for the lab-scale reactor operating at 10 mL/min and the CFIR operating at 20 L/h were characteristic for plug flow reactors, despite the actual residence times deviating somewhat from the calculated residence time. Either the conductivity response times were rather slow or some resistance to flow may have been observed due to the increased viscosity of ammonium sulphate in the mixture.

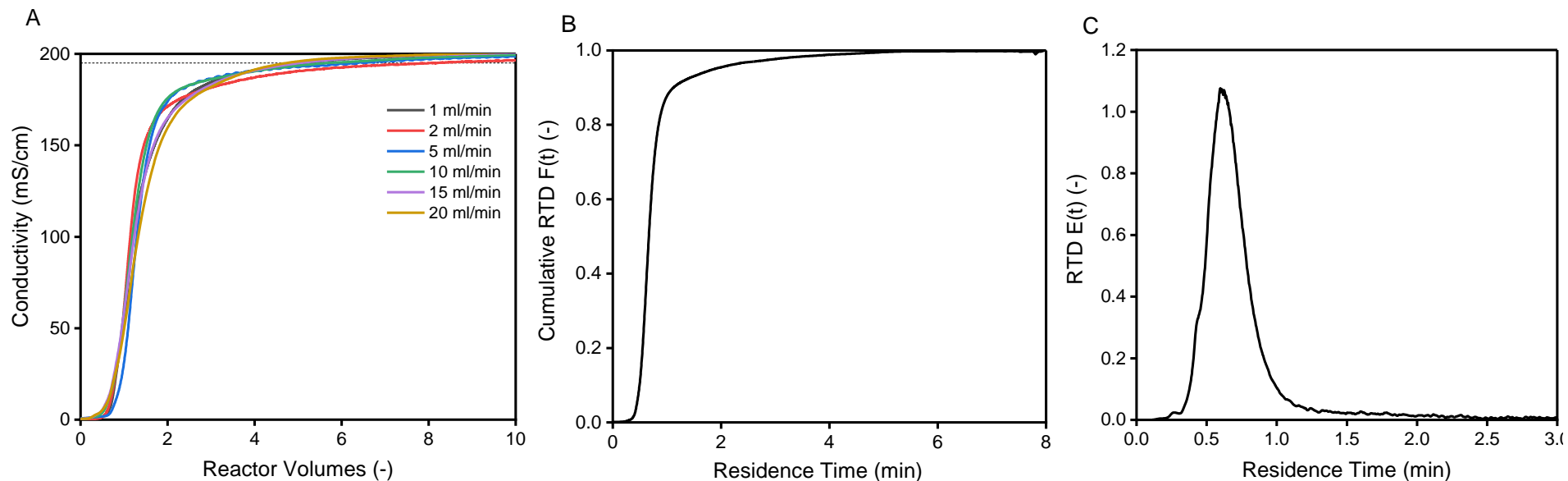


Figure 4-6. Residence time distribution experiments in the lab-scale continuous reactor. (A) Conductivity profiles of the ammonium sulphate positive step input through the lab-scale tubular reactor fitted with 1 mm diameter tubing at various flow rates ranging from 1 to 20 mL/min. Black dashed line corresponds to the expected final conductivity value of the mixture as determined by a batch dilution (~ 190 mS/cm). (B) The measured cumulative time distribution and (C) residence time distribution corresponding to a flow rate of 10 mL/min.

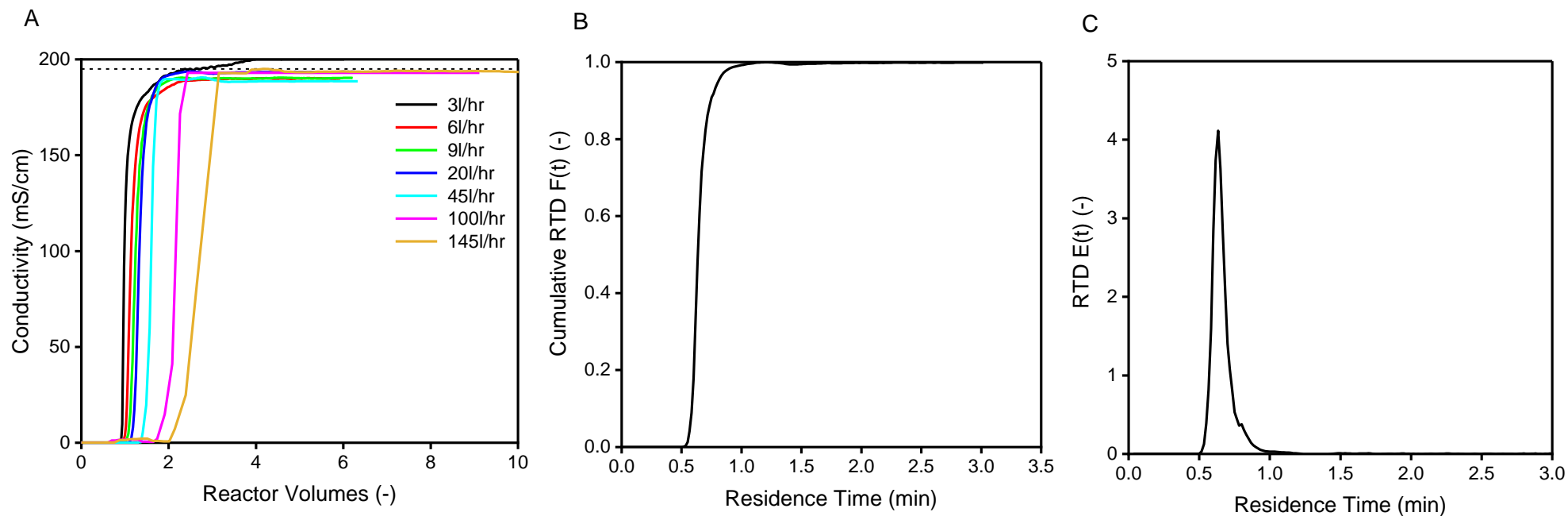


Figure 4-7. Residence time distribution experiments in the pilot-scale reactor. (A) Conductivity profiles of the ammonium sulphate positive step input through the CFIR tubular reactor at various flow rates ranging from 3 to 145 L/hr. Black dashed line corresponds to the expected final conductivity value of the mixture as determined by a batch dilution (~ 190 mS/cm). (B) The measured cumulative time distribution and (C) residence time distribution corresponding to a flow rate of 20 L/hr.

4.6 Micro-mixing tests results

4.6.1 Micro-mixing in stirred batch reactor

In a baffled tank with fully developed turbulence, the characteristic micro-mixing time, t_m , can be estimated based on the incorporation model proposed by Baldyga and Bourne according to the relation:

$$t_m = 17.2 \sqrt{\frac{\varepsilon}{\nu}}$$

Equation 4-8. Calculation to estimate micro-mixing time, t_m , in a baffled vessel with fully developed turbulence (i.e. $Re > 10^4$).

where ε is the local energy dissipation rate in the stirred vessel, in W/kg, and ν is the fluid kinematic viscosity in m^2/s . Since $Re < 10^4$, we cannot simply estimate the micro-mixing times using the above equation and must therefore be experimentally determined.

In order to ensure the predominance of micro-mixing in a batch vessel whilst mitigating meso- and macro-mixing effects, slow additions must be made such that the addition time, t_{add} , exceeds the critical injection time, t_{crit} . Determination of t_{crit} occurs at the point when the value of X_s begins to plateau as t_{add} increases. In our experiments, t_{crit} was determined using the slowest mixing speed, 100 rpm, and t_{add} in the range 96 to 1200 s. The values of t_{add} corresponded to acid flow rates of 0.1 to 1.25 mL/min. The effect of viscous additions, as in the macro-mixing experiments, was also investigated. Figure 4-8 displays the change of X_s as a function of t_{add} for acid injections with 1 and 2.5 mPa.s viscosities. For both viscosities, it can be seen that X_s begins to plateau from $t_{add} = 480$ s which is therefore the determined value of t_{crit} .

In the next set of experiments, the effect of impeller speed on the micro-mixing at the value of t_{crit} was investigated. From the determined values of X_s , these were converted to the corresponding α values which enabled the determination of micro-mixing times from the relations presented in section 4.3. Figure 4-9 shows the relationship between mixing speed and α at t_{crit} . For a given viscosity, as the impeller speed increases, so does α as a result of increased energy dissipation. When comparing the two viscosities, in general there was a similar level of micro-mixing quality. The small differences between the plots can be attributed to the sensitivity of the method. Table 4-1 displays the estimated micro-mixing times for each of the experiments.

Table 4-1. Summary of micro-mixing results from batch mixing experiments. Addition time for acid, t_{add} , was fixed at 480 s according to determination of t_{crit} . Micromixedness ratios, α , and micro-mixing times, t_m , correspond to the mean values from triplicate experiments.

Addition Time, t_{add} (s)	Addition Rate (ml/min)	Impeller speed (rpm)	$\mu_{inj} = 1 \text{ mPa.s}$		$\mu_{inj} = 2.5 \text{ mPa.s}$	
			$\alpha(-)$	t_m (ms)	$\alpha(-)$	t_m (ms)
480	0.25	100	3.2	53	2.8	71.3
		200	6.1	13.1	6	13.3
		300	10.4	5.2	10.9	5.5
		400	13.1	4.1	15.4	3.3
		500	16.8	2.6	19.1	2.2

Greater effects on the micro-mixing quality may have been observed if acid injections of significantly higher viscosities had been employed. More significant changes could also be expected if glycerol was used as an additive to the borate-iodate bulk solution instead given the higher viscous volume that would need to be mixed relative to the volume of acid injected (Guichardon, Falk and Villermaux, 1997). In the context of precipitation, this would be more relevant for feeding low viscous protein-rich solutions into a bulk precipitant solution. However, it is more common and beneficial to increase the saturation of feed via the addition of precipitant than the other way around.

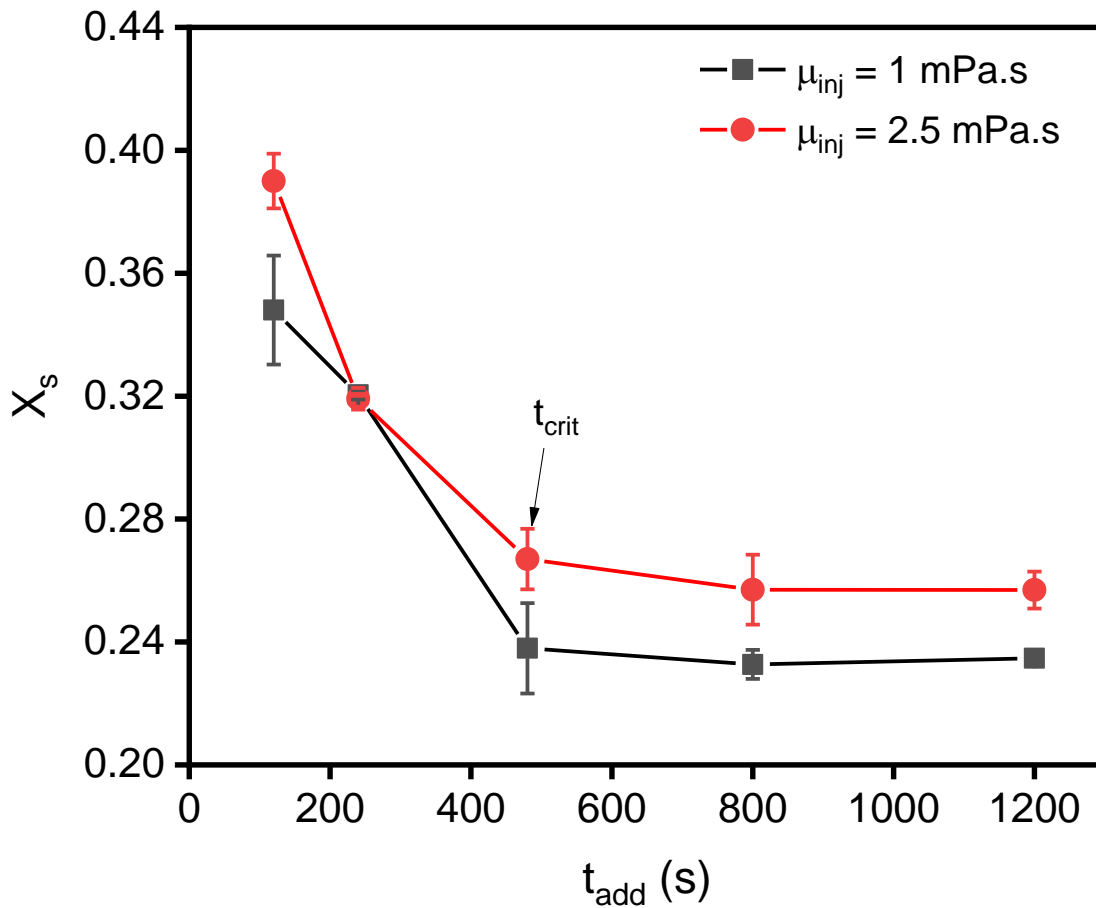


Figure 4-8. Effect of the sulphuric acid injection time (t_{add}) at 100 rpm impeller speed on the segregation index at two different acid viscosity injections: 1 and 2.5 mPa.s. Reagent concentrations: $[H_2SO_4] = 0.5$ M, $[H_3BO_3] = 0.1818$ M, $[KIO_3] = 0.023$ M, $[KI] = 0.017$ M. Viscosity increase to 2.5 mPa.s was performed using glycerol as an additive to 26 % v/v final concentration. Each data point represents the mean X_s value from triplicate experiments with error bars corresponding to one standard deviation. The point of the critical injection time (t_{crit}) is highlighted.

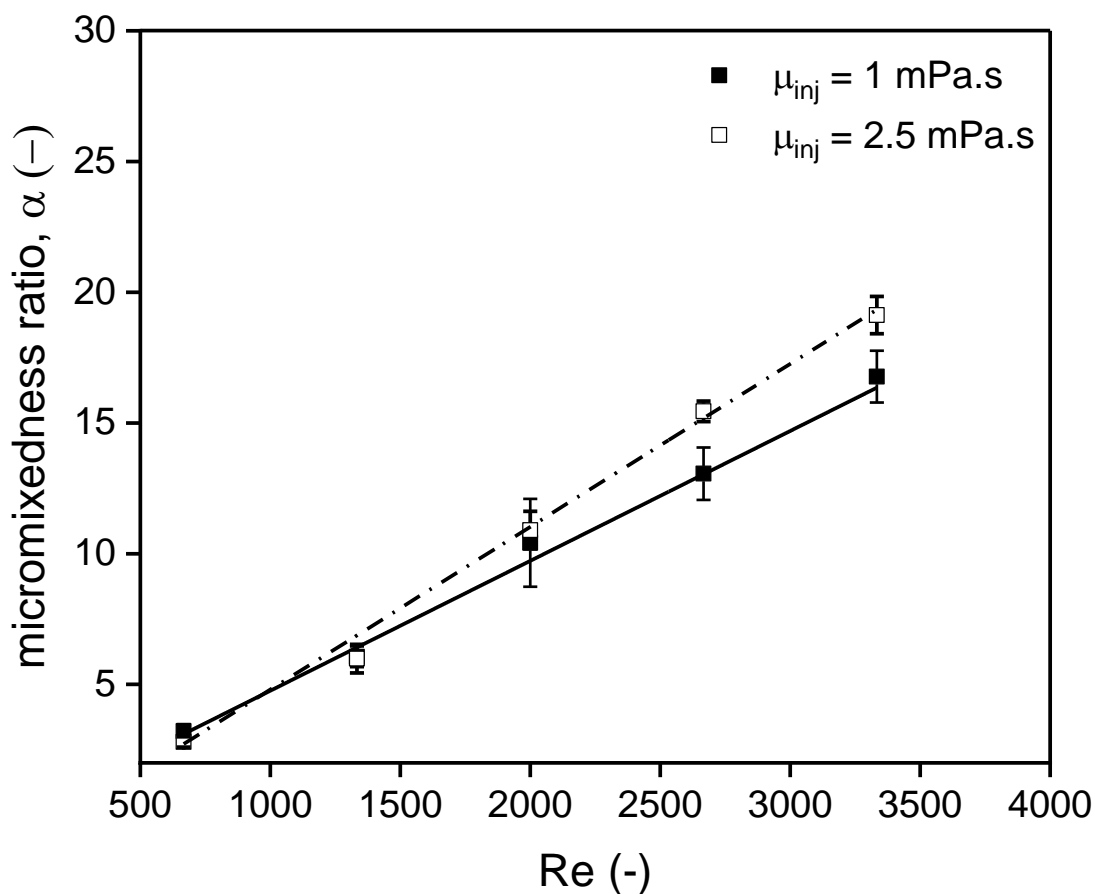


Figure 4-9. Effect of Reynolds number on the micromixedness ratio, α , at the critical injection time, t_{crit} ($t_{add} = 480$ s), and at two different viscosities: 1 and 2.5 mPa.s. Reagent concentrations: $[H_2SO_4] = 0.5$ M, $[H_3BO_3] = 0.1818$ M, $[KIO_3] = 0.023$ M, $[KI] = 0.017$ M. Viscosity increase to 2.5 mPa.s was performed using glycerol as an additive to 26 % v/v final concentration. Each data point represents an average of triplicate measurements with error bars of one standard deviation around the mean displayed. Reynolds numbers in the range 670 – 3300 correspond to an impeller speed range 100 – 500 rpm.

4.6.2 Micro-mixing characterisation in the lab-scale and pilot-scale continuous reactors

Figure 4-10 and Figure 4-11 display the effect of Reynolds number, Re , through the various continuous tubular reactor systems on t_m (as determined from experimental X_s values). It can be seen that for both reactors and for a given tube diameter and solution viscosity, t_m decreases as Re increases. This is due to the combined effect of increased collision energy between the incoming streams at T during initial mixing and an increase in the linear flow rate which creates more vortices and subsequently enhances engulfment flow even under laminar conditions. In the lab-scale reactor, t_m was in the range 0.001 to 0.0012 s (Figure 4-10). At constant tube diameter, longer t_m is observed with the inclusion of glycerol in the fluid medium at low Re due to the increased viscosity. The effect of viscosity is however minimised towards the upper limit of the Re range. At similar Re , reduced t_m values were observed when 0.5 mm diameter tubing was used over the 1 mm and 2mm diameter tubing. This is due to the improvement of the rate of diffusion by reducing the length of molecular diffusion between lamellae in a smaller tube size. This finding is consistent from previous observations made by Gobert *et al* (Gobert *et al.*, 2017). Longer t_m was expected in the 2 mm diameter tubing over the 1 mm diameter tubing. However, Figure 4-10 indicates that the micro-mixing quality is similar with constant Re . The similarity may be attributed to the 1 mm diameter tubing placed upstream which potentially contributed to the overall mixing efficiency. In support of this, Panić *et al* (Panić *et al.*, 2004) have demonstrated that short capillary lengths (< 1 m) are sufficient in completing micro-mixing.

The micro-mixing tests for the pilot-scale reactor gave t_m values in the range 0.0005 to 0.0035 s (Figure 4-11). Only small differences in t_m can be observed between exclusion and inclusion of glycerol in the medium as a function of Re . Interestingly, the pilot-scale reactor was capable of delivering superior micro-mixing relative to that of the lab-scale system. We postulate that the combination of increased turbulence and reactor design (i.e. helical coiling of tubing inducing radial mixing) contributed to very fast micro-mixing, particularly at higher Re .

In comparison to the micro-mixing times determined from the batch mixing experiments, we were able to attain much faster mixing times using continuous tubular reactors depending on the operating conditions. Consequently, faster mixing times with increased mass flow improves overall productivity.

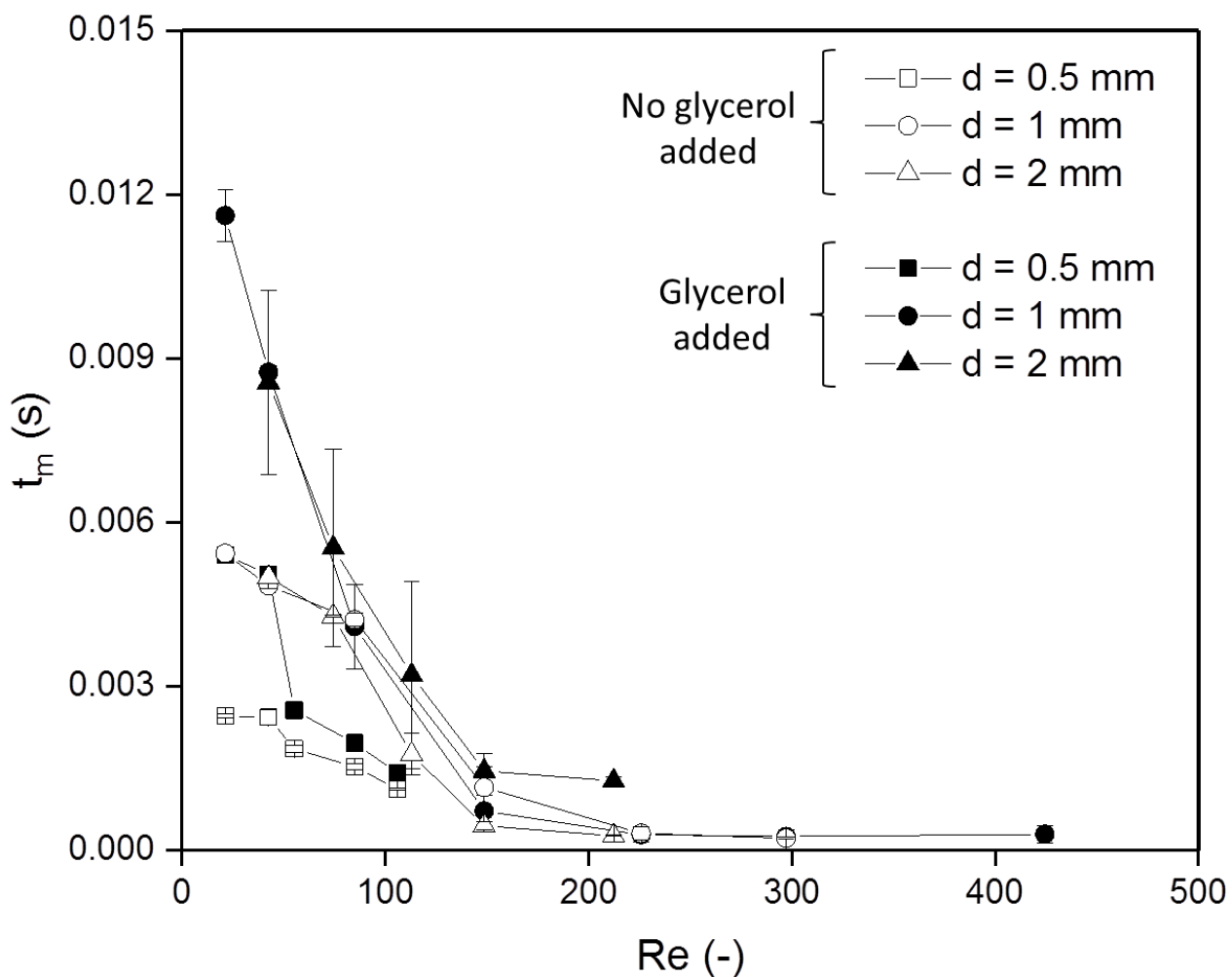


Figure 4-10. Re vs estimated t_m from lab-scale continuous reactor micro-mixing experiments. Reagent concentrations: $[\text{H}_2\text{SO}_4] = 0.02 \text{ M}$, $[\text{H}_3\text{BO}_3] = 0.045 \text{ M}$, $[\text{KIO}_3] = 0.003 \text{ M}$, $[\text{KI}] = 0.016 \text{ M}$. Reactor dimensions: Tee diameter = 0.5 mm, tubing length = 5 m. d corresponds to the diameter of the tubing at the T outlet with the exception of the 2 mm diameter tubing which had a short 1 mm diameter tubing section ($\sim 5 \text{ cm}$) upstream to enable connection. Glycerol was added to the borate-iodate buffered solution to a final concentration of 21 % v/v ($\mu = 2 \text{ mPa}\cdot\text{s}$ at $22.5 \text{ }^\circ\text{C}$). A minimum of 5 reactor volumes were processed before samples were withdrawn and analysed for I_3^- . Data represent the mean value of t_m with $\pm 1 \text{ SD}$ from triplicate experiments.

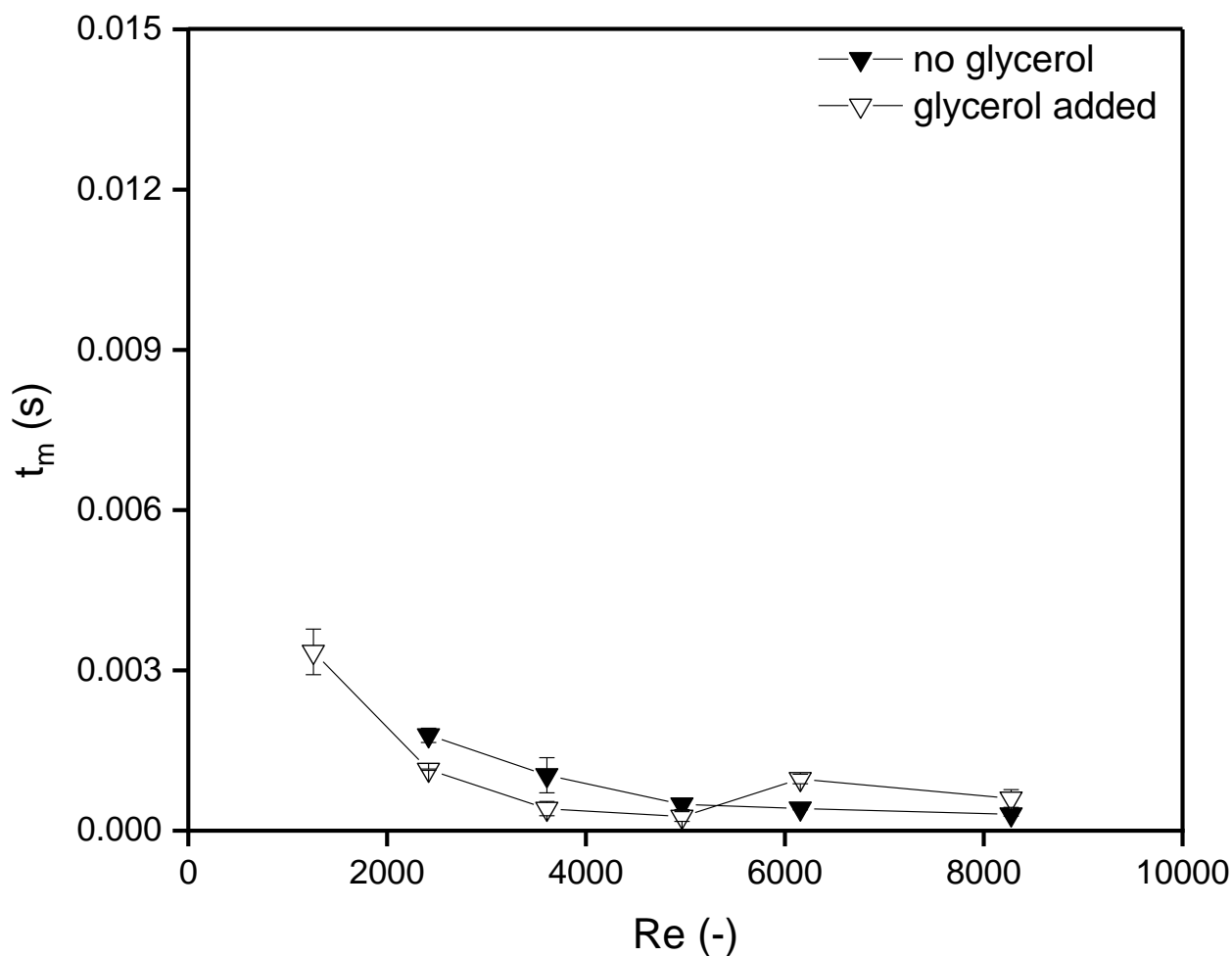


Figure 4-11. Re vs estimated t_m from pilot-scale continuous reactor (CFIR) micro-mixing experiments. Reagent concentrations: $[\text{H}_2\text{SO}_4] = 0.02 \text{ M}$, $[\text{H}_3\text{BO}_3] = 0.045 \text{ M}$, $[\text{KIO}_3] = 0.003 \text{ M}$, $[\text{KI}] = 0.016 \text{ M}$. Reactor dimensions: Tee diameter = 4.8 mm, tubing diameter = 6.4 mm, tubing length = 5 m. Glycerol was added to the borate-iodate buffered solution to a final concentration of 21 % v/v ($\mu = 2 \text{ mPa}\cdot\text{s}$ at 22.5 °C). A minimum of 5 reactor volumes were processed before samples were withdrawn and analysed for I_3^- . Data represent the mean value of t_m with $\pm 1 \text{ SD}$ from triplicate experiments.

4.7 Summary

Reactor designs for the application of a protein precipitation process were presented. Since mixing has been demonstrated to influence the output of these reactions, it was important to characterise different reactor set-ups and operating conditions based on the quality of mixing that could be attained. Here, we assessed the mixing quality from a conventional stirred batch vessel system operated in semi-batch mode and tubular reactor systems operating with continuous flow. Assessment of mixing was conducted using a pH-responsive dye on the macroscopic scale, whilst Villermaux's iodide-iodate test was employed and/or adapted for mixing at the microscopic scale. RTD experiments for the continuous flow experiments were also conducted by positive step inputs of salt to determine the likely flow pattern which was shown to emulate plug-flow like behaviour.

Continuous flow systems exhibited superior mixing efficiencies relative to conventional stirred batch mixing depending on the operating flow rates and the given pressure drop. Whilst improvements to the batch reactor design can be made to match the levels of mixing governed by continuous flow systems, it can be limiting to the application in question. At least for protein precipitation, vigorous mixing can often lead to protein denaturation from the generation of air-liquid interfaces. Another point is that to limit the mixing process to micro-mixing, feeding must be sufficiently slow which reduces overall productivity. In contrast, improved productivity is accompanied by the attainment of reduced mixing times with high flow rates in continuous flow systems. One drawback is when the studied process requires a minimum residence time to achieve a desired output which dictates the length of a tubular reactor. This factor would be addressed in the subsequent chapter. Given the advantages of continuous flow systems, it was of more interest to take a scale-up approach based on a continuous flow system over a batch system.

In this study, we only considered micro-mixing effects for continuous flow systems operating with a 1:1 flow ratio. It would have been interesting to investigate the influence of different ratios of flow rates between both streams. As an alternative, computation fluid dynamics (CFD) can also be a useful tool for the design of mixers and/or a more accurate method for estimating micro-mixing times from precise pressure drop and mixer volume calculations.

Chapter 5: Micro-mixing on protein precipitation as a tool for scale-up

5.1 Introduction

The complexity of precipitation processes brings the difficult task in being able to define the physical and chemical parameters which influence the quality of the precipitate product. This is particularly important when scaling-up to an industrial precipitation process which can operate robustly. As the size of a precipitation vessel increases, some parameters will be more influential on the precipitation performance than others. However, it is usually difficult to control these especially in the presence of interaction effects which may play a pivotal role. A typical approach to the scale up of a precipitation or crystallisation process is by means of maintaining geometric, dynamic and kinematic similarities between scales. The dimensionless groups including Reynolds number, Damköhler number, Peclet number and Camp Number have all been proposed as suitable scale-up criteria (Hoare, 1982b; Ayazi Shamlou *et al.*, 1994; Mahajan and Kirwan, 1996). Scale-up becomes feasible when all the dimensionless groups controlling the process are maintained at the same value between different scales. In most cases, however, this cannot be established and scale-up becomes an empirical process which consequently reduces the development timeframe for launching new therapeutics using precipitation-based processes. Also, where one approach is suitable for a particular system, the same approach may not be feasible for others, suggesting the need to explore multiple strategies. Reports which successfully demonstrate the scale-up of precipitation processes are rather sparse in the literature.

The influence of mixing on product quality with respect to the physical properties of chemical and biological-based precipitates has been studied vigorously (Salt *et al.*, 1982; Momonaga, Yazawa and Kagara, 1992; Iyer and Przybycien, 1994). In stirred batch vessels, the quality of mixing is influenced by mixer type, the size of the mixer, mixer speed, the localisation of the feed point in particular for a semi-batch process, the rate of addition and the solution viscosity. Scale-up on the basis of mixing using the specific power input and tip speed constants have been proposed. The challenge arises when more than one mixing mechanism is controlling the process and thus the output of the product due to the variation of flow patterns between scales. Therefore, using a constant tip speed or constant specific energy input could lead to unsatisfactory large-scale predictions. Some authors have although shown that when the mixing mechanism is limited to micro-mixing, constant power

per unit volume provides good scale-up predictions (Phillips, Rohani and Baldyga, 1999; Zauner and Jones, 2000). In the case of a meso-mixing limited process, constant tip speed has been suggested. Hence, control of the process to one of the multistep mixing mechanisms facilitates the establishment of a scale-up strategy. When operating at fully turbulent conditions i.e at $Re > 10^4$, theoretical values of the mixing time constants for meso-mixing and micro-mixing can be defined. The mixing mechanism with the largest value is likely the mechanism which controls the process. In non-turbulent flows, experimental characterization of the mixing must be performed to determine regions of meso-mixing, micro-mixing or a combination thereof. In order to ensure a micro-mixing-controlled process, the rate of feeding has to be an order of magnitude slower than the circulation rate governed by macro-mixing. Indeed, the throughput of a batch precipitation process would be limited to such feeding rates.

Continuous tubular reactors offer an alternative to the conventional batch-operated processes which carry the potential in achieving much higher throughputs. These rely on short mixing components to bring precipitant and feed solutions into contact, of which include T-mixers, Y-mixers and static mixers. The mixing quality in these reactors becomes dependent on the specific design of the mixer, the tubing size at the outlet and the mass flow rate. Despite the abundance of studies concerning mixing phenomena in these systems, few demonstrate approaches to scaling up precipitation processes based on continuous mixing. So far a suitable scale-up approach based on micro-mixing concerning the precipitation of the pharmaceutical Lovastatin using a two-impinging jets (TIJ) precipitator has been established by Mahajan and Kirwan (Mahajan and Kirwan, 1996). They were able to demonstrate how the magnitude of the micro-mixing time to the nucleation time affected the PSD of Lovastatin precipitates. Therefore, the Damköhler constant was proposed for scale-up. Moreover, they concluded that the TIJ precipitator was capable of completing micro-mixing before nucleation occurs, allowing the control of PSD. This study amongst others come to a general agreement that localised supersaturation gradients influenced by mixing is the key factor in controlling particle size and PSD by influencing nucleation and growth rates.

Owing to the fast kinetics of precipitation on the basis of salting-out, it becomes a critical task to consider the mixing mechanisms at the molecular scale. Therefore, we attempted to understand whether a scale-up approach based upon micro-mixing could be established for our antibody precipitation process. Specifically, we aimed to correlate micro-mixing to the control of precipitate formation with respect to particle size, PSD and particle strength, all of which are critical for subsequent centrifugal clarification. Micro-mixing effects have been

extensively characterised for reactive crystallisation or precipitation for small inorganic compounds, but much less so on biologics.

We use the relation of the micro-mixing model, as detailed in Chapter 2, to our precipitation model on the basis of the competition between particle nucleation and growth rates as function of the micro-mixing efficiency. The importance of Camp Number on increasing particle strength during the precipitate aging process was also evaluated. This was investigated by determining the extent of particle breakage as a consequence of turbulent shear stress, which in turn impacts clarification. Even mechanically strong protein precipitate particles are susceptible to breakage with turbulent shear. This therefore raises the need to characterise such effect in order to determine the viability of a centrifugation step at large scale.

The work outlined in this chapter discusses the influence of reactor design and operating conditions, of which directly relate to the mixedness, on the precipitation performance with regards to final precipitate properties. The USD centrifugation method is then applied to measure the shear sensitivity of the formed particles and its influence on the ease of clarification. The USD concept, developed at UCL, is to mimic pilot-scale centrifugation in the laboratory by applying a rotating disc device which can simulate the equivalent shear experienced in the feed zone of industrial centrifuges. Then, the ease of clarification is assessed using a laboratory scale centrifuge and validated with pilot-scale based on the concept of sigma theory. Taking this integrated approach allows the interaction between precipitation operation and subsequent centrifugal processing to be established.

5.2 Theoretical considerations

5.2.1 Particle fractal dimension

A particle in three-dimensional space is considered to be fractal if its density decreases with radial distance from the nucleus. An assessment of the fractal geometry of particles may provide a useful insight into the characterisation of protein precipitates which influence their behaviour during solid-liquid separation. Fractal dimension analyses were first described as a method of elucidating the process of diffusion-limited colloidal aggregation that leads to the formation of clusters with particular structures (Meakin, 1990). The fractal dimension, f_D , has a value less than 3 and is a non-integer. In the case of a straight line, f_D is 1; for a circle in two-dimensional space, f_D is 2, and for a perfectly spherical aggregate which is uniformly

packed of primary particles; f_D is 3. The typical branched and porous nature of particle structures often obtained from aggregation and/or precipitation processes, f_D will have a value less than 3.

In addition to acquiring PSD data from laser light scattering methods, it is also possible to extract scattering angle and light intensity data information which provides estimations of f_D . In the Malvern Mastersizer 3000, which has a particle size detector range of 0.1 μm to 1 mm, 68 detectors are placed at unique scattering angles that detect particles within a particular size range. The scattering wave vector, Q , is a function of the scattering angle, Θ , and corresponds to the inverse of a particular particle radius which is given by:

$$Q = \frac{4\pi n_i}{\lambda} \sin\left(\frac{\Theta}{2}\right)$$

Equation 5-1. Calculation of scattering wave vector, Q .

The scattering pattern of deflected laser light with intensity, I , at each Θ is a function of the number of aggregate particles at the corresponding particle size and is characteristic of the nature of the particle structures. The number of particles present within the aggregate is a function of f_D and I which is expressed as:

$$\text{Log}I = k - f_D \text{Log}Q$$

Equation 5-2. Log-log correlation of deflected laser light intensity, I , at each scattering angle, Θ , to estimate particle fractal dimension, f_D .

where k is a proportionality constant. Plotting $\text{Log}Q$ against $\text{Log}I$ gives a negative slope by which the fractal dimension is estimated from. Figure 5-1 shows the construction of the log-log plot to estimate the fractal dimension of precipitates subjected to an impeller mixing rate of 400 rpm. Data points corresponding to the scattering wave vector at particle size detectors 34 to 43 were used to construct the slope. The negative slope was determined with 95% confidence limits.

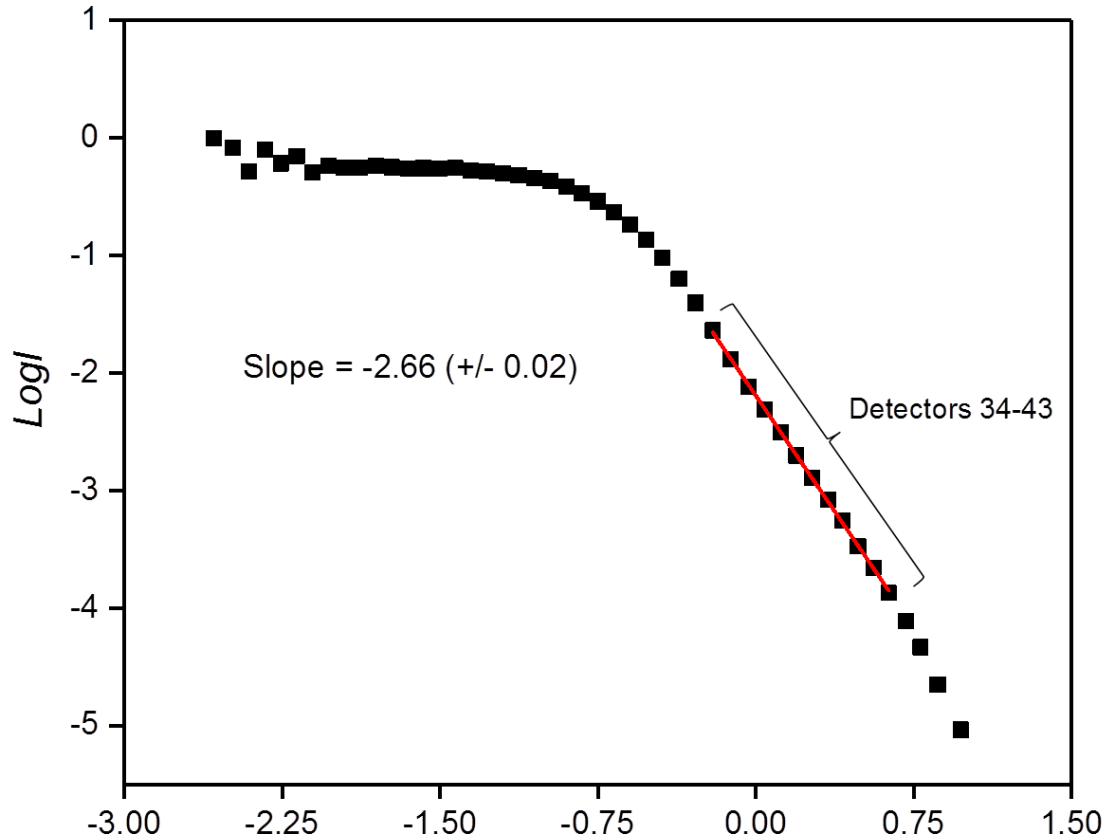


Figure 5-1. Log-log plot for the estimation of the fractal dimension, f_D , of a protein precipitates with laser light diffraction. This example corresponds to the light intensity, I , of the scattering pattern as a function of the scattering wave vector, Q , for a precipitate suspension formed in batch mode with mixing at 300 rpm. The negative slope is taken between the values of $LogQ$ corresponding to the scattering angles at detectors 34 to 43 in the Mastersizer 3000.

5.2.2 Sigma theory

The concept of sigma theory allows a centrifuge to be described in terms of its solid-liquid separation performance, independent of the operating conditions. The sigma factor, Σ , also referred to as the equivalent settling area, is defined as the required surface area of a gravity settling tank that provides equal clarification performance as the centrifuge under equivalent conditions. This factor is often used when comparing the performance of centrifuges of different types or for scale-up purposes. For a given centrifuge, the clarification performance is defined as the ratio of the volumetric rate, Q , and Σ . Therefore, based on the unique

correlations for calculating Σ for various centrifuges, similar clarification performances between centrifuges can be achieved according to the relation:

$$\frac{Q_1}{\Sigma_1} = \frac{Q_2}{\Sigma_2}$$

Equation 5-3. Sigma theory correlation between two types of industrial centrifuges which provide similar clarification.

where subscripts 1 and 2 each denote a different type of centrifuge. For a disc-stack centrifuge, the equivalent settling area is calculated by:

$$\Sigma_{ds} = \frac{2\pi z \omega^2 (R_o^3 - R_i^3)}{3g \tan\theta} C_{ds}$$

Equation 5-4. Calculation of equivalent settling area for disc-stack centrifuges.

where Σ_{ds} is the equivalent settling area of a disc stack centrifuge, z is the number of discs, ω is the angular velocity, R_o and R_i are the outer and inner disc radius, respectively, θ is the half disc angle and C_{ds} is a correction factor for non-ideal flow and has a value of 0.4. In the case of laboratory centrifuge, equivalent settling area is defined by the correlation:

$$\Sigma_{lab} = \frac{V_{lab} \omega^2}{2g \ln\left(\frac{2R_o}{R_o + R_i}\right)} C_{lab}$$

Equation 5-5. Calculation of equivalent settling area for laboratory centrifuges.

where Σ_{lab} is the equivalent settling area of a lab centrifuge, V_{lab} is the volume of feed processed in the centrifuge tube and C_{lab} is the correction factor, assumed to be equal to 1 for our purposes.

The volumetric flow rate through a disc-stack centrifuge can be mimicked in a lab centrifuge by the ratio of process material and the time of centrifugation, t_{lab} . Therefore, comparisons on the ease of sample clarification between laboratory centrifuges and large scale centrifuges using different settings can be performed with the following assumption:

$$\frac{V_{lab}}{\Sigma_{lab} t_{lab}} \approx \frac{Q_{ds}}{\Sigma_{ds}}$$

Equation 5-6. Sigma theory correlation to mimic clarification of an industrial centrifuge with a laboratory centrifuge.

5.3 Batch precipitation trials

5.3.1 Effect of mixing during micro-mixing-controlled precipitation

Precipitations of cell culture fluid using ammonium sulphate were carried out in the stirred batch vessel system using micro-mixing-controlled conditions, of which have been experimentally characterised in section 4.6.1. The reactor was first charged with 58 mL of CCCF solution, to which 42 mL of 3.6M ammonium sulphate was added via the 0.5 mm diameter bore at a constant rate of 0.25 mL/min. The final conditions were 1.5 M ammonium sulphate (corresponding to 42% saturation) and 0.8 mg/mL IgG₄. The precipitations were carried out at an ambient temperature and at pH 7. No pH adjustment was required following the addition of precipitant due to the phosphate buffering components of the ammonium sulphate and CCCF solutions. Impeller speeds during the additions were ranged between 100 and 500 rpm as in the mixing characterisation experiments performed in section 4.6.1.

In all the experiments, the induction of precipitation was observed when the ammonium sulphate concentration reached approximately 1 M, consistent with the predetermined IgG₄ solubility curves. Samples of the precipitate were withdrawn and analysed immediately after the end of feeding, after 5 minutes and then every 10 minutes for up to an hour. Mixing at 100 rpm was found to be too slow in keeping the mixture fully mixed as was evident by the sedimentation of the precipitate throughout the course of the experiment. Therefore the experiment was repeated at 150 rpm which minimised the presence of two phases. The mixing speed range was therefore adjusted from 150 to 500 rpm. Sampling of the precipitate mixture between the end of feeding and during the course of the experiment where the precipitate underwent constant mixing showed that, for a given mixing speed, there was no particular difference in the particle size or PSD (data not shown). This suggested that particles had already grown to their final equilibrium sizes upon a short time of reaching the target ammonium sulphate concentration.

Figure 5-2 displays the final mean particle size values, as a function of impeller speed from triplicate experiments. A 23% increase in the mean particle size was observed when the mixing speed was raised from 150 to 200 rpm, corresponding to micro-mixing times of 20 and 13.3 ms, respectively. The 200 rpm condition achieved a maximum mean particle size value of $15.6 \pm 0.6 \mu\text{m}$ over the mixing range. Thereafter, the mean particle size became an inverse function of the mixing speed and decreased to $8.6 \pm 0.5 \mu\text{m}$ at 500 rpm.

The broadness of the precipitate PSD was also influenced by the mixing regime, as illustrated in Figure 5-3. Broader PSDs were attained with low mixing speeds whilst high

mixing speeds yielded narrower PSDs. The rise in mean particle size between the 150 and 200 rpm condition suggests improved diffusion rates of mass transfer of solute into the vicinity of the protein molecules as a consequence of better mixing. Considering the low molecular weight of ammonium sulphate relative to that of proteins, the diffusion of its ions in solution will be much more rapid and hence the proteins can be considered as stationary whilst the salt ions being highly mobile. During low mixing, the rate of diffusion of ammonium sulphate to a protein particle is slow which in turn slows down the rate of consumption. Therefore, the solution is saturated with higher ammonium sulphate concentrations for a longer period until the final saturation level is reached when the mixing is complete. As a result, this leads to some highly supersaturated regions where nucleation rates are higher and particle sizes are generally lower. This effect of supersaturation is then minimised with increased mixing speeds. However, at high mixing speeds, corresponding to micro-mixing times in the range 2.2 to 5.5 ms in this system, whilst diffusion of mass transfer is faster, the mechanical energy from the mixer creates more forceful impacts between the particles causing particle disruption and in turn reduced the particle size. This phenomenon could be indicative of a secondary nucleation process taking place whereby abrasion of particles formed during the primary nucleation process readily occurs.

According to the micrographs in Figure 5-4, the precipitates form aggregates of primary particles with amorphous structures of distinct sizes depending on the level of mixing employed. For some particles, conglomerates of sizes greater than those measured from laser diffraction were seen. This could have been due to the stacking of smaller particles trapped between the glass slides and cover slips during the microscopic analysis of undiluted samples, thereby appearing as larger aggregates. During particle size measurements, the particles become dispersed in a cuvette and so this stacking effect would not be observed. Therefore, laser diffraction was primarily relied on to determine particle sizes, whilst microscopy was useful in informing gross structural differences between particle samples. Particularly at the 500 rpm mixing condition, the precipitates appeared to regularly form more globular and compacted structures than the rest.

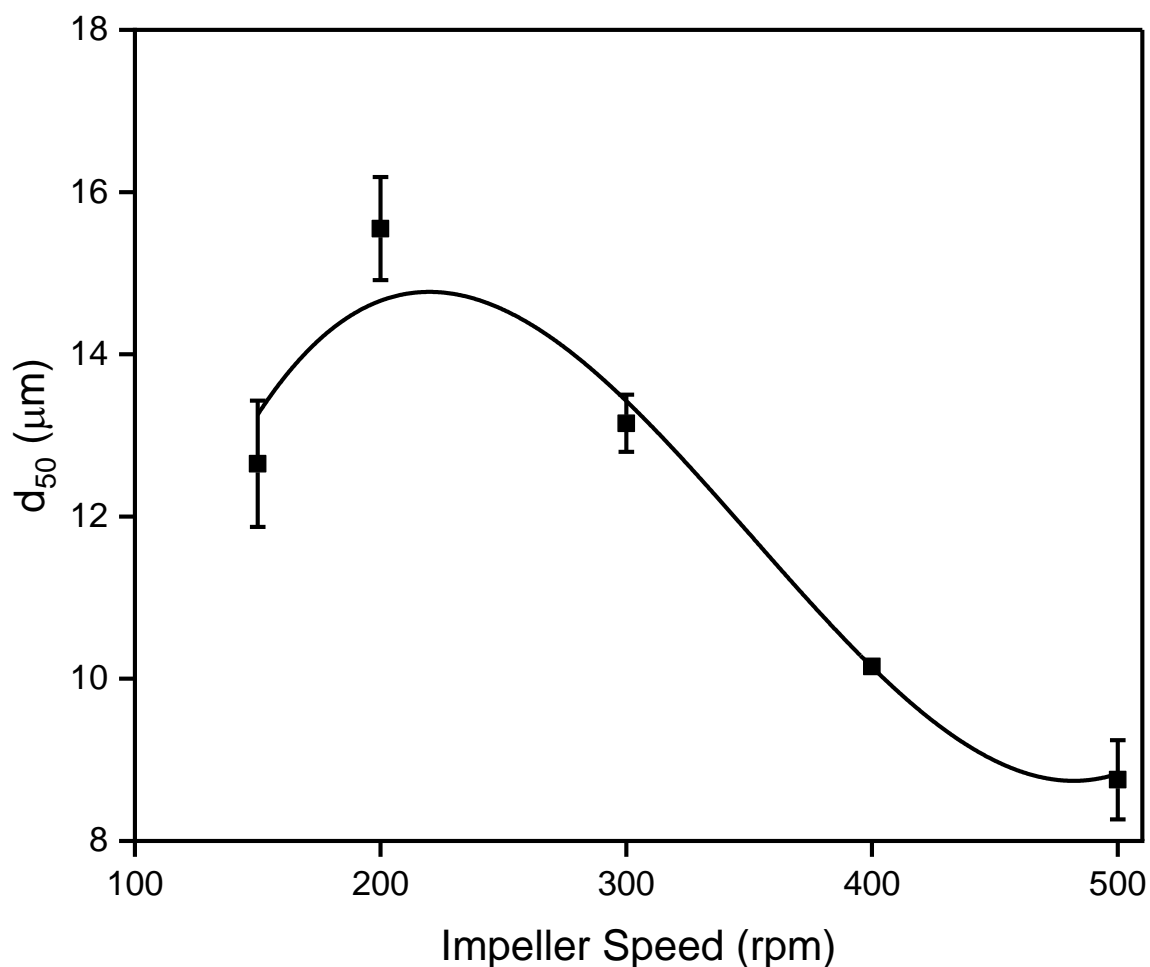


Figure 5-2. Effect of impeller speed on the average mean particle size, d_{50} , of CCCF precipitates with ammonium sulphate in a 150 mL baffled-stirred vessel under micro-mixing-controlled conditions. Batch vessel was pre-charged with CCCF containing 1.4 mg/mL IgG. 3.6 M ammonium sulphate was injected at a constant feed rate of 0.25 mL/min. Final solution conditions were 1.5 M ammonium sulphate and 0.82 mg/mL IgG. All precipitations were conducted at ambient temperature and at pH 7.0. Data are shown as averages of the final mean particle sizes from triplicate experiments with error bars corresponding to ± 1 standard deviation. Minimal differences in mean particle sizes were observed throughout the selected aging period of 0 to 60 min.

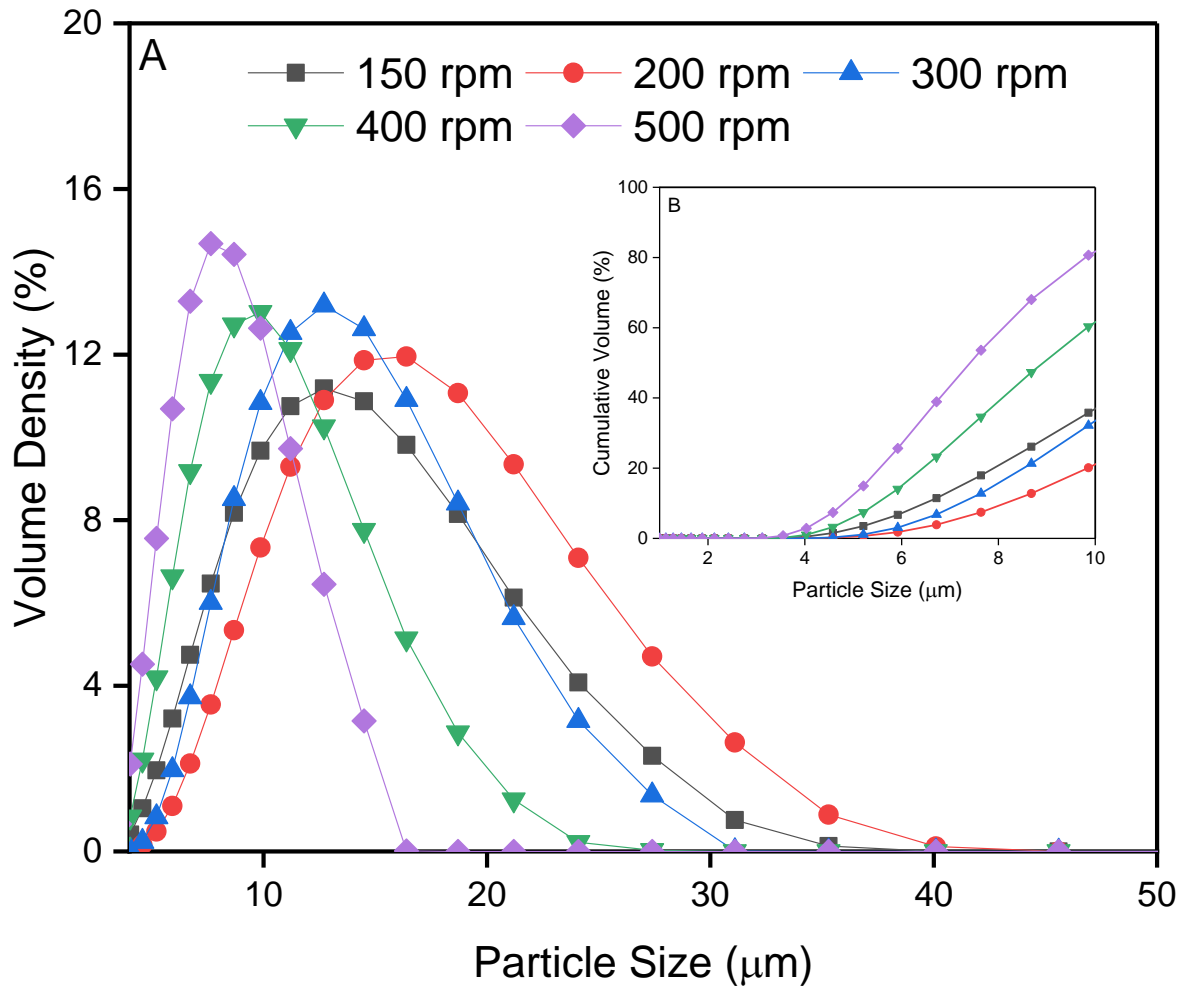


Figure 5-3. Effect of batch mixing speed on the PSD profiles of CCCF precipitates under micro-mixing-controlled conditions. (A) PSD, on the basis of volume density, shown on the linear scale in the range 0 to 50 μm (no additional peaks were observed beyond this quantity). (B) Cumulative PSD of particles $\leq 10 \mu\text{m}$, highlighting the differences in the quantity of particle fines between the mixing conditions. Distributions are presented as technical averages from $n = 5$ measurements for each triplicate experiment.

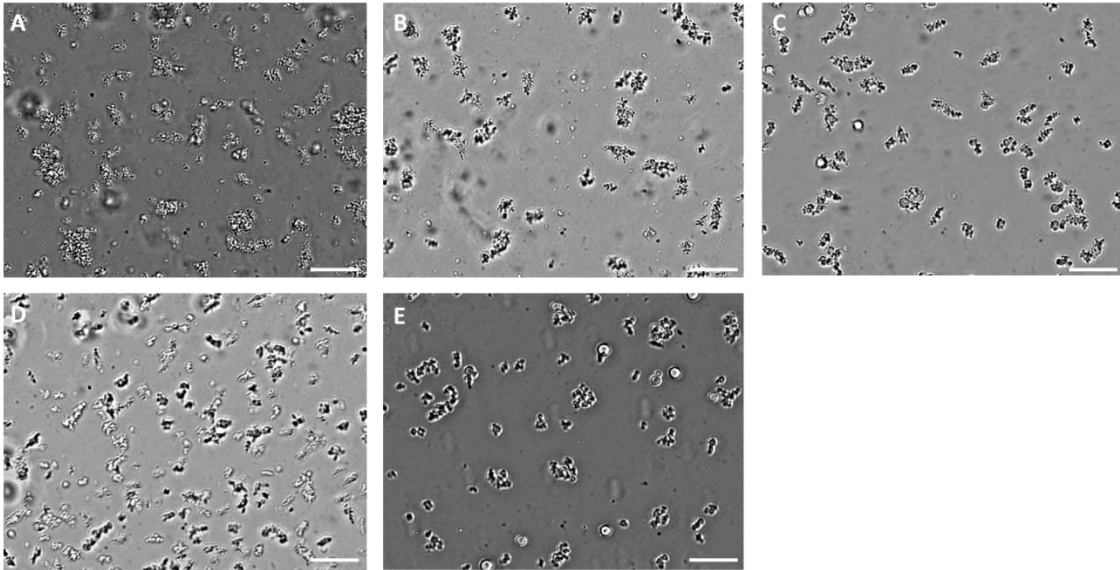


Figure 5-4. Representative micrographs of protein precipitate particles prepared during batch precipitation experiments. These were prepared corresponding to the mixing conditions: (A) 150 rpm, (B) 200 rpm, (C) 300 rpm, (D) 400 rpm and (E) 500 rpm mixing. Undiluted samples were used for visual observation. Post-image analysis was performed using ImageJ. Scale bar corresponding to 20 μm is displayed.

5.3.2 Effect of increased agitation on precipitates

An experiment was conducted to assess how precipitate aging approaches influence potential changes in the particles by exposing the final precipitated material to more intense mixing regimes than the mixing level used for the precipitation itself. A precipitation was first carried out with mixing at 200 rpm which gave the maximum mean particle size (d_{50} : $15.6 \pm 0.6 \mu\text{m}$). Increases in the mixing rate up to 600 rpm in 100 rpm increments were implemented for 10 minutes before increasing to the next required speed. Samples were taken prior to each speed increase.

As the mixing speed chosen yielded the widest PSD with the largest mean particle size, it would have been expected that increasing the mixing speed would induce particle fragmentation due to exposure to increased shear. In fact, we did not observe any changes in the particle size nor in PSD upon intensifying the mixing (data not shown). Based on these results, it can be suggested that the final particle size and PSD are primarily influenced by the mixing of solutions during injection and the aging process has minimal effect. This finding is in fact consistent with the study on acid precipitation of whey protein isolates in a similar system, conducted by Byrne and colleagues (Byrne *et al.*, 2002a). It can also be

hypothesised that once particles are fully formed, the increase in mechanical energy imposed from the more intense mixing regimes may not be sufficient to induce particle breakage.

5.3.3 Ultra scale-down centrifugation of batch precipitates

5.3.3.1 Particle breakage of batch-formed precipitates with the rotating disk device

Precipitate samples generated from the batch precipitation experiments were exposed to the turbulent shear stress in the rotating disc device, mimicking the feed zone of a disc-stack centrifuge prior to entering the settling region of the centrifuge. This device required small sample usage (~ 20 mL) which enables full characterisation of centrifugation conditions where sample is limited. As protein precipitates are generally vulnerable to these kinds of environments, it is important to identify the suitability of a large scale centrifuge for their recovery. Significant particle breakage becomes problematic as the centrifuge is less able to capture solids with particle sizes below a certain range. It is therefore desirable to obtain precipitates that are mechanically strong in withstanding such forces, which is related to the Camp number. It has been suggested that Camp numbers above 10^5 create compact flocks which minimise shear susceptibility and allow better separation from the liquid (Jungbauer, 2013).. From the semi-batch operated precipitation experiments, it was difficult to accurately determine a characteristic Camp number since it was not known at what point it should be determined from i.e. from the point of precipitation induction (at approximately 1 M salt) or from the end of feeding. Therefore for consistency, an aging time of 1 hour was included for each experiment which ensured the Camp numbers was kept above 10^5 .

The effect of exposing the precipitates formed under the various conditions to a shear stress of 6000 rpm, corresponding to a maximum energy dissipation rate of 0.045×10^6 W/kg, is shown through the PSD profiles of non-sheared versus sheared samples, as shown in Figure 5-5, and in micrographs displayed in Figure 5-6. This energy dissipation rate was considered to be representative of a hydro-hermetic feed zone according to Chatel *et al* (Chatel, Kumpalume and Hoare, 2014), which essentially avoids air-liquid interfaces in the feed disc.. This feature would be particularly important in avoiding potential damage of the protein precipitates due to the presence of such interfaces. Despite keeping the Camp numbers for each of the precipitates above 10^5 , various extents of particle breakage can be observed. The extent of breakage was shown to be dependent on the initial mixing strategy for the precipitation reaction. The maximum amount of particle breakage was observed for the precipitates formed with 150 and 200 rpm mixing, showing a 54 and 56 % reduction in

mean particle size, respectively. In contrast, precipitates formed at the highest mixing levels i.e. 400 and 500 rpm experienced the least amount of abrasion with only a 6 - 10 % reduction in the mean particle size. The micrographs in Figure 5-6 demonstrate that the large aggregates formed during low mixing fragment significantly into finer particles whilst particles generated at 300 and 500 rpm break to a much lesser extent. In some cases, precipitates which were formed during low mixing were 'aged' for longer periods to elevate the Camp number, similar to that of precipitates formed during high mixing to determine if the susceptibility to breakage could be reduced by aging. Yet, these particles eroded to a similar extent in comparison to a 1 hour aging period (data not shown). Therefore, increasing the aging time did not show to add any benefit in particle strength. This suggested that the initial mixing of protein and precipitant was more critical in controlling final precipitate characteristics.

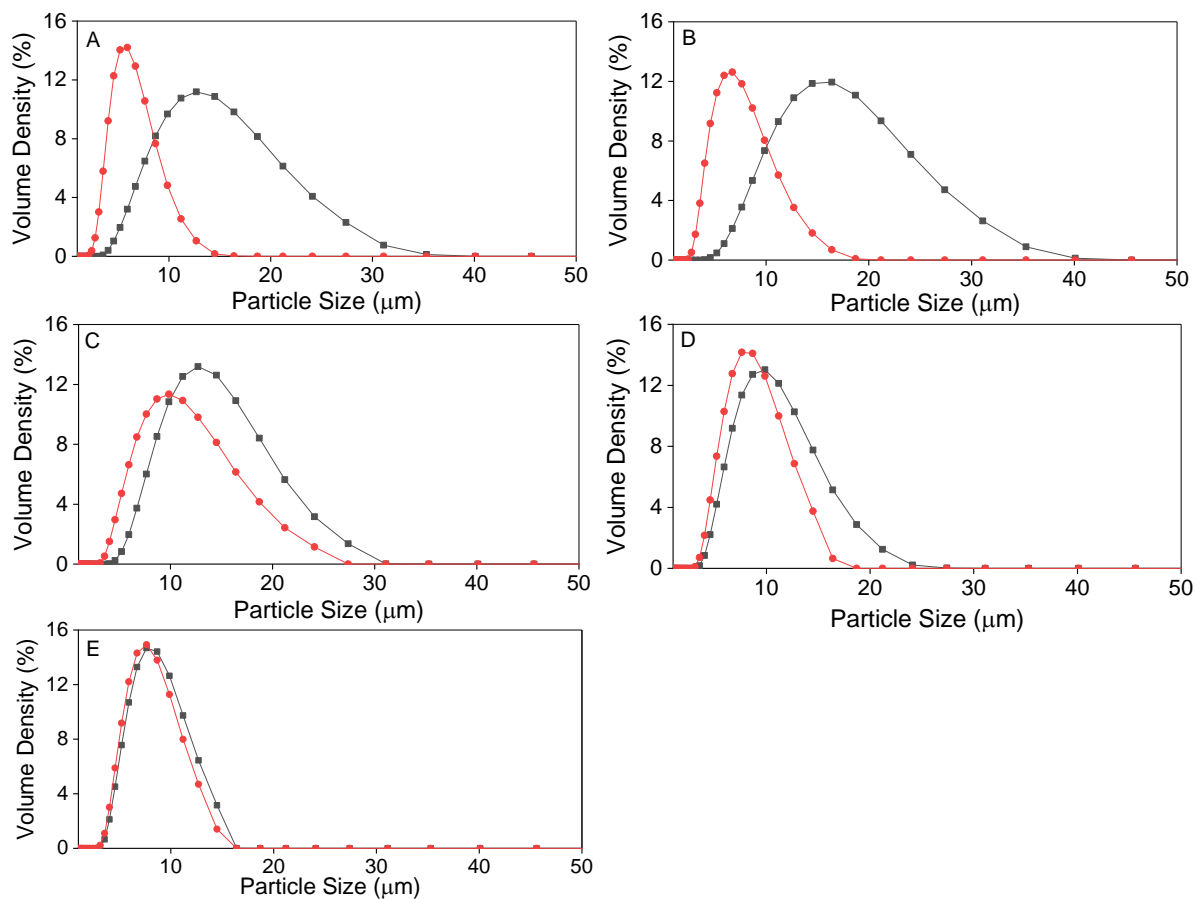


Figure 5-5. Effect of turbulent shear stress on batch precipitates. Distributions, on the basis of volume, are shown for the batch precipitate suspensions formed from the various mixing conditions (black curves) and subsequently exposed to shear stress in the rotating disc device (red curves). (A) 150 rpm mixing, (B) 200 rpm mixing, (C) 300 rpm mixing, (D) 400 rpm mixing and (E) 500 rpm mixing. Sheared samples were prepared by exposing the precipitate suspensions to the rotating disc device at 6000 rpm, corresponding to a maximum energy dissipation rate of 0.045×10^6 W/kg. Distributions are presented as technical averages from $n = 5$ measurements for each replicate experiment.

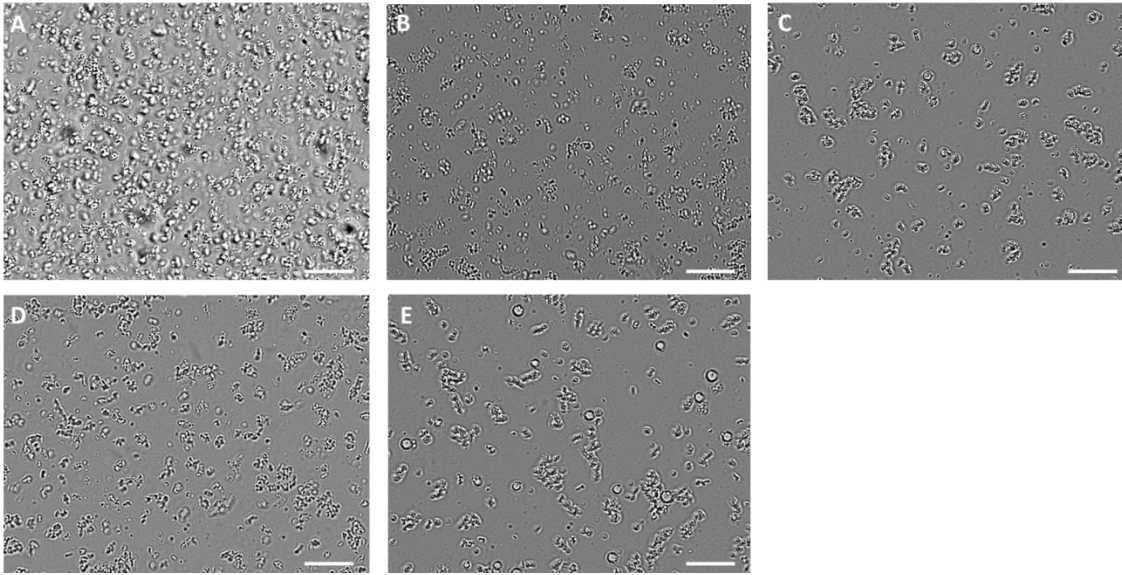


Figure 5-6. Representative micrographs of batch-formed precipitates after exposure to turbulent stress at 6000 rpm in the rotary disc device. A-E nomenclature from Figure 5-5 is used. Undiluted samples were used for visual observation. Post-image analysis was performed using ImageJ. Scale bar corresponding to 20 μm is displayed.

5.3.3.2 Fractal dimension values

Table 5-1 presents the estimated f_D values for the batch precipitate particles formed from the various mixing regimes. The samples exposed to turbulent shear in the rotating disc device were also characterised in terms of f_D . The trend shows an increase in f_D values for precipitates formed with better mixing and is in the range 2.53 to 2.77. As might be expected, particles with high f_D are more compact and more able to withstand the effects of turbulent processing in the rotating disc device. Correlating f_D with the changes in mean particle size with turbulent processing as a function of the mixing employed during precipitation shows good agreement with this theory. In addition, the newly fragmented particles possessed higher f_D , on a relative basis suggesting the formation of tougher and more highly compact structures.

Table 5-1. Determined f_D values of non-sheared and sheared batch precipitate samples as a function of mixing. Mean values of f_D are shown from $n = 3$ experimental runs ± 1 standard deviation.

		f_D	
		Non-sheared	Sheared
Mixing Condition	Shear Condition		
	150 rpm	2.53 \pm 0.02	2.71 \pm 0.08
	200 rpm	2.48 \pm 0.04	2.76 \pm 0.02
	300 rpm	2.50 \pm 0.06	2.77 \pm 0.06
	400 rpm	2.67 \pm 0.02	2.72 \pm 0.01
500 rpm	2.77 \pm 0.04	2.80 \pm 0.04	

Differences in the estimated f_D values for the precipitates produced at the various mixing conditions were statistically evaluated to confirm if these were statistically different. To this end, a one-way ANOVA test to compare the means was performed.

First, the one-way ANOVA was used to establish the presence of statistical significance between sample groups at the 95% confidence level ($\alpha = 0.05$). Second, a post-hoc test was followed to determine between which sample groups was there a statistically significant difference. The one-way ANOVA uses three assumptions: 1) the dependent variable is normally distributed in each group, 2) there is equal variance between the groups and 3) the sample cases should be independent of each other. The first assumption can be tested with SPSS statistics. Shapiro-Wilk test was used to test whether the spread of the data in each sample group was normally distributed. The second assumption can be ignored as the sample sizes between each sample group are equal. The third assumption was met due to each experiment being performed independently of each other.

The result of the Shapiro-Wilk test revealed that f_D data regarding the non-sheared precipitates and sheared precipitates were normally distributed according to the corresponding p-values ($p > 0.05$). The ANOVA test with equal variances revealed that there were statistical differences in f_D between the non-sheared precipitates ($p < 0.001$), but no statistical differences detected between f_D of sheared precipitates ($p = 0.226$). A post hoc Tukey's test showed that the f_D of precipitates formed at 100, 200 and 300 rpm did not differ significantly from each other ($p > 0.05$), whilst the f_D of precipitates formed at 400 rpm and 500 rpm differed significantly from the other four mixing conditions ($p > 0.05$).

5.3.3.3 Clarification results

Centrifugation conditions studied for the sedimentation behaviour of non-sheared and sheared samples were selected to represent those equivalent for a disc-stack centrifuge, $(Q/\Sigma) = (V_{lab}/t_{lab}|\Sigma_{lab}) > 3 \times 10^{-9}$ m/s. The clarification behaviour can be presented in two ways: clarification efficiency or percentage of solids remaining. For our purpose, it was decided to represent the performance of precipitate clarification in terms of solids remaining as this provides a better insight for sizing filters which are often implemented at the interface between centrifugation and chromatography. Also, if the clarification efficiencies between samples are high (> 95%), the differences expressed as percentage of solids remaining become clearer.

The comparison on the centrifugal recovery for non-sheared and sheared precipitates formed during batch processing, as a function of $V_{lab}/\Sigma_{lab}t_{lab}$, i.e. centrifuge throughput, in the range 9.25×10^{-9} to 4.8×10^{-8} m/s, is presented in Figure 5-7. As expected, for a given condition, the level of clarification was directly proportional to the centrifuge throughput. Since t_{lab} was a fixed value at 10 mins, increasing V_{lab} which additionally influences the settling area, the distance for a given solid to settle in suspension under centrifugal forces is greater. For the control samples which were not exposed to the rotating disc device, the 500 rpm condition provided the least amount of clarification over the whole range with 7.6% solids remaining at the highest centrifuge throughput. As expected, precipitates formed with 200 rpm mixing gave the optimal level of clarification with 2.4% solids remaining at the highest centrifugation throughput due to the presence of larger particles that ease the clarification. However, upon shearing the same samples, the trend in clarification performance was somewhat reversed. Clarification was severely impacted for sheared precipitates formed in the 150 and 200 rpm conditions. In both cases, the remaining solids were comparable in the range 14.7 to 20 %, depending on the throughput. This effect was minimised for sheared precipitates formed at the higher mixing speeds, giving improved centrifugal recoveries (7% at the highest centrifugation throughput).

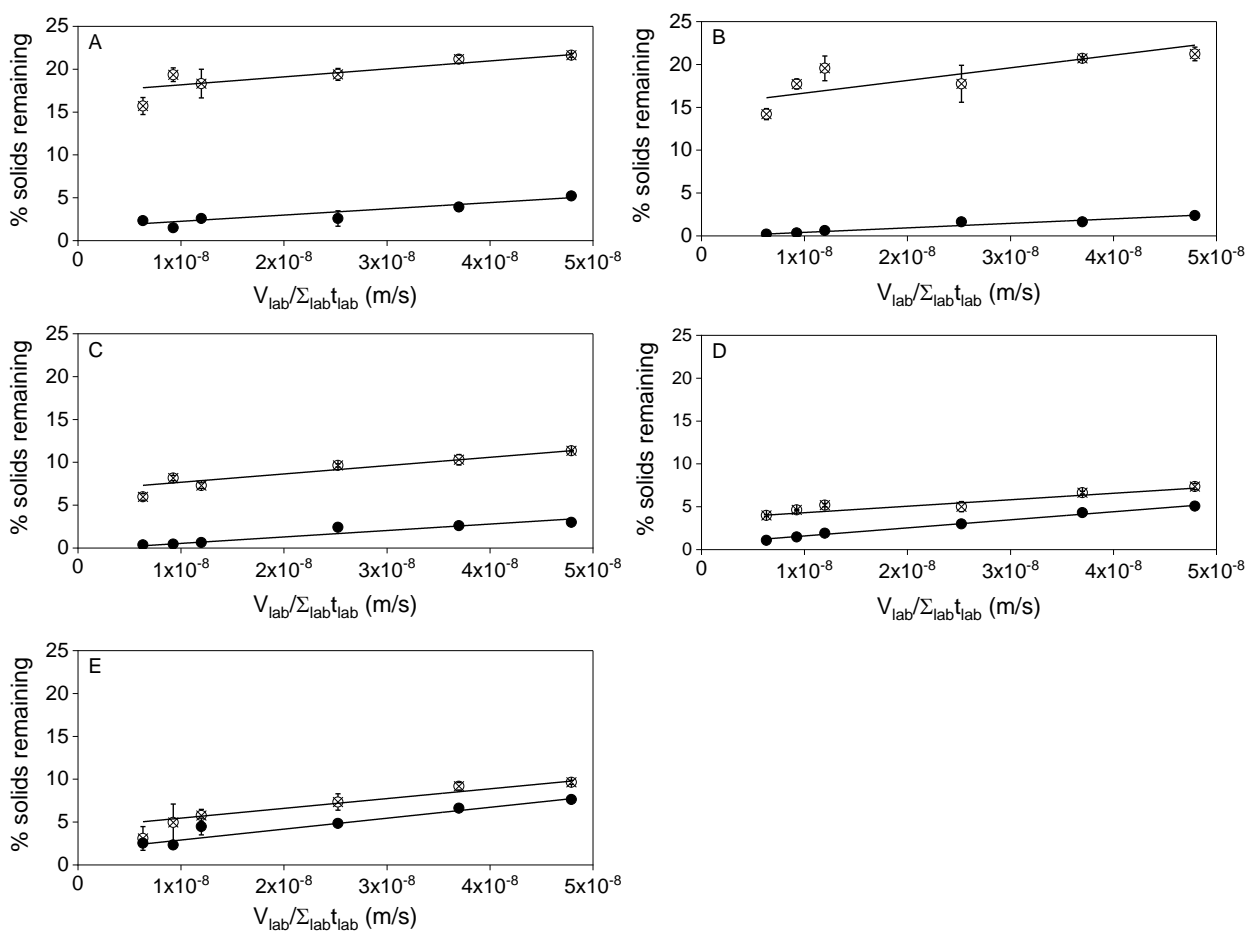


Figure 5-7. Ultra scale-down centrifugation analysis of non-sheared (black circles) and sheared (crossed open circles) precipitate samples from the batch precipitation experiments conducted at (A) 150 rpm, (B) 200 rpm, (C) 300 rpm, (D) 400 rpm and (E) 500 rpm mixing. Sheared samples were prepared by exposing the precipitate suspensions to a rotating disc device at 6000 rpm, corresponding to a maximum energy dissipation rate of 0.045×10^6 W/kg. Centrifugation performance is reported in terms of percentage of solids remaining in the supernatant fraction with respect to various centrifuge throughputs. Data are presented as averages of $n = 4 \pm 1$ standard deviation and fitted with linear regression.

5.4 Continuous precipitation trials

5.4.1 Lab-scale continuous precipitation

Precipitations in the continuous tubular reactor were carried out by feeding CCCF containing a desired concentration of antibody and 3 M ammonium sulphate solution through T mixers in a 1-to-1 volumetric ratio. The final precipitation condition was 1.5 M ammonium sulphate and constant antibody concentration. Similarly to the batch experiments, precipitations were maintained at pH 7, as measured at the outlet, and performed at ambient temperature. During operation, samples were taken after 5 reactor volumes had been processed. Most continuous precipitation experiments were performed with an antibody concentration of 0.8 mg/mL. Otherwise, the effect of antibody concentration in the precipitate stream was evaluated in section 5.4.3.

5.4.2 Effect of flow rate and residence time on particle size, PSD and yield

From the results presented in section 4.6.2, it was observed that mixing is influenced by the mean energy dissipation of the flow rates of the feed solutions through the system. Therefore, the influence of mixing on the basis of flow rate was used to evaluate precipitation performance in continuous flow systems. The reactor length required to complete the precipitation was determined in the lab-scale reactor using 1 mm diameter tubing. Precipitations were first carried out using a length of 10 m which followed reduction to 5, 4, 3, 2 and 1 m. The flow rate through the system was manually adjusted to 1, 2, 4, 10, 14 or 20 mL/min. Precipitation was assumed to be complete when the mean particle size was at a stable value.

The evolution of mean particle size at the various flow rates over the reactor lengths are displayed in Figure 5-8. It can be seen that for 1, 2 and 4 mL/min, the initial mean particle size changed over a few meters of tubing up to 5 m, corresponding to residence times in the range 47 to 190 s depending on the flow rate. Thereafter, the same particle size was obtained at 10 m. To ensure the precipitation was complete, the reactor effluent for each of the conditions was collected in a batch reactor and continuously stirred at 300 rpm with a mechanical stirrer for up to an hour. No further change in particle size was observed indicating precipitation had already been completed in the continuous reactor. At the higher flow rates, the initial particle sizes did not seem to change during the course of the process or when similarly aged in a batch vessel. This suggested that the final equilibrium particle

size was obtained very quickly at fast micro-mixing times. Moreover, the mean particle size decreased as the flow rate increased, as did the spread of PSD (Figure 5-9). This could be explained through enhanced mixing which increases the shear exposure on the precipitates, and in turn induce particle breakage events.

Figure 5-10 displays representative micrographs of the precipitates obtained at 1, 2, 4, 7 and 14 mL/min. In the case of the 20 mL/min condition, a similar result to the 14 mL/min condition was obtained. The micrographs corroborate with the decrease in mean particle size as the operating flow rate increases, as well as an increased abundance in the smaller particles.

The shift of the mono-modal PSDs, as had been observed for batch precipitation, confirmed the predominance of a micro-mixing regime controlling the precipitation reaction. In adopting the micro-mixing model to the nucleation and growth reactions, we can propose that nucleation is more highly favoured over precipitate growth at high flow rates i.e. with short micro-mixing times, which results in the generation of smaller particles. In contrast, when the micro-mixing is longer due to low flow rates, the rate of precipitate growth is enhanced and particles are allowed to grow to larger sizes. The spread of the PSDs between the conditions can be attributed to the presence of supersaturation gradients due to temporal heterogeneity of conditions in the system. Since these gradients are maximised during low mixing, particle nucleation and growth occur before micro-mixing is complete. The space time for supersaturation gradients is then minimised during superior levels of mixing governed by high flow rates and increased turbulence, giving narrower PSDs. As the flow rate progressively increases, and as does the mixing, the change in the d_{50} values and PSD shifts become less apparent. It even appears that the value of d_{50} begins to approach a minimum by which enhanced levels of mixing would have no further influence in the particle formation. Given this, it's possible that we were able to identify a mixing window in which the mixing time is less than or of the same order of magnitude as the precipitation induction time. These findings were consistent with reports which attempted to relate the micro-mixing quality based on micro-mixing times towards the rapid precipitation of pharmaceutical products in a TIJ precipitator based on the identification of characteristic micro-mixing and precipitation induction times (Liu, Ma and Wang, 2015).

Precipitates obtained after processing through 5 and 10 m of tubing were recovered by centrifugation and/or filtration through 0.22- μ m PES membranes and re-solubilised up to half the original volume with 50 mM sodium phosphate buffer. In all experiments, the antibody yield was in the range 91.3 to 94.6%. The small differences in these values indicated that flow rate does not have a clear impact on the yield. Since no change in the yield and particle

size result was observed after 5 m of processing, future precipitation experiments were performed at this length.

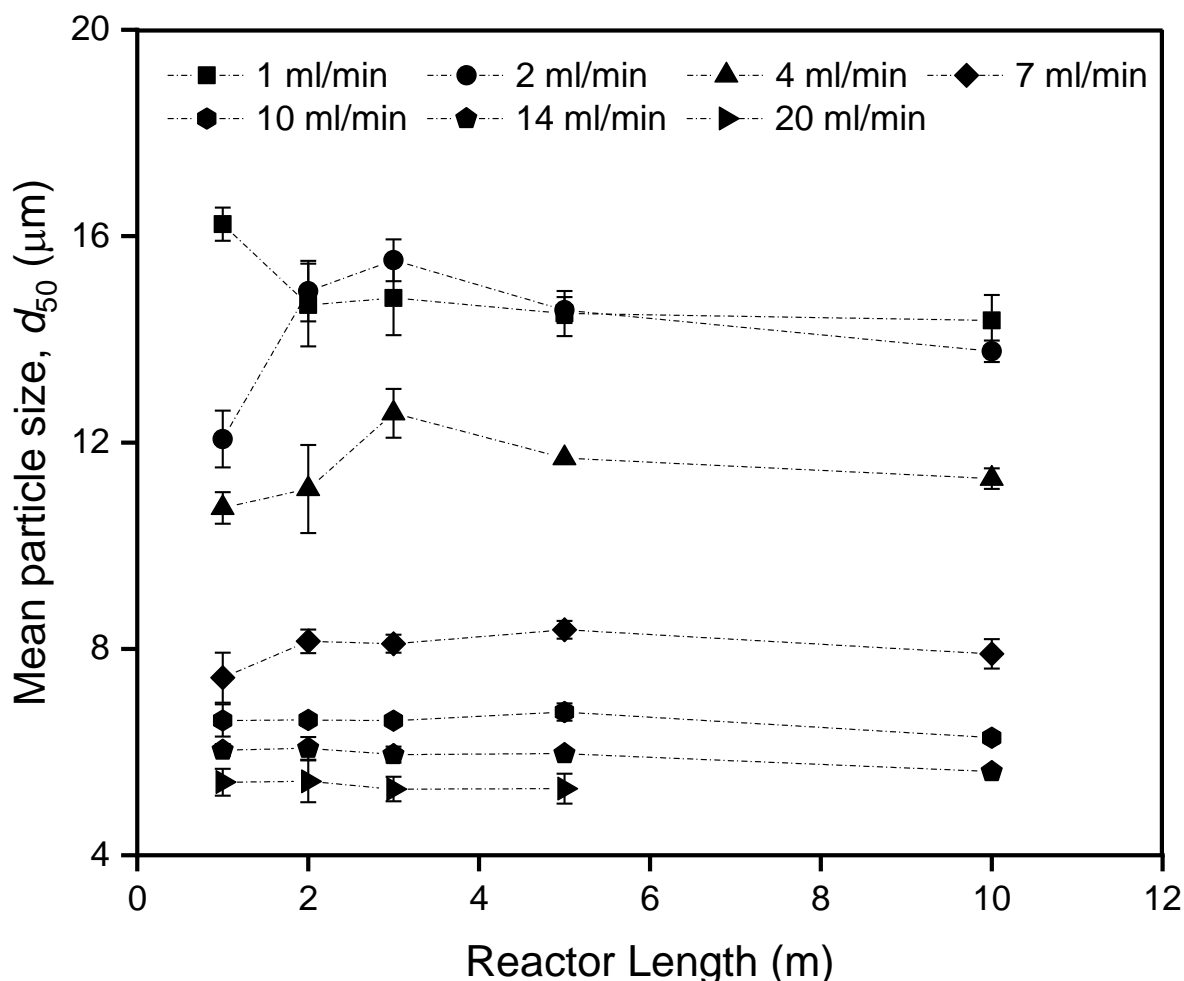


Figure 5-8. Change in the mean particle size, d_{50} , of clarified cell culture fluid protein precipitates as a function of flow rate over various reactor lengths in 1 mm diameter tubing. Solutions were mixed in a 1-to-1 ratio (3 M ammonium sulphate to CCCF comprising 1.5 mg/mL IgG) in a micro T with 0.5 mm internal diameter. Outlet tubing diameter was fixed at 1 mm. Tube length was adjusted through the connections of 1 m or 5 m sections using PEEK unions of 1 mm internal diameter. Final precipitation conditions: 1.5 M ammonium sulphate and 0.8 mg/mL IgG₄ in CCCF at ambient temperature and pH 7. Data represent the average mean particle size values with ± 1 SD from triplicate experiments. Mean particle size data are shown as technical averages of $n = 5$ measurements taken from the Mastersizer.

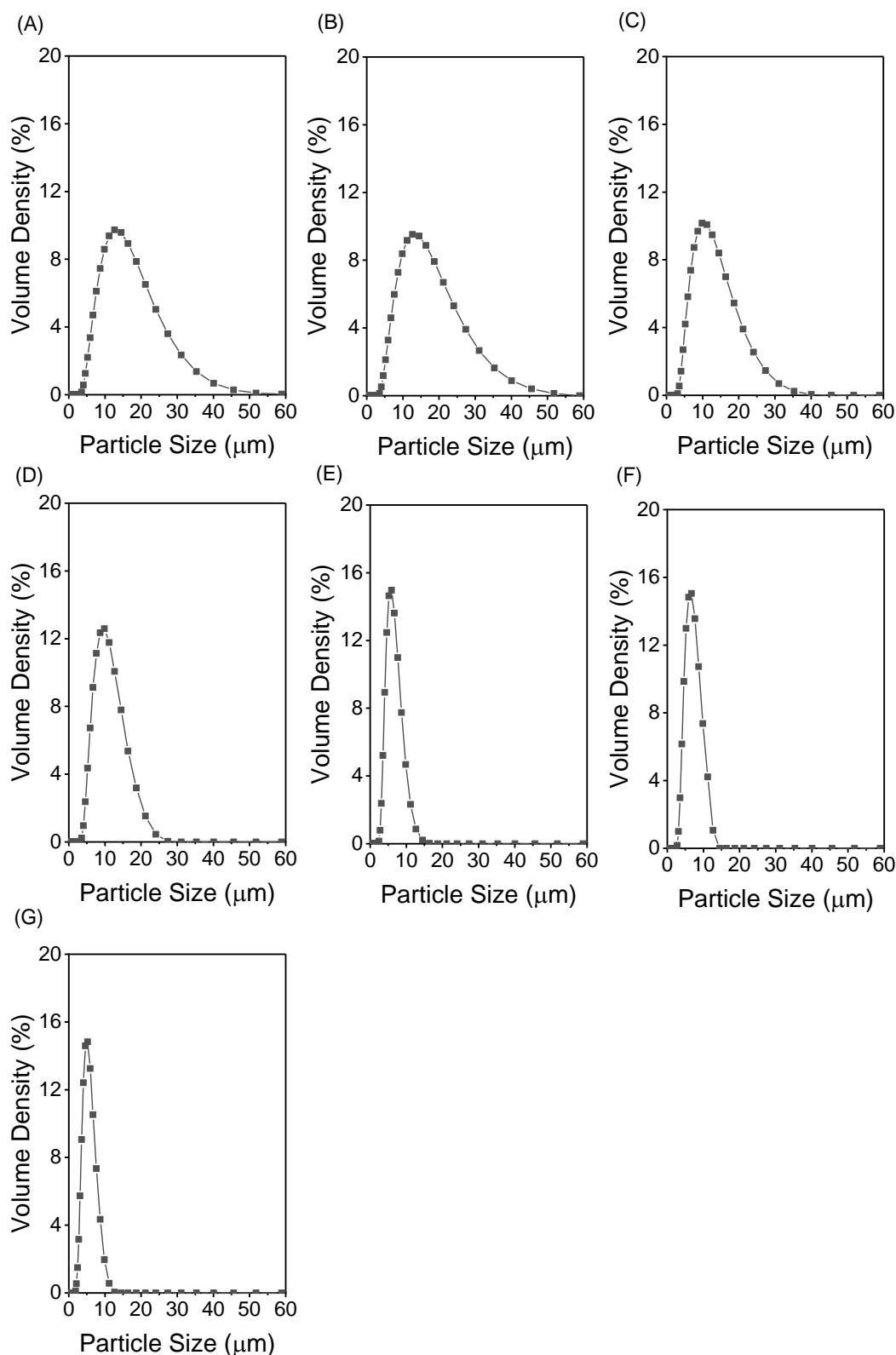


Figure 5-9. Representative particle size distributions (PSD) of protein precipitates formed at (A) 1 mL/min, (B) 2 mL/min, (C) 4 mL/min, (D) 7 mL/min, (E) 10 mL/min, (F) 14 mL/min and (G) 20 mL/min. Each profile corresponds to the technical average measurement of $n = 5$ particle size measurements and is shown in terms of volume percentage.

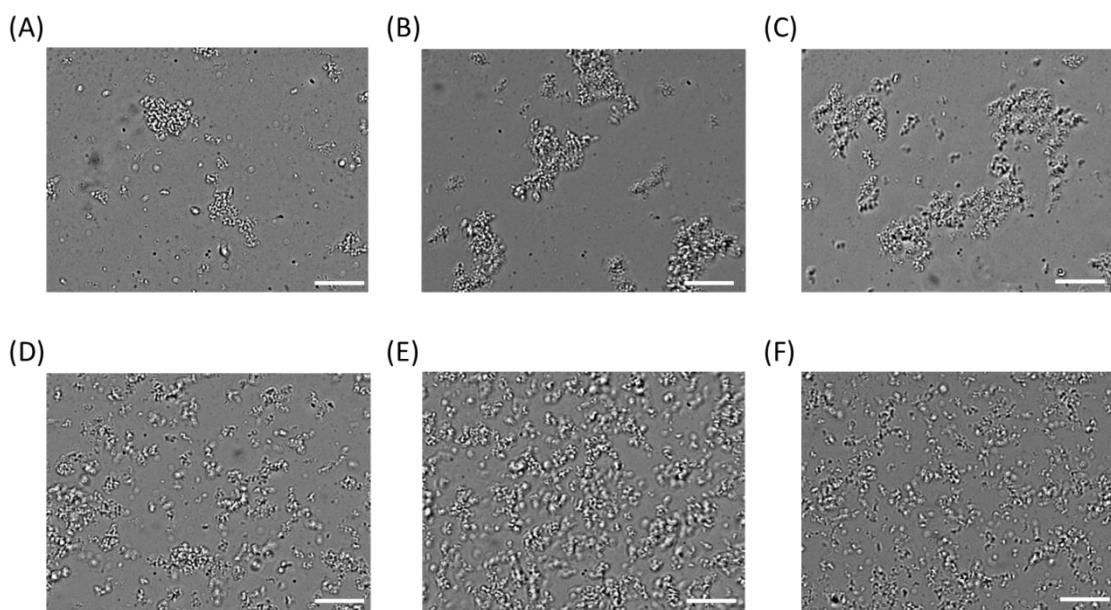


Figure 5-10. Representative micrograph images of protein precipitates obtained at (A) 1 mL/min, (B) 2 mL/min, (C) 4 mL/min, (D) 7 mL/min, (E) 10 mL/min, (F) 14 mL/min. Undiluted samples were used for visual observation. Post-image analysis was performed using ImageJ. Scale bar corresponding to 20 μm is displayed.

5.4.3 Effect of antibody concentration on particle size

The effect of antibody concentration in the CHO supernatant using the same precipitation and flow rate conditions employed in section 5.4.2 on particle size was evaluated. In order to adjust the IgG₄ concentration, CCCF was spiked with a stock of purified antibody (from PrA purification) to final antibody concentrations of 4.5, 7 and 15 g/L. Precipitations on the non-spiked CCCF sample were also performed for comparison. The reactor length for these experiments was maintained at 5 m. It can be generally seen from Figure 5-11 that larger mean particle sizes were obtained as the concentration of antibody in the CCCF increased. This effect however becomes negligible at higher flow rates. As the protein concentration in the sample increases, so does the number of particles that precipitate out of solution. Consequently, the particle collision frequency is enhanced to the second power due to the reduction of the diffusional distance barriers between primary particles (Bell, Hoare and Dunnill, 1983) (assuming a collision is governed by two particles and results in their adhesion with a 100% success rate). At low mass flow rates, these collisions lead to incremental particle adhesion which ultimately forms larger aggregates under the low shear

environments. Conversely, the minimal effect of protein concentration on particle size at high flow rates suggested a hydrodynamic force exposure limitation was imposed on particle growth as a result of forceful impacts between particles. Thus, leading to enhanced particle disruption.

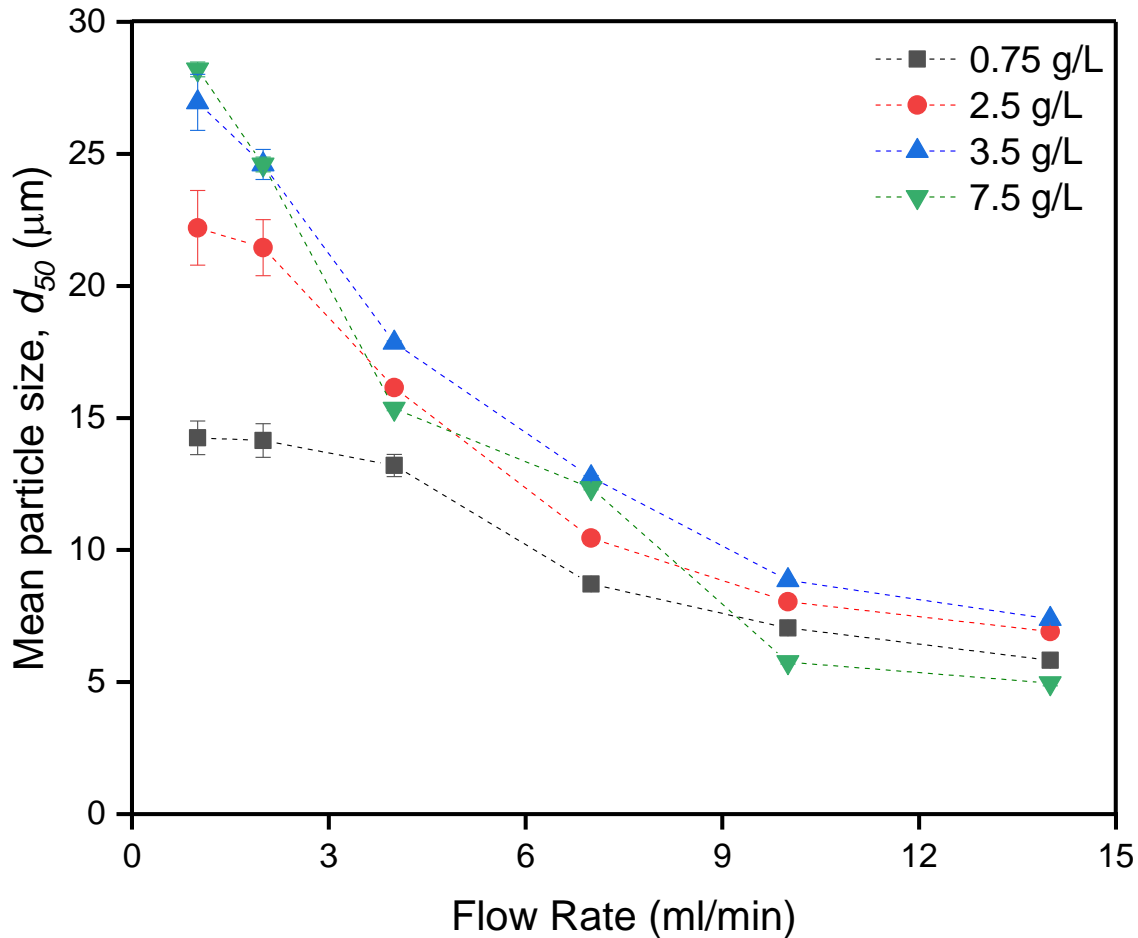


Figure 5-11. Effect of CCCF antibody concentration on the mean particle size, d_{50} , of continuous protein precipitates as a function of total flow rate. Data represents the average mean particle size values with ± 1 SD from triplicate experiments. In some cases, error bars are too small to be displayed.

5.4.4 Effect of tube diameter in the lab-scale reactor

In these next set of experiments, we desired to evaluate the effect of changing the tube diameter at the T-mixer outlet on the precipitation performance since this has an effect on the quality of mixing as pre-characterised in Chapter Four. Therefore, we replaced the 1 mm diameter tubing with either 0.5 or 2 mm diameter tubing, keeping all other reactor components and reactor dimensions the same. Precipitations were performed at each flow rate condition at least in duplicate. Figure 5-12 displays the precipitate sizes obtained using the 0.5, 1 and 2 mm diameter tubing as a function of flow rate. The same flow rates used during the micro-mixing experiments were employed to demonstrate the relation between micro-mixing times and mean particle size. It can be seen that at a constant Re value for $Re < 110$, larger mean particle sizes were obtained as the tube diameter increased. When switching to the 2 mm diameter tubing, precipitate settling in the tube was encountered at < 8 mL/min ($Re < 80$) due to un-sustained mixing across the reactor; thus providing unreliable particle size measurements. Despite the short 1 mm diameter contraction providing better initial mixing at low flow rates, increased flow rates were required to ensure continuous mixing of the precipitate with the mother liquor. Therefore, the flow rate range in these experiments was adjusted to 8 – 85 mL/min. This range may have been more applicable to assess micro-mixing without the 1 mm diameter tubing contraction.

When normalising the data to the mean energy dissipation rate, ϵ , it was found that similar particle sizes were obtained between the three tube sizes at similar mean energy dissipation rates (Figure 5-13). This suggests that the mechanistic and transport processes involved during precipitate formation to a desired particle size can be controlled with constant ϵ which provides similar micro-mixing behaviour.

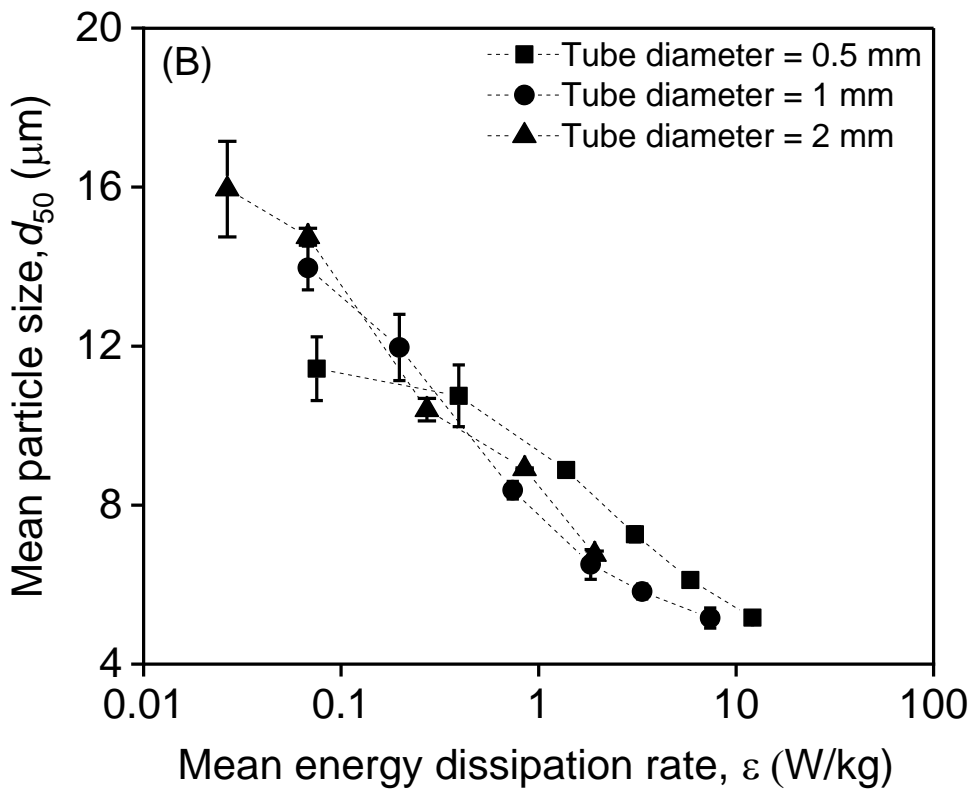
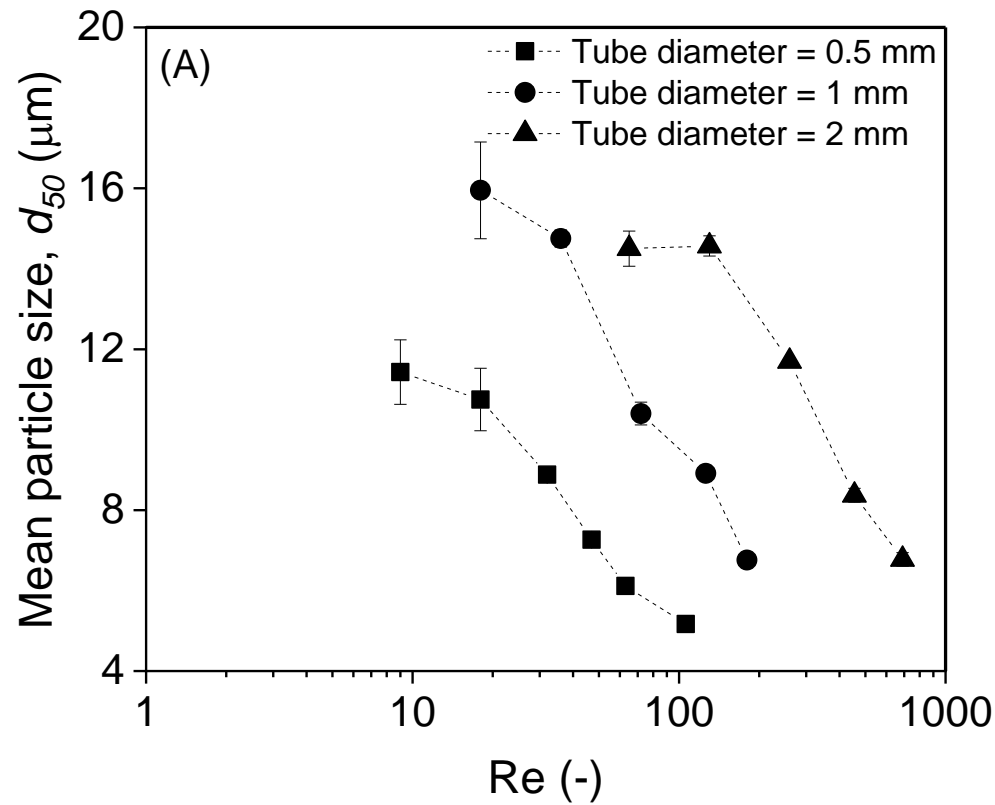


Figure 5-12. Mean particle sizes in various tubing diameters for continuous precipitation at lab-scale. (A) Effect of tube diameter on mean precipitate sizes as a function of Re . (B) Mean energy dissipation correlation with mean particle size. The reactor length for all experiments was fixed at 5 m. Mean particle sizes are shown as an average of $n = 3$ experimental runs ± 1 standard deviation.

5.4.5 Pilot-scale precipitation results

In order to demonstrate a proof of concept for scale-up of a continuous protein precipitation step, runs were performed in the CFIR system. Details of this system are described in Chapter 3. Flow rates through the system were selected to be in range of the calculated shear rates and mean energy dissipation rates from the lab-scale system. Dummy runs with water were performed to determine the pressure drop range achievable with the pump flow rates of the AKTA Ready system, as measured by the UNICORN software interface. As only the Low-Flow kit was available for use, flow rates were limited to the range 3 – 150 L/h, providing a maximum pressure drop over a 5 m tubular reactor (and additional tubing for flow cell connections) of 0.5 bar. From this, precipitations in the pilot-scale reactor were performed using flow rates in the range 9 to 150 L/H. Table 5-2 details the experimental conditions.

Table 5-2. Experimental conditions employed for the pilot-scale precipitation runs in a CFIR. Mean energy dissipation and shear rates are calculated on the basis of pressure drop readings from the AKTA Ready.

Flow Rate (L/h)	Residence Time (s)	Mean energy dissipation rate (W/kg)	Shear Rate (s ⁻¹)
9	64	0.03	155
20	29	0.13	306
90	6	2.84	1550
150	4	11.8	3165

The mean particle sizes from duplicate runs are displayed in Figure 5-13A. Both sets of runs provided comparable results. As in the small-scale, the PSD shifted to smaller and narrower distributions with increasing flow rate (Figure 5-14). According to Figure 5-13B, at the lower end of the mean energy dissipation rate range, the mean particle sizes were smaller than those obtained in the small-scale reactor, but more similar at higher rates. This could be attributed to better micro-mixing times obtained at low mean energy dissipation rates using the specific reactor design. The micro-mixing times are more similar at the higher mean energy dissipation rate values. Similarly to small-scale, antibody yield was not significantly impacted by the operating flow rate given these were in the range 90.9 to 96.1 %.

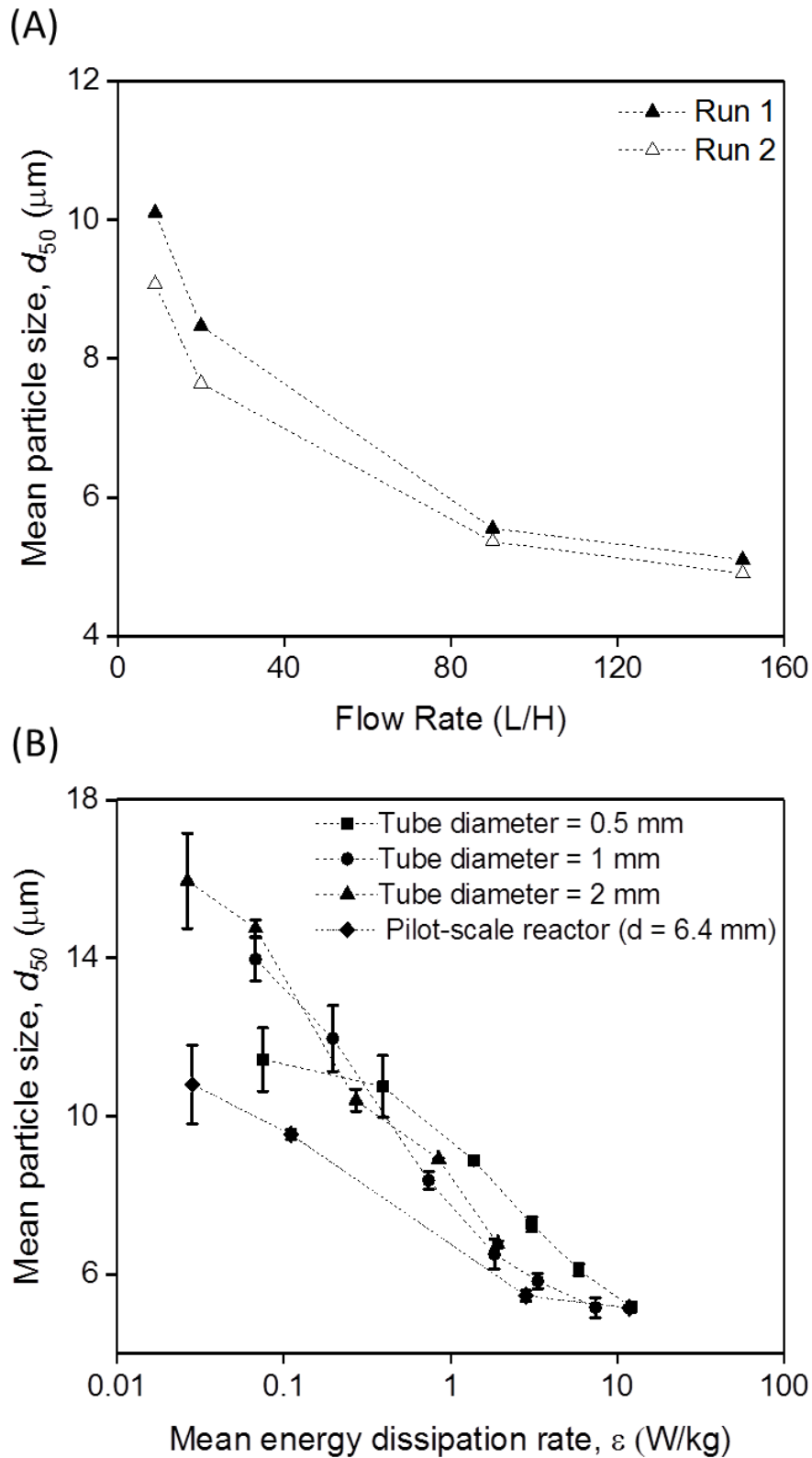


Figure 5-13. Pilot-scale precipitation results and comparison with small-scale data. (A) Mean precipitate sizes in the pilot-scale continuous tubular reactor from duplicate runs. (B) Mean energy dissipation vs. mean particle size for the lab-scale and pilot-scale reactors.

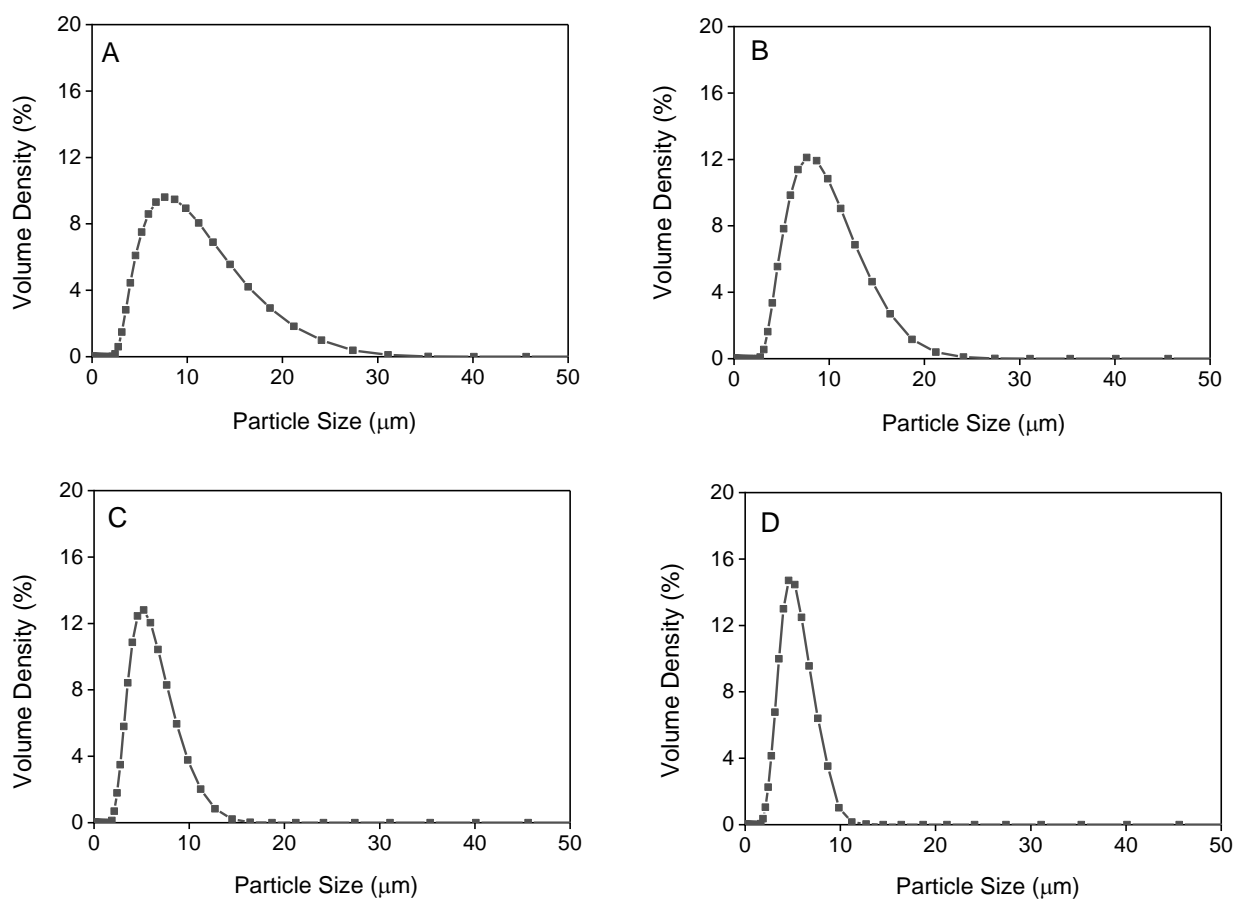


Figure 5-14. Effect of flow rate on the PSD, on a volume basis, of protein precipitates formed at pilot-scale in a CFIR. Precipitations were conducted at (A) 9 L/H, (B) 20 L/H, (C) 90 L/H and (D) 150 L/H, using a T-mixer with an internal diameter of 4.8 mm and outlet tubing of 6.4 mm internal diameter and 5 m in length. Reactor volume was ~160 mL. Samples were collected after five reactor volumes had passed. Distributions are presented as technical averages from $n = 5$ measurements for each replicate experiment.

5.5 Impact of turbulent processing on continuous protein precipitates

In the same way as described in section 5.3.3, suspensions from the continuous precipitation experiments were exposed to the rotating disc device to assess particle breakage. Using the shear rate of 6000 rpm, the change in mean precipitate particle sizes for the various process conditions was evaluated. In addition, the precipitates were characterised in terms of their f_D values to describe particle strength based on the relative breakage observed. For these experiments, precipitate samples generated from the lab-scale reactor using 1 mm diameter tubing and from the pilot-scale were tested. The results are summarised in Figure 5-15 and Figure 5-16.

Flow Rate (ml/min)	1	2	4	7	10	14	20
Reactor Shear Rate (s^{-1})	116	240	480	850	1248	1648	2502
Mean Particle Size d_{50} (μm) (\pm 95% Confidence Intervals)	14.7 (\pm 1.12)	14.0 (\pm 1.37)	11.9 (\pm 0.76)	8.37 (\pm 0.60)	6.51 (\pm 0.48)	5.83 (\pm 0.58)	5.2 (\pm 0.72)
Fractal Dimension, f_D (-) \pm Std. Deviation	2.27 \pm 0.01	2.31 \pm 0.01	2.42 \pm 0.02	2.53 \pm 0.01	2.74 \pm 0.05	2.84 \pm 0.02	2.87 \pm 0.02
Rotary Disc Shear Device (Disc Speed= 100 rps)							
Mean Particle Size d_{50} (μm) (\pm 95% Confidence Intervals)	5.88 (\pm 1.29)	5.45 (\pm 2.11)	6.44 (\pm 2.98)	4.73 (\pm 0.82)	4.29 (\pm 0.37)	4.32 (\pm 0.75)	4.17 (\pm 1.04)
Percentage Size Reduction (%)	60	56	46	44	34	26	20

Figure 5-15. Effect of turbulent processing in a rotating disc device on lab-scale protein precipitates formed from various flow rate conditions. 20 mL of precipitate samples were processed in the shear device at a disc speed of 6000 rpm (100 rps) for 20 s, and measured immediately for particle size with laser light diffraction. Tube diameter of 1 mm was used for the continuous precipitation experiments. d_{50} values are displayed as the average of triplicate experiments with the 95 % confidence interval.

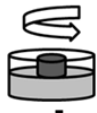
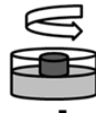
Flow Rate (L/H)		9	20	90	150
Reactor Shear Rate (s^{-1})		155	306	1550	3165
Mean Particle Size d_{50} (μm)	Run 1	10.1	9.45	5.36	5.1
	Run 2	11.5	9.62	5.55	5.19
Fractal Dimension, f_D (-)	Run 1	2.31	2.37	2.73	2.86
	Run 2	2.35	2.42	2.72	2.83
		↓	↓	↓	↓
Rotary Disc Shear Device (Disc Speed = 100 rps)					
		↓	↓	↓	↓
Mean Particle Size d_{50} (μm)	Run 1	4.3	4.2	4.25	4.55
	Run 2	4.8	4.38	4.83	4.33
Percentage Size Reduction (%)	Run 1	57	55	21	11
	Run 2	58	54	13	17

Figure 5-16. Effect of turbulent processing in a rotating disc device on pilot-scale protein precipitates formed from various flow rate conditions. 20 mL of precipitate samples were processed in the shear device at a disc speed of 6000 rpm (100 rps) for 20 s, and measured immediately for particle size with laser light diffraction. d_{50} values obtained from duplicate runs are displayed

At both scales, there was a clear positive correlation between the applied flow rate and particle breakage upon turbulent shear stress. Larger particles formed at low flow rates, or low mixing, were more susceptible to breakage than the smaller particles formed at high flow rates, or with faster mixing. For example, the maximum percentage size reduction was 60% for the large precipitates, whilst the smaller precipitates reduced in size by 26% or less. Moreover, there was a second correlation with the precipitate fractal dimension. Based on studies conducted on whey precipitation by Byrne *et al.* (Byrne *et al.*, 2002b), smaller precipitates possess higher fractal dimensions due to their increased compactness, and are

tougher than larger particles with lower fractal dimensions. The results shown here are in agreement with their observations. Although large precipitates are ideal to facilitate separation, the precipitates were weak and fragmented easily with industrial processing, which may in turn reduce centrifugal efficiency. The impact of the relative particle breakage on clarification efficiency is evaluated and discussed in section 5.7

It appeared that the mean particle sizes of all suspensions were reduced to similar values after turbulent processing. To determine if the particle sizes between samples after shear testing were statistically different, a one-way analysis of variance (ANOVA) test was performed.

Using the same approach described as in section 5.3.3.2, it was found that the data around shear testing of lab and pilot-scale precipitates were normally distributed according to the corresponding p-values ($p > 0.05$). The ANOVA test with equal variances revealed that there were statistical differences between the shear tested lab scale precipitates ($p < 0.001$), but that there was no statistical difference between the shear tested pilot scale precipitates ($p = 0.031$). The post hoc Tukey test showed that for precipitate sample groups obtained at 1 and 2 ml/min, the mean particle sizes after shear did not differ significantly from each other ($p > 0.05$), but did differ significantly from the other sample groups ($p < 0.05$). In the case of precipitate samples which were obtained at 7 ml/min and higher, the mean particle sizes after shear did not differ significantly from each other ($p > 0.05$). Precipitates obtained at 4 ml/min and then sheared tested gave mean particle sizes which were statistically different than the rest ($p < 0.05$). This result was likely due to the larger particle sizes obtained after shear testing as well as the wider confidence interval. Given the lack of statistical difference in the shear tested pilot scale precipitates, as well as the lack of statistical difference in the shear tested lab scale precipitates produced at the high flow rates, it is likely that these precipitate samples share similar characteristics.

5.6 Effect of Camp Number on strength of continuous precipitates

Camp numbers for the continuous tubular precipitates were calculated using the average shear rate in the reactor, as a function of the pressure drop, and the mean residence time for a given flow rate, assuming plug flow. In the previous experiments, the precipitate Camp number was consistently below 10^5 . In order to target Camp numbers above 10^5 , which allowed us to evaluate its importance for the characterisation of the strength of precipitates from a continuous process, various approaches could be employed. This included increasing

the reactor length, introducing turbulent promoters via constriction and dilation of tubing and subsequent aging in a batch reactor. As previously shown, a relation between Camp number and precipitate particle strength in the batch precipitation experiments was not established. However, it was still interesting to determine whether it had any significance for a continuous precipitation process based on a tubular reactor, particularly since the Camp numbers in the process were an order of magnitude lower than those characterised for the batch precipitates (10^4 vs 10^5).

Precipitations were performed at lab-scale either at 2 or 14 mL/min, representing low and high flow rate conditions, respectively. For a given reactor length, assuming the average shear rate increases proportionally with total mass flow rate, the precipitate Camp numbers would be equivalent. Attempts to increase the Camp number to above a value of 10^5 involved 1) increasing the reactor length up to 22 m in order to prolong the shear history, 2) aging the precipitate suspension from the outlet in the 150 mL stirred batch vessel for one hour with constant mixing at 300 rpm and 3) incorporating constrictions of 0.5 mm diameter tubing connections of 5 cm in length at regular intervals in-between sections of 1 mm diameter tubing. Precipitates created from these various approaches were then exposed to the rotating disc device to evaluate a link between Camp number and particle strength.

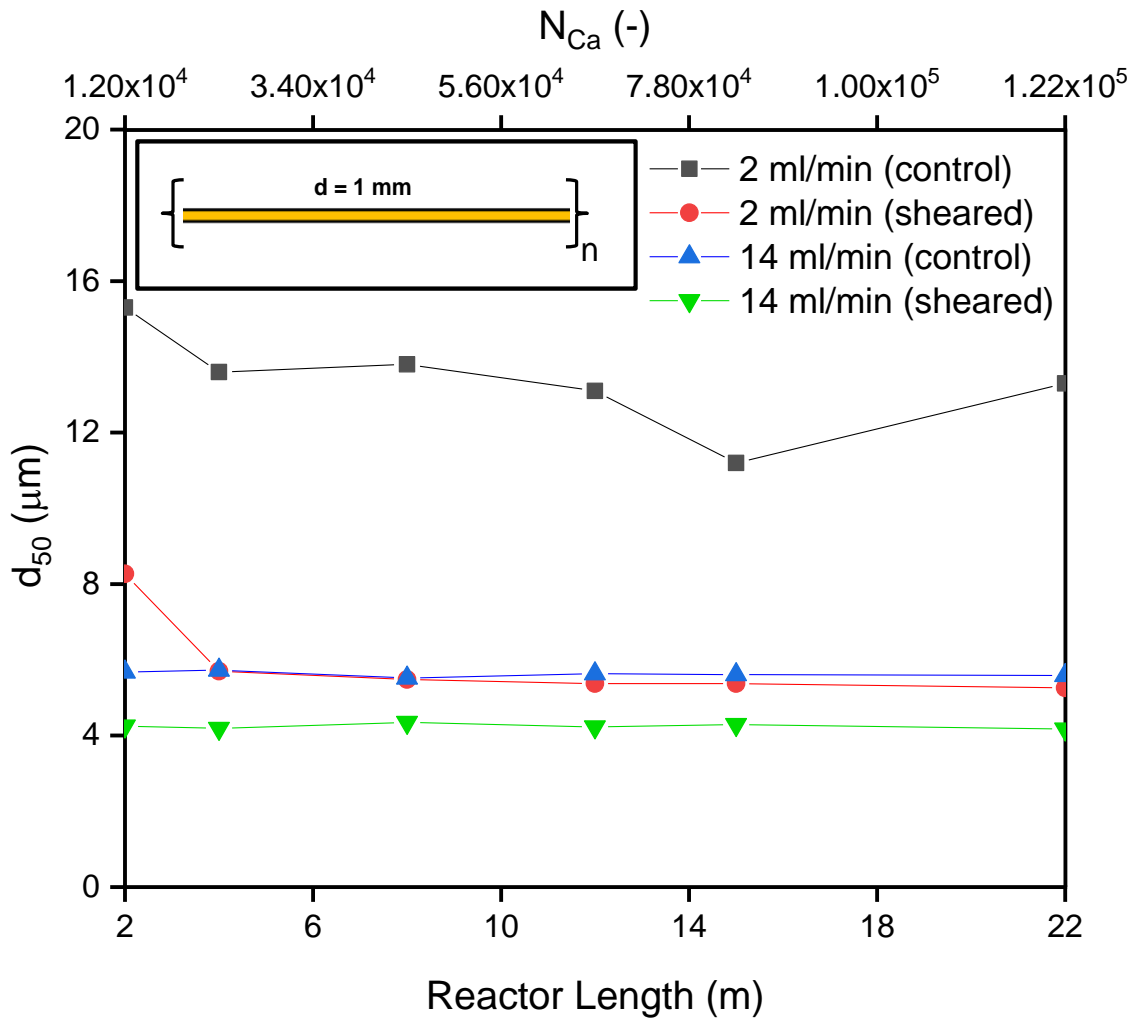


Figure 5-17. Effect of precipitate Camp Number, N_{Ca} , by varying reactor length, on the change of mean particle size, d_{50} , with exposure to turbulent shear stress in the rotating disc device. Continuous precipitation was performed at 2 and 14 mL/min using 1 mm diameter tubing connected with PEEK unions of 1 mm internal diameter to increase reactor length up to 22 m. At constant reactor length, N_{Ca} was assumed to be equal for both flow rates. Sheared samples were prepared by exposing the precipitate suspensions to a rotating disc device at 6000 rpm, corresponding to a maximum energy dissipation rate of 0.045×10^6 W/kg.

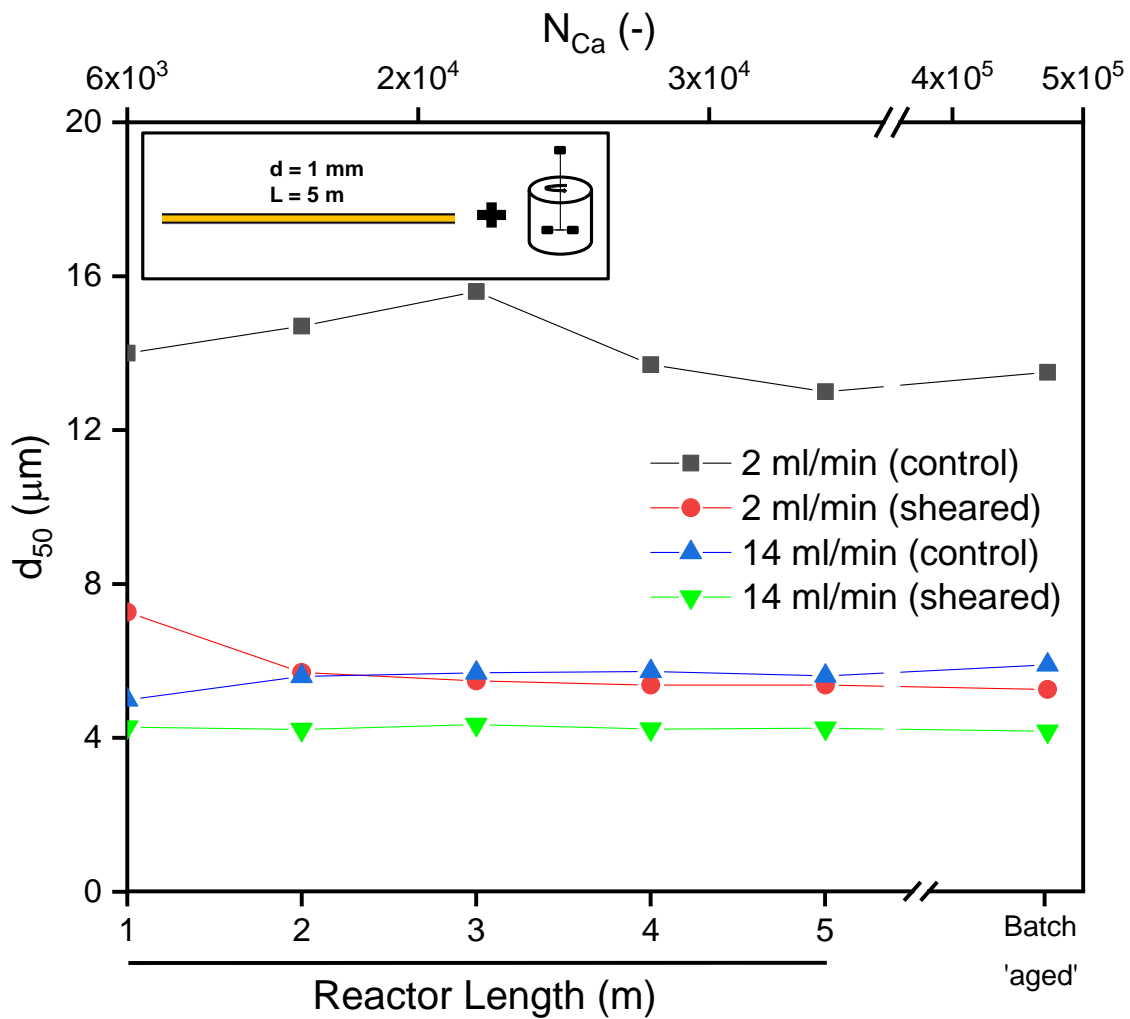


Figure 5-18. Effect of batch aging on the mean particle size, d_{50} , and strength of continuous tubular precipitates. Continuous precipitation was performed at 2 and 14 mL/min using 1 mm diameter tubing connected with PEEK unions of 1 mm internal diameter to increase reactor length up to 5 m. At constant reactor length, N_{Ca} was assumed to be equal for both flow rates. Suspensions from the reactor outlet were then aged in a 150 mL baffled batch vessel with constant mixing at 300 rpm for one hour, Sheared samples were prepared by exposing the precipitate suspensions to a rotating disc device at 6000 rpm, corresponding to a maximum energy dissipation rate of 0.045×10^6 W/kg. The final precipitate N_{Ca} from batch aging was taken as the sum of calculated N_{Ca} values for the continuous precipitation and batch aging process. Sheared samples were prepared by exposing the precipitate suspensions to a rotating disc device at 6000 rpm, corresponding to a maximum energy dissipation rate of 0.045×10^6 W/kg.

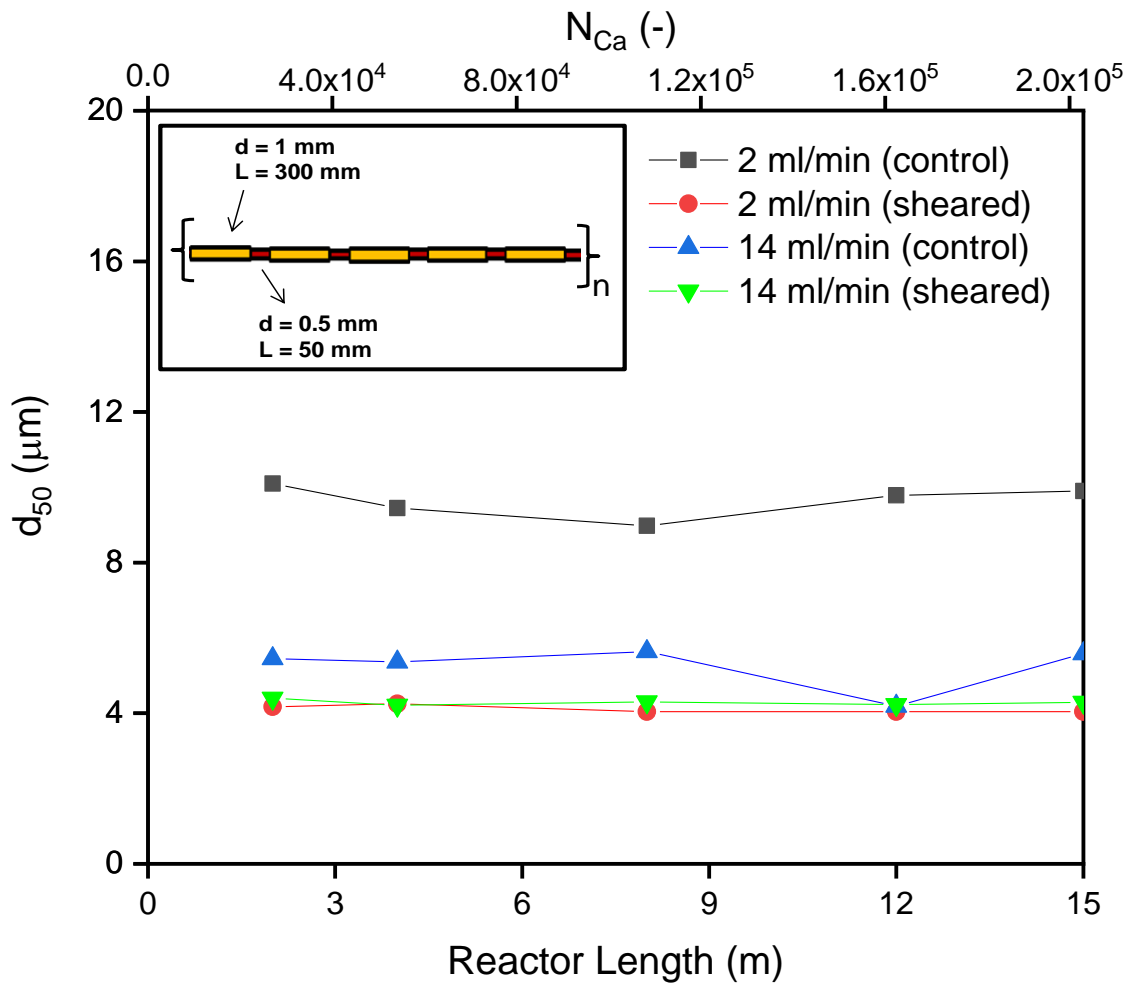


Figure 5-19. Effect of tube constrictions on the mean particle size, d_{50} , and strength of continuous tubular precipitates. Continuous precipitation was performed at 2 and 14 mL/min with varying reactor length up to 15 m. 5 cm tubing of 0.5 mm internal diameter were spaced evenly between 30 cm sections of 1 mm diameter tubing, connected via PEEK unions of 0.5 mm internal diameter. Sheared samples were prepared by exposing the precipitate suspensions to a rotating disc device at 6000 rpm, corresponding to a maximum energy dissipation rate of 0.045×10^6 W/kg.

As can be seen from Figure 5-17, the extent of particle breakage for a given flow rate condition was independent of the Camp number with a longer shear history. In Figure 5-18, batch aging also did not show any discernible effect on improving the precipitate strength despite a substantial increase in Camp number approaching 5×10^5 . The value of Camp number using this combined approach was taken as the sum of the Camp numbers from the continuous and batch operating conditions. From Figure 5-19, the insertion of tube restrictions at regular intervals along the length of the reactor appeared to reduce the mean particle sizes for both flow rates, more so for the 2 mL/min flow rate. This was most likely due to the presence of 'shear bursts' from the constriction of the tubing, particularly in the region immediately downstream of the T where most particle formation occurs during mixing. Similarly, no particular benefit in improving the precipitate strength was observed with increasing Camp number. However, the particle size can be adjusted through constriction and dilation of the tubing. A similar approach was implemented for the continuous precipitation of soya protein isolate whereby increasing the turbulence via tube constriction induced greater break up rates, thus producing smaller particles (Virkar *et al.*, 1982).

Regardless of the reactor length, precipitates formed in the continuous reactor under high mixing intensities or high shear rates were mechanically stronger and more resistant to breakup. Taken together, the result demonstrates the importance of the initial mixing for the rapid salting-out process having a much greater influence on the particle characteristics. After which, the remaining residence time spent in the reactor can be considered as much less necessary for the precipitation reaction. This finding is useful as it suggests a much less requirement for the design of very long continuous reactors.

5.7 Ultra scale-down centrifugation study

The centrifugation conditions studied for the sedimentation behaviour of non-sheared and sheared samples were equivalent to those studied for the batch precipitates i.e. $(Q/\Sigma) = (V_{lab}/t_{lab}/\Sigma_{lab}) > 3 \times 10^{-9}$ m/s. The comparison of the centrifugal recovery for non-sheared and sheared precipitates formed during lab-scale and pilot-scale continuous processing, as a function of $V_{lab}/\Sigma_{lab}t_{lab}$, i.e. centrifuge throughput, in the range 9.25×10^{-9} to 4.8×10^{-8} m/s, is presented in Figure 5-20 and Figure Figure 5-21, respectively.

For the control samples which were not exposed to shear in the rotating disc device, solids remaining were in the range 0.06 to 0.9% for the lab-scale reactor (Figure 5-20), whilst for the pilot-scale reactor, the range was 0.01 to 1.2 % (Figure 5-21). For the sheared samples,

solids remaining were in the range 0.4 to 2.7 % and 0.01 to 1.5 % for the lab and pilot-scale reactors, respectively. For a given centrifuge throughput, the clarification of sheared and non-sheared samples were more similar in the pilot-scale reactor than in the lab-scale reactor. The results demonstrate that the clarification of precipitates formed at higher flow rates or with better mixing is less impacted after being exposed to turbulent shear.

In comparison to the batch-formed precipitates, an overall improved clarification was observed for the continuous-formed precipitates under the same centrifugation conditions and when particle sizes are comparable. This may suggest that precipitates prepared from continuous processing in the tubular reactors exhibit faster hindered settling rates. Visual observations from the micrographs presented in Figure 5-4 and Figure 5-10 demonstrate that the tubular reactor precipitate particles form looser networks. These structures tend to sediment rapidly and sweep up the fine particles with low settling rates from underneath. In contrast, the particles in a batch-formed precipitate are more compact and regular in structure and so are less hindered which results in a less clarified supernatant. This phenomenon had been previously observed in the gravity settling behaviour of soy protein precipitates prepared by isoelectric precipitation in batch and tubular reactor configurations (Bell and Dunnill, 1982b).

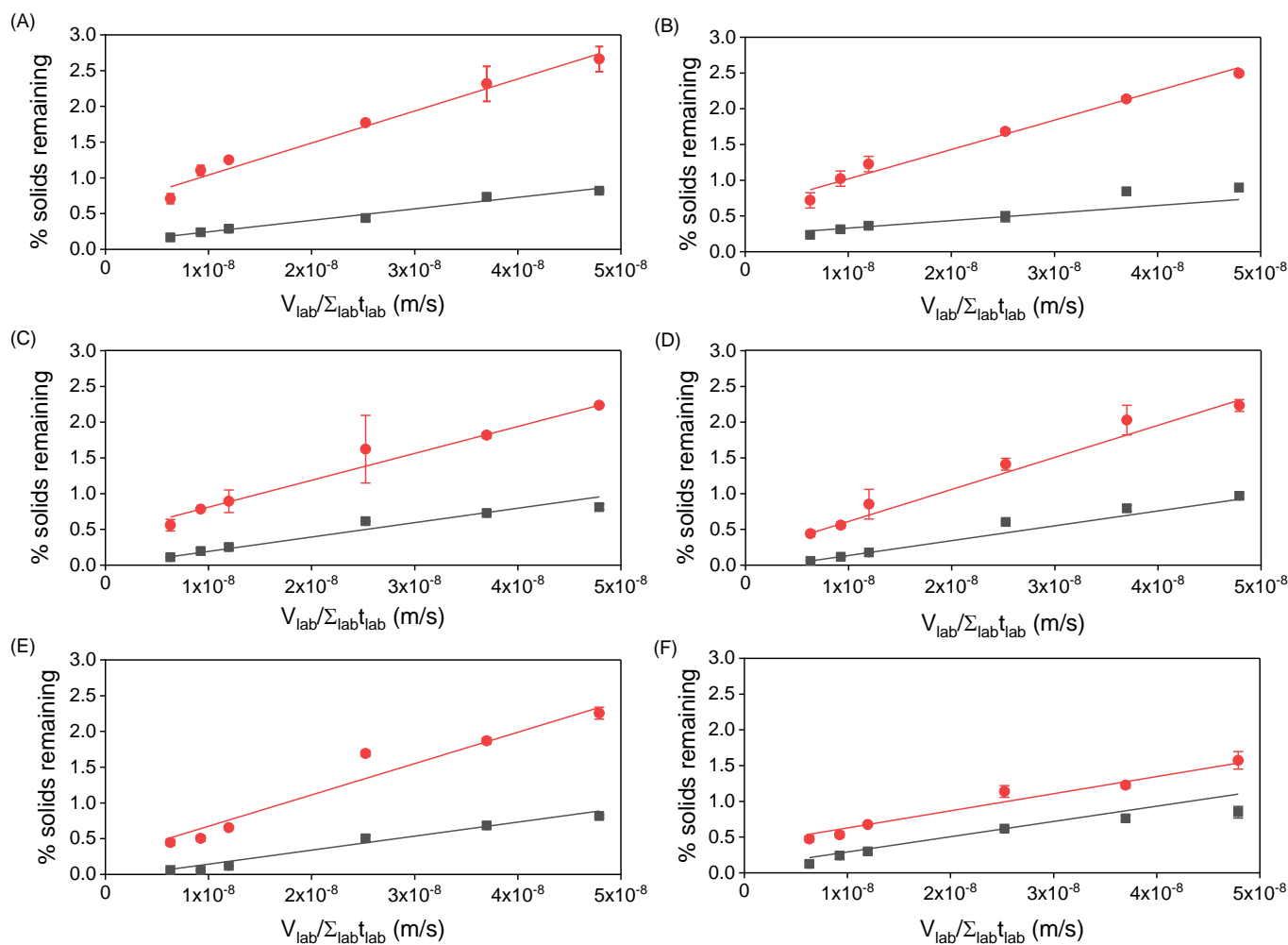


Figure 5-20. Ultra scale-down centrifugation analysis of non-sheared (black squares) and sheared (red circles) lab-scale precipitate samples. Centrifugal efficiency is characterised in terms of percentage of solids remaining, S , in the supernatant as a function of centrifuge throughput. Precipitates were prepared at (A) 1 mL/min, (B) 2 mL/min, (C) 4 mL/min, (D) 7 mL/min, (E) 10 mL/min, (F) 14 mL/min and (G) 20 mL/min in the lab-scale reactor with 1 mm diameter tubing. Data are presented as averages of $n = 4 \pm 1$ standard deviation and fitted with linear regression.

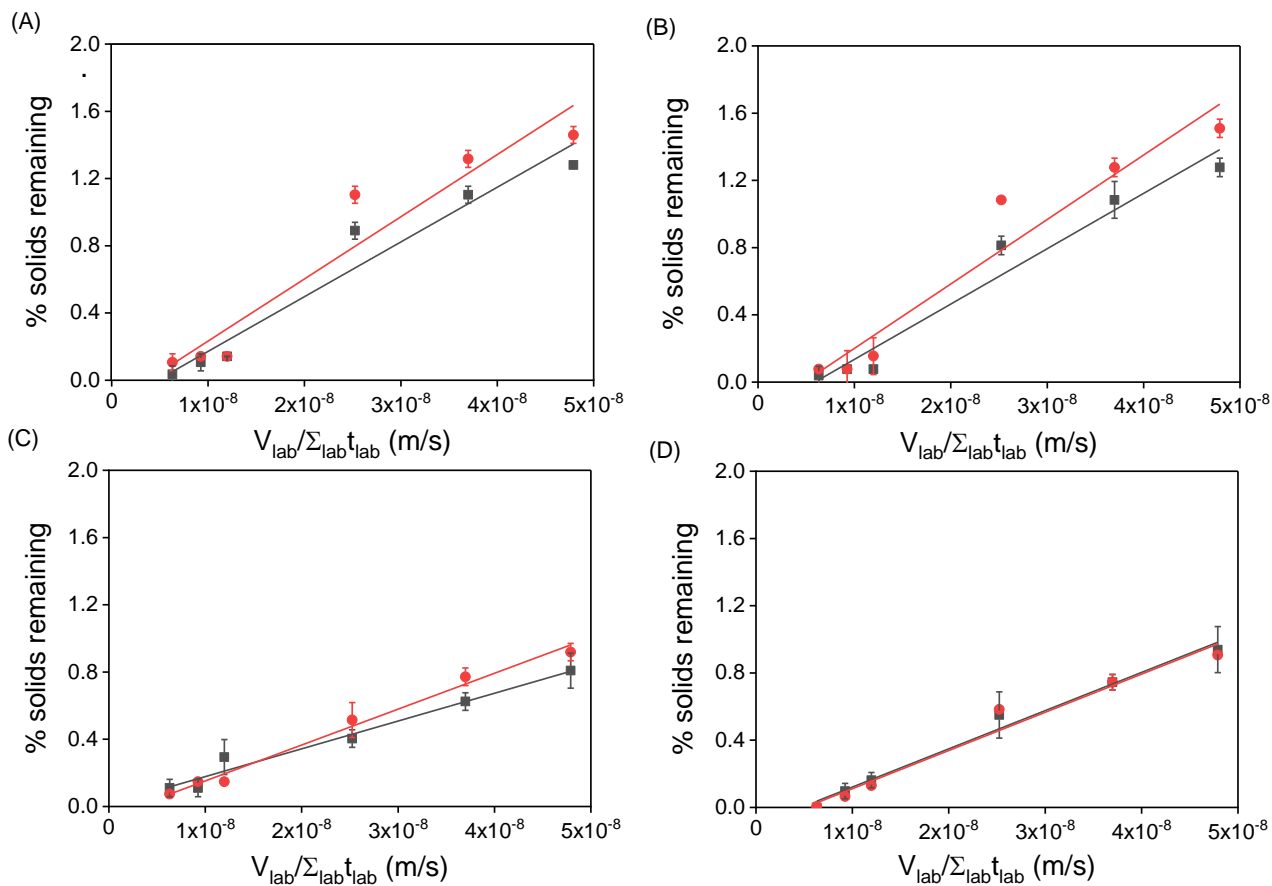


Figure 5-21. Ultra scale-down centrifugation analysis of non-sheared (black squares) and sheared (red circles) pilot-scale precipitate samples. Centrifugal efficiency is characterised in terms of percentage of solids remaining, S , in the supernatant as a function of centrifuge throughput. Precipitates were prepared at (A) 9 L/H, (B) 20 L/H, (C) 90 L/H and (D) 150 L/H. Data are presented as averages of $n = 4 \pm 1$ standard deviation and fitted with linear regression.

5.8 Disc-stack centrifugation

In order to validate the USD centrifugation method in predicting precipitate recovery at large scale, a process run on a Pathfinder PSC-1 was performed. Precipitate feed was first prepared in the CFIR using a flow rate of 150 L/h which enabled a fast process without affecting protein recovery (93.5%). Due to the limited availability of feed material, it was only possible to conduct a single run on the Pathfinder. Approximately 4 L of feed was processed through the Pathfinder at a feed flow rate of 35 L/H, which corresponded to a Q/Σ value of 2.52×10^{-8} m/s as selected from the median of the centrifuge throughput tested range. As per the manufacturer's recommendation, the seal of the centrifuge bowl was tested by feeding water at a defined flow rate in order to ensure effective opening and closing of the bowl via the sliding piston. Glycol was used as a cooling agent and circulated to minimise excessive heat generation from high centrifuge speeds. Prior to pumping feed, 50 mM sodium phosphate pH 7 buffer was pumped through the system at the selected flow rate as an equilibration step. After which point, the feed line was switched to the feed bucket as quickly as possible to minimise the introduction of air bubbles. Collection of the supernatant pool began approximately after 1 bowl volume had passed (~ 1 L). In ideal circumstances, samples would be taken to determine at which point steady state is attained prior to commencing the collection of the bulk material; however this was not performed given how quickly the material was processed. A precipitate wash step on the captured solids was performed by flushing the bowl with ammonium sulphate solution and directing this to waste. To isolate the captured solids, three complete discharges of the bowl were performed.

A useful component of the PSC-1 design is the sight glass incorporated in the feed and supernatant lines which enable monitoring of liquid clarity in real-time, and provide a qualitative indication of centrifugal performance. Also, this allowed monitoring of solids breakthrough as the bowl reaches capacity, at which point the solids discharge mechanism should take place. Initially, a clear supernatant was observed during the first minute of operation. After this, the clarity of the liquid decreased and appeared to be constant for the rest of the run, which could indicate steady state. Visual observation of the supernatant pool showed the presence of solids which were not effectively clarified with the PSC-1. Samples of the centrate were taken for A_{600} measurements and compared to those for the supernatant samples in the USD centrifugation study. The PSC-1 centrate sample showed an average absorbance of 0.39, which was markedly different to the absorbance of the USD centrifugation supernatant samples ($A_{600} < 0.05$). As a result, the PSC-1 run achieved a clarification of 73.8%, or equivalent to 26.2% solids remaining in solution, as shown in Figure 5-22. This indicated an over-prediction of the USD method. (0.55 ± 0.14 % solids remaining).

Replicates would be required to confirm the observation as a real result. It is unlikely that solids breakthrough due to reaching bowl capacity would have occurred since the total amount of solids loaded were approximately 100 g and the capacity of the bowl is about 850g. When the solids present in the supernatant sample were characterised in terms of PSD, a very broad additional peak showing particle sizes in the range 20 -120 μm , in relation to the feed material, was observed, as shown in Figure 5-23. This could be attributed to the remains of potential air-liquid interfaces formed despite back pressure having been applied on the supernatant discharge.

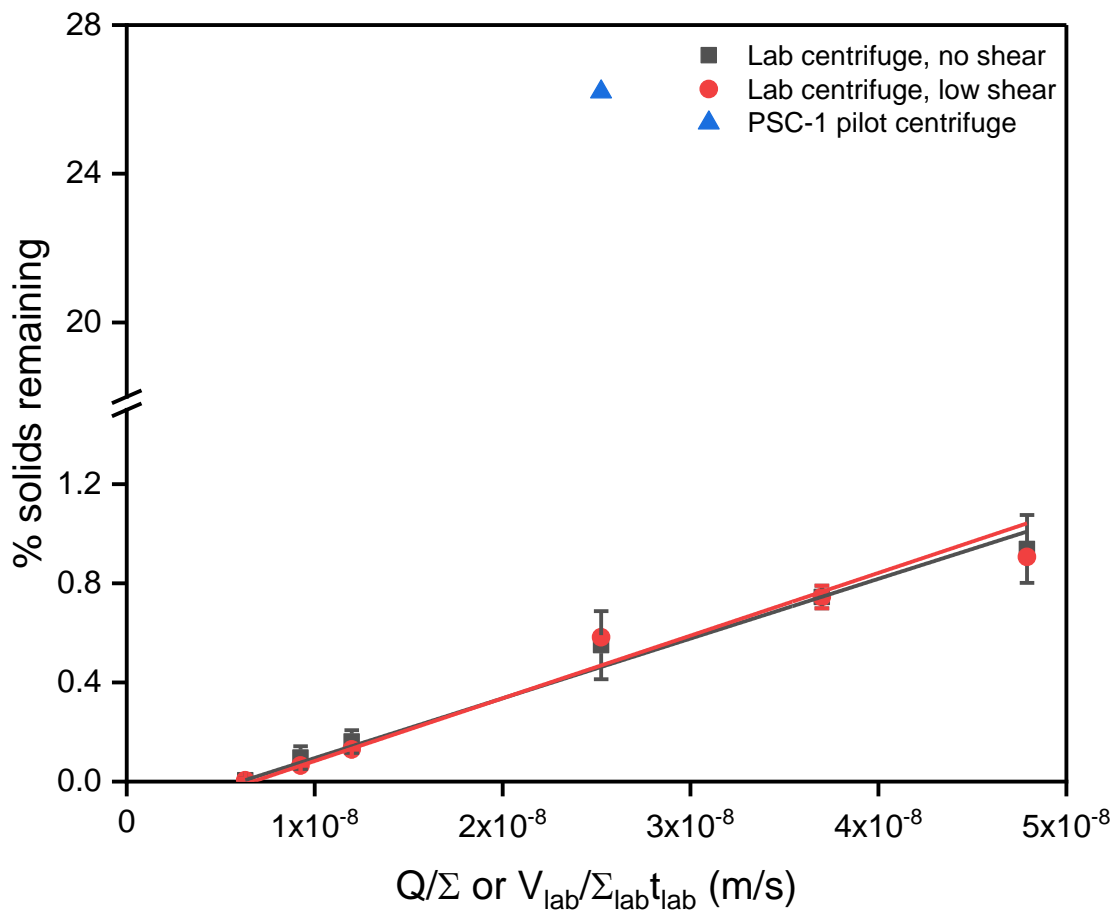


Figure 5-22. Validation of the USD method for the prediction of CCCF precipitate recovery by disc-stack centrifuge with Pathfinder PSC-1. CCCF precipitates were prepared with pilot-scale continuous precipitation in a CFIR using ammonium sulphate at an operating flow rate of 150 L/h. This figure is an adaptation of Figure 5-21 which incorporates the data point for the PSC-1 run which corresponds to an operating flow rate of 35 L/h.

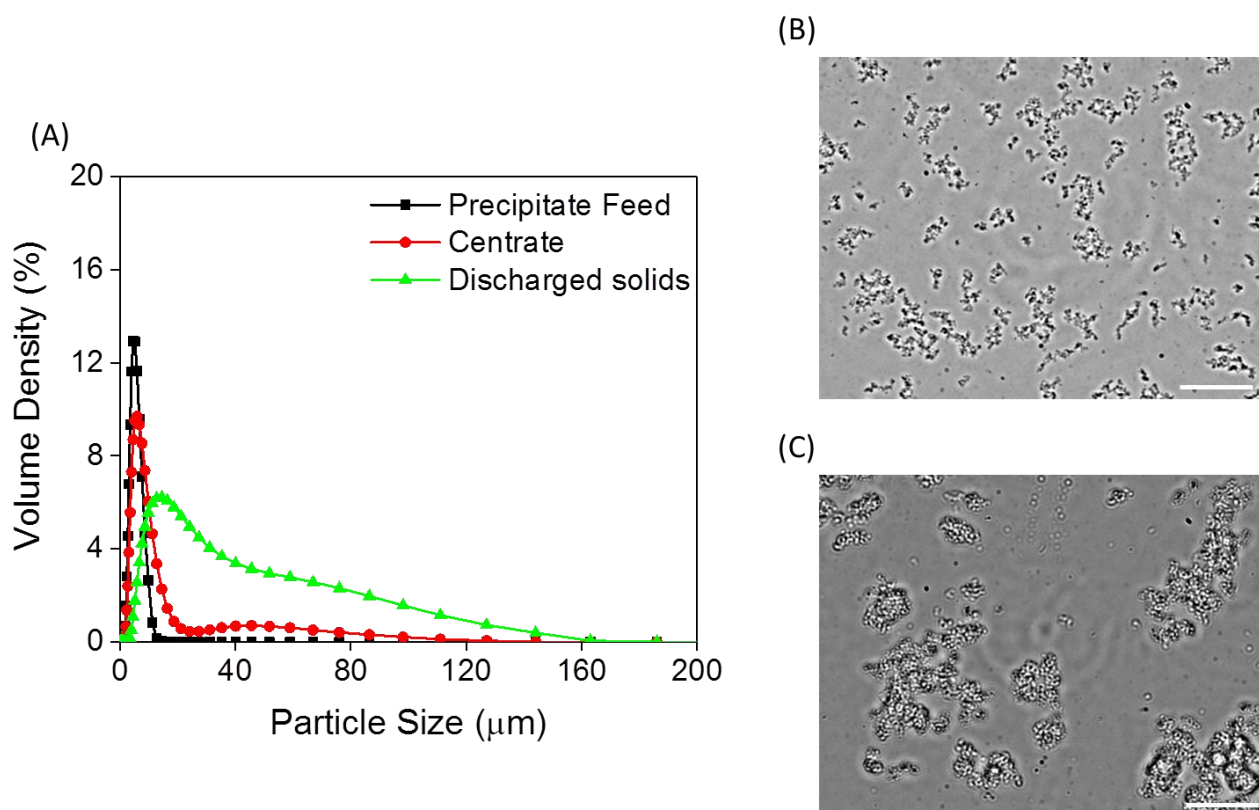


Figure 5-23. Effect of disc-stack centrifugation on CCCF precipitate recovery. (A) PSD profiles of precipitate feed, centrate and discharged solids during processing on Pathfinder PSC-1 centrifuge. Each profile corresponds to the technical average measurement of $n = 5$ particle size measurements and is shown in terms of volume percentage. (B) Representative micrograph of precipitate feed from the pilot-scale reactor operating at 150 L/H. (C) Representative micrograph of precipitate solids discharged from centrifuge bowl. Disc-stack centrifugation was performed at 13000 x g and 35 L/h.

An important factor to consider is the time between sample shearing and clarification. In the USD method, some time passes from the moment of shear exposure in the disc device to the centrifugation step. In a disc-stack centrifuge, the time between particles passing through the feed zone to the settling region is very short. It is possible that during USD characterisation at laboratory scale, the precipitates undergo a reformation phase shortly after initial breakage which does not occur in the disc-stack centrifuge because of the very short residence time. Consequently, the phenomenon of hindered settling increases the clarification performance with the USD method. For a more accurate comparison, precipitates could be diluted for the USD experiments to minimise potential reformation.

The integrity of the precipitate solids upon discharge was assessed and thus indicated the potential of disc-stack centrifugation for separation. For some centrifuges, it is possible to sample the bowl without the need for discharging. This approach allows in understanding the impact of entry into the bowl imposed on the feed particles during operation. This was however not possible for the PSC-1. Instead, we attempted to isolate any solids material which may not have been effectively discharged at the end of the run; however we failed to observe any notable material which could be sampled. The USD experiments consider the shear levels encountered in the feed zone of a disc-stack centrifuge but they do not consider the shear stress field present during solids discharge. It is expected that the shear from discharge is markedly higher than what can be predicted with our USD method. Discharge on the precipitate solids was initially thought to either show comparability in the integrity of particles with the feed material or induce particle fragmentation due to very high levels of shear. However, as can be seen from Figure 5-23A, a clear shift in the PSD profile towards larger sizes relative to the feed material with a much broader distribution is observed. When comparing the micrographs in Figure 5-23B and Figure 5-23C, it can be seen that the feed particles conglomerated into large aggregates. This is likely to be an effect of concentrating the solids within the confined volumes between the bowl discs. Not to our surprise, the level of solids dewatering was rather poor due to not operating the centrifuge optimally. As a result, much of the liquid phase was collected with the solids in the solids collection vessel. Therefore, further work in optimising a disc-stack centrifuge for this application is needed.

5.9 Summary

In this chapter, we aimed to demonstrate the relationship between mixing and the precipitation performance in batch and continuous reactors which could provide insight into a suitable approach for scale-up. In the context of a bioprocess, it was necessary to establish the link between precipitate formation and centrifugal recovery operations. Provided the rapid kinetics of precipitation exhibited by our system, it was important to understand the impact of mixing on the precipitation performance at the molecular scale.

Final particle sizes and PSD were shown to be dependent on the level of mixing owing to various levels of supersaturation affecting nucleation and growth rates as well as influencing particle fragmentation. Scale-up on the basis of mean energy per dissipation rate in a continuous tubular reactor demonstrated a good method for the control of particle properties between scales. The tubular precipitator carries the advantage of being a simple and inexpensive design, requiring a small holdup volume to complete the precipitation. Operating

at fast flow rates did not impact performance in terms of antibody recovery, indicating that the process can be made high throughput depending on the pump and pressure drop limitations. An approach employing the Dahmkohler constant for scale-up, which relates the precipitation reaction time to the micro-mixing time, could be a suitable alternative as in the case of continuous Lovastatin precipitation (Mahajan and Kirwan, 1996). However, with current methods it was not possible to accurately determine the induction time or this value has not been reported in the literature.

Applying the USD method to protein precipitate suspensions for mimicking centrifugal clarification enabled rapid investigation of the interaction between precipitation and centrifugation conditions using small process volumes. The combined method of the rotating disc device and laser light diffraction measurements in estimating particle f_D was useful in understanding particle characteristics contributing to mechanical strength. From a single centrifugation run at large scale, the clarification was overestimated from USD predictions which could be attributed to factors including hindered settling phenomena. This therefore necessitates dilution of samples for USD characterisation and the application of a hindered settling correction factor which provides a more accurate comparison between the two scales. Alternative methods including TFF and depth filtration could be more suitable for the solid-liquid separation stage and in fact exhibit lower shear stress where particle breakage is of major concern to the clarification.

All in all, the results presented in this chapter highlight the need to integrate the design of a precipitator which ultimately depicts the nucleation and growth kinetics of complex precipitation processes, and the solid-liquid separation operations. The next chapter of this thesis will address how the precipitation step can be further integrated into a downstream process to improve antibody purity, with the goal to provide purification levels of which compete with conventional Protein-A chromatography operations.

Chapter 6: Integrating salt precipitation with chromatography

6.1 Introduction

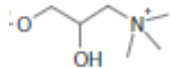
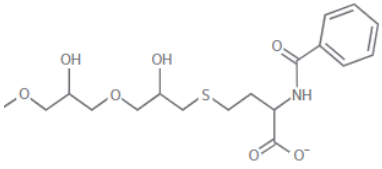
In monoclonal antibody platform processes, chromatography steps provide the major workhorse for purification. Despite observing some level of purification from the precipitation of crude harvest using ammonium sulphate, capture with PrA chromatography remains superior. This is not surprising considering the mechanisms by which both purification methods govern separation. In the salting-out procedure, alterations in the solution environment influence a solubility change of all the solutes, rather than via specific targeting. For some precipitants, such as PEG, evidence of target specificity has been presented (Hönig and Kula, 1976; Oelmeier, Ladd-Effio and Hubbuch, 2013). Nonetheless, the conventional precipitation strategies often fail to provide reasonable protein purity without additional process steps. Therefore, an integrated approach to incorporate chromatography with precipitation was implemented to govern a suitable bioprocess which could compete with conventional affinity-based bioprocesses. The goal would be to yield a purified IgG₄ that is of pharmaceutical grade.

Anion-exchange (AEX) and mixed-mode chromatography (MMC) offer potential as polishing steps, aiding in the removal of bulk impurities such as HCP and DNA at reduced costs. These various modes were investigated to determine their suitability and compatibility for antibody purification post a salt-driven precipitation step. AEX in antibody purification processes are often employed in flow-through (FT) mode, meaning that loading conditions for the chromatography step are selected based on minimising product binding on the matrix whilst retaining the majority of impurities. Product binding is determined by the overall net charge at a specified pH, requiring knowledge of the target's pI. Purification with MMC is much more complex due to the presence of multiple interactions which influence binding. Thus, development of MMC processes is significantly more challenging since multi-parameter screening is necessary for its optimisation. High-throughput methods can however alleviate the development time by enabling simultaneous experimentation of many conditions whilst minimising sample usage. Examples of high-throughput applications to chromatography development include Predictor plates and Robocolumns, which can then be validated with lab-scale chromatography.

The work in this chapter aims to demonstrate a non-affinity based downstream bioprocess using precipitation and chromatography steps that is capable of purifying an antibody to

clinical grade standards. To this end, chromatography steps following the ammonium sulphate precipitation step were developed and evaluated in respect to the removal of HCP and DNA species. A microscale experimental approach was conducted on Predictor plates for the primary evaluation, with subsequent verification demonstrated using lab-scale chromatography. Table 6-1 details the chromatography adsorbents used in the study. AEX was performed using Capto Q, a strong anion exchanger fixed onto a matrix of agarose beads, and operated in FT mode. Capto MMC was used for the mixed-mode step in bind-and-elute mode. The Capto MMC ligand combines weak cation-exchange and hydrophobic interaction properties. Optimal conditions from screening studies were carried forward and verified with column chromatography, and subsequently compared with PrA chromatography. A multi-step process incorporating both Capto Q and Capto MMC steps was also proposed to demonstrate the potential of a non-affinity based three-step process.

Table 6-1. Details of Capto Q and Capto MMC resin media.

Adsorbent Name	Capto Q	Capto MMC
<i>Proposed Binding Mechanism</i>	Strong anion exchanger	Weak cation-exchange and hydrophobic interaction
<i>Base Matrix</i>	Agarose	Agarose
<i>Ligand</i>		
<i>Particle Size</i>	90 µm	75 µm
<i>Purpose</i>	HCP and DNA removal	HCP and Product-related species removal

6.2 IgG₄ purification with Capto Q in FT-mode

6.2.1 Determination of IgG₄ binding conditions with microscale chromatography screening

6.2.1.1 *Experimental Layout*

Primary evaluation was conducted by determining suitable loading conditions for IgG₄ to assess binding behaviour. In FT-mode, the aim is to deduce the conditions in which the antibody of interest does not bind to the resin. The effect of pH with no added salt was examined. PrA-purified IgG₄ feedstock was used for the study to provide a rapid examination of binding at the various conditions. Samples were dialysed into various mobile phase conditions with a pH range 6.5 to 9 and low conductivity i.e. no salt, and adjusted to 2 mg/mL IgG₄ by dilution. For pH 6.5 to 7.5, a 20 mM phosphate buffer was used whilst for pH 8 to 9, 20 mM tris was used. All sample conductivities were below 4 mS/cm at 22.5 °C.

The workflow methodology for the Predictor plate screening study is presented in Figure 6-1. Removal of the 20 % ethanol storage solution and equilibration of the wells was performed in accordance with the manufacturer's recommendations. Each well was equilibrated with the recommended volume of corresponding mobile phase buffer (~200 µL) for a total of five equilibrations, with liquid removal performed via centrifugation for 2 min at 500 rpm. Antibody samples were loaded to the corresponding wells to a target load challenge of 10 µg IgG₄ per µL resin, as per UCB's recommendation. Each loading condition was performed in triplicate. The plate was then incubated at room temperature with mixing at 1000 rpm on an orbital shaker for 1 hour. Three total washes of the wells were performed with the respective buffers. In order to remove all bound components, a strip step was performed with 2 M NaCl. All fractions consisting of FT, the three wash steps, and strip were collected and analysed separately with a plate reader (Tecan Safire 2, Tecan) to formulate a complete IgG₄ mass balance. Well volumes were determined using absorbance measurements at 990 nm with a reference wavelength of 900 nm. This was on the basis of the distinctive absorbance peak of water at near infrared (McGown and Hafeman, 1998). A set of calibrations using buffer were prepared to equate volumes with the specific absorbance at this wavelength. Path lengths could then be determined from the cross-sectional area of the wells, based on which sample concentrations could be deduced.

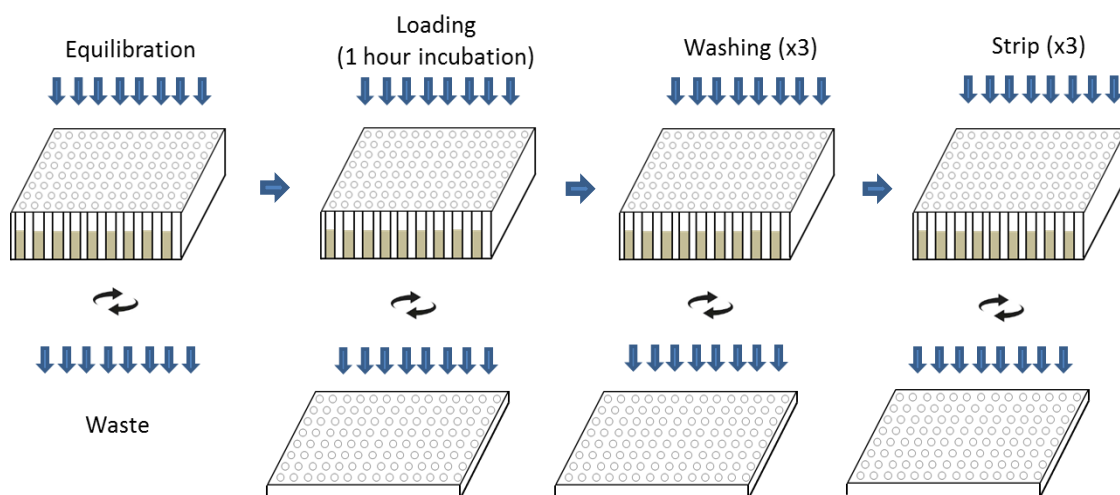


Figure 6-1. High-throughput workflow using 50 μ L Cpto Q 96-well Predictor plates for the development of an anion exchange (AEX) chromatography step. Resin wells were re-suspended in the 20% ethanol storage solution, followed by removal of the solution via centrifugation. Wells were equilibrated with the respective mobile phases for 2 minutes at 1100 rpm in an orbital shaker, after which the solutions were removed by centrifugation and discarded to waste. This step was repeated for a total of five times. Samples were loaded to a target load challenge of 10 μ g IgG₄ per μ L resin and incubated for 1 hour with mixing at 1000 rpm. Well washing was performed with the equivalent mobile phase loading buffers. 2 M NaCl solution was used for the strip/elution step. Flow-through (FT), wash and strip fractions were collected separately into UV-transparent microplates and analysed.

6.2.1.2 Effect of loading pH on IgG₄ binding

Analyses of the chromatographic fractions revealed the effect of mobile phase pH on IgG₄ binding to Cpto Q ligand. It can be seen from Figure 6-2 that IgG₄ binding to Cpto Q increases for pH >8 as a reduced amount of IgG₄ is recovered in the FT and wash fractions. The binding behaviour corroborates with the theoretical pI of the IgG₄ molecule (~ 7.9). Above this value, IgG₄ would be expected to exhibit an overall net negative charge which drives the binding to Cpto Q ligand via electrostatic interactions. IgG₄ binding is then reversed in the presence of 2 M NaCl as shown by the recoveries in the strip fractions. The determined recoveries from the wash steps primarily constitute recovery from the first wash step which was expected to be sufficient in maximising recovery. Maximum recoveries from the pool of FT and wash samples were in the range 82 to 86 % when operating Cpto Q in FT-mode at \leq pH 7.5.

The lower than expected total mass balances (< 100%) may have been a result of the inaccuracies associated with manual liquid volume handling of such small volumes as well as potential volume losses between centrifugation steps. Therefore, recoveries in the FT or strip samples are likely underestimated.

The next step in the Capto Q evaluation study was to determine the influence of loading conditions on the separation efficiency between IgG₄ and the process-related impurities. The knowledge gained from Capto Q process development, according to UCB's expertise, informs that the capture of impurities is typically at an optimum when operating at high pH and low conductivity (< 4mS/cm). Generally, HCPs and DNA have relatively low pI (< 6). Therefore, operating at the highest possible pH without promoting antibody binding is preferred. Based on this, Capto Q purification evaluation on post-precipitated samples was performed with loading at the highest pH value where IgG₄ binding occurs at a minimum i.e. pH 7.5, and within a range of salt concentration.

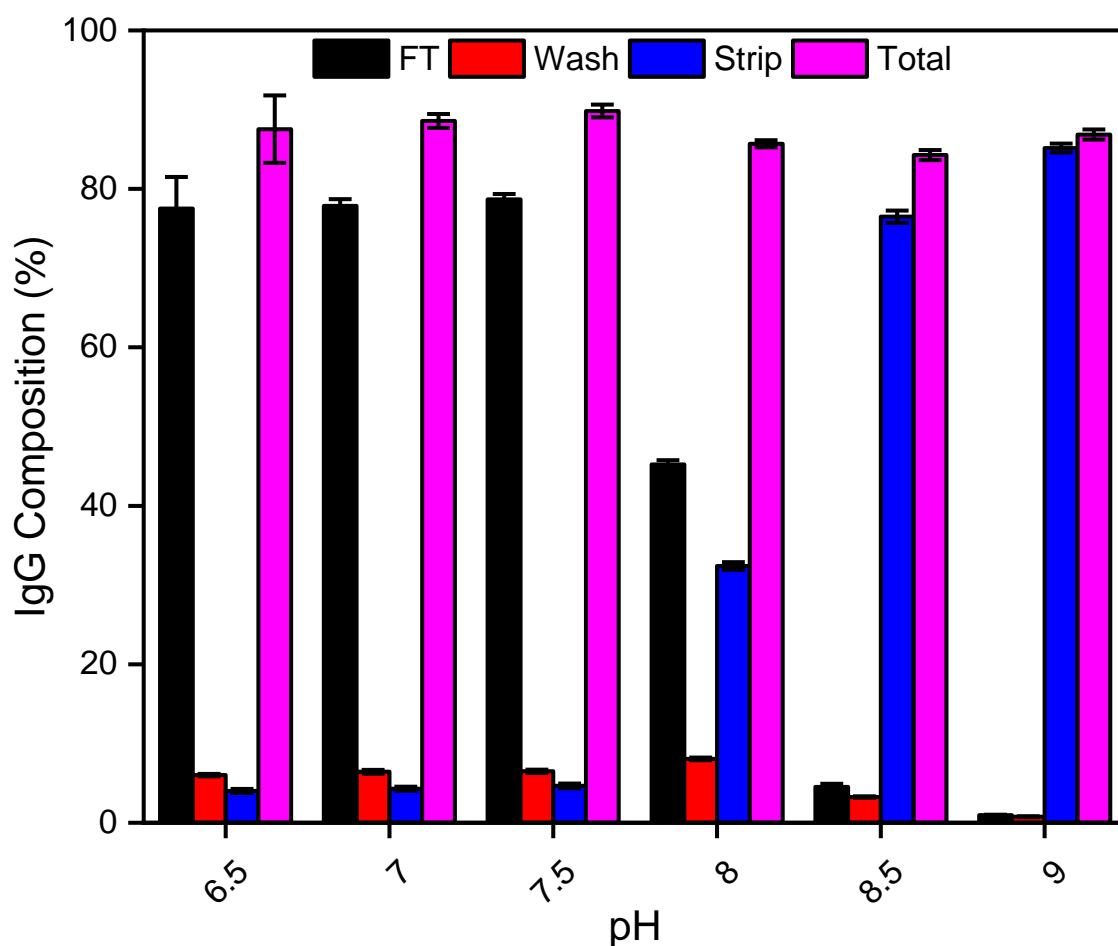


Figure 6-2. Cpto Q screening to determine IgG₄ loading conditions. Buffer exchanged Protein-A purified antibody samples were loaded onto Cpto Q 96-well Predictor plates with 50 μ L resin per well. 500 μ g of sample was loaded to each well to provide a target load challenge of 10 μ g IgG₄ per μ L resin. FT, wash and strip fractions were recovered via centrifugation. IgG₄ content was determined by absorbance at 280 nm in microtitre plates and expressed in terms of yield for each fraction. Data is presented as the average IgG₄ composition percentage relative to the total loading amount in the various fractions from differing loading conditions from n = 3 experiments with error bars of \pm 1 standard deviation displayed. Total represents the full IgG₄ mass balance from the sum of the fractions.

6.2.2 Evaluation of loading conditions on IgG₄ yield and impurity removal

6.2.2.1 Sample preparation

A series of CCCF precipitations were first conducted in batch mode at 100 mL scale with constant mixing at 300 rpm with ammonium sulphate feed rates of 1 mL/min. Precipitates were filtered through 0.22- μ m Rapid-Flow Nalgene disposable filter units, washed twice with ammonium sulphate and subsequently solubilised in-line with phosphate buffers at pH 7 with varying NaCl concentration in the range 0 to 125 mM. Due to the expected residuals of ammonium sulphate present in the precipitate, the resolubilised samples underwent dialysis into the respective mobile phase condition in preparation for loading onto Capto Q. Final sample conductivities were in the range 3.8 to 15 mS/cm. Yields from the buffer exchange step were generally above 90% with some losses observed due to insoluble aggregate formation and potential cake formation on the membrane. These were processed through 0.22- μ m syringe filters in order to remove these.

A series of control experiments were included for the Capto Q assessment which involved direct IgG₄ purification from CCCF samples. This was performed to demonstrate the efficacy of salt precipitation as a 'pre-treatment' step which may impact Capto Q performance. CCCF samples were dialysed in the same manner as for the post-precipitated samples.

6.2.2.2 Predictor plate results

The same workflow presented in Figure 6-1 was employed for the study with the focus on examining IgG₄ yields and product HCP levels in the FT fractions. Figure 6-3 demonstrates the effect of loading mobile phase on IgG₄ yield and remaining HCP composition in the flow-through, for post-precipitated and non-precipitated CCCF samples. The data shows that, for a given loading condition, the antibody yields were comparable for both feed types. A slightly increasing trend in yield was observed with higher salt concentrations which could indicate non-specific interactions contributing to yield losses at low salt concentrations. Higher yields could have been obtained with the inclusion of the wash step fractions but at the risk of greater HCP levels. Both sets of data demonstrate an increasing removal of HCPs with increasing salt up to 75 mM. HCP levels then rise with a further increase in salt concentration. At the optimum, Capto Q in FT-mode alone achieved an 88-fold removal in HCPs alone (11200 \pm 2900 ppm), whilst pre-treatment with ammonium sulphate precipitation, followed by Capto Q achieved 178-fold removal (5970 \pm 2000). Such a significant reduction

in HCPs from both feeds from a Capto Q flow-through method was surprising since an overall 2 log removal in total HCPs was observed. It was then noted that the 1 hour incubation employed provided a significant amount of time for HCPs to bind to the resin thereby aiding their separation from unbound antibody. The results would need to be validated with lab-scale chromatography.

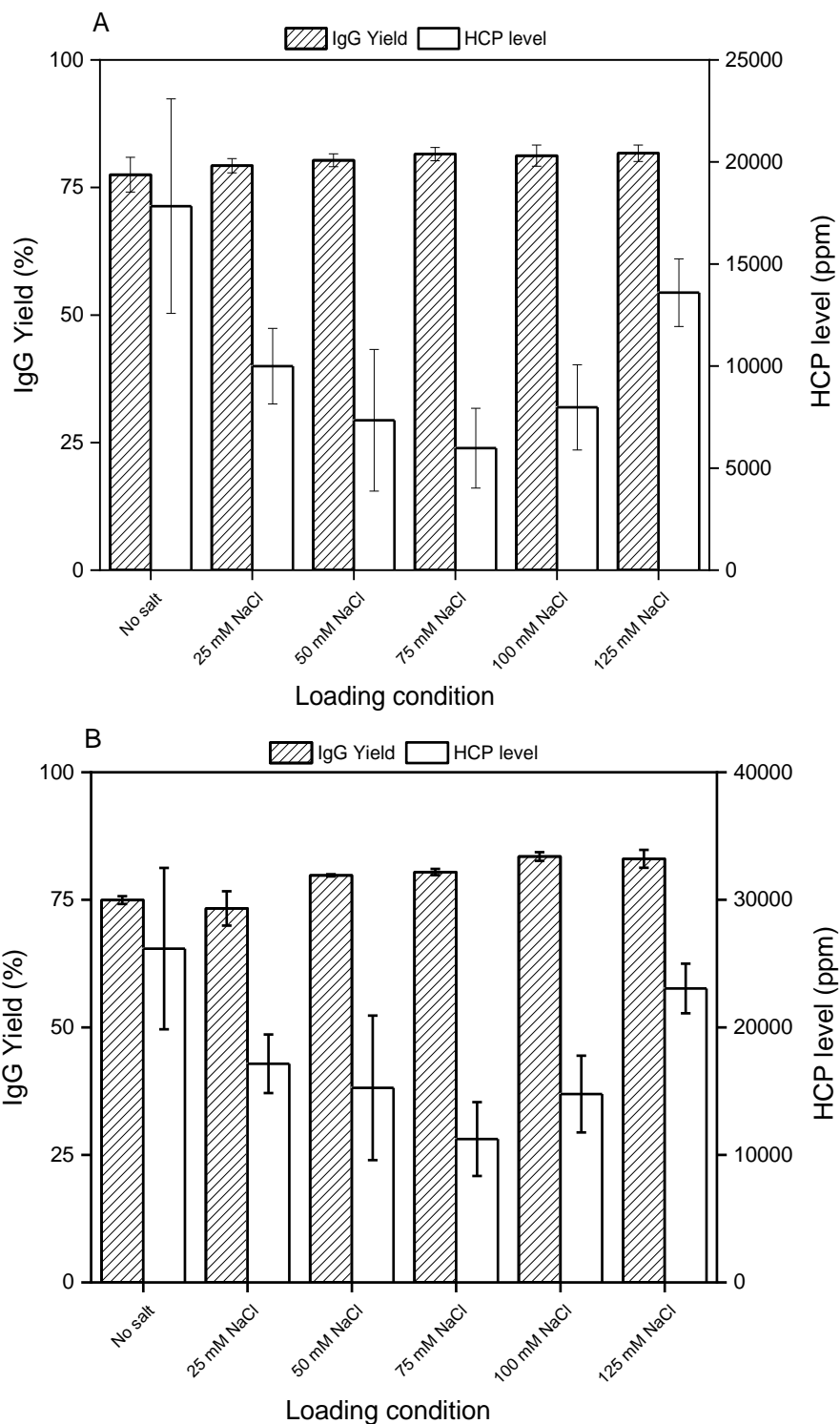


Figure 6-3. Effect of salt concentration on antibody yield and remaining HCP levels in CptoQ processing of (A) post-precipitated and (B) non-precipitated CCF samples at microscale. Loading was performed with a target load challenge of 10 μg IgG₄ per μL resin with mixing at 1100 rpm for 1 hour. Well samples were recovered with centrifugation. Yields were determined via PrG-HPLC analyses. HCP concentrations were examined with CHO-HCP ELISA kits and converted to ng HCP per mg IgG₄ (ppm). Data represents the average IgG₄ yields and HCP levels, in ppm, present in the FT fractions from the various loading conditions performed in 96-well Predictor plates. Error bars are displayed as 1 standard deviation of n = 3 experiments.

6.2.2.3 Verification of Capto Q loading conditions on IgG₄ purification with lab scale chromatography

Results presented from the Predictor plate screening experiments were validated with a 1 mL HiTrap Capto Q column (7 mm ID x 25 mm L) on an AKTA Pure 25 system. The column was prepared by pre-charging the resin with 20 mM phosphate, 2 M NaCl pH 7.5 for three column volumes (CV), washing with MilliQ water, and finally equilibrating with the corresponding mobile phase buffer for a minimum of 3 CVs or until the conductivity trace was stable at the expected value. Sample loading was carried out at a linear flow rate of 78 cm/h, corresponding to 0.5 mL/min volumetric flow rate and a total residence time of 2 min, using the equivalent load challenge (10 mg per mL resin). The method on UNICORN was programmed to commence product collection when the UV exceeded 50 mAU and end when it fell below during the loading and wash steps. The wash step was performed for 3 CVs. Strip with 2M NaCl was performed for 10 CVs in order to ensure the removal of all bound materials in preparation for the next cycle. Duplicate experiments were performed. Representative chromatograms for Capto Q processing of post-precipitated and non-precipitated samples are presented in Figure 6-4.

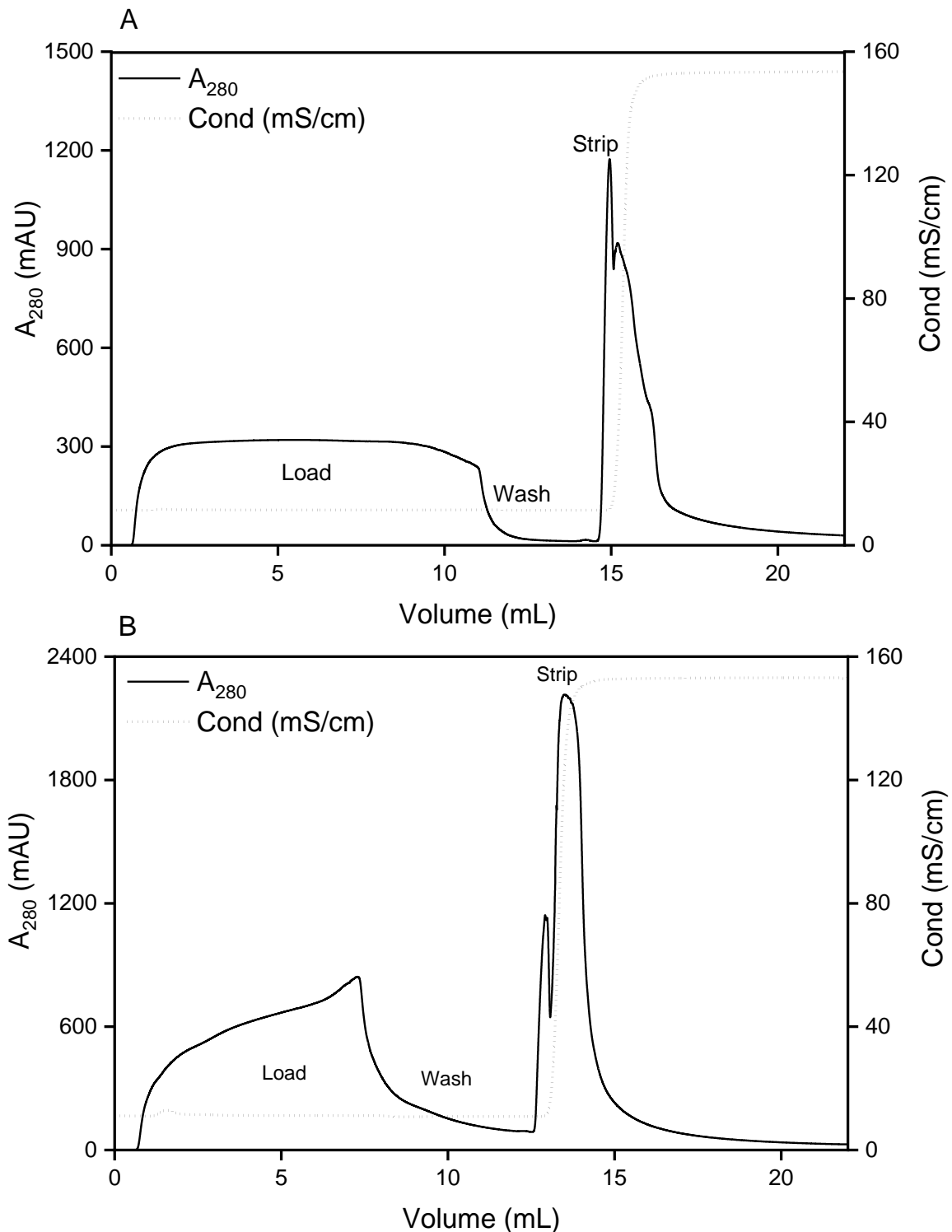


Figure 6-4. Capto Q chromatogram profiles representing IgG₄ purification from (A) post-precipitated and (B) non-precipitated CCCF samples in a 1 mL HiTrap column. Both profiles correspond to IgG₄ loading at 10 mg IgG₄ per mL Capto Q resin at pH 7.5, 75 mM NaCl. Samples were directly loaded to the column at a linear flow rate of 78 cm/h, corresponding to 0.5 mL/min volumetric flow rate and 2 min total residence time. Corresponding UV peaks of load, wash and strip are displayed. Sample collection commenced when UV during loading exceeded 50 mAU and ended when it fell below during the wash step.

Figure 6-5 presents the yield and HCP level results from Capto Q processing at the various loading conditions for post-precipitated and non-precipitated CCCF samples. Capto Q yields for post-precipitated samples were in the range 82 to 98%, whilst for the non-precipitated samples, yields were in the range 90 to 98%. Consistent with the microscale data, step increases in yield were observed with increasing salt concentration, again supporting the hypothesis of non-specific protein-ligand interactions occurring at low salt concentrations.

In terms of HCP, the levels in samples from the 1 mL HiTrap were far greater than those from the microscale experiments, which is likely a consequence of the very different residence times between both methods. Nonetheless, the lab-scale chromatography experiments verify the 75 mM NaCl condition as the optimal loading strategy in maximising HCP removal for both feed types. Using this loading condition, Capto Q alone achieved a 5-fold reduction in HCPs. In combination with ammonium sulphate precipitation, HCP removal was enhanced by 4-fold (20-fold total HCP removal from CCCF). The samples from these experiments were also analysed for DNA content. As illustrated in Figure 6-6, DNA levels are significantly reduced by Capto Q, especially for the non-precipitated CCCF sample (initial DNA concentration: 1533 ng/mg)

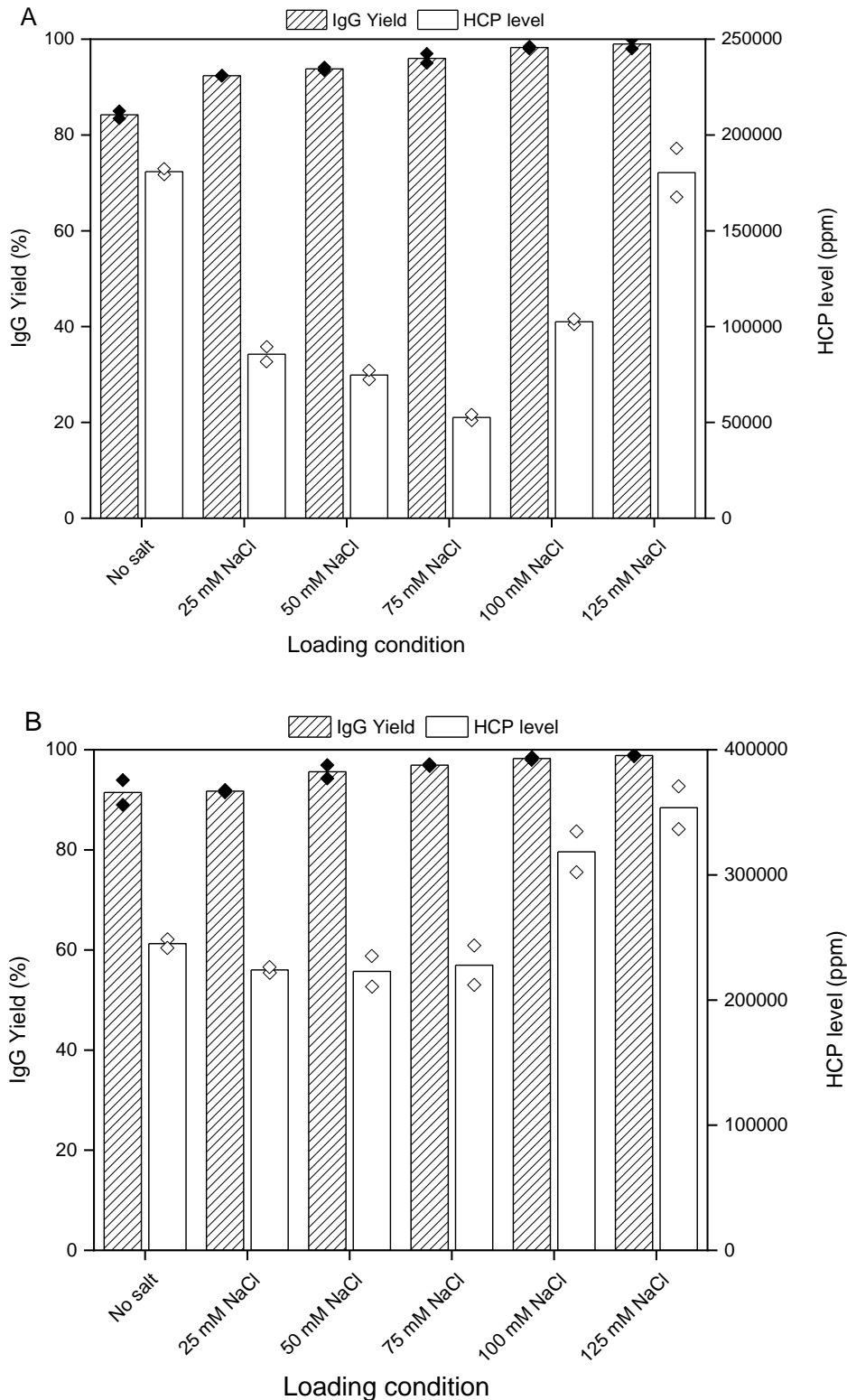


Figure 6-5. Effect of salt concentration on antibody yield and HCP levels in Capto Q processing of (A) post-precipitated and (B) non-precipitated CCCF samples in FT-mode using lab-scale chromatography. Samples were loaded onto a 1 mL HiTrap Capto Q column at a linear flow rate of 78 cm/h, corresponding to 0.5 mL/min volumetric flow rate and 2 min total residence time, and with a load challenge of 10 mg IgG₄ per mL resin. Columns bars represent the average yield and HCP levels in FT samples from duplicate experiments, whilst data points correspond to each experimental run.

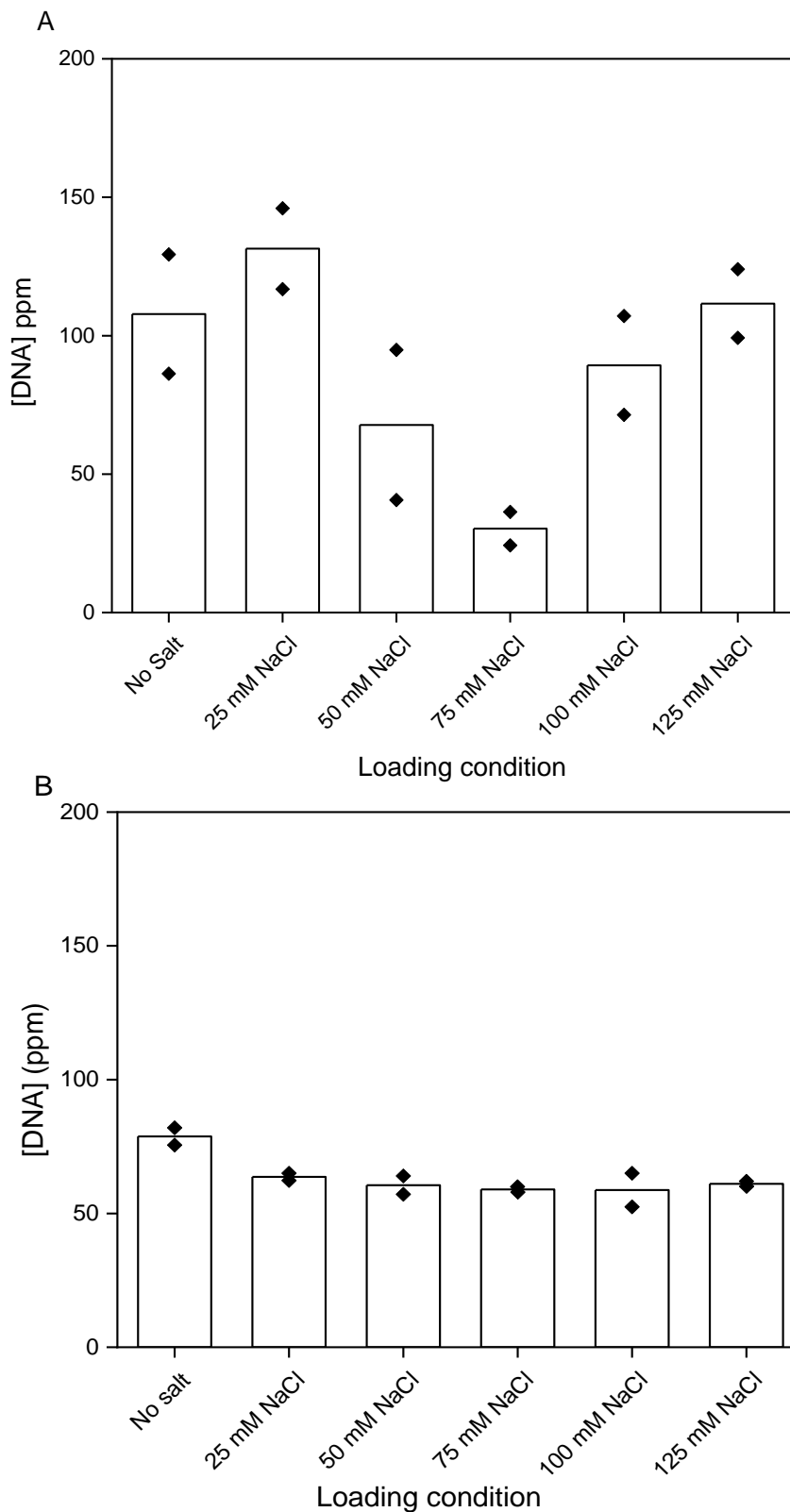


Figure 6-6. Effect of salt concentration on residual DNA levels in Capto Q processing of (A) post-precipitated and (B) non-precipitated CCCF samples in FT-mode using lab-scale chromatography. Samples were loaded onto a 1 mL HiTrap Capto Q column at a linear flow rate of 78 cm/h, corresponding to 0.5 mL/min volumetric flow rate and 2 min total residence time, and with a load challenge of 10 mg IgG₄ per mL resin. Column bars represent the average DNA levels in FT samples from duplicate experiments, whilst data points correspond to each experimental run.

6.3 IgG₄ purification with Capto MMC in bind-and-elute mode

Similarly to Capto Q, suitable IgG₄ loading conditions were investigated with Capto MMC in bind-and-elute mode using microscale chromatography. Owing to the mixed ionic and hydrophobic properties of the Capto MMC ligand by which binding occurs, the influence of pH, salt type and salt concentration during loading was evaluated. Ranges for each parameter were selected based on previous research conducted in the department (Wenger, 2010). Ammonium sulphate and sodium chloride were chosen as salt constituents in buffers of pH ranging between 5 and 7. Salt concentrations had to be tested to establish a working range in which non-precipitating or non-aggregating feed conditions were met as a prerequisite for Capto MMC loading. Samples were dialysed in a universal buffer mixture of 10 mM sodium phosphate, 10 mM sodium acetate and 10 mM HEPES at the desired pH.

6.3.1 Determination of non-precipitating loading conditions

A solubility screen on post-precipitated CCCF was conducted using sodium chloride and ammonium sulphate at 1 mg/mL IgG₄, the concentration at which primary evaluation of Capto MMC was to be carried out. Solutions were dialysed into pH 5, 6 or 7 buffers and combined with salt at concentrations up to 1.25 M and at the desired pH using 3 M stock solutions. After 1 hour of incubation with gentle agitation, solubility was then assessed by measuring sample absorbance at 600 nm. Sample precipitation and/or aggregation was indicated based on absorbance measurements being at least 3-fold above the background signal i.e. > 0.03 for a buffer sample. The solubility screen results are presented in Table 6-2. As expected, aggregation and/or precipitation begins to occur at ammonium sulphate concentrations ≥ 1 M with a slight pH dependency. Sodium chloride did not present any clear indication on aggregation or precipitation behaviour with respect to pH or salt concentration. Therefore, the upper salt concentration for the sample loading range fixed to an upper limit of 0.75 M to ensure fully soluble conditions across the pH range to be examined.

Table 6-2. Examination of non-precipitating and precipitating conditions across a salt range from 0 to 1.25 M sodium chloride (SC) and ammonium sulphate (AS) for Capto MMC chromatography loading. Final antibody concentration in the well was fixed to 1 mg/mL. Absorbance at 600 nm was measured in 96-well UV-transparent microtitre plates. Values above three times the background signal (i.e. ≥ 0.08) are shown in bold and considered indicative of precipitation.

[Salt], M	0	0.25	0.5	0.75	1	1.25
SC, pH 5	0.032	0.035	0.0436	0.059	0.039	0.065
SC, pH 6	0.028	0.0331	0.044	0.038	0.036	0.061
SC, pH 7	0.041	0.042	0.0434	0.0385	0.0361	0.054
AS, pH 5	0.0351	0.0316	0.0336	0.0412	0.0361	1.567
AS, pH 6	0.0363	0.033	0.0392	0.0344	0.213	1.214
AS, pH 7	0.0311	0.0354	0.0394	0.0352	0.190	1.627

6.3.2 Microscale purification study

6.3.2.1 Experimental layout

The Predictor plate workflow scheme for IgG₄ purification on post-precipitated samples using Capto MMC is outlined in Figure 6-7. The wells were first equilibrated with the corresponding mobile phases for a total of five equilibration steps. Dialysed samples were then loaded to a target load challenge of 5 µg IgG₄ per uL resin. Wells were incubated on an orbital shaker at 1100 rpm for 1 hour and at room temperature to ensure optimal IgG₄ binding at the various conditions. Primary assessment was conducted on the FT fractions to determine antibody capture and HCP removal as a function of pH, salt concentration and salt-type. Then, a secondary evaluation was conducted to determine the effect of elution strength on reversible IgG₄ binding, whilst assessing co-elution of HCPs during purification. Elution was carried out in a staircase fashion using sodium chloride up to 1.5 M in 0.25 M increments, buffered in 50 mM HEPES pH 8. The salt type and pH combination has been previously shown to maximise IgG₄ desorption from Capto MMC ligand, and thus was taken forward as an extension to this study (Wenger, 2010). Elution at each salt concentration was performed twice in sequence to recover as much sample as possible from the wells prior to performing elution at the next increment. Fractions of FT, wash and eluates were collected separately in microtiter plates for individual analyses.

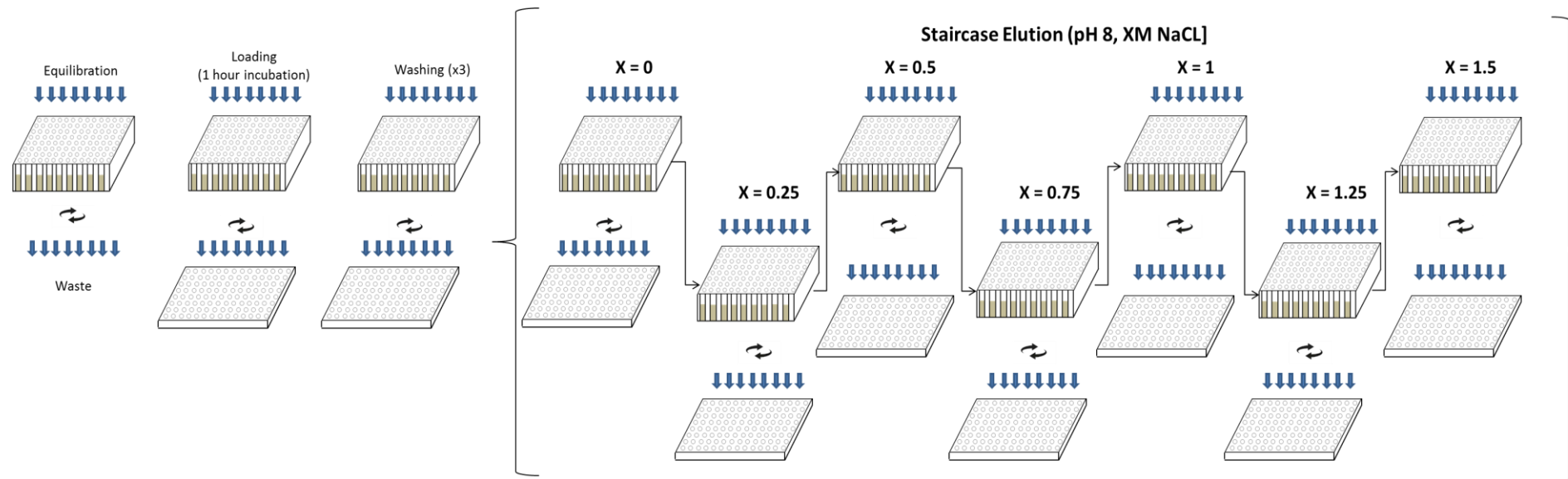


Figure 6-7. Capto MMC Predictor Plate workflow schematic for antibody purification screening. Each well consisted of 50 μL MMC resin and were equilibrated with the desired mobile phase prior to loading. Each well was loaded with 5 μg IgG₄ per μL resin (Total IgG₄ load amount = 250 μg) and incubated for 1 hour with mixing. Following, the wells were washed for a total of three washes with the same buffers used for equilibration. IgG₄ elution was performed using sodium chloride buffered with HEPES at pH 8.0 in a staircase fashion using 0.25 M salt incremental steps in the range 0 to 1.5 M. All fractions were collected by centrifugation into separate plates and analysed accordingly.

6.3.2.2 Data analysis to select leading conditions

Statistical DoE was implemented to facilitate data analysis from the Capto MMC experiments, enabling simultaneous evaluation of multiple variables on one or more response factors. Whilst DoE was not implemented in the experimental design, the software was used to summarise the data and generate useful models which describe main effects and reveal factor interactions where visual inspection could not. Moreover, specifications could be placed on the data such that optimal sets of conditions are outlined to maximise, minimise or provide a target range for one or more of the specific response factors. The desirability plot output is a useful tool which highlights specific operating windows that provide a balance between the response factors, with 0 being the least desirable condition and 1, the most desirable. Design Expert software (version 12.0) from Stat-Ease was used to analyse the data from the microscale Capto MMC results. Data was initially fitted with a cubic polynomial model, and then, if required, refitted with lower order models when aliased terms in the cubic model were detected and therefore not recommended for analysis.

6.3.2.3 Effect of mobile phase on IgG₄ binding and HCP removal

The response maps illustrated in Figure 6-8 demonstrate a dependence of pH, salt type and salt concentration on the binding behaviour of IgG₄ and HCPs on Capto MMC ligand. In the case of loading with sodium chloride, IgG₄ and HCP binding is reduced with higher pH and salt concentration. For the 0.75 M sodium chloride at pH 7 loading condition, almost minimal to no antibody could bind to the resin and most if not all HCPs were carried along with it. The reduction in binding with sodium chloride at pH ≥ 6 indicates that electrostatic interactions dominate in this range. IgG₄ binding was much less affected when loading with ammonium sulphate within the equivalent pH and salt concentration range. This implies that in this case binding is driven by hydrophobic interactions at high salt concentrations. A valley in the response surface was observed which represented a reduction in the antibody binding occurring at ≥ 0.25 M salt at above pH 6, but then appears to increase at ≥ 0.5 M. This behaviour suggests that hydrophobic interactions supersede electrostatic interactions at higher ammonium sulphate concentrations.

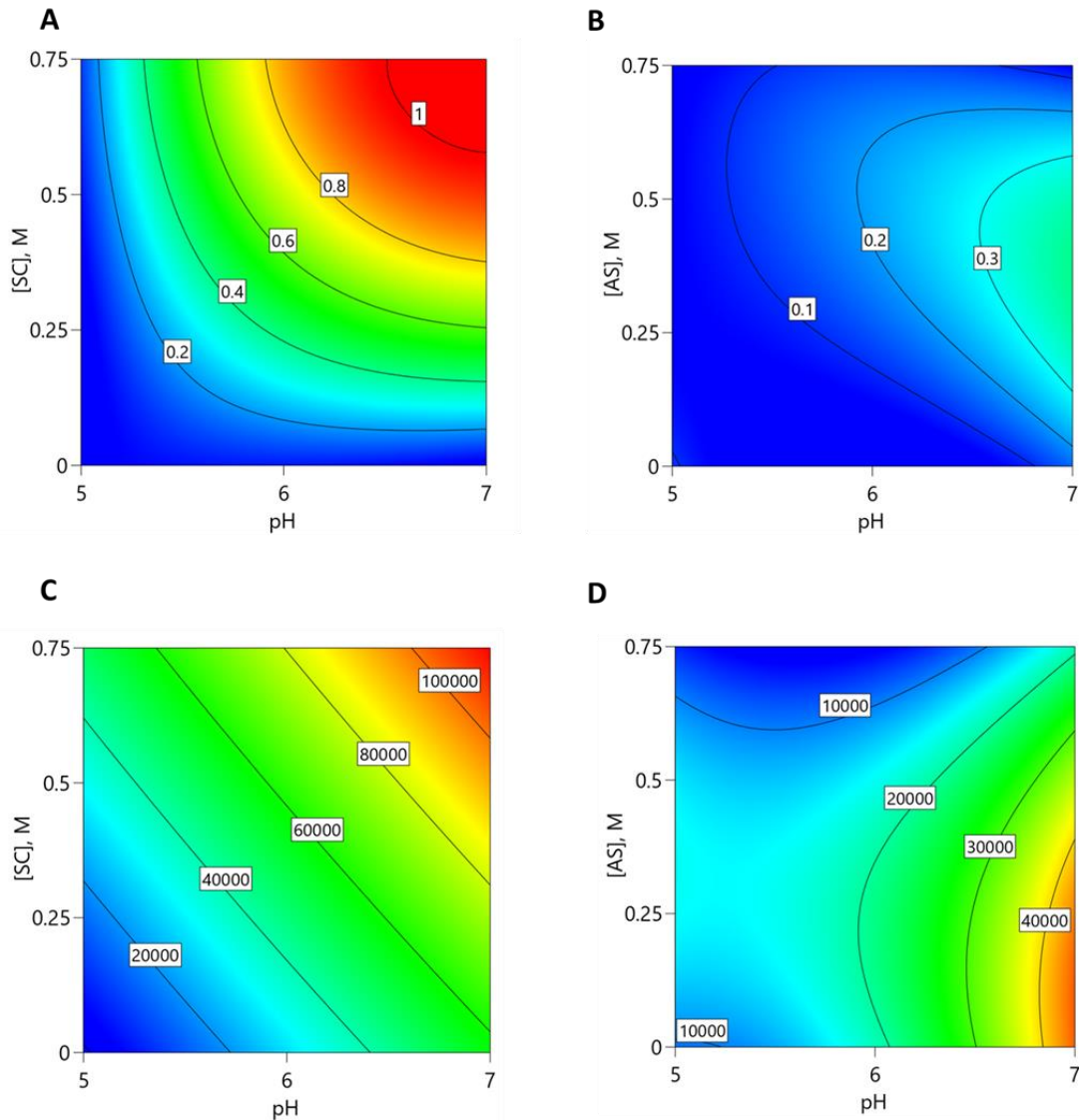


Figure 6-8. Contour plots showing the effect of pH, salt type and salt concentration of IgG₄ binding to Capto Q resin and HCP removal during loading in 50 μ L Predictor plates as a function of pH and salt concentration. (A) Fraction of post-precipitated unbound IgG₄ in the presence of sodium chloride (SC), (B) Fraction of post-precipitated unbound IgG₄ in the presence of ammonium sulphate (AS), (C) HCP levels in ng/mL with sodium chloride, (D) HCP levels in ng/mL with ammonium sulphate. Response maps were generated from duplicate experiments and modelled with Design Expert 12.0. Response maps (A)-(B) and (D) were fitted using the quadratic model whilst (C) was fitted with the linear model. Unbound fraction responses: adjusted $R^2 = 0.93$, predicted $R^2 = 0.91$; HCP level responses: adjusted $R^2 = 0.838$, predicted $R^2 = 0.81$.

Visual observation of the desirability plots presented in Figure 6-9 demonstrate operating regions in which loading conditions are favourable to give a maximum threshold of 35 % unbound IgG₄ and maximum HCP levels. Comparison of both plots revealed that ammonium sulphate provided a more robust window of desirable loading conditions over sodium chloride. Both sets of data are in agreement that desired loading occurs at high pH and low salt i.e. pH 7 with no added salt, suggesting Capto MMC is performing better as a cation-exchanger. In addition to the pH 7 with no added salt condition, two conditions were identified: pH 6.5 with no added salt and pH 5.8, 0.34 M ammonium sulphate. The latter was specifically taken forward because of its robust operating window with respect to changes in pH and salt concentration.

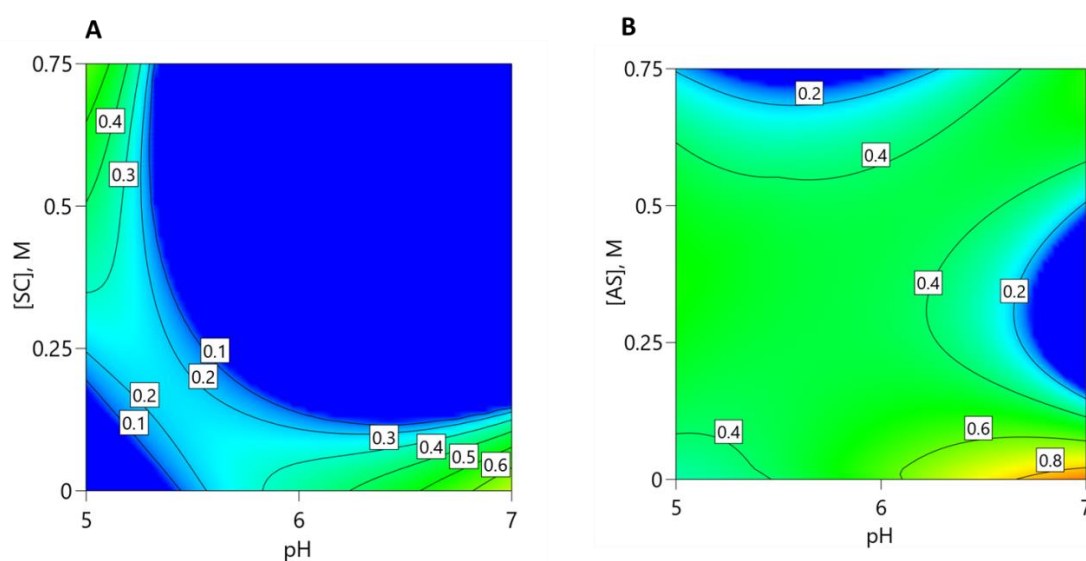


Figure 6-9 Desirability plots highlighting leading loading conditions from sodium chloride, SC, (A) and ammonium sulphate, AS, (B) screening using Design Expert 12. Contour lines represent areas of desirability with 0 being the least optimal and 1, the most desirable. Unbound IgG₄ and HCP levels were weighted with equal importance, with a maximum level of unbound IgG₄ set to 30 % and HCP levels set to a maximum. Optimal loading conditions were selected based on visual inspection of the contour plots and designated.

6.3.2.4 Evaluation of IgG₄ reversible binding with sodium chloride elution strength

The IgG₄ elution profiles from the secondary assessment of Cipto MMC using sodium chloride buffered at pH 8 is displayed in Figure 6-10. For each of the conditions employed for IgG₄ loading, where IgG₄ was found to effectively bind to Cipto MMC, it can be seen that elution at pH 8 up to 1.5 M NaCl was sufficient in complete IgG₄ desorption with the majority of antibody eluting at ≥ 0.25 M. In pooling the 0.25, 0.5 and 0.75 M elution strength fractions, a maximum step recovery of 85 % could be attained, depending on the loading condition.

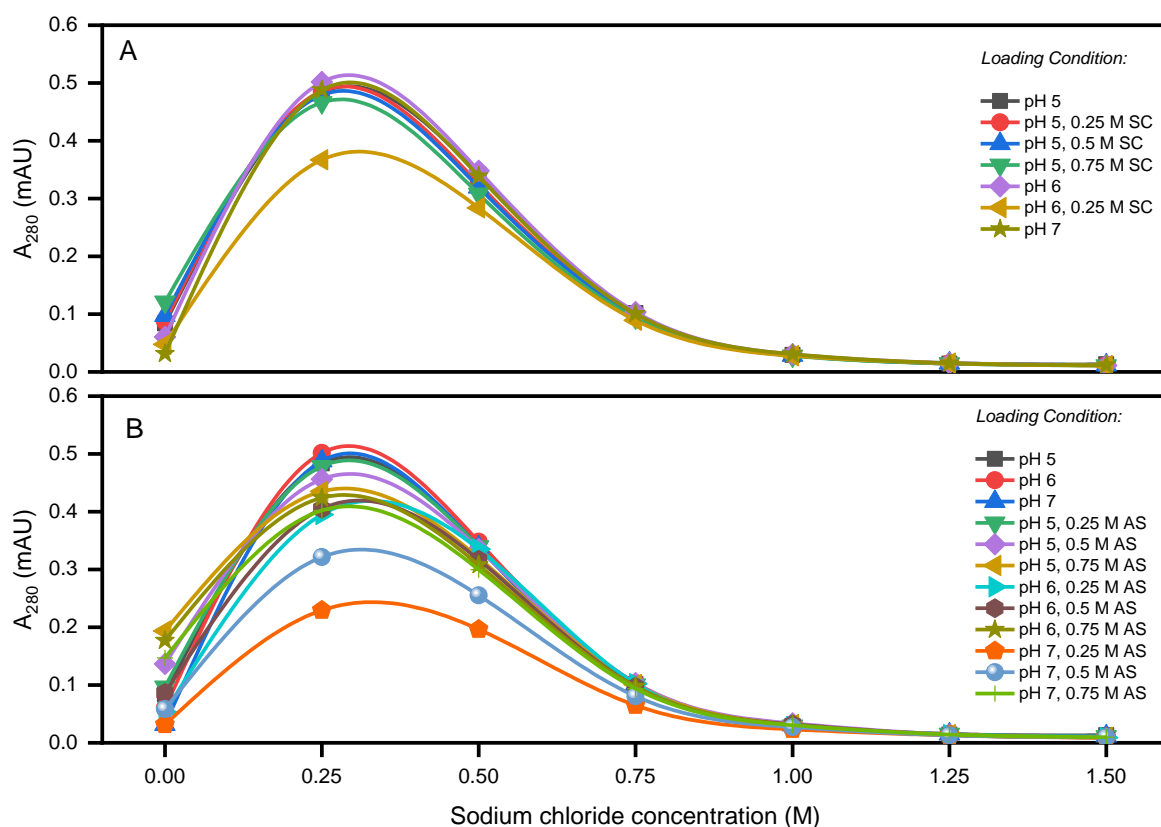


Figure 6-10. IgG elution profiles with sodium chloride at pH 8. (A) IgG₄ loaded at various pH and sodium chloride (SC) concentrations. (B) IgG₄ loaded at various pH and ammonium sulphate (AS) concentrations. Elution was performed with increasing elution strength with each elution performed twice. A₂₈₀ values were taken from affinity-HPLC analyses.

With regards to potential HCP co-elution, considering the vast amount of samples which could be analysed, it was decided to pool the eluates from 0.25 M and 0.5 M salt elution strengths, of which most antibody reside in, and take these forward for HCP analyses. Whilst including the 0.75 M salt condition would augment the step yield, only slightly, it would however be expected that HCPs captured on the resin are more likely to co-elute as the elution strength increases. Therefore, elution at the 0.25-0.5 M salt range represented a good compromise between antibody step yield and HCP removal. IgG₄ yields and residual HCP levels in these fractions are displayed in the contour maps illustrated in Figure 6-11. Desirable operating regions are presented in the desirability plot illustrated in Figure 6-11C which balances optimal IgG₄ yield based on a minimum threshold of 65 % and the maximum extent of HCP removal. Both responses were weighted with equal importance. According to the model, a maximum yield of 84% with a minimum HCP level of 28100 ppm can be obtained from a Capto MMC step when loading is operated > pH 6.5 with no added salt. The pH 5.8, 0.34 M ammonium sulphate condition was also identified by the model predicting 79.7 % yield and 35000 ppm HCPs, and also provides a robust operating window. The selected lead conditions were taken forward for validation.

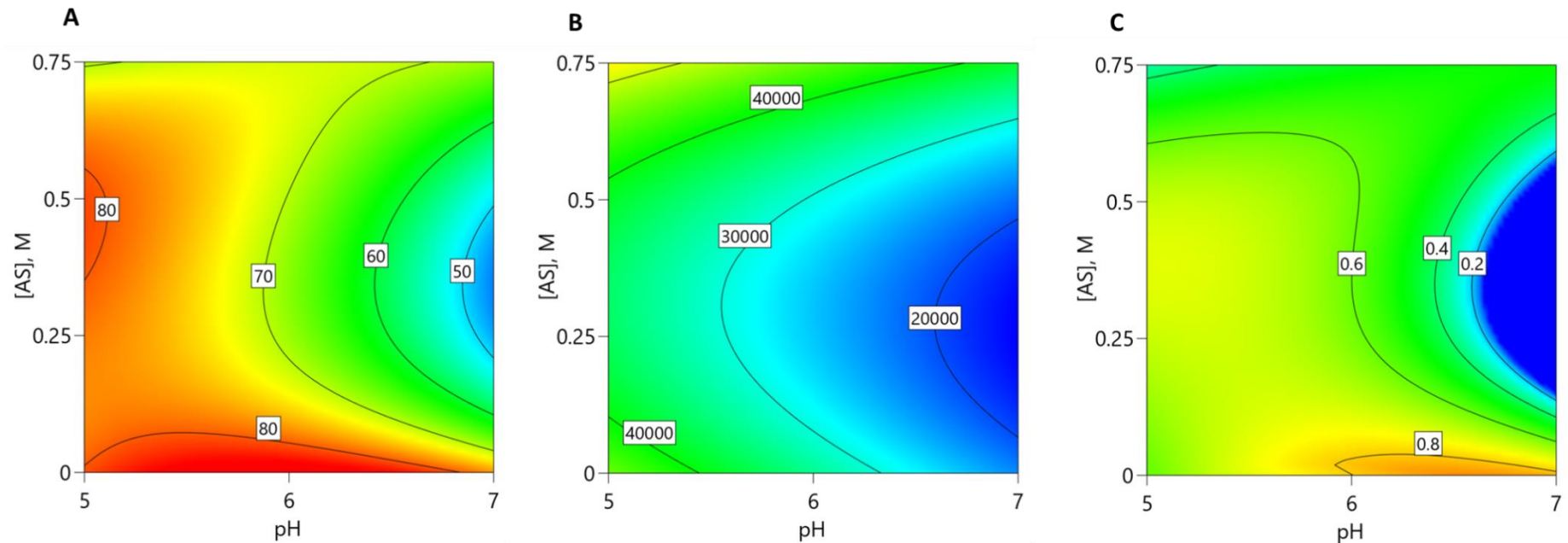


Figure 6-11. Contour maps showing antibody yield and HCP eluate pools from the various loading conditions in the presence of ammonium sulphate. (A) IgG₄ yields, (B) residual HCP levels (in ppm), (C) desirability plot balancing optimal IgG₄ yield (minimum threshold > 65 %) with optimal HCP removal at equal weighting importance. Data from two sets of replicate experiments were used to generate the response map and fitted using a quadratic model. *Yield* - Adjusted R²: 0.845, predicted R²: 0.767; *HCP levels* - Adjusted R²: 0.769, predicted R²: 0.656.

6.3.3 Verification of IgG₄ purification using selected lead conditions with lab scale chromatography

The selected conditions tested for verification on a 1 mL HiTrap Capto MMC column were as follows: pH 6.5 with no added salt, pH 7.0 with no added salt and pH 5.8, 0.34 M ammonium sulphate. Direct loading of the post-precipitated sample (pH 7.0 \pm 0.2; conductivity < 15 mS/cm) to the column was performed in lieu of the pH 7 condition (no salt added). For the other conditions, samples were exchanged into the desired solutions. Samples were loaded directly onto the column at 78 cm/h, corresponding to a total residence time of 2 minutes, with a load challenge of 5 mg of IgG₄ per mL of resin as per the microscale screening experiments. Product elution was performed via a linear gradient of sodium chloride at pH 8 (buffered with HEPES) from 0 to 1 M over twenty CVs, with 1 mL fractions collected along the gradient. A 1 M NaOH cleaning step was implemented for 3 CVs post-elution to remove any strongly bound components in order to prevent carry over to the next purification cycles. Experiments were carried out in duplicate.

The representative chromatographic profiles from these runs are shown in Figure 6-12. The replicates from these runs matched comparably and therefore only one replicate for each run is displayed. It can be seen that two separate peaks consistently evolved during elution whereby the smaller peak appears upon concomitant increase to pH 8. This was then followed by the main peak which reaches a maximum absorbance at 280 nm at approximately 0.4- 0.45 M NaCl which is consistent with the elution profiles in Figure 6-10. Analysis of the eluate fractions revealed the absence of IgG₄ in the pre-peak, indicating that this primarily corresponded to process-related impurities including HCP, DNA and potential free antibody light chain which is known to elute at pH 8. It also appears that the intensity of the smaller peak is dependent on the intensity of the FT peak. In other words, if more HCPs are removed during loading, then fewer HCPs are removed at the start of elution and vice versa.

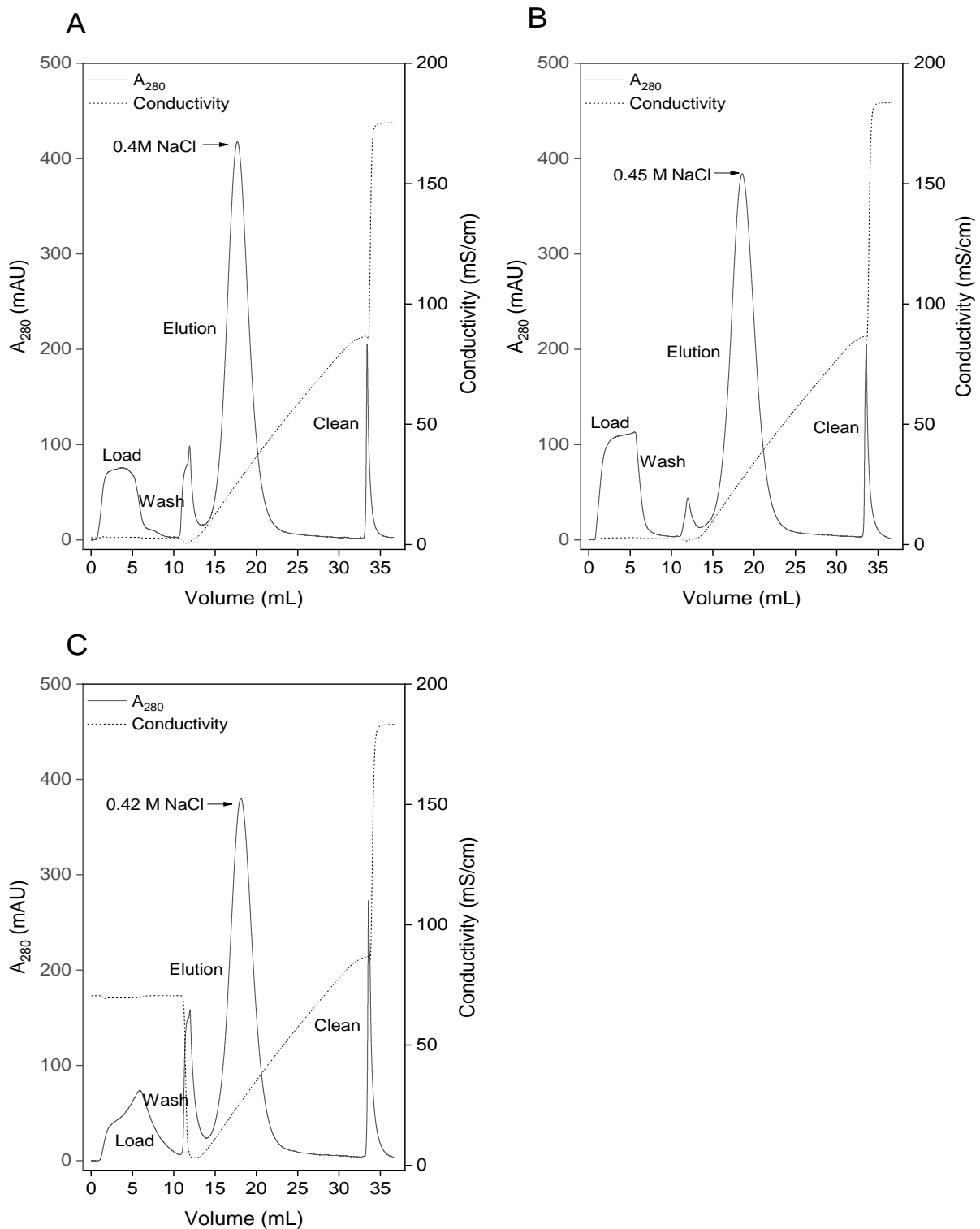


Figure 6-12. UV chromatograms of post-precipitated antibody samples loaded onto 1 mL HiTrap Canto MMC and eluted with sodium chloride at pH 8 with a linear gradient over 20 CVs. Corresponding loading conditions are as follows: (A) pH 6.5, no added salt, (B) direct loading of post-precipitated sample (pH 7, $< 15\text{ mS/cm}$) and (C) pH 5.8, 0.34 M ammonium sulphate. Samples were loaded at 78 cm/h, corresponding to a residence time of two minutes. Elution strength is represented by the conductivity profiles corresponding to the linear salt concentration change from 0 to 1 M sodium chloride. Corresponding elution salt concentrations at max peak absorbance of the main peak are displayed. Column cleaning and maintenance was performed with 1 M NaOH for a minimum of 3 CVs.

Column cleaning with 1 M NaOH showed to remove the strongly bound components which could not be desorbed from the matrix even at the highest elution strength. We did not expect the representative peak to contain any antibody and thus assumed complete IgG₄ elution prior to cleaning.

For each of the loading conditions, antibody recoveries in the equivalent eluate fractions were comparable. A complete mass balance was taken on the generated fractions from the portion of the linear gradient corresponding to the range 0.2 – 0.6 M salt which demonstrated that total yields for all runs were similar (82-87%). These fractions also revealed the part of the salt gradient where HCPs would co-elute with antibody. According to Figure 6-13, it can be seen that for each of the loading conditions, the majority of HCPs are present in the early fractions which correspond to elution at a salt concentration below 0.3 M. Since the corresponding fractions clearly carry much less antibody, these could be discarded to significantly improve overall antibody purity with respect to HCPs.

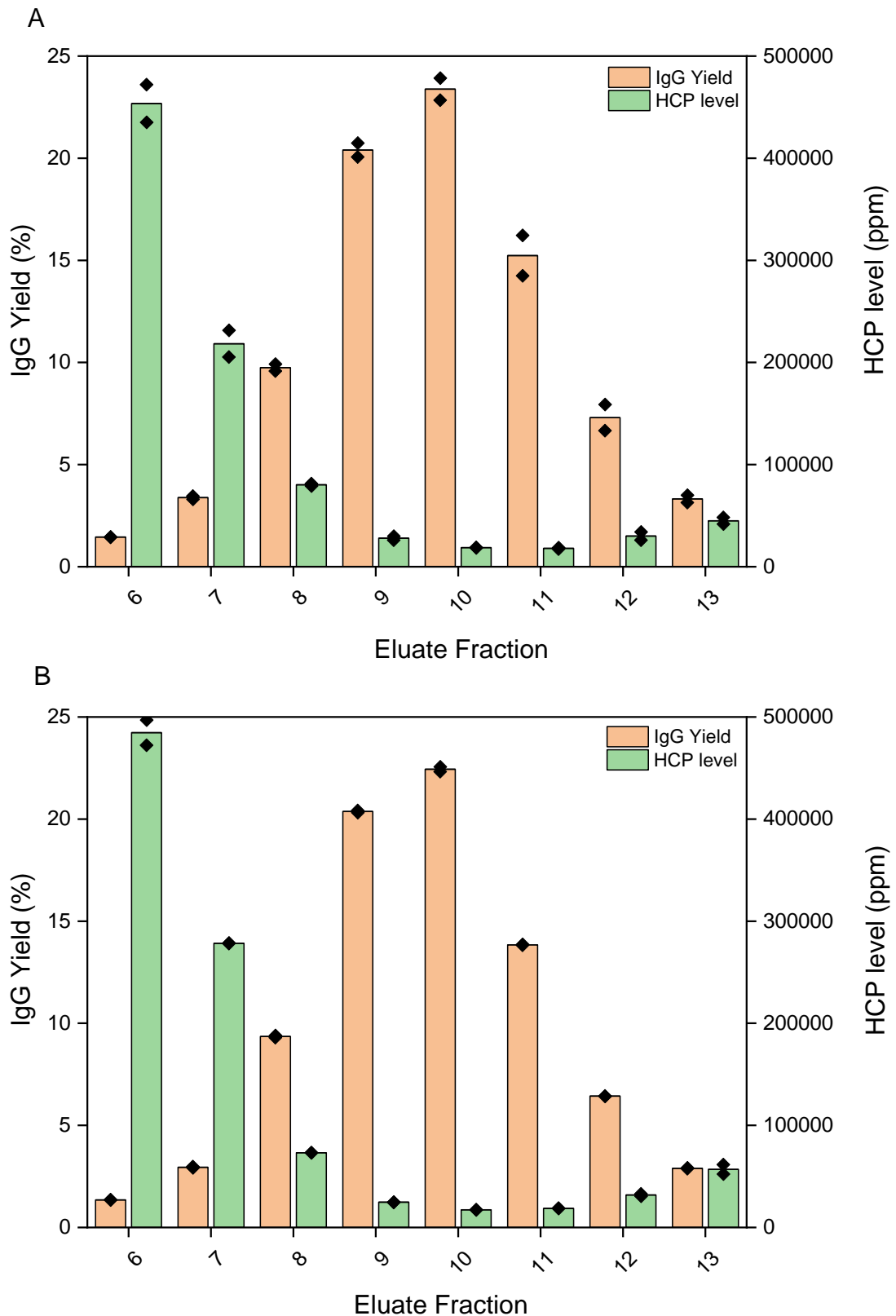


Figure 6-13. Antibody and HCP level compositions in Capto MMC eluate fractions corresponding to the main peak in the chromatograms presented in Figure 6-12. (A) pH 6.5, no added salt loading, (B) direct loading of post-precipitated sample (pH 7, < 15 mS/cm), (C) pH 5.8, 0.34 M ammonium sulphate loading. HCP levels in ng/mL determined by ELISA were converted to ppm. Error bars correspond to one standard deviation of duplicate experiments.

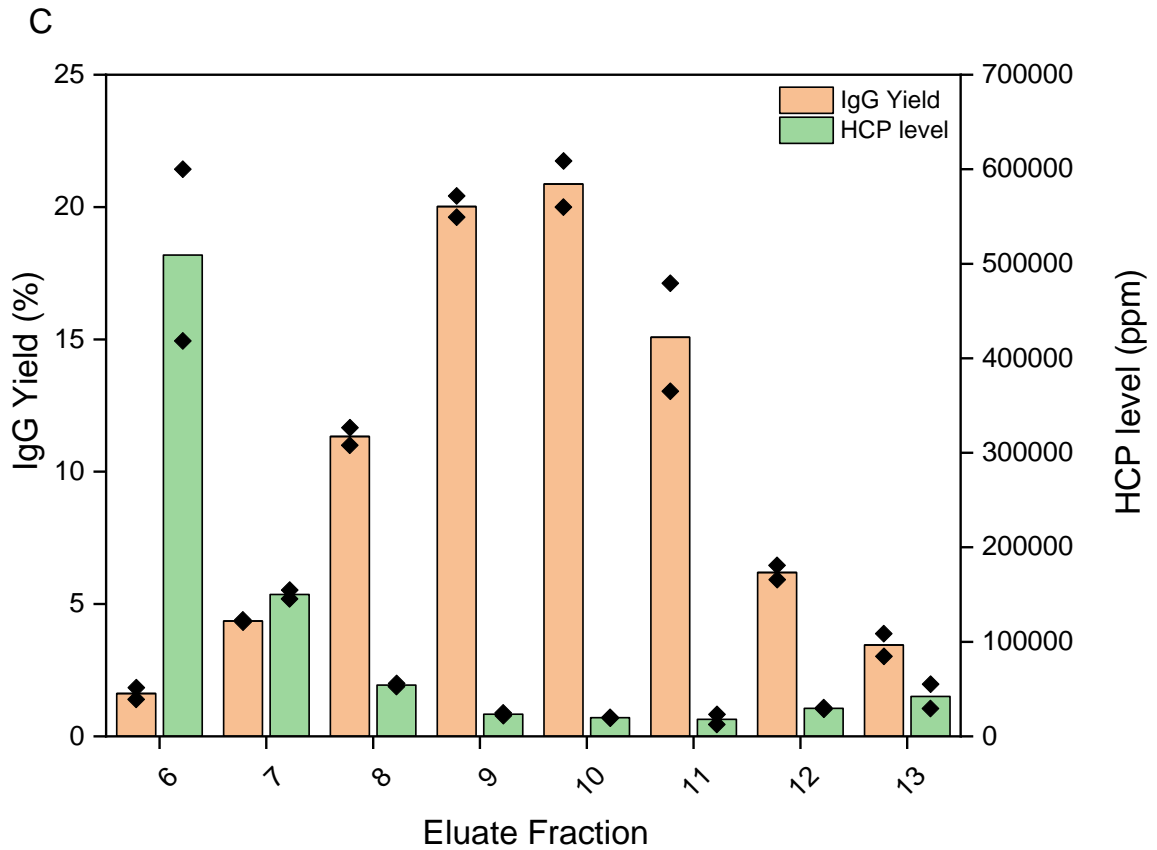


Figure 6-13 (continued). Antibody and HCP level compositions in Capto MMC eluate fractions corresponding to the main peak in the chromatograms presented in Figure 6-12. (A) pH 6.5, no added salt loading, (B) direct loading of post-precipitated sample (pH 7, < 15 mS/cm), (C) pH 5.8, 0.34 M ammonium sulphate loading. HCP levels in ng/mL determined by ELISA were converted to ppm. Error bars correspond to one standard deviation of duplicate experiments.

Table 6-3 compares the overall IgG₄ yields and HCP levels attained between the runs which consider the pooling of the eluate fractions consisting HCP levels below 100000 ppm. HCP levels were thus in the range 25278 – 33050 ppm, depending on the loading condition, which were initially predicted from the response surface model based of microscale experiments. Moreover, antibody purification from post-precipitated samples using Capto MMC chromatography in bind-and-elute showed improved HCP removal in comparison to Capto Q in flow-through mode, but reduced removal in DNA. It is suffice to say that the final IgG₄ purity from either step remains inadequate to compete with IgG₄ capture using PrA chromatography. However, further optimisation on Capto MMC could be performed via investigating additional process factors and wider ranges. Alternatively, both chromatography steps may be implemented in sequence to tackle the impurity burden and hence was proposed in the final stage of the study.

Table 6-3. Purification results of selected leading conditions for Capto MMC on a 1 mL HiTrap column. Yield, HCP and DNA levels were determined through pooling data of the individual eluate fractions 8 through 13.

Loading Condition	HCP level (E8-13 pool)	Total Yield (E8-13 pool)	DNA level (ppm, E8-E13 pool)
<i>pH 6.5, no added salt</i>	30600 ± 740	81.5 ± 2.1 %	33.2 ± 0.71
<i>Post-precipitated sample direct loading (pH 7, ~15 mS/cm)</i>	25000 ± 440	75.4 ± 0.2 %	38.3 ± 3.9
<i>pH 5.8, 0.34 M ammonium sulphate</i>	33100 +2000	77 ± 1.6 %	39.1 ± 0.92

6.4 Integration of precipitation and two-step chromatography process

Both Capto Q and Capto MMC processes have individually demonstrated reasonable removal of impurities; however final antibody purities were not yet adequate. Therefore, a final evaluation involving the combination of both steps in sequence for the purification was performed. The purification sequence was defined as follows: ammonium sulphate

precipitation – Capto Q (in FT mode) – Capto MMC (in bind-and-elute mode). These data were then compared to that of standard non-optimised PrA chromatography runs.

6.4.1 Purification with Capto Q on an XK 16 column

Bulk purifications with Capto Q were performed in a 10 mL column to generate sufficient material for Capto MMC evaluation. Post-precipitated samples were first buffer exchanged into 20 mM sodium phosphate, 75 mM NaCl pH 7.5 solution (as per the optimal condition identified in section 6.2.2.3). Sample loading was performed using the equivalent conditions specified for the 1 mL HiTrap experiments (load challenge: 10 mg IgG₄ per mL resin, 2 minutes residence time, 78 cm/h linear velocity). Two chromatography cycles were performed. The results from these runs gave an average yield of 90 ± 6.3%, 64210 ± 3532 ppm HCP and 35 ± 3.5 ppm DNA, which was consistent with the 1mL HiTrap experiments.

6.4.2 Capto MMC Loading Range selection

The loading range for Capto MMC evaluation for the purification of Capto Q–FT samples was chosen based on the previous range finding study. Only ammonium sulphate and not sodium chloride was taken forward, considering the prior established binding behaviour of IgG₄. As the feed type was different in terms of the presence of impurities, it was necessary to examine loading effects on HCP removal and consequently IgG₄ purity. Primary evaluation was performed as previously in 50 µL Predictor plates with all loading and elution conditions kept identical. Samples were equivalently dialysed into the respective mobile phases using a buffer exchange step. No indication of precipitation or aggregation was observed upon dialysis.

6.4.3 Predictor plate purification results

For this study, only IgG₄ yields and HCP levels in the eluate samples were considered in building the DoE model to define desirable loading conditions based on statistical analysis. The contour maps in Figure 6-14 resemble comparable response surfaces to those in Figure 6-11 representing purification on post-precipitated samples. Very similar desirable loading conditions based on the specific yield and HCP level criteria (\geq 65% yield and minimum HCP

level, both weighted with equal importance) were also identified. The model demonstrates that the highest desirability corresponding to both optimal yield (> 80%) and HCP removal is when $\text{pH} > 5.8$ and when the salt concentration is very low. At $\text{pH} 5.2$, 0.34 M ammonium sulphate, yield is increased but higher levels of HCP are present. This region does however provide a robust operating region. Both conditions were taken forward for verification with lab-scale chromatography.

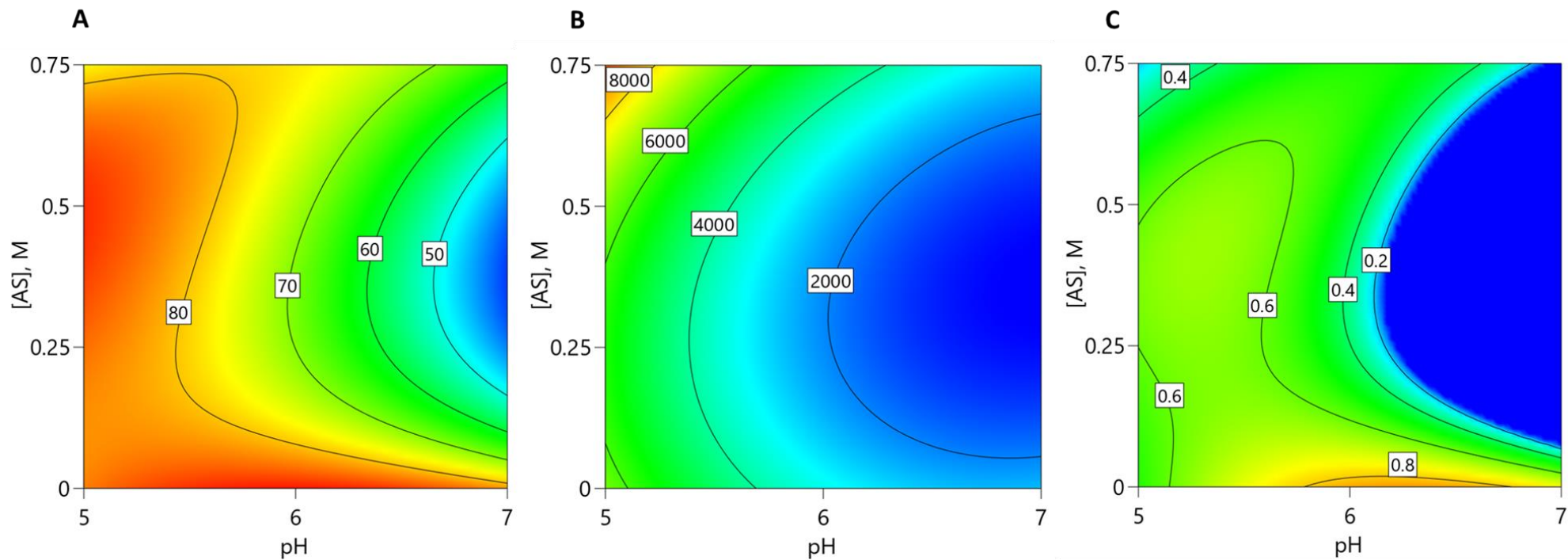


Figure 6-14. Contour maps showing from Capto MMC Predictor screening on post- Capto Q samples using ammonium sulphate (AS). Axes correspond to the sample loading conditions. (A) Antibody yields (Adjusted R^2 : 0.917, Predicted R^2 : 0.876) and (B) HCP levels from eluate fraction pools (Adjusted R^2 : 0.917, Predicted R^2 : 0.876). (C) Desirability plot highlighting optimal operating windows in maximising yield with a minimum threshold of 65 % and minimising HCP levels. Responses were weighted with equal importance.

6.4.4 Verification of IgG₄ purification using selected lead conditions with lab scale chromatography

Verification of the microscale purification results were performed by taking forward the selected loading conditions: pH 6.2 no added salt and pH 5.2, 0.4 M ammonium sulphate. All loading and elution conditions were performed as before. The UV chromatograms for each of the runs, which represent one of duplicate experiments, are presented in Figure 6-15.

Less intense flow-through peaks are observed as a result of fewer impurities in the sample of which were removed in the Capto Q step. Consistent with the previous experiments, a pre-peak is displayed during the very start of the gradient and is shortly followed by the main peak reaching a maximum absorbance at approximately 0.4 M NaCl. As expected, no antibody was detected in the pre-peak. Consistent with the previous Capto MMC experiments, increasing HCP levels were detected at low ionic strength which gradually decreased along the gradient (data not shown). Treatment of the appropriate fractions gave an average yield of $80 \pm 1.5\%$ and HCP levels of 3787 ± 332 ppm for the pH 6.2 with no added salt condition, whilst for the pH 5.2 and 0.34 M ammonium sulphate condition, an average yield of $87.6 \pm 2.1\%$ and HCP level of 6621 ± 505 ppm was attained. These results were within the prediction of the DoE model. Residual DNA analysis of the samples gave 8.6 ± 2.3 and 42.3 ± 7.3 ppm for the pH 6.2 and pH 5.2, 0.34 M ammonium sulphate loading conditions, respectively.

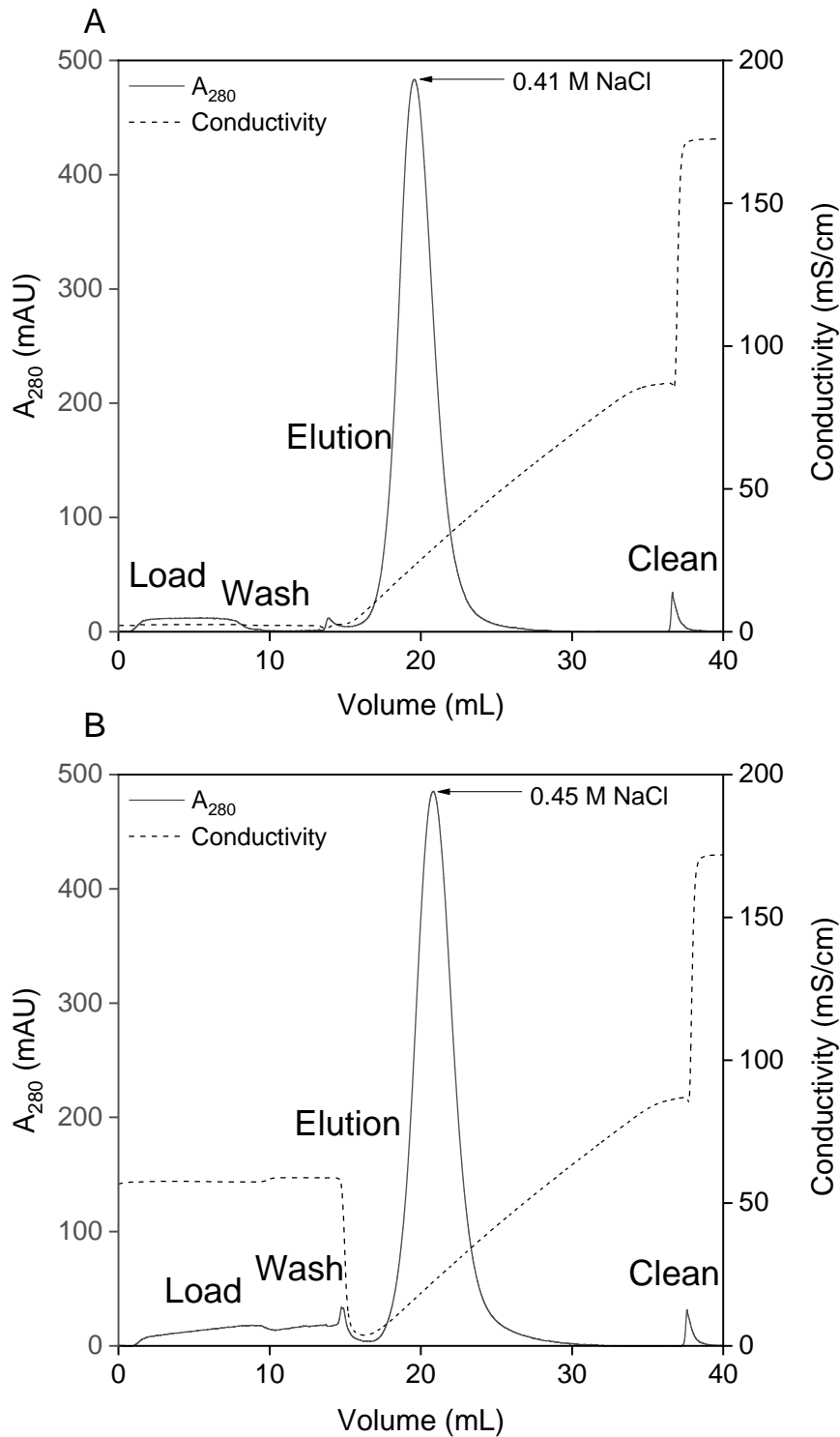


Figure 6-15. UV chromatograms representing Cpto MMC purification of Cpto Q FT samples. (A) pH 6.2 with no added salt loading, (B) pH 5.2, 0.34 M ammonium sulphate loading. Samples were loaded at 78 cm/h, corresponding to a residence time of two minutes. Elution strength is represented by the conductivity profiles corresponding to the linear salt concentration change from 0 to 1 M sodium chloride. Corresponding elution salt concentrations at max peak absorbance of the main peak are displayed. Column cleaning and maintenance was performed with 1 M NaOH for a minimum of 3 CVs.

6.5 Comparison of integrated processes with PrA chromatography

Table 6-4 displays the final purification results of the precipitation and integrated chromatography steps. Purification levels from a PrA chromatography step are also displayed for comparison. The purification data for each of the integrated processes correspond to the optimal conditions identified in the study. It can be seen that the three step process (precipitation + Capto Q + Capto MMC) provides a level of IgG₄ purification which almost approaches to that of PrA; however suffers from a significant loss of yield due to gradual losses between each purification step. Therefore, the data suggests superior purification performance using PrA chromatography.

Table 6-4. Comparison of integrated precipitation and chromatography purification processes for IgG₄ from CCCF with each other and with standard and UCB platform PrA capture chromatography processes. Values are expressed to 3 significant figures.

Purification step/Process	IgG₄ Yield (%)	HCP level (ppm)	DNA level (ppm)
<i>Cell Culture Harvest</i>	-	1180000	1900
<i>PrA (standard process)</i>	>90	500 - 10000	-
<i>PrA (UCB Platform Process)</i>	90 ± 2.5	1700 ± 520	1.1 ± 0.3
<i>Precipitation + Capto Q</i>	84.1 ± 2.3	54500 ± 3700	48 ± 32
<i>Precipitation + Capto MMC</i>	77.6 ± 1.2	25300 ± 330	33.2 ± 0.71
<i>Precipitation + Capto Q + Capto MMC</i>	67.3 ± 3.5	3800 ± 428	8.6 ± 2.3

An economic evaluation comparing our three-step process with PrA would add value in making informed decisions for bioprocess development. Also, where chromatography is unable to pick up the slack, the salt precipitation step could offer a stability advantage particularly for rather labile products. A more detailed analysis of product quality in sample analogous to those typically conducted at the end of a process could have been performed including SDS-PAGE, SEC-HPLC, charge variant analysis, 2D-DiGE, activity/potency assay, and CD spectroscopy. Such techniques add value in the identification of a stable, pure and active antibody product.

Although being beyond the scope of the work, resin re-use studies would demonstrate the value of conducting precipitation on crude harvest. The number of cycles that a chromatography step can run for is often limited by the presence of lipids in a sample. Assuming complete removal of the lipid phase upon precipitation, the extent of column fouling over time is minimised and in turn improves chromatography performance overall.

Chapter 7: Conclusions and Future Work

7.1 Conclusions

The main focus of the thesis was to demonstrate the potential of a downstream process for mAb purification based on precipitation, giving emphasis on the establishment of a scalable precipitation process using continuous manufacturing. It was of particular interest to demonstrate the engineering approach in producing viable protein precipitates which can be recovered at scale.

Benchmark studies sought to reproduce mAb precipitation behaviour with neutral salts over a range of process conditions. Initial experiments on a purified mAb enabled to identify the key process parameters that influence precipitation and these were then taken forward to link with precipitation from mammalian cell culture harvest. Depending on the salt employed, differences in the settling behaviour of protein precipitates with centrifugation were observed between purified and crude mAb systems making recovery from the latter difficult. This led to the identification of ammonium sulphate, which did not exhibit such effect, as the most suitable precipitating agent which would allow the later centrifugation studies outlined to be performed.

On the basis of micro-mixing theory and assumptions on the mean energy dissipation, micro-mixing times in batch and continuous tubular reactors were evaluated. The work then sought to determine the relevance of the mixing mechanism to protein precipitation behaviour with respect to creating protein precipitates with desirable properties. Based on the micro-mixing evaluation, the continuous tubular reactors demonstrated superior mixing times over the conventional batch reactor configuration. In addition, using the continuous precipitation approach enables a significantly higher throughput and allows more flexibility in varying demand of process volumes since process volume in a batch reactor is limited by its size. In some cases, potential fouling caused by precipitation in continuous tubular reactors can lead to cleaning challenges and, in the worst case, even lead to complete process shutdown. Therefore, batch precipitation approaches would be more appropriate to prevent and control this. Fouling due to precipitation was however not observed in the continuous precipitation experiments and these were operated without interruption.

Final particle properties were demonstrated to be a function of the micro-mixing efficiency as well as being dependent on the reactor design employed. Through the control of supersaturation and hydrodynamic-controlled shear during mixing, particles of a certain size

and distribution as well as strength could be obtained. When mixing time is important such that complete mixing should be obtained prior to the start of precipitate nucleation, the continuous reactors were capable of delivering rapid micro-mixing times. Faster mixing times as those reported in the literature for similar systems could not be achieved due to pump limitations. However, the data suggests that faster micro-mixing times may not provide any added benefit to the precipitation process. The scale-up of the continuous precipitation process based on the mean energy dissipation proved to be suitable in showing comparability between the precipitates with respect to the quality attributes. The nature of precipitates was characterised not only in terms of the relative PSD, but also with regards to the fractal dimension. Using microscopy as an orthogonal technique, precipitate particles with higher fractal dimensions as result of increased micromixing were shown to be smaller but more compact which led to the hypothesis that these particles were inherently stronger. This hypothesis was then verified by employing a USD approach to determine particle susceptibilities to turbulent break up, of which is critical for the success of large-scale centrifugal recovery.

The USD approach proved to be a useful methodology in examining the strength of precipitate particles which corroborated with fractal dimension analyses. Those particles with higher fractal dimensions were shown to be less susceptible to the turbulent shear stress in the rotating disc device. This allowed a correlation between f_D and particle break-up to be established. The USD data also showed that protein precipitates prepared in a continuous tubular reactor were much better clarified than those prepared in batch mode. This indicated that precipitates prepared during continuous precipitates possess higher hindered settling rates. To verify the USD methodology in predicting industrial precipitate recovery, a disc-stack centrifuge run was performed. Based on a single pilot-scale run, the USD method presented an over prediction of pilot-scale clarification. It is suggested that hindered settling occurring in the laboratory centrifuge led to the over prediction of clarification in the disc stack centrifuge where hindered settling is less likely to occur. A more accurate comparison requires dilution of precipitate samples for the USD method to minimise the potential reformation of precipitate flocs that account for hindered settling. Therefore, the scale-up challenge of a recovery process remains.

While ammonium sulphate was capable of reversibly precipitating the mAb of interest with solubilised yields above 90% and enabled a massive reduction of process volume, a considerable amount of HCPs, DNA and other process-related impurities was also detected in the precipitate. The extent of purification achieved with ammonium sulphate precipitation under the tested conditions was inferior in comparison to conventional capture methods used in mAb downstream processing, such as Protein A. Therefore, additional purification

methods were required. To this end, a bioprocess integration strategy was implemented in order to alleviate the impurity burden by processing precipitates through non-affinity based chromatography steps: anion exchange (Capto Q) and mixed-mode (Capto MMC) chromatography. These were challenged with the task in providing mAb purification to clinical grade levels. As a two-step or three-step integrated process, the typical specifications of a clinical mAb from a standard three-step processes were not met. Further optimisation in one or more steps or investigation into other suitable technologies would be required.

7.2 Scope for future work

This section explores aspects for future development of the precipitation-based downstream process. This is addressed in terms of short-term, mid-term and long-term plans. Short-term activities would take a few months to address, mid-term up to a year and long-term activities would span a few years of investigation.

7.2.1 Short-term

7.2.1.1 Testing process robustness in regard to alternative antibody therapeutics and variations in cell broth quality

All experiments in the EngD used a specific IgG₄ molecule. The established precipitation and subsequent downstream processing methods could be applied for different antibody classes including other IgG isoforms, Fabs, multimeric antibodies and antibody-drug conjugates. This will show whether the trends found in the EngD translate to other protein systems. However, since protein size, pI and surface characteristics (e.g. charge distribution and number of hydrophobic patches) likely play an important role for protein precipitation, a different performance might be observed between the different protein systems. Furthermore, changes in the upstream process often lead to variations in pH, conductivity, product titre and contaminant/impurity profile which also influence precipitation performance. In particular, it is critical to establish a precipitation process which can cope with variations in impurities and contaminants when considering a robust process that delivers the same product quality.

The effect of variations of cell broth quality on PEG-induced mAb precipitation has been previously reported (Großhans, Suhm and Hubbuch, 2019). The study indicated that different protein-contaminant interactions with low and high molecular weight impurities were the reason for differences in yield and purity. If, for example, a change in the cell broth resulted in the increase of high molecular weight impurities, an ammonium sulphate-induced mAb precipitation would struggle to remove these. This is due to the higher propensity of high molecular weight impurities to precipitate at similar concentrations of ammonium sulphate needed to precipitate mAbs. Therefore, it is critical to gain a deep understanding of the phase behaviour of complex protein solutions which can simplify precipitation process development. In addition, it highlights the importance of integrated up- and downstream process studies. This ought to be investigated in future work.

7.2.1.2 *Analytics of protein precipitate*

A range of analytical methods have been applied throughout the EngD to understand the influence of process parameters on precipitate formation, as well as estimate the level of purification achieved with salt-driven precipitation

In regards to determining purity, the HCP-ELISA method used to quantify HCP levels in the starting material and precipitated protein sample gave highly variable results. This was due to the relatively high levels of HCPs in these samples which required serial dilutions, which likely added an inaccuracy in the quantification of HCPs. As a result, the relative level of purification achieved was likely not very accurate. The method was probably more suited for later stage samples such as those obtained from the downstream chromatography experiments. An alternative method is proteomic mass spectrometry which enables the identification of a wider population of individual HCPs, without the requirement of antibody-specific reagents found in ELISA assay kits. It is important to note that mass spectrometry should be not be used as a replacement, but as an orthogonal technique to ELISA to increase the range of detectable HCPs. Particularly, mass spectrometry is more sensitive to low abundance HCPs, which may not be detected in ELISAs.

Light microscopy was used to inform the gross structures of protein precipitates obtained in the batch and continuous precipitation studies; however higher-resolution methods such as transmission electron microscopy (TEM) and scanning electron microscopy (SEM) could be used to examine the internal structure of the precipitate particles. As the protein precipitate contains some leftover ammonium sulphate, its presence is likely to interfere during the

analysis. Therefore, a sample preparation method needs to be developed to ensure precipitate detection whilst maintaining the precipitate structures driven by the precipitation reaction itself. Sample preparation would need to involve removing as much salt as possible to reduce sensitivity, whilst keeping the protein in a precipitated state to perform the analysis.

In contrast to ammonium sulphate precipitation, sodium citrate and sodium sulphate precipitations on cell culture fluid created the centrifugation challenge whereby the solid precipitate phase was less dense than the liquid phase. An in-depth analysis of the precipitates from the three salting-out methods would be informative in attributing the components responsible for this behaviour. The lower precipitate density was initially hypothesised to be due to the co-precipitation of lipids, which are known to be more buoyant than other cellular components, and suspected to bring proteins along with them. Such less dense precipitates would therefore be more suitable for recovery by filtration. If indeed lipids are present, this may present issues with column fouling in subsequent purification with chromatography.

7.2.2 Mid-term

7.2.2.1 *Designing effective continuous in-line mixers*

It has been demonstrated that in-line T-mixers are capable of rapid initial mixing which is important in the reproducible operation of fast reaction systems, such as in protein precipitation. Moreover, this method of mixing followed by a continuous tubular reactor provides significantly lower residence times over batch processing. Mixing experiments were conducted at the same flow rates which aided in the determination of mixing times based on the assumptions of the mean energy dissipation. Mixing times (or energy dissipation rates) were correlated to the performance of protein precipitation.

The iodide-iodate test in the characterisation of micro-mixing can also be applied to explore flow rate ratios other than 1:1. This would be relevant for a precipitation reaction in which the amount of precipitant to protein solution desired is small. This carries the advantage of minimising precipitant usage which in turn reduces precipitant waste disposal. The concept of unsymmetrical T-mixer designs could be considered useful in enhancing the mixing of two solutions. In principle, the viscous precipitant solution would be passed through the inlet with a smaller diameter such that the incoming velocity is higher relative to the protein solution which is passed through the larger diameter inlet.

Much of the foundation of this work has been previously laid out in various other reactor designs (Cozewith *et al.*, 1991). A potential starting point regarding mixing characterisation is modelling fluid dynamics using CFD. This provides a useful tool in building mixer designs and computing mixing times over a range of process conditions. Then, CFD predictions should be validated against experimental observations in order to guide an improved mixer design.

7.2.2.2 Evaluating CoGs for precipitation-based process

Taking the data presented in the work together with data obtained in future investigations in regards to developing a high performing precipitation-based purification process that meets target criteria, e.g. DSP yield and an acceptable level of residual HCPs, DNA and aggregates, can be used to establish a process cost model. BioSolve is a software tool that models the CoGs of standard protein production processes including mAbs and Fabs; however, it has the flexibility of modelling custom processes to the user's demands. This is particularly useful when a novel process is to be modelled. It comprises of an extensive data library of equipment, consumables, materials, labour and utilities which are used to calculate variable and fixed costs.

Upon generating a cost model for the precipitation-based process, the CoGs can be compared against generic mAb processes. The outcome of the cost model comparisons could drive an initiative into exploring precipitation-based unit operations for future bioprocess designs. Moreover, batch processes can be compared against continuous processes to determine the processing mode which is more economically viable. Provided that the continuous precipitation process designed in the work only requires simple tubing, T-mixers and pumps, the consumable and equipment costs are expected to be low. At larger scale, the costs would not be expected to increase significantly. Also, the use of disposables can be considered, making cleaning-in-place and sanitisation-in-place procedures redundant, further reducing the costs (Hammerschmidt *et al.*, 2014).

In many cases, real data for industrial antibody production processes are not often shared within the scientific community due to intellectual property, and therefore creates the challenge of building an accurate cost model. Consequently, many assumptions have to be made. It would also be required to include the cost of filters wherever relevant, although these can be assumed to be relatively low in comparison to the other unit operations. Nonetheless, a good cost model can justify the decisions to direct developmental efforts into

process changes for various production scenarios (e.g. pre-clinical, Phase 1, Phase 2, Phase 3, commercial).

7.2.2.3 *Stability studies on the storage of precipitate process intermediate*

Hold steps between unit operations are common given the flexibility of the manufacturing process but often introduce a challenge in achieving product quality which is dependent on the storage conditions of process intermediates. As an important element of process validation, it is recommended to evaluate the impact of hold steps and mid-manufacturing storage on protein alterations and stability at all stages of the process (European Medicines Agency, 2016). This is particularly relevant during unexpected process interruptions or if materials need to be shipped to another site. As recombinant antibodies are susceptible to modifications that compromise functionality and stability, it is important to define optimum storage conditions. The potential for improving antibody stability as a precipitated process intermediate during storage as compared to Protein A chromatography (or other methods) would be an interesting avenue to explore. In order to track product variations and alterations, a broad palette of analytical tools would be required. For example, SEC and MS would provide information on product degradation whilst CD is useful in tracking protein structural changes. Given the stabilising effect of ammonium sulphate on proteins, there is potential for increased storability. Moreover, precipitation posed the advantage of reducing the process volume by approximately 40-fold, which makes the storage of the precipitate more practically feasible and overall decreases storage costs.

7.2.3 Long term

7.2.3.1 *Alternative precipitants*

Ammonium sulphate is limited in its ability to selectively precipitate target proteins of interest based on the understood mechanism of salting-out, and thus precipitation carries over many of the process-related impurities (particularly high molecular weight impurities) Based on Protein G-HPLC data, purification of IgG₄ using ammonium sulphate precipitation provides ca. 58% overall purity which also includes a precipitate washing step. For this reason, additional purification steps are needed to improve purity. To improve purification performance with precipitation, other precipitants such as PEG, ethanol and polyelectrolytes could be investigated. PEG in particular is low cost and is available in various polymer

lengths which can be screened to select the polymer providing the highest selectivity towards the antibody of interest. Alternatively, synergistic approaches involving the combination of two or more precipitants, e.g. ammonium sulphate with PEG, could also be investigated. Exploiting the different mechanisms governed by such precipitants with the control of other process parameters potentially allows increased selectivity, which in turn enhances purification. Furthermore, there is likely scope for reducing the required amount of each precipitant which lowers the overall cost. These can be rapidly screened with high-throughput experimental procedures. The use of a precipitant or combination of precipitants must however take into account the scale-up implications, which may limit suitability in an industrial process. This would include cost, viscosity, safety and potential recyclability considerations.

7.2.3.2 Alternative large scale precipitate recovery methods

The recovery of protein precipitate at pilot scale was demonstrated with a disc-stack centrifuge using selected process conditions based on the USD methodology. The difference in the clarification between the scales was suggested to be a result of the differences in particle hindered settling. A follow-up would look to remove this phenomenon by diluting the suspensions prior to exposing to shear in the USD shear device and re-evaluating the clarification at the various centrifuge throughputs. Data gathered could then confirm the hypothesis.

As has been observed, disc-stack centrifugation achieved a poor dewatering level on the precipitate, and therefore reduced the separation efficiency. Alternative centrifugation technologies such as the tubular bowl or multi-chamber bowl can provide improved dewatering and a drier paste; however the challenge is their limitation in capacity to operate in a continuous manner. UF/DF rigs, depth filters and belt filters are also options to investigate. In these systems, the suspension is processed through a membrane where the precipitated material is retained on the membrane surface whilst the soluble material passes through. Thereafter, the solids are flushed and simultaneously recovered in re-solubilisation buffer. The choice of filter membrane requires a suitable pore size that retains the solids whilst reduces the extent of fouling and flow reduction to maximise productivity. It would be expected that precipitate processing by filtration exposes lower shear on the precipitate particles and thus reduces the extent of breakage impacting separation. A filtration step also has the potential in enabling precipitate separation, washing and solubilisation in a single system. In contrast, when using centrifugation, an additional hold tank would be required to contain the precipitate, to which buffer is added for precipitate resuspension.

7.2.3.3 Improving downstream steps and considering viral inactivation

In order to provide a three-step downstream process which can yield a mAb of clinical grade, improvements in the currently designed process must be made. This could be in the form of optimising the precipitation step using different precipitants and process conditions as aforementioned or investigating other suitable chromatography techniques. In terms of improving precipitation, one option which was not presented but considered in the early stages was a negative precipitation step involving pre-conditioning the starting material by reducing the pH (to between pH 3.5 and 5). Based on published reports, doing so would precipitate a mixture of HCP, DNA and media impurities, whilst maintaining soluble IgG and showing minimal product loss (Sommer *et al.*, 2015; Trapp *et al.*, 2018). Since low pH conditions are typically employed as a viral inactivation step post Protein-A, it would be advantageous to implement a low-pH driven precipitation purification regime to clean up the feed stream of many HCPs, DNA and viral proteins prior to the product precipitation step. A range of inorganic acids and polyelectrolytes would be relevant for such a step.

In preparation for further processing of protein precipitates with chromatography, samples underwent buffer exchange steps to remove residual ammonium sulphate as well as to exchange the samples into the respective buffers corresponding to the desired loading conditions. Indeed, buffer exchange steps, typically in the form of UF/DF, adds capital costs, increases process time and contributes to yield loss. One method to improve the downstream process involves avoiding the need for a buffer exchange step altogether. A future investigation would look to dissolve the precipitate in various buffer systems (as explored in Chapter 3) to provide re-suspended material which is compatible for loading onto different chromatography media without additional steps. Afterwards, resin screening studies can be performed to compare antibody purification performance between different media. PreDicator resin screening plates available from GE Healthcare, in combination with automation resources and high-throughput experimentation, facilitates a rapid and efficient comparison in order to identify an optimal resin. Thereafter, optimization studies involving the investigation of loading, wash and elution conditions would be performed.

Chapter 8: Process Validation

8.1 Regulatory considerations for bioprocess manufacturing

The sponsoring company UCB, by whom much of the work has been funded, currently develop and manufacture a wide range of small molecules and complex biological therapeutics for the treatment of immunological and neurodegenerative indications. As is the case for many biopharmaceutical companies, UCB constantly faces key regulatory issues associated with the commercial release of developed products. For instance, it is the responsibility of the business to ensure that its operations are compliant with the regulations and laws set out in order to control what is submitted to the health authorities and assure public health and safety. In particular, the Food and Drug Administration (FDA) and European Medicines Agency (EMA) have created the ICH guidelines as a means to harmonise the pharmaceutical standards required that should be adhered to in order to produce safe and efficacious product. Some of these guidelines outline the relevant studies that the company should perform and the relevant thresholds for product characterisation and impurity testing.

Within process development, a challenge is being able to fully understand the nature of a new molecule coming into development and the impact of upstream and downstream processing variables on product quality which would require robust and precise testing. Particularly in the development of biologics, the inherent complexity of these molecules requires that a huge toolbox of analytics is available for characterising the behaviour of the drug which should be built into the process. However, from a regulatory point of view, it is the responsibility for the company to establish the important analytical assays as product and process understanding increases as well as ensuring such methods are reproducible, robust and easily interpretable for GMP batch release testing. In some cases, where product understanding is high, the business may decide to implement process changes such that productivity is improved. However, the key challenge here is the ability to demonstrate comparability studies or bridging studies such that the final drug substance still meets the target specification with regards to efficacy and product safety. Moreover, the company has a clear responsibility to demonstrate to the regulators that the product with the defined attributes is consistently produced each time, batch to batch. Failure to do so will affect the ability to continue through development and incur huge costs, as well as damage the reputation of the business long-term.

Another challenge that UCB may face, as drug development proceeds, is the motivation to make changes to CMC (Chemical, Manufacturing and Controls) within the IND (investigational new drug) application with regards to, but not limited to, the manufacturing process and analytics. This requires that such changes are supported with sufficient data and justification. However, issues with CMC submissions carries the down effect of delaying manufacturing activity and thereby inducing a global shortage of approved drugs.

Having multiple manufacturing facilities worldwide, approval of new drug application (NDA) submissions for marketing authorization in multiple countries by UCB requires regulatory approval. This requires, particularly in meeting FDA expectations, extensive facility and process validation data as well as clinical trial data to be included in the submission. Change in the process scale can be challenging due to the differences of technology and equipment with scale-up, hence a full tech-transfer process must be completed before production batches to ensure that all critical process parameters can be monitored and all process specifications would be met within the desired ranges. Another key regulatory issue concerns the implementation of new technologies for current manufacturing processes or process changes due to not knowing how the regulator bodies will perceive these. With regards to process changes, small-scale studies are conducted to characterise these changes on the product profile and re-define the design space to work within the newly acceptable ranges. As new technologies and innovate methods of operation are emerging, companies begin to take an interest to consider these innovations in order to improve the drug development process, whilst maintaining market competitiveness.

8.2 Regulatory considerations for implementation of precipitation processes

Precipitation for purification applications of therapeutics is not a new concept as evident from the established plasma fractionation process. From blue-skies research, this has sufficiently progressed to industrial application. However, the reluctance to implement new or alternative technologies for the production of mAbs is not surprising considering the current chromatography-based methods are well understood and well validated for mAb platform processes which keep the regulatory authorities satisfied.

Investigation of precipitation as an individual unit operation raises the question of how efficient the product can be recovered from a crude mixture such as CHO cell culture supernatant as well as the impact on the product itself (e.g. protein stability, activity) and

other associated critical quality attributes (CQAs), whether process or product related. These would include but not limited to residual HCP and DNA levels, protein modifications affecting efficacy and potency, protein dimers, residual precipitation agent, residual particles, protein activity and stability. Moreover, the potential of its integration into existing mAb processes needs to be addressed in order to be considered for industrial application. Therefore, thorough process validation data is required to satisfy regulatory needs.

A new standard in bio-manufacturing practices is the use of the quality by design (QbD) approach which is based on validated process modelling to establish optimal operating parameters that result in consistent quality. Such an approach can be implemented in the development of precipitation processes. Figure 8-1 shows the QbD scheme for quality assurance. The approach begins with defining a quality target product profile (QTPP) based on structural information of the drug product, followed by the identification of CQAs. In the next stage, a risk assessment is conducted to establish links between resources, equipment and process parameters (i.e. critical process parameters, CPPs) on the CQAs, in the form of Ishikawa diagrams and failure-mode-effect-analysis (FMEA). From the parameters identified as high within the scope of FMEA, a design space is derived, supported by DoE, high-throughput experiments and, in some cases, model simulations. A control strategy to continuously monitor and control the process is finally implemented through process analytical technologies (PAT), enabling continual improvement of the manufacturing process. In regards to precipitation, the QbD approach can provide a comprehensive evaluation of known and hypothetical parameters, with specified ranges, influencing product yield and purity during the precipitation reaction and on the dissolution of the precipitate.

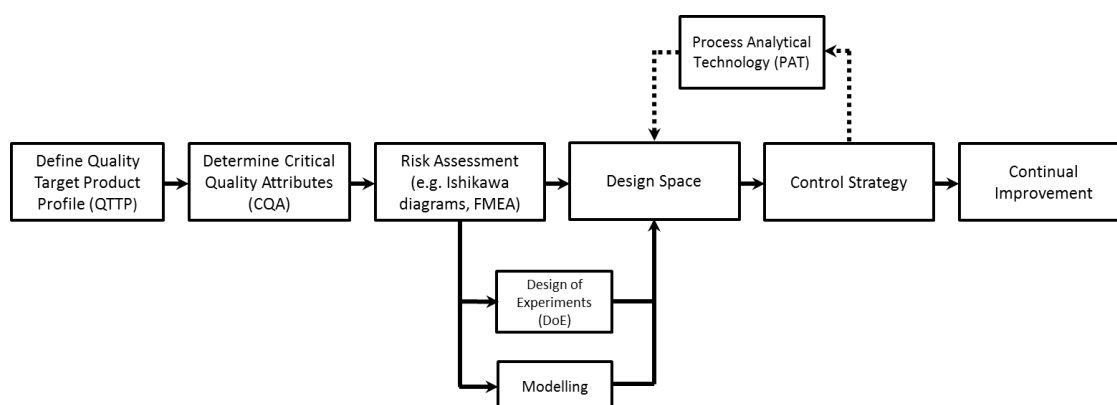


Figure 8-1. Quality by design (QbD) approach for quality assurance.

As the researcher, screening studies of the main factors affecting some of the CQAs mentioned above with precipitation techniques, either early on or late in the purification train, would be required followed by optimisation experiments to define acceptable ranges and interaction effects. Since the current knowledge of protein precipitation is relatively weak in the context of bioprocessing, thorough experimentation is performed in order to take into account all of the important factors. Nevertheless, high throughput experimentation in conjunction with powerful statistical methodologies can provide rapid characterisation and establish design spaces based on the CQAs and the acceptable ranges, whilst improving productivity and process robustness. Detection of these CQAs would be addressed by analytical experts with a range of analytical techniques which would require validation to ensure the reliability of the data output from the process. Performing several GMP batches with a precipitation-integrated process may convince the regulators given that it is demonstrated to work efficiently and can produce the same result each time. Moreover, comparability of the final specifications of a precipitation-integrated process compared to fully chromatography-based processes may provide further convincing evidence for the regulators.

Since it is widely accepted that precipitation occurs via a mechanism of aggregation, it is important that the researcher can demonstrate that the precipitation can be reversed with further purification and such aggregates are no longer present from an activity and safety perspective. Selecting an appropriate precipitation method which facilitates this is critical. The identification of appropriate redissolution solvents is also required, which consist of components capable of maintaining product stability in a soluble form. For some applications, precipitation becomes an irreversible process and the target protein cannot go back into solution, rendering the method useless.

Also concerning safety is the use of some of the precipitating agents commonly used in the type of research by which a process incorporating these would have to demonstrate their complete removal by the end of the process. Appropriate analytical techniques will need to be developed and validated to ensure that these can be detected even at low concentrations. Moreover, disposal of large precipitant amounts as would be expected at production scale would be problematic due to high disposal costs, but also has an impact on the environment. Therefore, this should be validated early-on in process development to ensure the company fulfils its social responsibilities and complies with current environmental laws.

From a manufacturing perspective, the implications towards the use of certain precipitating agents which pose validation concerns must be considered. For instance, the corrosive nature of ammonium sulphate on stainless steel equipment can have a long-term impact on equipment performance if the cleaning procedure is not validated. Also, it is widely known that performing ammonium sulphate precipitation above pH 8 releases toxic ammonia gas which compromises safety to operators and therefore a control strategy must be put in place to reduce the risk. Uses of ethanol and other organic solvents for precipitation applications bring about concerns of flammability hazards, particularly in large quantities. A facility must ensure the appropriate controls are in place to minimise the safety risk. These two examples highlight the necessity for good acquired knowledge of chemical properties when designing a precipitation step so that the operation is performed within an appropriate range that does not compromise process performance and safety. Another example is the use of PEG which although serves useful in precipitation applications, the increase in solution viscosity with PEG additions can cause problems during recovery in centrifugation and filtration.

Another example is ethanol precipitation which has been recently reported for mAb precipitation. The flammability issues concerning use of this reagent in large quantities one would envisage to be extremely cautious and hence the facility must ensure controls are in place to minimise the safety risk.

References

- Adair, J. H., Suvaci, E. and Sindel, J. (2001) 'Surface and Colloid Chemistry', in *Encyclopedia of Materials: Science and Technology*, pp. 1–10. doi: 10.1016/b0-08-043152-6/01622-3.
- Ahmad, S. S. and Dalby, P. A. (2011) 'Thermodynamic parameters for salt-induced reversible protein precipitation from automated microscale experiments', *Biotechnology and Bioengineering*, 108(2), pp. 322–332. doi: 10.1002/bit.22957.
- Albertsson, P. Åke and Frick, G. (1960) 'Partition of virus particles in a liquid two-phase system', *BBA - Biochimica et Biophysica Acta*, 15(37), pp. 230–237. doi: 10.1016/0006-3002(60)90228-6.
- Ameur, H., Kamla, Y. and Sahel, D. (2018) 'Performance of Helical Ribbon and Screw Impellers for Mixing Viscous Fluids in Cylindrical Reactors', *ChemEngineering*, 2(2), p. 26. doi: 10.3390/chemengineering2020026.
- Arakawa, T. and Timasheff, S. N. (1984) 'Mechanism of protein salting in and salting out by divalent cation salts: balance between hydration and salt binding', *Biochemistry*. American Chemical Society, 23(25), pp. 5912–5923. doi: 10.1021/bi00320a004.
- Arunakumari, A. and Ferreira, G. M. (2011) 'Protein purification by citrate precipitation. US Patent 8063189B2'.
- Asakura, S. and Oosawa, F. (1958) 'Interaction between particles suspended in solutions of macromolecules', *Journal of Polymer Science*, 33, pp. 183–192. doi: 10.1002/pol.1958.1203312618.
- Ayazi Shamlou, P. *et al.* (1994) 'Growth-independent breakage frequency of protein precipitates in turbulently agitated bioreactors', *Chemical Engineering Science*, 49(16), pp. 2647–2656. doi: 10.1016/0009-2509(94)E0077-4.
- Balasundaram, B., Sachdeva, S. and Bracewell, D. G. (2011) 'Dual salt precipitation for the recovery of a recombinant protein from *Escherichia coli*', *Biotechnology Progress*. Wiley Subscription Services, Inc., A Wiley Company, 27(5), pp. 1306–1314. doi: 10.1002/btpr.645.
- Baldwin, R. L. (1996) 'How Hofmeister ion interactions affect protein stability.', *Biophysical Journal*, 71(4), pp. 2056–2063.
- Bałdyga, J., Bourne, J. R. and Hearn, S. J. (1997) 'Interaction between chemical reactions and mixing on various scales', *Chemical Engineering Science*, 52(4), pp. 457–466. doi: 10.1016/S0009-2509(96)00430-7.
- Bałdyga, J. and Pohorecki, R. (1995) 'Turbulent micromixing in chemical reactors — a review', *The Chemical Engineering Journal and the Biochemical Engineering Journal*. Elsevier, 58(2), pp. 183–195. doi: 10.1016/0923-0467(95)02982-6.
- Bell, D. J. and Dunnill, P. (1982a) 'Shear disruption of soya protein precipitate particles and the effect of aging in a stirred tank.', *Biotechnology and bioengineering*. United States, 24(6), pp. 1271–1285. doi: 10.1002/bit.260240604.
- Bell, D. J. and Dunnill, P. (1982b) 'The influence of precipitation reactor configuration on the centrifugal recovery of isoelectric soya protein precipitate.', *Biotechnology and*

bioengineering, 24(11), pp. 2319–36. doi: 10.1002/bit.260241104.

Bell, D. J. and Dunnill, P. (1984) 'Mechanisms for the acoustic conditioning of protein precipitates to improve their separation by centrifugation', *Biotechnology and Bioengineering*, 26(7), pp. 691–698. doi: 10.1002/bit.260260710.

Bell, D. J., Hoare, M. and Dunnill, P. (1983) 'The Formation of Protein Precipitates and Their Centrifugal Recovery', in *Advances in biochemical engineering/biotechnology*. New York: Springer, pp. 1–72.

Berre, F. Le, Chauveteau, G. and Pefferkorn, E. (1998) 'Perikinetic and orthokinetic aggregation of hydrated colloids', *Journal of Colloid and Interface Science*, 199(1), pp. 1–12. doi: 10.1006/jcis.1997.5307.

Bhat, R. and Timasheff, S. N. (1992) 'Steric exclusion is the principal source of the preferential hydration of proteins in the presence of polyethylene glycols.', *Protein Science: A Publication of the Protein Society*. Cold Spring Harbor Laboratory Press, 1(9), pp. 1133–1143.

Bourne, J. R. and Dell'ava, P. (1987) 'Micro- and Macro-mixing in Stirred Tank Reactors of Different Sizes.', *Chemical Engineering Research and Design*, 65a, pp. 180–186.

Brown, D. L. and Glatz, C. E. (1987) 'Aggregate breakage in protein precipitation', *Chemical Engineering Science*, 42(7), pp. 1831–1839. doi: 10.1016/0009-2509(87)80188-4.

Burgess, R. R. (2009) 'Protein precipitation techniques.', *Methods in enzymology*, 463, pp. 331–42. doi: 10.1016/S0076-6879(09)63020-2.

Byrne, E. P. *et al.* (2002a) 'Influence of shear on particle size and fractal dimension of whey protein precipitates: implications for scale-up and centrifugal clarification efficiency', *Chemical Engineering Science*, 57(18), pp. 3767–3779. doi: 10.1016/S0009-2509(02)00315-9.

Byrne, E. P. *et al.* (2002b) 'Influence of shear on particle size and fractal dimension of whey protein precipitates: implications for scale-up and centrifugal clarification efficiency', *Chemical Engineering Science*. Pergamon, 57(18), pp. 3767–3779. doi: 10.1016/S0009-2509(02)00315-9.

Camp, T. R. (1955) 'Flocculation and Flocculation Basins', *Transactions of the American Society of Civil Engineers*. American Society of Civil Engineers, 20(1), pp. 1–16.

Carol, K. *et al.* (2009) 'High-throughput screening techniques for rapid PEG-based precipitation of IgG4 mAb from clarified cell culture supernatant', *Biotechnology Progress*. American Chemical Society (ACS), 26(3), pp. 697–705. doi: 10.1002/btpr.357.

Çelikbilek, M. (2012) 'Crystallization Kinetics of Amorphous Materials', in Ersundu, A. E. (ed.) *Advances in Crystallization Processes*. Rijeka: IntechOpen, p. Ch. 6. doi: 10.5772/35347.

Chan, M. Y., Hoare, M. and Dunnill, P. (1986) 'The kinetics of protein precipitation by different reagents.', *Biotechnology and bioengineering*, 28(3), pp. 387–93. doi: 10.1002/bit.260280312.

Chatel, A., Kumpalume, P. and Hoare, M. (2014) 'Ultra scale-down characterization of the impact of conditioning methods for harvested cell broths on clarification by continuous centrifugation-Recovery of domain antibodies from rec *E. coli*', *Biotechnology and Bioengineering*, 111(5), pp. 913–924. doi: 10.1002/bit.25164.

- Chayen, N. E. (2005) 'Methods for separating nucleation and growth in protein crystallisation', *Progress in Biophysics and Molecular Biology*, 88(3), pp. 329–337. doi: 10.1016/j.pbiomolbio.2004.07.007.
- Chen, Y. S. *et al.* (2006) 'Characteristics of micromixing in a rotating packed bed', *Journal of the Chinese Institute of Chemical Engineers*, 37(1), pp. 63–69.
- Chi, E. Y. *et al.* (2003) 'Physical stability of proteins in aqueous solution: Mechanism and driving forces in nonnative protein aggregation', *Pharmaceutical Research*, 20(9), pp. 1325–1336. doi: 10.1023/A:1025771421906.
- Clark, K. M. and Glatz, C. E. (1987) 'Polymer Dosage Considerations in Polyelectrolyte Precipitation of Protein', *Biotechnology Progress*, 3(4), pp. 241–247. doi: 10.1002/btpr.5420030408.
- Clark, K. M. and Glatz, C. E. (1992) 'A binding model for the precipitation of proteins by carboxymethyl cellulose', *Chemical Engineering Science*, 47(1), pp. 215–224. doi: 10.1016/0009-2509(92)80215-X.
- Cohn, E. J. (1925) 'The physical chemistry of proteins', *Physiol. Rev.*, 5(3), pp. 349–437.
- Cohn, E. J. *et al.* (1940) 'Preparation and Properties of Serum and Plasma Proteins. I. Size and Charge of Proteins Separating upon Equilibration across Membranes with Ammonium Sulfate Solutions of Controlled pH, Ionic Strength and Temperature', *Journal of the American Chemical Society*. American Chemical Society, 62(12), pp. 3386–3393. doi: 10.1021/ja01869a030.
- Cohn, E. J. *et al.* (1946) 'Preparation and Properties of Serum and Plasma Proteins. IV. A System for the Separation into Fractions of the Protein and Lipoprotein Components of Biological Tissues and Fluids 1a,b,c,d', *Journal of the American Chemical Society*. American Chemical Society, 68(3), pp. 459–475. doi: 10.1021/ja01207a034.
- Commonge, J.-M. and Falk, L. (2011) 'Villermaux–Dushman protocol for experimental characterization of micromixers', *Chemical Engineering and Processing: Process Intensification*, 50(10), pp. 979–990. doi: 10.1016/j.cep.2011.06.006.
- Cozewith, C. *et al.* (1991) 'Computer simulation of tee mixers for nonreactive and reactive flows', *Industrial & Engineering Chemistry Research*. American Chemical Society, 30(1), pp. 270–275. doi: 10.1021/ie00049a043.
- Crowe, K. M. (2014) 'Optimizing protein precipitation efficiency for assessing the contribution of low molecular weight compounds to serum antioxidant capacity.', *Clinical biochemistry*, 47(15), pp. 116–8. doi: 10.1016/j.clinbiochem.2014.06.021.
- Crowell, A. M. J., Wall, M. J. and Doucette, A. A. (2013) 'Maximizing recovery of water-soluble proteins through acetone precipitation.', *Analytica chimica acta*, 796, pp. 48–54. doi: 10.1016/j.aca.2013.08.005.
- Danzon, P. M. (2007) 'At what price?', *Nature*, 449(7159), pp. 176–179. doi: 10.1038/449176a.
- David Leonard Chapman (1913) 'A Contribution to the Theory of Electrocappilarity', *The London, Edinburgh and Dublin philosophical magazine and journal of science*, 25(148), pp. 475–481.
- Derjaguin, B. V. *et al.* (1987) 'The Derjaguin—Landau—Verwey—Overbeek (DLVO) Theory of Stability of Lyophobic Colloids', in *Surface Forces*, pp. 293–310. doi: 10.1007/978-1-4757-6639-4_8.

DiMasi, J. a., Hansen, R. W. and Grabowski, H. G. (2003) 'The price of innovation: New estimates of drug development costs', *Journal of Health Economics*, 22(2), pp. 151–185. doi: 10.1016/S0167-6296(02)00126-1.

Dunnill, P. *et al.* (1967) 'Large-scale isolation of prolyl-tRNA synthetase from *Phaseolus aureus*', *Biotechnology and Bioengineering*, 9, pp. 343–356. doi: 10.1002/bit.260090307.

Dunnill, P., Currie, J. A. and Lilly, M. D. (1970) 'Continuous enzyme processing: The isolation of prolyl-tRNA synthetase from *Phaseolus Aureus*', *Biotechnology and Bioengineering*, 12, pp. 63–74. doi: 10.1002/bit.260120106.

Edmond, E. and Ogston, A. G. (1970) 'Phase separation in an aqueous quaternary system.', *The Biochemical journal*, 117(1), pp. 85–89. doi: 10.1042/bj1170085.

Espuny Garcia del Real, G., Davies, J. and Bracewell, D. G. (2014) 'Scale-down characterization of post-centrifuge flocculation processes for high-throughput process development', *Biotechnology and Bioengineering*, 111(12), pp. 2486–2498. doi: 10.1002/bit.25313.

European Medicines Agency (2016) *Guideline on process validation for the manufacture of biotechnology-derived active substances and data to be provided in the regulatory submission, Committee for Medicinal Products for Human Use (CHMP) Guideline.*

Fahrner, R. L. *et al.* (2011) 'Polyelectrolyte precipitation and purification of antibodies. US Patent 7947813'.

Faizal Wong, F. W., Ariff, A. B. and Stuckey, D. C. (2017) 'A biocompatible surfactant, methyl ester sulphonate (MES), as a precipitating ligand for protein purification', *Biochemical Engineering Journal*, 117, pp. 30–40. doi: 10.1016/j.bej.2016.09.020.

Falk, L. and Commenge, J.-M. (2010) 'Performance comparison of micromixers', *Chemical Engineering Science*. Pergamon, 65(1), pp. 405–411. doi: 10.1016/J.CES.2009.05.045.

Farid, S. S. (2007) 'Process economics of industrial monoclonal antibody manufacture', *Journal of Chromatography B: Analytical Technologies in the Biomedical and Life Sciences*. doi: 10.1016/j.jchromb.2006.07.037.

Fischer, H., Polikarpov, I. and Craievich, A. F. (2009) 'Average protein density is a molecular-weight-dependent function', *Protein Science*, 13(10), pp. 2825–2828. doi: 10.1110/ps.04688204.

Forney, L. J. and Gray, G. E. (1990) 'Optimum design of a Tee mixer for fast reactions', *AIChE Journal*. American Institute of Chemical Engineers, 36(11), pp. 1773–1776. doi: 10.1002/aic.690361122.

Foster, P. R., Dunnill, P. and Lilly, M. D. (1973) 'The precipitation of enzymes from cell extracts of *Saccharomyces cerevisiae* by polyethyleneglycol', *BBA - Protein Structure*, 317(2), pp. 505–516. doi: 10.1016/0005-2795(73)90243-2.

Foster, P. R., Dunnill, P. and Lilly, M. D. (1976) 'The kinetics of protein salting-out: Precipitation of yeast enzymes by ammonium sulfate', *Biotechnology and Bioengineering*, 18(4), pp. 545–580. doi: 10.1002/bit.260181019.

Fournier, M. C., Falk, L. and Villermaux, J. (1996) 'A new parallel competing reaction system for assessing micromixing efficiency - Experimental approach', *Chemical Engineering Science*, 51(23), pp. 5187–5192. doi: 10.1016/0009-2509(96)00270-9.

Frank, H. S. and Evans, M. W. (1945) 'Free volume and entropy in condensed systems III.

Entropy in binary liquid mixtures', *Journal of Chemical Physics*, 13, pp. 507–532.

Fredericq, E. and Neurath, H. (1950) 'The Interaction of Insulin with Thiocyanate and other Anions. The Minimum Molecular Weight of Insulin¹', *Journal of the American Chemical Society*. American Chemical Society, 72(6), pp. 2684–2691. doi: 10.1021/ja01162a094.

Fuchs, N. . (1964) 'The Mechanics of Aerosols', in *Physics Today*. Pergamon Press, p. 73.

Gao, Z. *et al.* (2015) 'Chinese Journal of Chemical Engineering Micromixing efficiency in a T-shaped confined impinging jet reactor ☆', 23, pp. 350–355.

Ghanem, A. *et al.* (2014) 'Static mixers: Mechanisms, applications, and characterization methods – A review', *Chemical Engineering Research and Design*, 92(2), pp. 205–228. doi: 10.1016/j.cherd.2013.07.013.

Gholap, R. V., Sergio, P. and Bourne, J. R. (2018) 'Influence of viscosity on product distribution of fast competitive chemical reactions', *Chemical Engineering & Technology*. Wiley-Blackwell, 17(2), pp. 102–107. doi: 10.1002/ceat.270170206.

Giese, G. *et al.* (2013) 'Purification of antibodies by precipitating impurities using Polyethylene Glycol to enable a two chromatography step process.', *Journal of chromatography. B, Analytical technologies in the biomedical and life sciences*, 938, pp. 14–21. doi: 10.1016/j.jchromb.2013.08.029.

Glatz, C. E., Hoare, M. and Landa-Vertiz, J. (1986) 'The formation and growth of protein precipitates in a continuous stirred-tank reactor', *AIChE Journal*, 32(7), pp. 1196–1204. doi: 10.1002/aic.690320717.

Gobert, S. R. L. *et al.* (2017) 'Characterization of Milli- and Microflow Reactors: Mixing Efficiency and Residence Time Distribution', *Organic Process Research & Development*. American Chemical Society, 21(4), pp. 531–542. doi: 10.1021/acs.oprd.6b00359.

Gouy, M. (1910) 'Sur la constitution de la charge électrique à la surface d'un électrolyte', *Journal de Physique Théorique et Appliquée*, 9(1), pp. 457–468. doi: 10.1051/jphystap:019100090045700.

Greene, D. G. *et al.* (2018) 'Mechanisms of precipitate formation during the purification of an Fc-fusion protein', *Biotechnology and Bioengineering*, 115(10), pp. 2489–2503. doi: 10.1002/bit.26746.

Großhans, S., Suhm, S. and Hubbuch, J. (2019) 'Precipitation of complex antibody solutions: influence of contaminant composition and cell culture medium on the precipitation behavior', *Bioprocess and biosystems engineering*. 2019/03/18. Springer Berlin Heidelberg, 42(6), pp. 1039–1051. doi: 10.1007/s00449-019-02103-y.

Guichardon, P. and Falk, L. (2000) 'Characterisation of micromixing efficiency by the iodide-iodate reaction system. Part I: experimental procedure', *Chemical Engineering Science*, 55(19), pp. 4233–4243. doi: 10.1016/S0009-2509(00)00068-3.

Guichardon, P., Falk, L. and Andrieu, M. (2001) 'Experimental Comparison of the Iodide-iodate and the Diazo Coupling Micromixing Test Reactions in Stirred Reactors', *Chemical Engineering Research and Design*. Elsevier, 79(8), pp. 906–914. doi: 10.1205/02638760152721433.

Guichardon, P., Falk, L. and Villermaux, J. (1997) 'Extension of a chemical method for the study of micromixing process in viscous media', *Chemical Engineering Science*. Pergamon, 52(24), pp. 4649–4658. doi: 10.1016/S0009-2509(97)85419-X.

Guichardon, P., Falk, L. and Villermaux, J. (2000) 'Characterisation of micromixing efficiency by the iodide-iodate reaction system. Part II: kinetic study', *Chemical Engineering Science*. Pergamon, 55(19), pp. 4245–4253. doi: 10.1016/S0009-2509(00)00069-5.

Hammerschmidt, N. *et al.* (2014) 'Economics of recombinant antibody production processes at various scales: Industry-standard compared to continuous precipitation', *Biotechnology Journal*. WILEY-VCH Verlag, 9(6), pp. 766–775. doi: 10.1002/biot.201300480.

Hammerschmidt, N. *et al.* (2015) 'Continuous precipitation of IgG from CHO cell culture supernatant in a tubular reactor', *Biotechnology Journal*. WILEY-VCH Verlag, 10(8), pp. 1196–1205. doi: 10.1002/biot.201400608.

Hammerschmidt, N., Hobiger, S. and Jungbauer, A. (2016) 'Continuous polyethylene glycol precipitation of recombinant antibodies: Sequential precipitation and resolubilization', *Process Biochemistry*, 51(2), pp. 325–332. doi: <http://dx.doi.org/10.1016/j.procbio.2015.11.032>.

Handlogten, M. W. *et al.* (2013) 'Nonchromatographic Affinity Precipitation Method for the Purification of Bivalently Active Pharmaceutical Antibodies from Biological Fluids', *Analytical Chemistry*. American Chemical Society, 85(10), pp. 5271–5278. doi: 10.1021/ac4008286.

Harms, A. J. (1946) 'Abnormal precipitation of proteins from antitoxic horse plasma in the presence of phenolic compounds', *Nature*, 157(3990), p. 514. doi: 10.1038/157514a0.

Harrison, R. (1994) *Protein purification process engineering*.

Hekmat, D. (2015) 'Large-scale crystallization of proteins for purification and formulation', *Bioprocess and biosystems engineering*, 38(7), pp. 1209–1231. doi: 10.1007/s00449-015-1374-y.

Hekmat, D. *et al.* (2017) 'Continuous Crystallization of Proteins in a Stirred Classified Product Removal Tank with a Tubular Reactor in Bypass', *Crystal Growth & Design*. American Chemical Society, 17(8), pp. 4162–4169. doi: 10.1021/acs.cgd.7b00436.

Higgins, J. J. *et al.* (1978) 'Investigation of the unit operations involved in the continuous flow isolation of β -galactosidase from *Escherichia coli*', *Biotechnology and Bioengineering*, 20, pp. 159–182. doi: 10.1002/bit.260200202.

Higuchi, W. I. *et al.* (1963) 'Kinetics of rapid aggregation in suspensions. Comparison of experiments with the Smoluchowski theory', *Journal of Pharmaceutical Sciences*, 52(1), pp. 49–54. doi: 10.1002/jps.2600520110.

Hill, R. D. and Zadow, J. G. (1978) 'Recovery of whey proteins from precipitated complexes of carboxymethyl cellulose and protein', *Journal of Dairy Research*, 45(1), pp. 77–83. doi: 10.1017/S0022029900016228.

Hoare, M. (1982a) 'Protein precipitation and precipitate aging .1. Salting-out and aging of casein precipitates.', *T I Chem ENG-LOND*, 60(2), pp. 79–87.

Hoare, M. (1982b) 'Protein precipitation and precipitate aging .2. Growth of protein precipitates during hindered settling or exposure to shear.', *T I Chem ENG-LOND*, 60(3), pp. 157–163.

Hoare, M., Dunnill, P. and Bell, D. J. (1983) 'Reactor Design for Protein Precipitation and Its Effect on Centrifugal Separation', *Annals of the New York Academy of Sciences*, 413, pp. 254–269. doi: 10.1111/j.1749-6632.1983.tb47898.x.

Hönig, W. and Kula, M.-R. (1976) 'Selectivity of protein precipitation with polyethylene glycol

- fractions of various molecular weights', *Analytical Biochemistry*, 72(1–2), pp. 502–512. doi: 10.1016/0003-2697(76)90560-1.
- Hutchinson, N. *et al.* (2006) 'Shear stress analysis of mammalian cell suspensions for prediction of industrial centrifugation and its verification', *Biotechnology and Bioengineering*, 95(3), pp. 483–491. doi: 10.1002/bit.21029.
- Iverius, P. H. and Laurent, T. C. (1967) 'Precipitation of some plasma proteins by the addition of dextran or polyethylene glycol', *BBA - Protein Structure*, 133(2), pp. 371–373. doi: 10.1016/0005-2795(67)90079-7.
- Ives, K. J. (1978) *The scientific basis of flocculation*. doi: 10.1016/0043-1354(79)90079-4.
- Iyer, H. and Przybycien, T. (1994) 'Protein precipitation: Effects of mixing on protein solubility', *American Institute of Chemical Engineers Journal*, 40(2), pp. 349–360.
- Janoschek, L., Freiherr von Roman, M. and Berensmeier, S. (2014) 'Protein A affinity precipitation of human immunoglobulin G.', *Journal of chromatography. B, Analytical technologies in the biomedical and life sciences*, 965, pp. 72–8. doi: 10.1016/j.jchromb.2014.06.011.
- Jewett, W. R. (1974) 'Method and apparatus for treating multi-phase systems. US Patent 3826740'.
- Juckles, I. R. M. (1971) 'Fractionation of proteins and viruses with polyethylene glycol', *BBA - Protein Structure*, 229(3), pp. 535–546. doi: 10.1016/0005-2795(71)90269-8.
- Jungbauer, A. (2013) 'Continuous downstream processing of biopharmaceuticals.', *Trends in biotechnology*, 31(8), pp. 479–92. doi: 10.1016/j.tibtech.2013.05.011.
- Kang, Y. K. *et al.* (2013) 'Development of a novel and efficient cell culture flocculation process using a stimulus responsive polymer to streamline antibody purification processes', *Biotechnology and Bioengineering*, 110(11), pp. 2928–2937. doi: 10.1002/bit.24969.
- Kateja, N. *et al.* (2016) 'Continuous precipitation of process related impurities from clarified cell culture supernatant using a novel coiled flow inversion reactor (CFIR).', *Biotechnology journal*, 11(10), pp. 1320–1331. doi: 10.1002/biot.201600271.
- Kaufman, J. and Kalaitzandonakes, N. (2011) 'The economic potential of plant-made pharmaceuticals in the manufacture of biologic pharmaceuticals', *Journal of Commercial Biotechnology*. Nature Publishing Group, 17(2), pp. 173–182. doi: 10.1057/jcb.2010.37.
- Kauzmann, W. (1959) 'Some Factors in the Interpretation of Protein Denaturation', *Advances in Protein Chemistry*, 14, pp. 1–63. doi: 10.1016/S0065-3233(08)60608-7.
- Kim, J. Y., Kim, Y.-G. and Lee, G. M. (2012) 'CHO cells in biotechnology for production of recombinant proteins: current state and further potential', *Applied Microbiology and Biotechnology*, 93(3), pp. 917–930. doi: 10.1007/s00253-011-3758-5.
- Klein, D. H. (1965) 'Kinetics of precipitation (Nielsen, Arne E.)', *Journal of Chemical Education*. American Chemical Society, 42(5), p. A428. doi: 10.1021/ed042pA428.1.
- Kling, K. and Mewes, D. (2004) 'Two-colour laser induced fluorescence for the quantification of micro- and macromixing in stirred vessels', *Chemical Engineering Science*. Pergamon, 59(7), pp. 1523–1528. doi: 10.1016/J.CES.2004.01.015.
- Koehler, K. C. *et al.* (2019) 'Enhancing Protein A performance in mAb processing: A method to reduce and rapidly evaluate host cell DNA levels during primary clarification',

Biotechnology Progress, 35(6), p. 2019. doi: 10.1002/btpr.2882.

Kolbl, A. and M, K. (2003) 'On the Use of the Iodide Iodate Reaction Method for Assessing Mixing Times in Continuous Flow Mixers', *VTT Publications*, 57(504), pp. 3–194. doi: 10.1002/aic.

Krepper, W. *et al.* (2019) 'Mid-manufacturing storage: Antibody stability after chromatography and precipitation based capture steps', *Biotechnology Progress*. American Chemical Society (ACS), 36(2), p. e2928. doi: 10.1002/btpr.2928.

Kuczewski, M. *et al.* (2010) 'PEG Precipitation: A Powerful Tool for Monoclonal Antibody Purification', *Biopharm International Supplement*, 23, pp. 46–47.

Kurinomaru, T. *et al.* (2014) 'Protein–Poly(amino acid) Complex Precipitation for High-Concentration Protein Formulation', *Journal of Pharmaceutical Sciences*. Elsevier, 103(8), pp. 2248–2254. doi: 10.1002/JPS.24025.

Leavis, P. C. and Rothstein, F. (1974) 'The Solubility of Fibrinogen in Dilute Salt Solutions', *Archives of Biochemistry and Biophysics**Archives of Biochemistry and Biophysics*, 161, pp. 671–682.

Lehwald, A., Thévenin, D. and Zähringer, K. (2010) 'Quantifying macro-mixing and micro-mixing in a static mixer using two-tracer laser-induced fluorescence', *Experiments in Fluids*, 48, pp. 823–836. doi: 10.1007/s00348-009-0769-4.

Li, Z. *et al.* (2019) 'Continuous precipitation for monoclonal antibody capture using countercurrent washing by microfiltration', *Biotechnology Progress*, 35(6), p. e2886. doi: 10.1002/btpr.2886.

Liu, W. *et al.* (2019) 'Salt-enhanced permeabilization for monoclonal antibody precipitation and purification in a tubular reactor with a depth filtration membrane with advanced chromatin extraction', *Biochemical Engineering Journal*, 151, p. 107332. doi: <https://doi.org/10.1016/j.bej.2019.107332>.

Liu, W. J., Ma, C. Y. and Wang, X. Z. (2015) 'Novel impinging jet and continuous crystallizer design for rapid reactive crystallization of pharmaceuticals', *Procedia Engineering*. Elsevier B.V., 102, pp. 499–507. doi: 10.1016/j.proeng.2015.01.199.

Livingstone, J. R., Spolar, R. S. and Thomas Record, M. (1991) 'Contribution to the Thermodynamics of Protein Folding from the Reduction in Water-Accessible Nonpolar Surface Area', *Biochemistry*, 30(17), pp. 4237–4244. doi: 10.1021/bi00231a019.

Low, D., O'Leary, R. and Pujar, N. S. (2007) 'Future of antibody purification.', *Journal of chromatography. B, Analytical technologies in the biomedical and life sciences*, 848(1), pp. 48–63. doi: 10.1016/j.jchromb.2006.10.033.

Ma, J. *et al.* (2010) 'Using precipitation by polyamines as an alternative to chromatographic separation in antibody purification processes', *Journal of Chromatography B: Analytical Technologies in the Biomedical and Life Sciences*, 878, pp. 798–806. doi: 10.1016/j.jchromb.2010.01.044.

Madhusudhan, M. C., Raghavarao, K. S. M. S. and Nene, S. (2008) 'Integrated process for extraction and purification of alcohol dehydrogenase from Baker's yeast involving precipitation and aqueous two phase extraction', *Biochemical Engineering Journal*. Elsevier, 38(3), pp. 414–420. doi: 10.1016/J.BEJ.2007.08.007.

Mahajan, A. J. and Kirwan, D. J. (1996) 'Micromixing effects in a two-impinging-jets precipitator', *AIChE Journal*. Wiley-Blackwell, 42(7), pp. 1801–1814. doi:

10.1002/aic.690420702.

Martinez, M. *et al.* (2019) 'Precipitation as an Enabling Technology for the Intensification of Biopharmaceutical Manufacture', *Trends in Biotechnology*, 37(3), pp. 237–241. doi: 10.1016/j.tibtech.2018.09.001.

McDonald, P. *et al.* (2009) 'Selective antibody precipitation using polyelectrolytes: A novel approach to the purification of monoclonal antibodies', *Biotechnology and Bioengineering*, 102(4), pp. 1141–1151. doi: 10.1002/bit.22127.

McGown, E. L. and Hafeman, D. G. (1998) 'Multichannel pipettor performance verified by measuring pathlength of reagent dispensed into a microplate', *Analytical Biochemistry*, 258(1), pp. 155–157. doi: 10.1006/abio.1998.2621.

McKinney, M. M. and Parkinson, A. (1987) 'A simple, non-chromatographic procedure to purify immunoglobulins from serum and ascites fluid', *Journal of Immunological Methods*, 96(2), pp. 271–280. doi: 10.1016/0022-1759(87)90324-3.

Meakin, M. Y. L. and H. M. L. and D. A. W. and R. K. and R. C. B. and P. (1990) 'Universal diffusion-limited colloid aggregation', *Journal of Physics: Condensed Matter*, 2(13), p. 3093.

Melander, W. and Horváth, C. (1977) 'Salt effects on hydrophobic interactions in precipitation and chromatography of proteins: An interpretation of the lyotropic series', *Archives of Biochemistry and Biophysics*, 183(1), pp. 200–215. doi: 10.1016/0003-9861(77)90434-9.

Mellanby, B. Y. J. (1904) *GLOBULIN*.

Mellanby, J. (1907) 'The precipitation of the proteins of horse serum', *J.Physiol*, 36(288).

Merrill, M. H. and Fleisher, M. S. (1932) 'Factors involved in the use of organic solvents as precipitating and drying agents of immune sera', *Journal of General Physiology*, 16(2), pp. 243–256. doi: 10.1085/jgp.16.2.243.

Middaugh, C. R. *et al.* (1980) 'Thermodynamic basis for the abnormal solubility of monoclonal cryoimmunoglobulins', *Journal of Biological Chemistry*, 255(14), pp. 6532–6534.

Miyake, T., Kung, C. K. H. and Goldwasser, E. (1977) 'Purification of human erythropoietin', *Journal of Biological Chemistry*, 252(15), pp. 5558–5564.

Momonaga, M., Yazawa, H. and Kagara, K. (1992) 'Reactive crystallization of methyl ac-methoxyimino acetoacetate', *Journal of Chemical Engineering of Japan*, 25, pp. 237–242. doi: 10.1252/jcej.25.237.

Morris, C. W. (2019) 'Protein Precipitation for the Purification of Therapeutic Proteins', *UCL Doctoral Thesis*.

Muendges, J. *et al.* (2015) 'Single stage aqueous two-phase extraction for monoclonal antibody purification from cell supernatant', *Fluid Phase Equilibria*, 385, pp. 227–236. doi: 10.1016/j.fluid.2014.10.034.

Muralidhara, H. S., Ensminger, D. and Putnam, A. (1985) 'Acoustic Dewatering And Drying (Low And High Frequency): State Of The Art Review', *Drying Technology*, 3(4), pp. 529–566. doi: 10.1080/07373938508916296.

Nelson, C. D. and Glatz, C. E. (1985) 'Primary particle formation in protein precipitation', *Biotechnology and Bioengineering*, 27(10), pp. 434–444. doi: 10.1002/bit.260271007.

- Nonaka, T. *et al.* (2018) 'A new pH-responsive peptide tag for protein purification', *Protein Expression and Purification*. Academic Press, 146, pp. 91–96. doi: 10.1016/J.PEP.2018.02.004.
- Oelmeier, S. A., Ladd-Effio, C. and Hubbuch, J. (2013) 'Alternative separation steps for monoclonal antibody purification: Combination of centrifugal partitioning chromatography and precipitation', *Journal of Chromatography A*, 1319, pp. 118–126. doi: 10.1016/j.chroma.2013.10.043.
- Oss, C. J. (1989) 'On the mechanism of the cold ethanol precipitation method of plasma protein fractionation', *Journal of Protein Chemistry*, 8(5), pp. 661–668. doi: 10.1007/BF01025606.
- Oss, C. J. V. and Good, R. J. (1989) 'Surface tension and the solubility of polymers and biopolymers: The role of polar and apolar interfacial free energies', *Journal of Macromolecular Science: Part A - Chemistry*, 26(8), pp. 1183–1203. doi: 10.1080/00222338908052041.
- van Oss, C. J., Good, R. J. and Chaudhury, M. K. (1986) 'Solubility of proteins', *Journal of Protein Chemistry*, 5, pp. 385–405. doi: 10.1007/BF01025572.
- Panić, S. *et al.* (2004) 'Experimental approaches to a better understanding of mixing performance of microfluidic devices', *Chemical Engineering Journal*. Elsevier, 101(1–3), pp. 409–419. doi: 10.1016/J.CEJ.2003.10.026.
- Parker, T. G. and Dalgleish, D. G. (1977) 'The use of light-scattering and turbidity measurements to study the kinetics of extensively aggregating proteins: α s-Casein', *Biopolymers*, 16(11), pp. 2533–2547. doi: 10.1002/bip.1977.360161115.
- Percival, H. (1925) 'Observations on the Role of the Ether-Soluble Constituents of Serum in Certain Serological Reactions', *British journal of experimental pathology*, 6(4), pp. 180–196.
- Petenate, A. M. and Glatz, C. E. (1983) 'Isoelectric precipitation of soy protein. II. Kinetics of protein aggregate growth and breakage', *Biotechnology and Bioengineering*, 25(12), pp. 3059–3078. doi: 10.1002/bit.260251220.
- Phillips, R., Rohani, S. and Baldyga, J. (1999) 'Micromixing in a single-feed semi-batch precipitation process', *AIChE Journal*, 45(1), pp. 82–92. doi: 10.1002/aic.690450108.
- Pinot, J. *et al.* (2014) 'New protocol of the Villermaux–Dushman reaction system to characterize micromixing effect in viscous media', *Chemical Engineering Science*, 118, pp. 94–101. doi: 10.1016/j.ces.2014.07.010.
- Polson, A. *et al.* (1964) 'The fractionation of protein mixtures by linear polymers of high molecular weight', *Biochimica et Biophysica Acta (BBA) - General Subjects*, 82(3), pp. 463–475. doi: [https://doi.org/10.1016/0304-4165\(64\)90438-6](https://doi.org/10.1016/0304-4165(64)90438-6).
- Polson, A. (1977) 'A theory for the displacement of proteins and viruses with polyethylene glycol', *Preparative Biochemistry*, 7(2), pp. 129–154. doi: 10.1080/00327487708061631.
- Polson, C. *et al.* (2003) 'Optimization of protein precipitation based upon effectiveness of protein removal and ionization effect in liquid chromatography–tandem mass spectrometry', *Journal of Chromatography B*, 785(2), pp. 263–275. doi: 10.1016/S1570-0232(02)00914-5.
- Ramos-de-la-Peña, A. M., González-Valdez, J. and Aguilar, O. (2019) 'Protein A chromatography: Challenges and progress in the purification of monoclonal antibodies', *Journal of Separation Science*, 42(9), pp. 1816–1827. doi: 10.1002/jssc.201800963.

- Ramshaw, J. A. M., Bateman, J. F. and Cole, W. G. (1984) 'Precipitation of collagens by polyethylene glycols', *Analytical Biochemistry*, 141(2), pp. 361–365. doi: 10.1016/0003-2697(84)90056-3.
- Raphael, M. and Rohani, S. (1999) 'Sunflower protein precipitation in a tubular precipitator', *The Canadian Journal of Chemical Engineering*, 77(3), pp. 540–554. doi: 10.1002/cjce.5450770315.
- Rathore, A. S. *et al.* (2015) 'Continuous processing for production of biopharmaceuticals.', *Preparative biochemistry & biotechnology*, 45(8), pp. 836–49. doi: 10.1080/10826068.2014.985834.
- Rayat, A. C. *et al.* (2016) 'Ultra scale-down approaches to enhance the creation of bioprocesses at scale: impacts of process shear stress and early recovery stages', *Current Opinion in Chemical Engineering*, 14, pp. 150–157. doi: 10.1016/j.coche.2016.09.012.
- Reay, D., Ramshaw, C. and Harvey, A. (2013) 'A brief history of process intensification', in *Process Intensification, 2nd edition*, pp. 437–542. doi: 10.1016/B978-0-08-098304-2.00012-2.
- Ries-Kautt, M. M. and Ducruix, A. F. (1989) 'Relative effectiveness of various ions on the solubility and crystal growth of lysozyme.', *Journal of Biological Chemistry*, 264(2), pp. 745–748. doi: 066/11.
- Rothstein, F. (1994) 'Differential precipitation of proteins. Science and technology.', *Bioprocess technology*. United States, 18, pp. 115–208.
- Rousseaux, J. M. *et al.* (1999) 'Micromixing efficiency of a novel sliding-surface mixing device', *AIChE Journal*, 45(10), pp. 2203–2213. doi: 10.1002/aic.690451018.
- Salahuddin, A. *et al.* (1983) 'A possible relation between the salting-out behaviour of proteins & their surface hydrophobicity.', *Indian Journal of Biochemistry and Biophysics*, 20(3), pp. 127–131.
- Salt, D. J. *et al.* (1982) 'Factors influencing protein structure during acid precipitation: A study of soya proteins', *European Journal of Applied Microbiology and Biotechnology*, 14, pp. 144–148. doi: 10.1007/BF00497890.
- Sandberg, H. E. (1978) 'International Workshop on Technology for Protein Separation and Improvement of Blood Plasma Fractionation', *Proceedings of the International Workshop on Technology for Protein Separation and Improvement of Blood Plasma Fractionation: Reston, Virginia*. Bethesda, Md.: Dept. of Health, Education, and Welfare, Public Health Service, National Institutes of Health (DHEW publication ; no. (NIH) 78-1422).
- Sandor, G. (1966) *Serum Proteins in Health and Disease*. Baltimore, Md.: William and Wilkins.
- dos Santos, R., Carvalho, A. L. and Roque, A. C. A. (2017) 'Renaissance of protein crystallization and precipitation in biopharmaceuticals purification', *Biotechnology Advances*, 35(1), pp. 41–50. doi: 10.1016/j.biotechadv.2016.11.005.
- Saunders, L. (1951) 'Surface and Colloid Chemistry', *Journal of Pharmacy and Pharmacology*, 3(1), pp. 865–882. doi: 10.1111/j.2042-7158.1951.tb13130.x.
- Schellman, J. A. (1990) 'A simple model for salvation in mixed solvents. Applications to the stabilization and destabilization of macromolecular structures', *Biophysical Chemistry*, 37, pp. 121–140. doi: 10.1016/0301-4622(90)88013-l.

Schilling, K. *et al.* (1953) 'Serum-Protein Fractionation by Means of Ammonium Sulfate in the Presence of Phenolic Compounds', *Acta Chemica Scandinavica*, 7, pp. 1007–1009. doi: 10.3891/acta.chem.scand.07-1007.

Schubert, P. F. and Finn, R. K. (1981) 'Alcohol precipitation of proteins: The relationship of denaturation and precipitation for catalase', *Biotechnology and Bioengineering*, 23, pp. 2569–2590. doi: 10.1002/bit.260231114.

Scopes, R. K. and Scopes, R. K. (1982) 'Separation by Precipitation', in *Protein Purification*, pp. 41–71. doi: 10.1007/978-1-4757-1770-9_3.

Shaughnessy, A. F. (2012) 'Monoclonal antibodies: magic bullets with a hefty price tag', *BMJ (Online)*, 345, p. e8346. doi: 10.5642/steam.20150201.16.

Shih, Y. C., Prausnitz, J. M. and Blanch, H. W. (1992) 'Some characteristics of protein precipitation by salts.', *Biotechnology and bioengineering*, 40(10), pp. 1155–64. doi: 10.1002/bit.260401004.

Sim, S.-L. *et al.* (2012) 'Branched polyethylene glycol for protein precipitation.', *Biotechnology and bioengineering*, 109(3), pp. 736–46. doi: 10.1002/bit.24343.

Sim, S. L. *et al.* (2012) 'Protein precipitation by polyethylene glycol: A generalized model based on hydrodynamic radius', *Journal of Biotechnology*, 157(2), pp. 315–319. doi: 10.1016/j.jbiotec.2011.09.028.

Sinanoğlu, O. (1980) 'The solvophobic theory for the prediction of molecular conformations and biopolymer bindings in solutions with recent direct experimental tests', *International Journal of Quantum Chemistry*, 28, pp. 381–392. doi: 10.1002/qua.560180207.

Smoluchowski, M. (1917) 'Mathematical theory of the kinetics of the coagulation of colloidal solutions', *Z physik Chem*, 92, pp. 129–168.

Sommer, R. *et al.* (2014) 'Combined polyethylene glycol and CaCl₂ precipitation for the capture and purification of recombinant antibodies', *Process Biochemistry*, 49(11), pp. 2001–2009. doi: 10.1016/j.procbio.2014.07.012.

Sommer, R. *et al.* (2015) 'Capture and intermediate purification of recombinant antibodies with combined precipitation methods', *Biochemical Engineering Journal*, 93, pp. 200–211. doi: 10.1016/j.bej.2014.10.008.

Stern, O. (1924) 'Zur Theorie der Elektrolytischen Doppelschicht', *Zeitschrift fur Elektrochemie*, 30, pp. 508–516. doi: 10.1002/bbpc.192400182.

Sternberg, M. and Hershberger, D. (1974) 'Separation of proteins with polyacrylic acids', *BBA - Protein Structure*, 342(1), pp. 195–206. doi: 10.1016/0005-2795(74)90121-4.

Swartz, A. R. *et al.* (2018) 'High-efficiency affinity precipitation of multiple industrial mAbs and Fc-fusion proteins from cell culture harvests using Z-ELP-E2 nanocages', *Biotechnology and Bioengineering*. Wiley-Blackwell, 115(8), pp. 2039–2047. doi: 10.1002/bit.26717.

Titchener-Hooker, N. J. *et al.* (1992) 'The effect of fluid-jet mixing on protein precipitate growth during low-frequency conditioning', *Chemical Engineering Science*, 47(1), pp. 75–86. doi: 10.1016/0009-2509(92)80202-N.

Titchener-Hooker, N. J. and McIntosh, R. V. (1992) 'Enhancement of protein precipitate strength and density by low-frequency conditioning', *Bioprocess Engineering*, 8(1–2), pp. 91–97. doi: 10.1007/BF00369270.

- Trapp, A. *et al.* (2018) 'Multiple functions of caprylic acid-induced impurity precipitation for process intensification in monoclonal antibody purification', *Journal of Biotechnology*. Elsevier, 279, pp. 13–21. doi: 10.1016/J.JBIOTEC.2018.05.001.
- Tscheliessnig, A. *et al.* (2014) 'Ethanol precipitation for purification of recombinant antibodies.', *Journal of biotechnology*, 188, pp. 17–28. doi: 10.1016/j.jbiotec.2014.07.436.
- Tummers, M. J., Jacobse, J. and Voorbrood, S. G. J. (2011) 'Turbulent flow in the near field of a round impinging jet', *International Journal of Heat and Mass Transfer*, 54(23), pp. 4939–4948. doi: 10.1016/j.ijheatmasstransfer.2011.07.007.
- Turkevich, J., Stevenson, P. C. and Hillier, J. (1951) 'A study of the nucleation and growth processes in the synthesis of colloidal gold', *Discussions of the Faraday Society*, 11, pp. 55–75. doi: 10.1039/DF9511100055.
- Villiermaux, J. (1986) 'Macro and Micromixing Phenomena in Chemical Reactors', in *Chemical Reactor Design and Technology*, pp. 191–244. doi: 10.1007/978-94-009-4400-8_6.
- Villiermaux, J. and Falk, L. (1994) 'A generalized mixing model for initial contacting of reactive fluids', *Chemical Engineering Science*, 49(24), pp. 5127–5140. doi: 10.1016/0009-2509(94)00303-3.
- Virkar, P. D. *et al.* (1982) 'Kinetics of the acid precipitation of soya protein in a continuous-flow tubular reactor.', *Biotechnology and bioengineering*, 24(4), pp. 871–87. doi: 10.1002/bit.260240410.
- Watanabe, E. O. *et al.* (2009) 'Phase equilibria for salt-induced lysozyme precipitation: Effect of salt type and temperature', *Fluid Phase Equilibria*, 281(1), pp. 32–39. doi: 10.1016/j.fluid.2009.03.021.
- Watt, J. G. (1970) 'Automatically Controlled Continuous Recovery of Plasma Protein Fractions for Clinical Use: A Preliminary Report', *Vox Sanguinis*. Blackwell Publishing Ltd, 18(1), pp. 42–61. doi: 10.1111/j.1423-0410.1970.tb01428.x.
- Wenger, M. D. (2010) 'Micro-tip chromatography ; a route to an integrated strategy for high throughput bioprocess development', *UCL Doctoral Thesis*, (December).
- Xu, J. *et al.* (2020) 'Biomanufacturing evolution from conventional to intensified processes for productivity improvement: a case study', *mAbs*, 12(1), pp. 1–13. doi: 10.1080/19420862.2020.1770669.
- Yang, H. J. *et al.* (2005) 'Micromixing efficiency in a rotating packed bed: Experiments and simulation', *Industrial and Engineering Chemistry Research*, 44(20), pp. 7730–7737. doi: 10.1021/ie0503646.
- Yang, K. *et al.* (2009) 'Micromixing Efficiency of Viscous Media in Micro-channel Reactor', *Chinese Journal of Chemical Engineering*. Elsevier, 17(4), pp. 546–551. doi: 10.1016/S1004-9541(08)60243-8.
- Zauner, R. and Jones, A. G. (2000) 'Scale-up of Continuous and Semibatch Precipitation Processes', *Industrial & Engineering Chemistry Research*, 39(7), pp. 2392–2403. doi: 10.1021/ie990431u.
- Zhang, C. *et al.* (2005) 'Lysozyme purification from tobacco extract by polyelectrolyte precipitation', *Journal of Chromatography A*, 1069(1), pp. 107–112. doi: 10.1016/j.chroma.2004.10.018.

Zhang, Y. and Cremer, P. S. (2006) 'Interactions between macromolecules and ions: The Hofmeister series.', *Current opinion in chemical biology*, 10(6), pp. 658–63. doi: 10.1016/j.cbpa.2006.09.020.

Zhang, Z., Chisti, Y. and Moo-Young, M. (1995) 'Isolation of a recombinant intracellular beta-galactosidase by ammonium sulfate fractionation of cell homogenates', *Bioseparation*, 5(6), pp. 329–337.

Zydney, A. L. (2015) 'Perspectives on integrated continuous bioprocessing—opportunities and challenges', *Current Opinion in Chemical Engineering*, 10, pp. 8–13. doi: 10.1016/j.coche.2015.07.005.

Appendix A: IgG₄ amino acid sequence

DIQMTQSPSS LSASVGDRVT ITCKASQNV R TVVAWYQQKP GKAPKTLIYL
ASNRHTGVPS RFSGSGSGTD FTLTISSLQP EDFATYFCLQ HWSYPLTFGQ
GTKVEIKRTV AAPSVFIFPP SDEQLKSGTA SVVCLLNNFY PREAKVQWKV
DNALQSGNSQ ESVTEQDSKD STYLSSTLT LSKADYEKHK VYACEVTHQG
LSSPVTKSFN RGECEVQLVE SGGGLVQPGG SLRLSCAASG FAFSTYDMSW
VRQAPGKGLE WVATISSGGS YTYLDSVKG RFTISRDKSS NTLYLQMNSL
RAEDTAVYYC APTTVVPFAY WGQGLVTVS SASTKGPSVF PLAPCSRSTS
ESTAALGCLV KDYFPEPVTV SWNSGALTSG VHTFPAVLQS SGLYSLSSV
TVPSSSLGTK TYTCNVDPK SNTKVDKRVE SKYGPPCPPC PAPEFLGGPS
VFLFPPKPKD TLMISRTPEV TCVVVDVSQE DPEVQFNWYV DGVEVHNAKT
KPREEQFNST YRVVSVLTVL HQDWLNGKEY KCKVSNKGLP SSIEKTISKA
KGQPREPQVY TLPPSQEEMT KNQVSLTCLV KGFYPSDIAV EWESNGQPEN
NYKTTTPVLS DGSFFLYSRL TVDKSRWQEG NVFSCSVMHE ALHNHYTQKS
LSLSLGKDIQ MTQSPSSLSA SVGDRVTITC KASQNVRTVV AWYQQKPGKA P
KTLIYLASN RHTGVPSRFS GSGSGTDFTL TISSLQPEDF ATYFCLQHWS YPLT
FGQGTK VEIKRTVAAP SVFIDPPSDE QLKSGTASVV CLLNNFYPRE AKVQW
KVDNA LQSGNSQESV TEQDSKDSTY SLSSTLTLSK ADYEKHKVYA CEVTHQ
GLSS PVTKSFNRGE CEVQLVESGG GLVQPGGSLR LSCAASGFAF
STYDMSWVRQ APGKGLEWVA TISSGGSYTY YLDSVKGRFT ISRDKSSKNTL
YLQMNSLRAE DTAVYYCAPT TVVPFAYWGQ GTLVTVSSAS TKGPSVFPLA
PCSRSTSEST AALGCLVKDY FPEPVTVSWN SGALTSGVHT FPAVLQSSGL
YSLSSVVTVP SSSLGKTYT CNVDHKPSNT KVDKRVESKY GPPCPPCPAP
EFLGGPSVFL FPPKPKDTLM ISRTPEVTCV VVDVSQEDPE VQFNWYVDGV
EVHNAKTKPR EEQFNSTYRV VSVLTVLHQD WLNGKEYKCK VSNKGLPSSI
EKTISKAKGQ PREPQVYTL PPSQEEMTKN QVSLTCLVKG FYPSDIAVEW
ESNGQPENNY KTTTPVLDS DGSFFLYSRLT VDKSRWQEGN VFSCSVMHEA
LHNHYTQKSL SLSLGK

Appendix B: IgG physicochemical properties

Molecular Weight, MW

144 kDa

Isoelectric point, pI

7.89

Extinction coefficient, ϵ_{280}

1.38 g L⁻¹ cm⁻¹